A Framework to Develop a Hybrid Methodology for Modeling of Diesel Particulate Matter Concentration in Underground Mine Ventilation Systems

by

Hongbin Zhang

A thesis submitted in partial fulfillment
of the requirements for the degree of
Doctor of Philosophy (Ph.D.) in Natural Resources Engineering

The Faculty of Graduate Studies
Laurentian University
Sudbury, Ontario, Canada

THESIS DEFENCE COMMITTEE/COMITÉ DE SOUTENANCE DE THÈSE
Laurentian Université/Université Laurentienne
Faculty of Graduate Studies/Faculté des études supérieures

Title of Thesis
Titre de la thèse

A Framework to Develop a Hybrid Methodology for Modeling of Diesel Particulate Matter Concentration in Underground Mine Ventilation Systems

Name of Candidate
Nom du candidat Zhang, Hongbin

Degree
Diplôme Doctor of Science

Department/Program
Département/Programme Engineering

Date of Defence
Date de la soutenance October 15, 2019

APPROVED/APPROUVÉ

Thesis Examiners/Examinateurs de thèse:

Dr. Ming Cai
(Co-Supervisor/Co-directeur de thèse)

Dr. Nick Vayenas
(Co-Supervisor/Co-directeur de thèse)

Dr. Lorrie Fava
(Committee member/Membre du comité)

Dr. Enrique Acuna
(Committee member/Membre du comité)

Dr. Hongliang Wang
(Committee member/Membre du comité)

Dr. Stephen Hardcastle
(External Examiner/Examinateur externe)

Dr. Andrew McDonald
(Internal Examiner/Examinateur interne)

Approved for the Faculty of Graduate Studies
Approuvé pour la Faculté des études supérieures
Dr. David Lesbarrères
Monsieur David Lesbarrères
Dean, Faculty of Graduate Studies
Doyen, Faculté des études supérieures

ACCESSIBILITY CLAUSE AND PERMISSION TO USE

Abstract

The purpose of this research is to develop a hybrid methodology for diesel particulate matter (DPM) modeling for underground mine ventilation systems. The hybrid methodology, which is an enhanced and complementary tool, is proposed to provide improved diesel input to a ventilation network solver by using a computational fluid dynamics (CFD) solver. The hybrid methodology uses the DPM results from a calibrated CFD model to update those from a network model at shared locations. A CFD approach for simulating DPM over an extended period has been proposed to make the hybrid methodology more adaptable to large ventilation systems. With the proposed CFD modeling approach, contaminants like DPM can be modeled accurately in a timely manner over an extended period of time. The results from this approach are then used to update the network model results at the shared outlets. The workflow to update DPM results from the network model using the calibrated CFD model is presented.

Two field studies were conducted in an underground mine in the western United States. Due to the low quality airflow and DPM data collected from the field, this study should be viewed as a qualitative study rather than a quantitative study. Corresponding CFD models, ventilation network models, and updated ventilation models were also established, and results from these models were compared with the experimental data. The limitations for both the instruments and the methodology were defined as well.

Keywords: hybrid methodology, mine ventilation, diesel particulate matter (DPM), network modeling, computational fluid dynamics (CFD)

Original Contributions

- Conducted a DPM simulation over an extended period of time (over one hour) in an underground dead-end heading using CFD models with a single DPM source and user-defined functions (UDF).
- Proposed a DPM modeling technique in a ventilation network solver.
- Developed a workflow for integrating a CFD model with a ventilation network solver.
- Proposed and tested a framework of a hybrid methodology for DPM modeling over an extended period of time in a dead-end heading.
- Provided the benefits of using the hybrid methodology and its potential applications.
- Using a CFD model, explored the impact of cycle time on DPM concentration over time
- Reduced the computing time for modeling DPM concentration over an extended period of time using CFD.
- Provided a new way to supply input to a ventilation network solver.
- Provided new numerical modeling approaches (i.e., the CFD modeling approach using a single stationary DPM source and the hybrid methodology) to predict future DPM concentration in underground mines.
- Defined the limitations of the current approach for both the instruments used and the methodology proposed.

Acknowledgments

Firstly, I would like to express my sincere gratitude to my research advisor Dr. Lorrie Fava, for the continuous support of my Ph.D. study and related research, for her guidance and motivation. Her guidance helped me in all the time of research and writing of this thesis. I could not have imagined having a better advisor and mentor for my Ph.D. study.

Besides, I want to express my sincere appreciation to my academic advisors: Prof. Ming Cai and Prof. Nick Vayenas for their insightful comments, encouragement, and guidance.

In addition, I want to thank Dr. Enrique Acuña for his advice on practical ventilation system design. I am also grateful for his suggestions on the thesis structure and ideas on how to proceed each milestone with confidence.

Moreover, I would like to thank Dr. Hongliang Wang and Prof. Redhouane Henda for their insightful comments and different views on my research.

I would like to express my special appreciation to MIRARCO Mining Innovation for providing an academic and professional atmosphere. I am proud to be a member of the Decision Support Software Center at MIRARCO and enjoyed working on the SOT+ project.

My sincere thanks also go to Newmont Mining Corporation, which provided me an opportunity to join their team as a researcher, trained me on how to drive a tractor, and helped me conduct field studies. Without their precious support, it would be difficult to do this research.

I would like to thank the Ultra-Deep Mining Network (UDMN) at the Centre for Excellence in Mining Innovation (CEMI) for their technical and financial contributions to this work.

I want to thank SHARCNET (www.sharcnet.ca) and Compute Canada (www.computecanada.ca) for providing high-performance computers for this research.

I am lucky to have friends who offer technical support for my research. I want to express my sincere appreciation to Darren Janeczek for technical assistance. I also want to express my sincere gratitude to Dr. Jozef Stachulak for his encouragement and suggestions for my career.

Furthermore, I want to thank CanmetMINING for offering me DPM data and some technical reports.

Last but not least, I would like to thank my family: my parents, my wife, and my baby girl for always being my patron and supporting me throughout my life in general.

Hongbin Zhang

MIRARCO Mining Innovation, Laurentian University

Sudbury, Ontario, Canada

Jan 17th, 2020

Table of Contents

List of Tables

List of Figures

List of Symbols

A	airway area
C_p	specific heat of fluid
E	energy
$\vec{F}$	external body force
f	coefficient of friction
g	gram
h	hour
h	sensible enthalpy
hp	horse-power
$\vec{J}_j$	diffusion flux of species
K	kelvin
k	Atkinson friction factor
k_{eff}	effective conductivity
kg	Kilogram
kW	Kilo-Walt
l	airway length
L_{eq}	equivalent length
M	mass flow rate
m	meter
min	minute
p	pressure
P_f	pressure increase through a fan
P_{shock}	shock loss
per	perimeter of the airway
Q	airflow quantity
Q_a	Assumed true airflow
R	Atkinson resistance
R_i	resistance of a single airway or net rate of production of species i by chemical reaction
R_{mine}	total resistance of airways
R_{shock}	shock resistance
s	second
S_f	slope of a fan curve
S_h	heat of chemical reaction and any other volumetric user-defined heat sources
S_i	rate of creation by addition from the dispersed phase plus any user-defined sources
S_m	additional mass added to the system from the user-defined sources or the dispersed second phase
t	time
T	temperature
T_{ref}	reference temperature
u	airflow velocity

$\vec{v}$	velocity vector
X	shock loss factor
Y_j	mass fraction of species *j*
°C	Celsius degree
ΔQ	difference between the true airflow and assumed true airflow
∇	partial derivative of a quantity in the Cartesian coordinate system
ρ	density
$\rho\vec{g}$	gravitational body force
$\bar{\bar{\tau}}$	stress tensor

List of Abbreviations

1D	One-dimensional
2D	Two-dimensional
3D	Three-dimensional
AMPL	Mathematical Programming Language
AMS	Air Monitoring Stations
CFD	Computational Fluid Dynamics
CPM	Critical Path Method
CSV	Comma-Separated Values
CTI	Control Time Interval
DCS	Distributed Control System
DES	Discrete Event Simulation
DOCF	Discounted Operating Cash Flow
DPM	Diesel Particulate Matter
EC	Elemental Carbon
ECS	Environment Control System
EE	Energy Efficiency
GA	Genetic Algorithm
HPC	High-Performance Computer
HS	Harmony Search
IP	Integer Programming
LHD	Load-Haul-Dump
LLSP	Laser-Light Scattering Photometry
LM	Load Management
LOM	Life-of-Mine
M/NM	Metal and Non-Metal
MILP	Mixed Integer Linear Programming
MIP	Mixed Integer Programming
MOGA	Multi-Objective Genetic Algorithm
MS	Microsoft
MSHA	Mine Safety and Health Administration
MSSO	Minesight Schedule Optimizer
MVO	Mine Ventilation Optimization
NIOSH	The National Institute for Occupational Safety and Health
NPV	Natural Ventilating Pressure or Net Present Value
OC	Organic Carbon
OMP	Open Mine Planner
PDM	Personal Dust Monitor
PERT	Program Evaluation and Review Techniques
PLCs	Programmable Logic Controllers
PPM	Parts Per Million
PSO	Particle Swarm Optimization
RTLS	Real-Time Location System
SHARCNET	The Shared Hierarchical Academic Research Computing Network

SOT	Schedule Optimization Tool
TC	Total Carbon
TLV	Threshold Limit Value
TWA	Time-Weighted Average
UDF	User Defined Functions
VCM	Ventilation Constraint Module
VFD	Variable Frequency Drive
VIV	Variable Inlet Vanes
VOD	Ventilation on Demand
VSD	Variable Speed Drive

Preface

The research work was completed at MIRARCO – Mining Innovation in Laurentian University, in Canada. The relevant field experiments were conducted in an underground gold mine in the U.S. The author worked for MIRARCO as a mining engineering research assistant on the SOT+ research project, sponsored by companies, Newmont Mining Corporation (U.S.), Vale (Canada), Agnico Eagle, Deswik, Map3D, Ventsim and the Ultra Deep Mining Network (UDMN) at the Centre for Excellence in Mining Innovation (CEMI).

SOT, which is short for Schedule Optimization Tool, is a mine production schedule optimization software. SOT optimizes the net present value of mine schedules with a genetic algorithm. However, constraints result from ventilation requirements, geo-technical stability, and ore grade or mineral price uncertainties, have not been accounted for. The SOT+ research project was initiated to consider these constraints when optimizing a mine production schedule. The author was working on the Ventilation Constraint Module (VCM), which is one of the three modules of the SOT+ project. VCM helps SOT generate feasible optimized schedules by taking ventilation constraints into account. The idea is VCM queries airflow and diesel particulate matter (DPM) information via a ventilation network solver and manipulates device settings in order to redistribute the airflow in the ventilation system to prevent the time-weighted average (TWA) DPM concentration being over the regulatory limit at any point of the Life-of-Mine (LOM) schedule. The airflow must reduce the TWA exposure of a worker to total carbon (TC) to not more than 400 $\mu g/m^3$ (Government of Ontario, 1990). TC is used as a substitute for DPM (Mine Safety and Health Administration, 2009). DPM is an important factor to account for when making mine production schedules because it is part of the diesel exhaust from diesel-powered equipment and it has a direct

relationship with the airflow needed in the mine. In Ontario, the law is that the airflow must be more than 0.06 m^3/s per kW power of the diesel equipment (Government of Ontario, 1990) and the Threshold Limit Values (TLVs) for biological or chemical agents in the airflow are within the regulatory range (Occupational Health and Safety Act, 1990).

Therefore, obtaining accurate DPM modeling results from the ventilation network solver is a key part of the schedule optimization process when using VCM. The challenge for the user is to ensure that the airflow and DPM data entered into Ventsim, which is a popular ventilation network solver, is accurate. If inaccurate diesel emission rates are entered into Ventsim, the DPM modeling results will be inaccurate. Ventsim, as a one-dimensional (1D) solver, takes area-average DPM data as input. The area-average DPM data input usually comes from underground measurements. When taking a DPM measurement in an underground mine, one real-time DPM monitor is often placed at one location in the cross-sectional area of a drift because the number of DPM monitors is often limited. As a result, it is hard to get area-average DPM data at different locations with multiple real-time DPM monitors installed at each cross-sectional area of the locations. Hence, either the measured TWA DPM concentration from the one monitor or the TWA DPM concentration with a correction factor (representing the area-average DPM concentration across the cross-sectional area) is used as the input to the ventilation network solver. However, the TWA DPM concentration from one monitor cannot represent the area-average DPM concentration and the correction factor may vary under different flow situations. Besides, the DPM simulation in the ventilation network solver is 1D and cannot provide detailed DPM distribution across a cross-sectional area.

Because of the mentioned uncertainties of DPM modeling in the ventilation network solver, the author decided to investigate the feasibility of using CFD for DPM modeling. With prior modeling

experience with CFD, the author knew that CFD simulation is time-consuming and computationally expensive but it is able to perform three-dimensional (3D) DPM modeling and it has high accuracy. Most importantly, a monitoring point can be created in a cross-sectional area in the CFD model at the same location as where the real-time-DPM monitor is in the experiment. Hence, the diesel input uncertainty can be eliminated in the CFD model.

Regarding the computing time, it will be feasible to model DPM distribution over time in one dead-end heading in the CFD model. However, DPM modeling at any point of the LOM with a large number of headings and development drifts in the CFD model will be impractical.

Therefore, the idea of a hybrid methodology for DPM modeling is proposed in this thesis. The hybrid methodology, which is an enhanced and complementary tool, is proposed to provide improved diesel input to Ventsim. DPM modeling in the dead-end headings will be conducted using CFD and the rest of the ventilation network will be modeled in Ventsim. The DPM results in the CFD model will be converted to equivalent diesel input at the shared outlet(s) in Ventsim so that the DPM data in Ventsim is updated. Besides, a CFD approach for DPM modeling over an extended period of time is also proposed to further reduce the computing time and better assist the hybrid methodology.

Chapter 1

1 Introduction

In general, the ventilation costs account for 40 to 50% of the total energy cost for an underground mine (Allen and Tran, 2011). However, most of the time, ventilation is over-provided for considering air leakage and for safety purposes, which has often resulted in a waste of energy and an increase of cost. In addition, mine ventilation is a constraint for both long-term and short-term mine schedules because a certain amount of airflow is required to dilute the diesel particulate matter (DPM) generated by various diesel equipment in metal/non-metal (M/NM) mines. Therefore, mine ventilation optimization is necessary for mine production schedule optimization.

Systematic research on ventilation optimization has been conducted since 1994 (Lilic and Kuzmanovl, 1994; Hardcastle *et al.*, 2005; Webber-Youngman, 2005; Sui *et al.*, 2011). Some ventilation network solvers, such as VNet (Mine Ventilation Services, 2016) and Ventsim (Chasm Consulting, 2016), are used to optimize ventilation networks. SOT and VCM is an example of a mine production schedule optimization software package, which has taken ventilation constraints into account by integrating with the ventilation network solvers. Common ventilation constraints include available airflow quantity, temperature threshold, the TLVs for biological or chemical agents in the airflow (Occupational Health and Safety Act, 1990), dust limit, and DPM limit. It is not reasonable to make a mine production schedule without considering ventilation availability because the ventilation constraints are regulated by mine safety agencies. For instance, the air volume needs to be at least 0.06 m^3/s per kW power of the diesel equipment working underground in Ontario, Canada (Government of Ontario, 1990). The regulatory DPM concentration in the U.S.

is 160 μg/m^3 (Mine Safety and Health Administration, 2001) and it is not feasible to create a mine schedule without considering the regulatory DPM limit.

This research is motivated by the need to narrow the gap between mine ventilation and production schedule optimization. The VCM, which is a software module developed by MIRARCO Mining Innovation in Canada, takes ventilation constraints into account while optimizing mine production schedules according to Zhang *et al.* (2016). The VCM is integrated with the ventilation network solver, Ventsim (Chasm Consulting, 2016). Ventsim is able to model the ventilation network. The challenge for the user is to ensure that the airflow and DPM data entered into Ventsim is accurate. If inaccurate diesel emission rates are entered into Ventsim, the DPM modeling results will be inaccurate. Ventsim, as a 1D solver, takes area-average DPM data as input. Because the number of real-time DPM monitors at mine sites is usually limited, it is hard to get area-average DPM data at different locations with multiple real-time DPM monitors installed at each cross-sectional area of the locations. Hence, a correction factor is needed to convert the point DPM data (recorded by a real-time DPM monitor) to area-average DPM data before entered into Ventsim. The correction factor may vary under different flow situations. A hybrid methodology, which is an enhanced and complementary tool, is proposed to provide improved diesel input to Ventsim. The airflow and DPM modeling results from Ventsim can then be used by VCM to constrain mine schedule optimization. The hybrid methodology is developed to combine two popular software packages and make full use of their advantages. The ventilation network modeling software, Ventsim, and a finite-volume-based CFD software, ANSYS Fluent (ANSYS Inc., 2009c), are coupled through the hybrid methodology in this research. The idea is to use DPM results from the CFD model to update those from the ventilation network solver at the outlet existing in both models. A DPM modeling technique in a ventilation network solver is proposed. A new CFD modeling approach

for modeling DPM over an extended period in underground mines is also proposed to reduce the computing time while sustaining high accuracy (80%) of the results. The hybrid methodology would not be practical without the new CFD modeling approach. With the hybrid methodology, the results are expected to be as accurate as those from the CFD model alone and the computing time is expected to be significantly less than those from the CFD model alone. Potentially, results from the updated ventilation network model using this hybrid methodology can be practically used by the VCM to constrain mine schedule optimization.

As mentioned above, addressing the gap between mine ventilation and production schedule optimizations is the motivation of this research. The hybrid methodology, the DPM modeling technique in a ventilation network solver, and the new CFD modeling approach to model DPM over an extended time (more than one hour) are the core contributions of this research.

Because it takes excessive effort and time to build an overall mine ventilation CFD model for an underground mine, the idea is to build it in a ventilation network solver. The first step is identifying the local areas of interest to build the CFD model. The next step is coupling the CFD model and the ventilation network model using the proposed hybrid methodology. On one hand, the ventilation network model is quick to solve and easy to establish compared with the CFD model, which is time-consuming to build, and computationally expensive. On the other hand, the CFD model can provide details of three-dimensional (3D) information of airflow (and other gas flows) better than the ventilation network model that only shows one-dimensional (1D) information of airflow. Here, 3D refers to three-dimensional movements of flow within a space. The data (e.g., air velocity and DPM concentration at a location in a drift) from the CFD model is not an average value. 1D refers to the longitudinal axis in the flow direction. The data from the ventilation network

model is an average value. Therefore, the hybrid methodology will make it possible to generate an updated ventilation model in less time compared with using a CFD model alone, while providing detailed airflow (and other gas flows) information in certain areas of interest.

1.1 Background

For underground M/NM mines, DPM is a main concern due to its carcinogenic effect on the human body after overexposure (Anon, 1988). DPM is generated by the diesel-powered equipment working underground and the shift-average DPM concentration is regulated by law in North America. Hence, it is crucial to understand and predict the DPM concentration distribution in underground mines. DPM concentration is affected by many factors such as airflow, diesel engine power, diesel emission rate, cycle time of diesel equipment, type of diesel engine, and after-treatment device attached to the diesel exhaust pipe. Both monitoring (Grenier *et al.*, 1991; Gillies *et al.*, 2008; Janisko and Noll, 2008, 2010; Wu and Gillies, 2008; Wu *et al.*, 2009; Gillies, 2012; Noll *et al.*, 2013; Khan and Gillies, 2015) and 3D CFD modeling (Zheng and Tien, 2008; Zheng, 2011; Zheng *et al.*, 2011, 2015, 2017; Thiruvengadam *et al.*, 2016; Chang *et al.*, 2019; Morla *et al.*, 2019) approaches have been investigated by various researchers to understand the DPM distribution in the confined underground environment.

However, none of the prior CFD modeling approaches are practical for application in the mining industry due to the computing time (e.g., more than 24 hours) required for transient simulation of DPM. The computing time of a transient simulation of DPM in the CFD model mainly depends on factors such as the size of the computational mesh, complexity of the geometry, flow characteristics, convergence criteria, number of governing equations, boundary conditions of the

flow domain, simulation time, and of course, processing power of the computer. Hence, a CFD modeling approach for DPM with less computing time is necessary for practical application.

Ventilation network solvers are also capable of DPM modeling and the computing time is negligible (e.g., 10 s) compared to the CFD modeling approach. As far as the author knows, no publications have been found on dynamic DPM modeling by using a mine ventilation network solver. There are few publications indicating DPM simulation in a ventilation network solver, but access to these publications is limited (e.g., membership restrictions). In addition, the abstracts of these publications indicate that no dynamic DPM modeling has been carried out. Hence, a DPM modeling technique using a ventilation network solver is proposed.

Although the computing time of the CFD modeling approach can be reduced, it will still be difficult to model the DPM distribution for an entire mine ventilation system in a timely manner because of the time needed to establish the model and to solve the large mesh. Therefore, the combination of ventilation network solver and CFD for DPM modeling can be a potential approach as long as a correct methodology can be defined to integrate the two.

Regarding the DPM monitoring approach, the Airtec real-time DPM monitor (Flir Systems, 2011), which is a popular real-time DPM monitor in North America, has a sensitivity of more than 70 $\mu g/m^3$ according to J. Noll (personal communication, June 12, 2018) from the National Institute for Occupational Safety and Health (NIOSH). Hence, the quality of the Airtec DPM monitors used is considered as not high. This research used the Airtec monitor because they were available at the mine site where the experiments were conducted.

1.1.1 Previous work conducted by the author

As detailed in the thesis published by Zhang (2015), a hybrid network-CFD model was built in a commercially available flow solver, Flownex (PADT, 2014b). The methodology of coupling CFD in Flownex is treating the CFD component as a "flow resistance" (PADT, 2014a). Both the inlet and outlet boundary conditions are transferred between the CFD component and Flownex. In addition, Flownex uses pressure/mass flow or temperature/heat difference as the convergence criteria for the hybrid model.

However, Flownex is not a standard mine ventilation solver, and no other studies using Flownex have been found related to mine ventilation other than Zhang's thesis (2015). Because it is a commercialized fluid network solver and has been coupled with the CFD solver (ANSYS Fluent), it is necessary to review the coupling methodology.

As seen in Fig. 1-1, Flownex iterates many times until the results match those from the CFD model. This provides accurate results but is time-consuming.

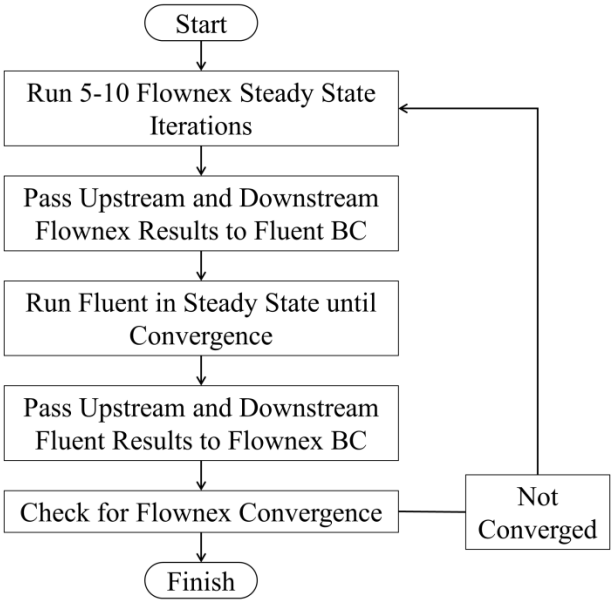

Fig. 1-1. Workflow of the hybrid Flownex-Fluent model (PADT, 2013).

In the thesis, a longwall working face was chosen as the CFD component in the hybrid model. However, because the geometry of the working face was simple and the real complex nature of the geometry was not modeled in the CFD component, results from the hybrid model matched those from the network model, but did not match those from the field studies. On the other hand, it did validate the hybrid model and proved that the CFD solver and the network solver could be integrated.

However, the hybrid model was applied in a coal mine, where the ventilation system was not as complicated as that in an M/NM mine. In addition, DPM modeling was not considered in the thesis.

1.2 Motivation

Ventilation costs account for 40 to 50% of the total energy cost for a Canadian base/precious metal mechanized mine (Hardcastle and Kocsis, 2004; Allen and Tran, 2011; De Souza, 2015). Total fan

power and the associated ventilation appliances at a mine site can exceed 10,000 kW easily (De Souza, 2015). With an electricity cost of $0.06 per kW·h, the annual ventilation cost can exceed $5.25 million. There are two main causes of such high ventilation cost. First, regional regulations (e.g., the air volume must be more than 0.06 m^3/s per kW power of the diesel equipment (Government of Ontario, 1990)) manages contaminants (particulates and gasses) as a whole. Second, the ventilation demand is not properly adjusted according to production flexibility (e.g., mining activities could change by hour but the air is not efficiently used in a traditional ventilation system which ventilates all potential workplaces). In addition, considerable duplication and redundancy lead to low utilization (50% at most) of the air resource (Hardcastle *et al.*, 2007). Therefore, an integration of mine production schedule optimization and mine ventilation should be considered to improve air utilization.

However, there is a gap between mine ventilation and mine production schedule optimization. The ventilation constraints such as airflow availability and airflow requirements for diesel equipment and personnel have not been studied in detail and considered in real underground mine production schedules, which brings up the motivation for this research. With the rapid development of computer technologies, a few schedule optimization tools have been developed for maximizing the LOM net present value (NPV). However, none of the tools has directly constrained the mine schedules in terms of ventilation availability. The VCM, which is developed by MIRARCO Mining Innovation, has been successfully coupled with the SOT and Ventsim.

There are different schedule optimization software packages used for both surface and underground mines. However, SOT, developed by MIRARCO, is the first commercialized schedule optimization software for underground mines in the market. It uses a genetic algorithm

and heuristics to generate a schedule while adhering to all precedence constraints and operational resource constraints. With the help of SOT, months of planning effort and millions of dollars could be added (Fava *et al.*, 2011, 2012, 2013).

VCM is coupled with Ventsim because the latter is widely used in the mining industry, which makes it easy to apply the VCM into the mining industry practically. VCM queries Ventsim for airflow and DPM information and redistributes the airflow in the ventilation system to prevent the DPM concentration being over the regulatory limit (e.g., 400 $\mu g/m^3$ in Ontario, Canada) at any point of the LOM. DPM is an important factor to account for when making mine production schedules because it is part of the exhaust from diesel-powered equipment and it has a direct relationship with the airflow needed in the mine. In Ontario, the law is that the airflow must be more than 0.06 m^3/s per kW power of the diesel equipment (Government of Ontario, 1990).

Therefore, obtaining accurate DPM modeling results from the ventilation network solver is a key part of the schedule optimization process when using VCM. The challenge for the user is to ensure that the airflow and DPM data entered into Ventsim, which is a popular ventilation network solver, is accurate. If inaccurate diesel emission rates are entered into Ventsim, the DPM modeling results will be inaccurate. Ventsim, as a 1D solver, takes area-average DPM data as input. The area-average DPM data input usually comes from underground measurements. When taking a DPM measurement in an underground mine, one real-time DPM monitor is often placed at one location in the cross-sectional area of a drift because the number of DPM monitors is often limited. As a result, it is hard to get area-average DPM data at different locations with multiple real-time DPM monitors installed at each cross-sectional area of the locations. Hence, either the measured time-weighted average (TWA) DPM concentration from the one monitor or the TWA DPM

concentration with a correction factor (representing the area-average DPM concentration across the cross-sectional area) is used as the input to the ventilation network solver. However, the TWA DPM concentration from one monitor cannot represent the area-average DPM concentration and the correction factor may vary under different flow situations. Besides, the DPM simulation in the ventilation network solver is 1D and cannot provide detailed DPM distribution across a cross-sectional area.

Because of the mentioned uncertainties of DPM modeling in Ventsim, the author decided to investigate the feasibility of using CFD for DPM modeling. With prior modeling experience with CFD, the author knew CFD is time-consuming and computationally expensive but it is able to perform 3D DPM modeling and it has high accuracy and capacity of solving complicated fluid dynamics problems. Most importantly, a monitoring point can be created in a cross-sectional area in the CFD model at the same location as where the real-time-DPM monitor is in the experiment. Hence, the diesel input uncertainty can be eliminated in the CFD model.

Regarding the computing time, it will be fine to model DPM distribution over time in one dead-end heading in the CFD model. However, DPM modeling at any point of the LOM with increasing number of headings and development drifts in the CFD model will be impractical.

Therefore, the idea of a hybrid methodology for DPM modeling is proposed in this thesis. The hybrid methodology, which is an enhanced and complementary tool, is proposed to provide improved diesel input to Ventsim. The author is a researcher at MIRARCO and is involved in the development and testing of VCM of the SOT+ project, further adding to the motivation to provide an improved diesel input for the DPM modeling in Ventsim with the hybrid methodology. DPM modeling in the dead-end headings is conducted using CFD and the rest of the ventilation network

is modeled in Ventsim. Due to the fact that DPM modeling is handled significantly different in terms of governing equations between CFD and Ventsim, the Ventsim results are updated with those from the CFD model at the outlet(s) existing in both the models. Computing time is saved by this means because the update is one-way and does not iterate back and forth. Besides, a CFD modeling approach for DPM modeling over an extended period of time (e.g., one hour) is also proposed to further reduce the computing time and better assist the hybrid methodology. As DPM modeling is the focus of this thesis and DPM is often measured over a shift, the CFD modeling approach needs to be capable of performing a transient simulation of DPM in a timely manner.

The DPM data over time or TWA DPM data obtained from the updated Ventsim model using the hybrid methodology from this research can be used in the VCM for schedule optimization in SOT.

1.3 Problem statement

DPM, generated from diesel engines, is the primary concern for ventilation systems of underground M/NM mines. As long as diesel equipment is deployed in a mine, DPM will continue being the focus of the mine ventilation system. Mining engineers usually design the ventilation system based on regulation and experience. Most of the time, fresh air is over-provided to ensure the safety and health of personnel working underground. Therefore, optimization of the ventilation system is necessary from an economic point of view. Using monitoring (such as real-time DPM monitors) and modeling (for instance, CFD) techniques, some research has been conducted on how to efficiently dilute the DPM in underground M/NM mines. However, due to the fact that field tests are hard to be conducted in an underground operation because of its busy production schedule, the modeling techniques are rarely validated to the field test data. In addition, typically there are not a sufficient number of DPM monitors available at a mine site to conduct accurate and

comprehensive DPM measurements. Even with enough monitors, they need to be placed in the targeted area to collect DPM data over time so that data on how the DPM distributes over time can be obtained. This process is time-consuming and costly. Most importantly, the DPM data collected from one field test will not generally be applicable to various conditions, such as the different geometry of headings, working paths and cycle times of diesel equipment, types of diesel engines, air volume from upstream, and auxiliary fan speeds. Therefore, accurate modeling techniques are required to investigate the DPM over time under various conditions. The modeling technique is not only cheaper but also more versatile compared with the field tests.

Conventional DPM modeling techniques using CFD are time-consuming and generally require the use of high-performance computers to conduct a short-period-of-time (i.e., less than 300 seconds) DPM simulation. It is not practical to model DPM with CFD over an extended period of time (i.e., more than an hour). Other than CFD, network solvers can perform DPM simulation, but they are simplified and cannot show 3D DPM concentration contours. Therefore, neither of the existing modeling techniques is quick and easy to model the distribution of airflow and DPM over time. For large and complex ventilation systems, it will be even harder to apply these techniques.

There are several commercial software packages available for making mine schedules by establishing precedence links between mining activities. However, the schedules outputted by the software are not optimized in terms of NPV. Before VCM was released, mine ventilation planning and production scheduling were conducted independently, and a manual process was needed to align the two. The ventilation constraints were not directly considered simultaneously with other constraints such as development rate and mine equipment availability when optimizing mine production schedules. Now with SOT and VCM, it is possible to consider ventilation and

production schedule optimizations at the same time but the challenge for the user is to ensure that the airflow and DPM data entered into Ventsim is accurate. If inaccurate diesel emission rates are entered into Ventsim, the DPM modeling results will be inaccurate. Ventsim, as a 1D solver, takes area-average DPM data as input. Because the number of real-time DPM monitors at mine sites is usually limited, it is hard to get area-average DPM data at different locations with multiple real-time DPM monitors installed at each cross-sectional area of the locations. Hence, a correction factor is needed to convert the point DPM data (recorded by a real-time DPM monitor) to area-average DPM data before entered into Ventsim. The correction factor may vary under different flow situations. A hybrid methodology, which is an enhanced and complementary tool, is proposed to provide improved diesel input to Ventsim.

This thesis is driven by the above problems and aims at providing solutions to these problems.

1.4 Research questions

The following four questions motivated this thesis research:

1) Why is there a gap between mine ventilation and mine planning?
2) Is there any methodology for mine planning while accounting for ventilation constraints?
3) Is there a CFD approach for simulating DPM over an extended period of time in underground mines?
4) What are the advantages of using an integrated 1D-3D model with a hybrid methodology instead of either CFD or network modeling alone for diluting the DPM in multiple dead-end headings?

1.5 Research objectives

The objectives of this research are as follows:

a) Establish a hybrid methodology.
    - Develop a CFD approach for DPM simulation over an extended period (one hour).
    - Investigate the main parameters affecting the DPM concentration in a heading.
    - Define a workflow to use CFD results to update the ventilation solver results.
    - Define the limitations of the new methodology.

b) Provide a consistent estimation of DPM concentration trend or TWA DPM data.

1.6 Research hypothesis

The hypothesis in this research is summarized as follows.

A hybrid methodology can be established to take advantages of both network modeling and CFD modeling.

The accuracy of the updated Ventsim model will be close to that of the CFD model. With the same geometry, the computational time of the hybrid model will be the sum of that of the CFD model and the network model. For a mine-scale ventilation system modeling, the computing time of the hybrid model (with CFD modeling applied to the dead-end headings and network modeling applied to the rest) will be between that of the CFD model and the network model.

A validated hybrid methodology will be able to better predict DPM in the following areas:

a) There is a truck, a load-haul-dump (LHD) machine, a bolter, or a drill jumbo moving.

b) Ventilation is not sufficient and efficient.

c) Downstream of production area

d) Low air volume areas

1.7 Research approaches

The entire mine ventilation system will be modeled in Ventsim, and CFD will be applied in the areas where Ventsim cannot be applied easily. The boundary conditions of the CFD model will be configured through the output results from the Ventsim model at the same inlets existing in both models. The results from the CFD model at the outlets existing in both models will be used to update those from the Ventsim model. Then the updated Ventsim results are carried over to the downstream of the ventilation network in Ventsim.

A new CFD approach for modeling DPM over an extended period can be proposed to quickly and accurately obtain the results with ANSYS Fluent. This approach is necessary because diesel equipment (e.g., a mine truck) usually stays and works in a working face for more than one hour, which is an extended period of time, which can take days to model using existing CFD approaches.

A DPM modeling technique using Ventsim is proposed to show how the DPM simulation is handled and to facilitate the integration with CFD.

Real-world DPM data will be collected and compared with the CFD model and the updated Ventsim model. Due to the low quality airflow and DPM data collected from the field, this study should be viewed as a qualitative study rather than a quantitative study.

1.8 Thesis summary

This chapter presents a brief introduction to the purpose of this research. Section 1.1 shows the background of this research. Motivation, problem statement, research questions, and research objectives are presented in Sections 1.2, 1.3, 1.4, and 1.5, respectively. The hypothesis made in this research is shown in Section 1.6. Research approaches taken are shown in Section 1.7.

Chapter 2 provides a comprehensive literature review on ventilation network solvers and their applications in the mining industry, CFD and its applications in the mining industry, hybrid models used in mining and other industries, ventilation network basics, equations and theories of underground mine ventilation, ventilation optimization techniques, mine production schedule optimization and common algorithms, integration of mine ventilation and production schedule optimizations, mine ventilation concerns and control strategies, methods for qualifying DPM, and DPM modeling using CFD.

Chapter 3 shows two approaches, which are a CFD modeling approach and a ventilation network modeling approach, to model DPM concentrations over an extended period in underground mines. This CFD approach is validated through result comparisons with the experimental data collected in an underground mine in the U.S. Similar DPM modeling is also conducted in a ventilation network solver. To the best knowledge of the author, this is also the first time that DPM in underground mines is modeled over an extended period in a ventilation solver.

Chapter 4 provides a hybrid methodology for investigating DPM concentration distribution in an underground mine. The idea of the hybrid methodology itself is not new in mine ventilation but the approach used in this research to achieve a successful and practically available hybrid

methodology for DPM modeling over an extended period of time is unique and novel. Details of the workflow for the hybrid methodology and how the CFD results are transferred to the ventilation network model are shown in this chapter as well. It is found that the workflow is feasible and the data transfer is well handled. Another idea of using structured cycle time of diesel equipment to predict DPM data over time is presented in this chapter as well. The benefits and practical applications of the hybrid methodology are also shown in this chapter.

Chapter 5 summarizes the main findings of this research and provides recommendations for future work as a continuation of this research. Suggestions on how the hybrid methodology can be practically applied in the mining industry are provided as well.

Chapter 2

2 Literature Review

Several key aspects related to the thesis such as mine ventilation, production schedule optimization, methods for quantifying DPM and control strategies, network modeling and CFD modeling of mine ventilation are reviewed in this chapter.

2.1 Ventilation network solvers and applications in the mining industry

Ventsim (Chasm Consulting, 2016) is a ventilation network software that has been used globally for many years (Walker, 2013). It is a 3D ventilation network software. Ventsim can not only conduct steady-state and dynamic airflow simulations but also computes airflow quantity, pressure, resistance, and other related properties (Şuvar *et al.*, 2012). The airflow calculations are implemented through the Hardy Cross method (Cross, 1936). Additionally, with a proper setup, Ventsim is capable of performing DPM simulation (Gorain and Pandey, 2015), multi-gas simulation, radon simulation, real-time airflow simulation (Gillies *et al.*, 2004), fire simulation (Stewart *et al.*, 2015), and financial optimization (Widzyk-Capehart and Watson, 2001).

VNet (Mine Ventilation Services, 2016) is another 3D ventilation network software which is adapted from a prior version of VnetPC (Mine Ventilation Services, 2016). Compared with VnetPC, VNet is more advanced in 3D graphics and user interface. Similar to Ventsim, VNet uses the Hardy Cross method and it can provide airflow and contaminant properties for ventilation planning as stated in Duckworth *et al.* (1995). VNet has been used for ventilation optimization

(Álvarez *et al.*, 2011), and it is capable of real-time airflow simulation (Ruckman and Prosser, 2010).

Similar to Ventsim and VNet, VUMA (Bluhm *et al.*, 2001) is a 3D ventilation network solver that also uses the Hardy Cross method. It can conduct airflow, heat, dust, radon, DPM, and several other simulations with various types of contaminants (VUMA Software ADCO (Pty) Ltd). Its interface is user-friendly, and it has been applied to ventilation planning and optimization (Bluhm *et al.*, 2014).

3D-CANVENT (Hardcastle, 1995) is also a 3D ventilation network solver based on the Hardy Cross method. What makes 3D-CANVENT special is that it has a sensitivity module incorporated, which can quickly solve the ventilation network for a user-defined change of the airflow parameters such as pressure, resistance, and fan speed. The solver can be used for ventilation system optimization with significant energy savings (Li *et al.*, 2011).

However, the airflow results from network solvers are often found inaccurate (Xu *et al.*, 2017) because of the erratic airway resistance input in the network solvers. In addition, due to the 1D network solvers, only area-average input is acceptable and detailed flow distribution across a cross-sectional area cannot be displayed and analyzed. The advantage of the network solver is its negligible computing time and strong adaptability with other software packages, which creates potential integration opportunities.

2.2 CFD and its applications in the mining industry

CFD is a computer-based numerical method for solving fluid flow problems under different boundary situations. Unlike the ventilation network modeling software discussed in the previous

section, CFD solves fluid dynamics equations such as mass conservation equation, momentum conservation equation, and energy equation to obtain flow properties (ANSYS Inc., 2009a). The equations are listed below.

Equation for mass conservation:

$$\frac{\partial \rho}{\partial t} + \nabla \cdot (\rho \vec{v}) = S_m \tag{2-1}$$

where ρ is density (kg/m^3), $\vec{v}$ is velocity vector, t represents time, S_m is the additional mass added to the system from the user-defined sources or the dispersed second phase, and ∇ refers to the partial derivative of a quantity in the Cartesian coordinate system, which is defined as

$$\frac{\partial}{\partial x}\vec{i} + \frac{\partial}{\partial y}\vec{j} + \frac{\partial}{\partial z}\vec{k} \tag{2-2}$$

Equation for momentum conservation:

$$\frac{\partial}{\partial t}(\rho \vec{v}) + \nabla \cdot (\rho \vec{v}\vec{v}) = -\nabla p + \nabla \cdot (\bar{\bar{\tau}}) + \rho \vec{g} + \vec{F} \tag{2-3}$$

where p is the static pressure, $\rho \vec{g}$ represents gravitational body force, $\vec{F}$ is the external body force, and $\bar{\bar{\tau}}$ is the stress tensor.

Equation for energy conservation:

$$\frac{\partial}{\partial t}(\rho E) + \nabla \cdot \left(\vec{v}(\rho E + p)\right) = \nabla \cdot \left(k_{eff} \nabla T - \sum_j h_j \vec{J_j} + (\bar{\bar{\tau}}_{eff} \cdot \vec{v}) \right) + S_h \tag{2-4}$$

where E represents energy, the three partial derivatives on the right-hand side of the equation represent energy transfer caused by conduction, species diffusion, and viscous dissipation, respectively. k_{eff} is the effective conductivity and $\vec{J_j}$ is the diffusion flux of species j. S_h represents the heat of chemical reaction and any other volumetric user-defined heat sources.

E in Eq. (2-4) is expressed as:

$$E = h - \frac{p}{\rho} + \frac{v^2}{2} \tag{2-5}$$

where sensible enthalpy h is defined for ideal gases as

$$h = \sum_j Y_j h_j \tag{2-6}$$

and for incompressible flows as

$$h = \sum_j Y_j h_j + \frac{p}{\rho} \tag{2-7}$$

In Eqs. (2-6) and (2-7), Y_j represents the mass fraction of species j, and

$$h_j = \int_{T_{ref}}^{T} C_{p,j} dT \tag{2-8}$$

where T_{ref} (reference temperature) is 298.15 K, C_p is the specific heat of fluid, and K stands for kelvin, the temperature unit.

Using the governing equations, CFD modeling is able to perform both steady-state and transient flow simulations. There are several widely-used, commercially available software packages on the market such as ANSYS Fluent, ANSYS CFX, Cradle, and OpenFOAM. ANSYS Fluent, which is a finite-volume-based solver, is considered a reliable and popular among the available packages. It can solve complex flow problems such as chemical reactions and heat transfers (ANSYS Inc., 2009a). In addition, CFD modeling has been applied to mining for airflow simulation (Ren and Balusu, 2010), DPM simulation (Zheng *et al.*, 2015), dust simulation (Ren and Wang, 2013), gob inertization (Balusu *et al.*, 2002), methane simulation (Toraño *et al.*, 2009), spontaneous combustion simulation (Yuan and Smith, 2009), and fire simulation (Edwards and Hwang, 1999, 2006), amongst others.

Although CFD modeling is powerful for obtaining detailed and accurate fluid properties, it requires computational power and takes a long time to calculate the results, especially when the computational domain is complex and extensive.

2.3 Hybrid models used in mining and other industries

Because neither the network solver nor the CFD solver can perform airflow simulations efficiently and at the same time accurately, the idea of the hybrid model has been raised.

Regarding hybrid model applications in the mining industry, Rueda (2017) built a co-simulation technology to study the contaminated gas concentration (mainly carbon monoxide) after a blast in an underground mine in Colombia. A Ventsim model for the mine and a CFD model for a stope were established. Results from the inlets in the Ventsim model were used as the input for the inlets in the CFD model. The results from the outlets in the CFD model were used to update the input of

the inlets in the Ventsim model by means of adding resistance. The process was repeated several times and stopped when the results from the two models matched, and the resistance was determined. This hybrid approach did not change the setup of the Ventsim model and added resistance to the inlet of the Ventsim model for calibration. However, it will take much longer if more than one area of interest needs to be calibrated at the same time due to the iterative process. In addition, the paper does not report any experiment was conducted to validate the accuracy of this method.

A multi-scale ventilation model (Wedding, 2014) was presented to model methane concentration distribution in a longwall gob area, which was a void zone filled with broken, falling rocks in an underground coal mine. A 3D CFD model was coupled with a 1D network model. Methane and airflow distribution in the gob area were modeled in the CFD model while airflow and methane in the entries and crosscuts surrounding the gob area were modeled in the network model. The finite-difference based 1D network model was developed in Matlab. The initial boundary conditions for the CFD model were read from the network model. Based on the CFD results, the boundary conditions for the network model were updated. The hybrid model was validated through a comparison with a calibrated ventilation model, and a good agreement of the results was obtained. One drawback of the hybrid model was that flow recirculation appeared when the number of coupling regions between the CFD model and the network model was increased. Extra time and effort are needed to ensure the coupling function works well and the boundaries are correctly formed. Because the network model was coded in Matlab and has not yet been commercialized, it is difficult to apply it in the mining industry, especially with competition from other widely-used and commercially available ventilation network solvers.

While the hybrid model is new in the mining industry, it is not new as discussed in the next paragraphs.

A 1D-3D coupled model (Prince, 2015) was proposed to simulate a subway tunnel ventilation network. An industry standard 1D network model and a 3D CFD model were combined, parts of the network being modeled in the CFD model were treated as pressure losses in the network model. The results were in agreement with the experimental data. In addition, the computational cost was much lower compared with a full 3D CFD model for the same ventilation network.

Diesel injection was successfully simulated in a co-simulation approach, which combined the 1D System AMESim and the 3D CFD EOLE software (Marcer *et al.*, 2010). The AMESim is a 1D system software used to describe the physical phenomena with few macroscopic parameters. The AMESim model consisting of tabulated models was used to simulate 1D flow in the complete injector. Flow near the injector nozzle was simulated by the 3D CFD EOLE model. Results from the hybrid model matched the experimental data well and this showed the hybrid model could potentially be applied in an industrial context.

A hybrid 1D-3D model was built to simulate the electrically active neurons and their calcium dynamics (Grein *et al.*, 2014). uG is a 3D simulation framework using the finite volume or the finite element method for discretization while NEURON is a 1D simulator for electrical signaling in neurons. In the hybrid model, the NEURON simulator was used as the 1D component, and the uG simulator was used as the 3D component. It was concluded that the hybrid model made it possible to simulate larger networks with detailed information on a fine scale.

A hybrid 1D-3D model, based on the Complex Automata and the Multiscale Modeling Language, was conducted to build an irrigation canal (Belgacem *et al.*, 2012). Water height and flow distribution were simulated. The research concluded that compared with the traditional methods the hybrid model could be efficient in more complex systems.

A combination of a 1D Environment Control System (ECS) model and a two-dimensional (2D) CFD model was established to simulate a smoke accident in an aircraft cabin (Chen *et al.*, 2015). The results from the simulation were accurate and proved that the accident could be simulated efficiently. The authors also suggested that a 1D-3D model should be built in the future for complex situations.

To summarize, the benefits of hybrid models include high efficiency, high accuracy, and strong adaptability to complex and extensive geometries. The hybrid model approach has been successfully applied in various industries including the mining industry. However, little is known about DPM simulation with the use of a hybrid approach.

2.4 Ventilation network basics

Every underground mine ventilation system consists of at least one fresh air intake, one contaminated/used air return, and various ventilation ducts/tunnels. Fans such as main fans, booster fans, and auxiliary fans are used underground (although booster fans are not allowed in coal mines in the U.S. (Gillies *et al.*, 2010)) to force the fresh air flow from surface to below the ground. Stoppings, seals, bulkheads, regulators, ventilation doors, airlocks, brattice curtains, and other devices are used underground to direct the airflow to working faces and improve the ventilation efficiency of the system.

In general, there are three ventilation systems, which are the exhausting system, blowing system, and push-pull system. The main fan locations differ from each other for the three systems as shown in Fig. 2-1.

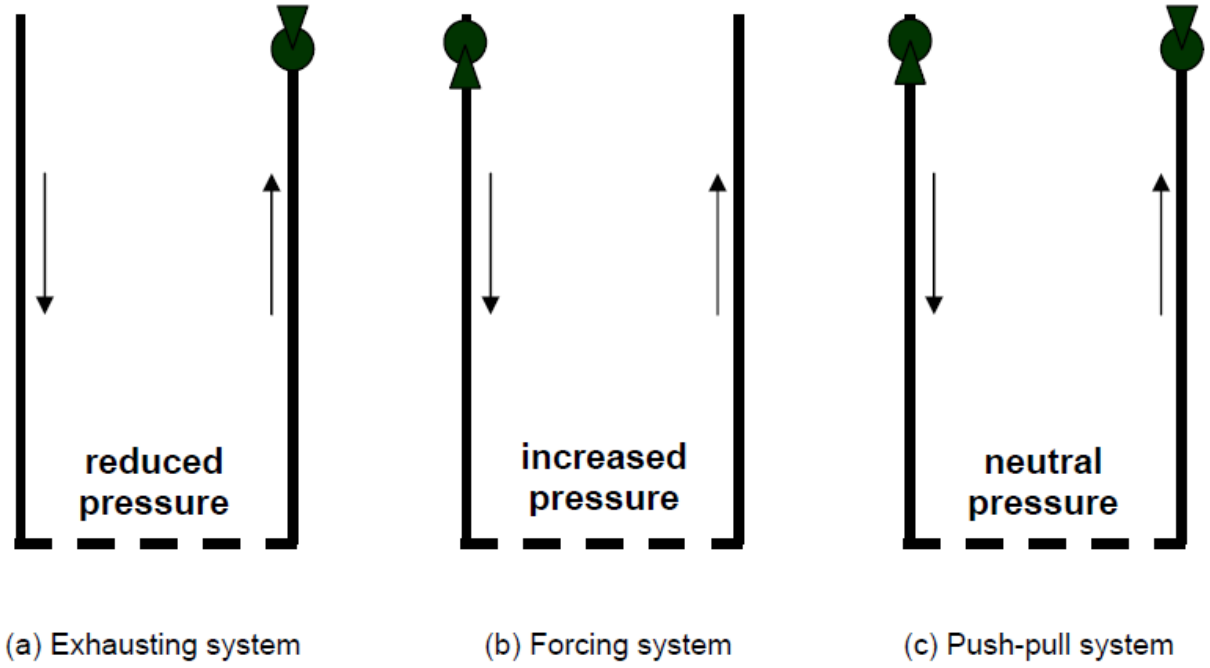

Fig. 2-1. Common underground ventilation systems and main fan locations on the surface (McPherson, 2009).

Due to inconsistent opening sizes, curved airways, and the difference in elevation, fresh air is resisted on its way to the return. In other words, the resistance of the mine prevents the fresh air flowing through the tunnels/ducts. The mine resistance is similar to the resistance of electric circuits. According to how the ducts/airways are connected, the mine resistance is calculated either in series or in parallel.

When the airways are in series, the mine resistance is calculated using Eq. (2-9)

$$R_{mine} = \sum_{i=1}^{n} R_i \tag{2-9}$$

where R_{mine} is the total resistance of airways in series, and R_i is the resistance of a single airway.

When the airways are in parallel, the mine resistance is calculated using Eq. (2-10)

$$\frac{1}{\sqrt{R_{mine}}} = \sum_{i=1}^{n} \frac{1}{\sqrt{R_i}} \tag{2-10}$$

where R_{mine} is the total resistance of airways in parallel.

The mine ventilation systems are categorized into two groups according to the mine layouts. One is U-tube, and the other one is through-flow. For the U-tube ventilation system, airflow is separated from the intakes in the return airways as illustrated in Fig. 2-2. The through-flow ventilation system is shown in Fig. 2-3, where intakes and returns are separated far from each other.

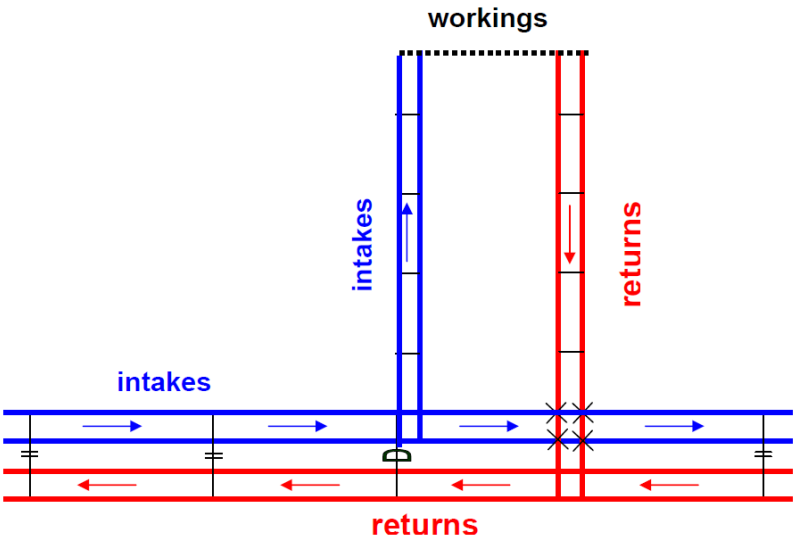

Fig. 2-2. U-tube ventilation (McPherson, 2009).

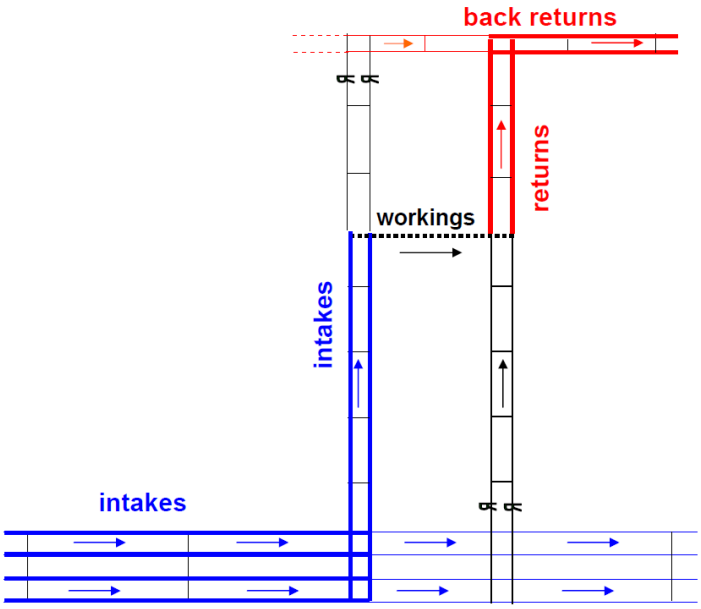

Fig. 2-3. Through-flow ventilation (McPherson, 2009).

In metal mines, through-flow ventilation systems are popular because the deposits are all on different levels as shown in Fig. 2-4.

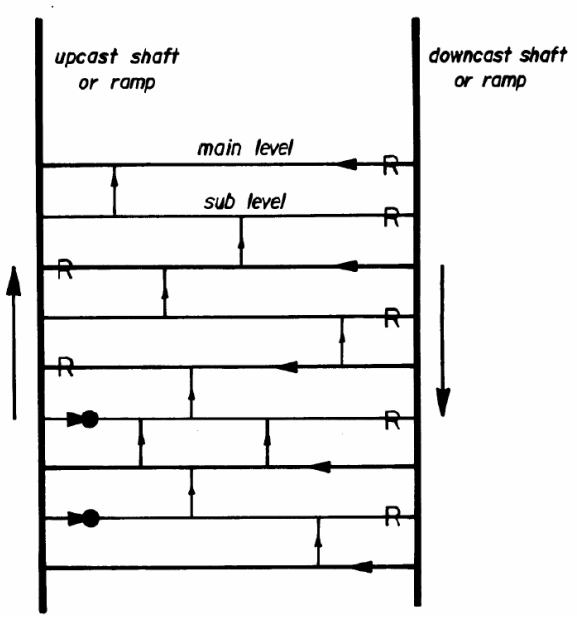

Fig. 2-4. A sectional view of a through-flow system in a metal mine (McPherson, 2009).

In addition to the main ventilation system, auxiliary ventilation is employed to ventilate a development heading or a working face. Auxiliary ventilation refers to the ventilation system using line brattices, duct system, fan, or ductless system (jet fans).

Similar to the main ventilation system, the auxiliary system also has three common systems. Blowing system, which uses soft ventilation ducts, is prevalent due to lower capital cost and easier maintenance compared with an exhausting system using hardlines. However, in some circumstances, neither the blowing nor the exhausting systems work well independently. Therefore, the combination of the two systems, which is called an overlap system (shown in Fig. 2-5), is often applied.

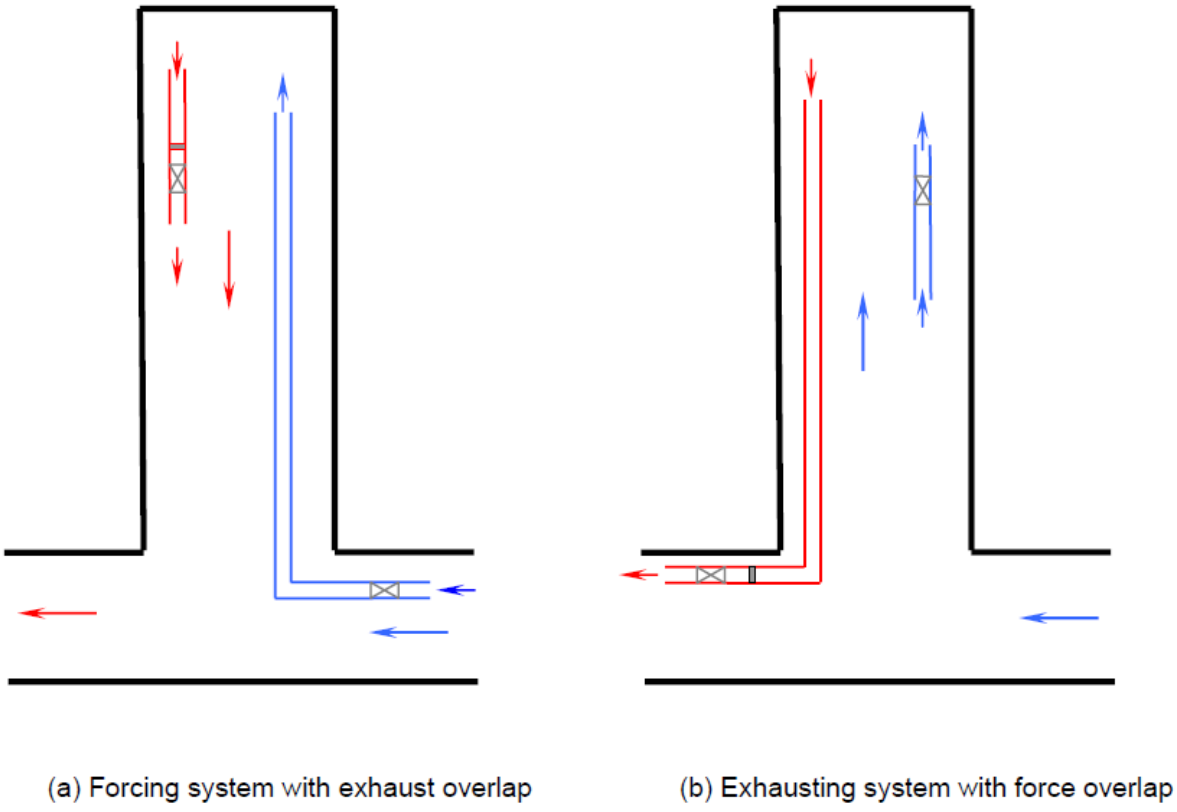

Fig. 2-5. Overlap systems of auxiliary systems (McPherson, 2009).

2.5 Equations and theories of underground mine ventilation

The equations and theories used in the underground mine ventilation system have already been well organized in McPherson's book (2009). Important equations and theories used in this thesis are summarized below.

2.5.1 The Atkinson equation and the square law

Friction and shock resistance make up the total resistance of an airway. The equations associated with the resistances are respectively provided as follows.

Atkinson Equation (Atkinson, 1854):

$$P = kL\frac{per}{A}u^2 \tag{2-11}$$

where

$$k = \frac{f\rho}{2} \tag{2-12}$$

P is the frictional pressure difference (Pa) across a given airway, *k* is the Atkinson friction factor, ρ is air density (kg/m^3), *f* is coefficient of friction (dimensionless), *per* is the perimeter of the airway, *L* is the airway length (m), *A* is the airway area (m^2), and *u* is airflow velocity (m/s).

The Atkinson resistance (Ns^2/m^8) of an airway is defined as

$$R = kL\frac{per}{A^3} \tag{2-13}$$

Because

$$Q = uA \tag{2-14}$$

where Q is the airflow quantity (m^3/s), Eq. (2-11) becomes

$$P = RQ^2 \tag{2-15}$$

Eq. (2-15) is the well-known Square Law.

Other than frictional loss, shock loss occurs when the airflow direction changes or the size of the airway changes. Eq. (2-16) is the shock loss equation.

$$P_{shock} = X\rho\frac{u^2}{2} = R_{shock}Q^2 \tag{2-16}$$

Similar to frictional loss, shock loss has a shock loss factor X (dimensionless), which is calculated using Eq. (2-16).

Based on Eqs. (2-14) and (2-16), we have

$$R_{shock} = \frac{X\rho}{2A^2} \tag{2-17}$$

where R_{shock} is shock resistance.

To calculate the total resistance, a new concept called “equivalent length” is introduced by McPherson (2009) to convert the shock resistance to equivalent frictional resistance. The equation for total resistance is

$$R_{total} = k(L+L_{eq})\frac{per}{A^3}\frac{\rho}{1.2} \tag{2-18}$$

where, L_{eq} is the equivalent length, and the shock resistance is

$$R_{shock} = kL_{eq}\frac{per}{A^3}\frac{\rho}{1.2} \tag{2-19}$$

According to Eqs. (2-17) and (2-19), we have

$$L_{eq} = \frac{1.2X}{2k}\frac{A}{per} \tag{2-20}$$

Based on the total resistance (Eq. (2-18)) and the Square Law (Eq. (2-15)), the total pressure drop needed to force a certain amount of fresh air to flow in the subsurface can be estimated. The power required for ventilation can be calculated by using the following equation.

$$Power = PQ \tag{2-21}$$

where P is the total pressure drop.

At last, ventilation engineers can come up with a reasonable ventilation plan with both operational cost and capital cost according to the power and airflow quantity required underground.

2.5.2 Kirchhoff's Laws

Kirchhoff's Laws are essential to analyze a ventilation network. Kirchhoff's first law is a mass conservation law, which is expressed by the following equation.

$$\sum_j M = 0 \tag{2-22}$$

where j represents a junction where all the mass flows join, and M is the mass flow rate (kg/s).

M can be calculated using the equation below.

$$M = Q\rho \tag{2-23}$$

where *Q* is volumetric flow rate (m^3/s) and ρ is air density (kg/m^3).

Because air density is assumed consistent underground,

$$\sum_j Q = 0 \tag{2-24}$$

Kirchhoff's second law is a pressure drop conservation law, which is expressed by the following equation.

$$\sum (P\text{-}P_f)\text{-}NPV = 0 \tag{2-25}$$

where *P* is frictional pressure drop, P_f is the pressure increase through a fan, and *NPV* represents natural ventilating pressure.

Based on the Kirchhoff's laws, two standard approaches, which are the analytical methods and numerical methods, can be used to analyze a ventilation network. The analytical methods use the Kirchhoff's laws and formulate equations which can be manually solved, and an exact solution can be obtained. The numerical methods use computers to solve the equations with a predefined accuracy by iterative approximation.

When a network is not complex, namely, there are less than two circuits in the network, it is not computationally expensive to manually solve the network. However, when a network is complex,

the numerical methods are more preferred. The Hardy Cross technique is an accepted numerical method for analyzing ventilation networks.

2.5.3 Hardy Cross technique

In general, ventilation network analysis is about correctly distributing airflow. With the Hardy Cross method, an airflow, Q_a, is assumed to represent the true airflow, Q, of a branch in a circuit. The relationship between Q_a and Q is shown in the following equation:

$$Q = Q_a + \Delta Q \tag{2-26}$$

where ΔQ is the difference between Q and Q_a.

Therefore, finding the value of ΔQ becomes the problem. After some mathematical manipulations, ΔQ can be represented as

$$\Delta Q = \frac{-\sum (RQ_a|Q_a| - P_f - NVP)}{\sum (2R|Q_a| + S_f)} \tag{2-27}$$

where S_f is the slope of the fan curves.

ΔQ can be iteratively solved and the value of ΔQ will fall close to zero as a result. With a given accuracy, Q of each branch in the ventilation network can be solved.

2.6 The gap between mine ventilation and mine production schedule optimization

Mine ventilation, as a significant and expensive component of an underground mining operation, has been investigated for optimization with algorithms (e.g., genetic algorithm) and technologies

(e.g., ventilation on demand). Mine production scheduling, which is another important component of a mining operation, has also been advanced for optimization by using various algorithms such as genetic algorithm. However, little research has been conducted to show the gap between mine ventilation optimization and mine production scheduling optimization.

2.6.1 Ventilation optimization

Hardcastle *et al.* (1999) reorganized the ventilation system at the Nanisivik mine and showed how air usage could be optimized. The ventilation concerns at the mine included insufficient total air volume (e.g., intake air being split into four flows), inadequate blast clearance (e.g., low air velocity and long re-entry times), "dead-zones" (e.g., drifts between the ventilation raises' discharges had low airflows because of booster fans being used in the raises), a compressor room in the fresh air route (i.e., potential fire hazard to the whole mine), seasonal variations of natural ventilation (i.e., air density changes due to seasonal temperature variations could reduce the air volume delivered to the lower ore zone), wind effects (e.g., the winds going into the portals could add resistance to the exhausting air), double handling of the air by fans (e.g., redundant booster fans were used to bring air to the lower zones), uncontrolled recirculation (i.e., air could recirculate between the lower ore zone and the main ore zone as a result of using the unnecessary booster fans), electrical power generation (i.e., the electricity was generated by the mine and limited), and thawing of strata (e.g., ice could form and build up on the floor). With a ventilation survey and a system simulation using a network simulator, a full redesign of the system was conducted. The measures taken to improve the condition were splitting the fresh air with two flows other than four by relocating the primary fans, sealing the unnecessary ventilation raises, and installing a regulator to control the fresh air entering into the compressor room. All the concerns were adequately

resolved after taking the measures. Consequently, a 45% reduction in fan motor size was achieved, which resulted in a power demand reduction. Furthermore, the updated ventilation system required less infrastructure (i.e., fans) and it was operated more efficiently.

Greberg and Sundqvist (2011) presented a case study on the Cadia East underground project in Australia to demonstrate the importance of simulation in mine planning and optimization. SimMine™ was used as the simulation software. The results of the study showed that simulation was able to assign resources optimally and visually validate development plans. The study offered some insights into using simulation for scheduling optimization. Kok (2014) provided some suggestions on ventilation designs in the feasibility study stage. Examples of fan locations, diesel emissions, heat, production requirements, and emergency plans were discussed. Some rules of thumbs, which are useful guidelines when establishing the ventilation design, were mentioned in the study. For example, 60% of diesel engine efficiency dissipated as heat and gas. Another rule of thumb is that 10 to 25% of total airflow contributes to leakage.

Sarac and Sensogut (2000) wrote a computer program combining the Hardy Cross method and the Steepest Descent method to solve ventilation network problems. The reason for writing the program was that convergence characteristics were uncertain for the Hardy Cross method. Based on the authors' experience, the solution time for their program would be at most half of that for the Hardy Cross method. Acuña and Lowndes (2014) reviewed not only the standard ventilation solvers in various countries but also recent ventilation optimization studies involving different techniques. The authors indicated that variants to be solved in a ventilation optimization problem could be classified into three groups, which were free-flow splitting, controlled flow splitting, and semi-controlled flow splitting.

Variable frequency drives (VFDs) and ventilation on demand (VOD)

Webber-Youngman (2005) demonstrated the importance of applying variable speed drive (VSD) fans for optimizing ventilation cost in mines with high temperatures. Active monitoring should be available to support and control the VSDs. He also indicated the relationship between air supplied and refrigeration requirements. Investigations were carried out at Target Mine in South Africa to confirm the possibility of performing real-time simulation in deep mines. According to the investigation results, variable inlet vanes (VIVs) could be used to change air velocities and potentially save energy. In addition, he suggested that VSDs for water pumps should be applied to control water flow rates to save energy.

The development of the VOD technology can be traced back to the 1990s. The idea of implementing VOD in underground mines was first brought up by Hardcastle *et al.* (1998). The main drivers for deploying VOD are reducing greenhouse gas emissions, decreasing ventilation-related energy cost, and foreseen more stringent diesel emissions regulations. It was found that the electricity generated by using fuels contributed to the increase in greenhouse gas emissions. The energy demand needs to be reduced to achieve lower greenhouse gas emissions. Further to this, air volume provided to an underground mine and air power have a cubic relationship, which is air power (kW) is proportional to the cubic of air volume (in m^3/s). Hence, a small increase in flow can increase the air power cost dramatically.

According to Hardcastle *et al.* (1998), it was common practice that ventilation was over provided to Canadian mines without incorporating proper management and optimization. For instance, auxiliary fans were often left running at the maximum speed continuously regardless of the demand for the mining activities. Hence, better ventilation management was necessary. A

management system, namely, VOD, was proposed and it contains remote control capacities on ventilation devices (e.g., fans, ventilation doors, and regulators), monitoring capacities on contaminants and status of the devices, vehicle tracking capacities, and ventilation network solving capacities with the use of a ventilation simulator. The operator of such a system could adjust the ventilation demand accordingly, which results in an optimized ventilation system with considerable energy savings.

The VOD concept was further evaluated at Barrick Gold's Bousquet Mine by Hardcastle *et al.* (1999). With the expansion of the mine, the conventional ventilation management system would not be able to fulfill the increasing airflow demand due to the increasing number of active headings and the size of the diesel engines. The VOD concept was accepted by the mine and it was found that the mine could continue operating without introducing additional air volumes into it. The VOD system was tested on a sublevel of the mine. Changes made to the existing ventilation system included using automated ventilation door with remote control abilities to replace the standard wooden regulator, installations of flow and gas sensors at strategic locations in the sublevel, fitting remote starters on the auxiliary fans, and installation of vehicle identification and detection system at the entrance. The vehicle identification mode and vehicle detection mode were the only two modes operated by the VOD system in the sublevel. A backfill truck and an LHD could be distinguished for turning on/off the auxiliary fans in the vehicle identification mode. In the vehicle detection mode, the active number of vehicles entering the sublevel was counted for adjusting the opening of the regulator. For air, gas, and diesel emissions monitoring, two types of methods were used for validation purposes. For instance, measurements taken by the airflow meters were confirmed with tracer gas injections. According to the gas monitoring results, the exhaust location in the sublevel had the potential to measure the air quality for ventilation management purposes.

However, whether the VOD system should be an air quantity or quantity based system remained unknown with the volumetric regulation (e.g., the airflow must be more than 0.06 m^3/s per kW power of the diesel equipment regardless of exhaust air quality (Government of Ontario, 1990)). The study showed the mine could easily adapt to an air quantity based system by equipping with advanced technologies and hardware such as automated regulators, automated auxiliary fans, vehicle detection and identification technologies, and accurate flow monitors.

Hardcastle and Kocsis (2004) described the ventilation challenges in deep mines and mentioned the importance of VOD for optimal efficiency. The four main components of the VOD system are decision logic (i.e., mine-wide and local vehicle tracking and identification systems), control devices (i.e., automated controls on the fans, doors, and regulators), compliance monitors (e.g., airflow and gas sensors), and communication/management infrastructure. Providing a safe and healthy working environment, maximizing the use of air, and lowering the power usage as well as the green gas emissions were the drivers for implementing VOD. VOD was a strategy suggested being used throughout the mine at depth with both heat and diesel concerns. When the heat became the dominant factor in deep mines, the integration of VOD and automation should be considered.

VOD could also facilitate a new ventilation design concept, which was a "life-cycle mine ventilation system", as introduced by Kocsis *et al.* (2004). The new ventilation design criterion was referred to as "life-cycle" airflow demand based on production rates and operating characteristics of a mine site. This approach could be treated as a "pay-as-you-go" approach, which meant the ventilation design would change with the mining conditions, compared with designing the ventilation system with the final requirements. According to Kocsis *et al.* (2004), auxiliary ventilation could consume about 50% of the total ventilation cost in an underground mine. VOD,

as one of the technologies mentioned by Kocsis *et al.* (2004), could be integrated into the new design criteria because of its capacity to control the auxiliary ventilation system. Further savings on production cost and power consumption with reductions on greenhouse gas emissions could be achieved using VOD with the new design criteria.

Baiden *et al.* (2005) introduced a process-simulation-based analysis technique for underground mine ventilation systems. The idea was basically VOD. As pointed out by those authors, the VOD system was not widely accepted by the industry due to the lack of a proper control system, deficient cost-benefit analysis, and considerable expense on retrofitting the existing infrastructure. It was noted that the minimum airflow was still required to ventilate a work area with no activities. A hypothetical mine with two production haulage levels, two production drilling levels, and two development levels were designed. The mining process, which referred to drill-blast-muck-condition, was simulated using AutoMod^{TM} (Norman and Farnsworth, 1993). The simulation has two parts: a mathematical model controlling the simulation environment and an animation showing real-time airflows and activities. Different schedules for activities were selected for the development and production levels. Results from the on-demand approach and the traditional approach, which continuously provided ventilation to all the areas, were compared. Compared with the traditional approach, the whole system ventilation savings using the on-demand approach ranged from 23% to 83% with different activities schedules (over a 5-day period) when combining the savings from both the production and development areas. It was concluded that the process simulations could help to justify the major capital investment and optimize the ventilation systems.

Hardcastle *et al.* (2007) stated that over-ventilating could exist in a mine with the best design. Due to leakages and system losses in the auxiliary ventilation system, the provided air volume could

be double of the required air volume. Redundancy of the design and operation of an auxiliary ventilation system includes selecting a fan and ventilation tubing based on the maximum requirement, designing the system for the maximum production/activity requirement, and ignoring the existence of mining activities with the continuous operation of the fans. A VOD study for a mechanized base metal mine was presented. The usage of the air generated by various auxiliary ventilation systems ranged from 7% to 31%. It was found that a less degree of redundancy could be found in a higher level of continuity of the operation. VOD could be used to distribute the air to where it was needed.

A VOD auxiliary fan project was undertaken in Creighton mine of Vale Canada Ltd by O'Connor (2008). Creighton mine, one of the world's deepest underground mines, has one of the highest energy cost resulted from the ventilation system requirements. VOD was used to reduce energy consumption from the auxiliary fans. A pilot VOD project was undertaken on two auxiliary fans on a sublevel of the mine. Variable frequency drive (VFD) starters were installed on both the auxiliary fans to supply air based on demand. Identification tags were used to identify both vehicles and personnel. Data such as equipment number and air volume requirements were programmed into the tags. Tag readers were installed at strategic locations to detect whether the equipment or personnel entered or left the active zone. The required volume from the fan was supplied through adjusting the fan speed. An airflow monitor was installed to ensure that the required air volume was achieved. Gas and temperature monitors were installed to ensure the acceptable environmental conditions were met. The relationship between the mining sequence and auxiliary ventilation system was provided in the study as well. The fan design and length of the tubing were determined based upon the development and production schedule. The durations (e.g., years), usage of equipment (e.g., 33% of 8 h for LHD mucking), and airflow requirements (e.g., 23.6 m^3/s for LHD

mucking) in the development and production phases were shown respectively. Over a ten-year period, the projected savings for a single auxiliary fan (112 kW) equipped with VFD was calculated to $168,648. It was mentioned that the success of the project depended on maintenance and ventilation personnel's commitment other than the operators.

Li *et al.* (2011) presented a new feature and the sensitivity analysis of the mine ventilation network solver 3D-CANVENT and explained how the sensitivity analysis could facilitate the mine-wide VOD system. The sensitivity analysis repeatedly solves the ventilation network for any given ventilation parameter changes. As a result, delays could be avoided when operators wanted to know the effects on the ventilation system due to any changes made by the VOD system. Three parameters, which could be changed using the sensitivity analysis, are airway resistance, fan pressure, and fan speed. The change rates (%) were determined by the user. The sensitivity analysis would generate a matrix of sensitivity factors (or air volume changes) for each parameter change. It was mentioned that the accuracy of the results from the sensitivity analysis relied on the number and magnitude of the changes in the three parameters. A case study was conducted and it was found that increasing the speed of one fan would be more efficient (e.g., less air power (kW)) than increasing the speed of another fan to achieve the airflow requirements with the use of the sensitivity analysis. In another case study, the speed of the exhaust fan could be reduced by 40% but still met both the local and mine-wide air volume requirements. Li *et al.* (2011) concluded that the sensitivity analysis could minimize the ventilation cost by providing the most cost-effective fan speed factors. The sensitivity analysis could promote the application of the mine-wide VOD system and be used for ventilation system design and short-term and long-term ventilation planning.

Allen and Tran (2011) explained how the VOD technique was applied in Coleman mine, Canada. VOD was utilized in the mine to decrease the ventilation cost and to expand the mine without introducing more vent raises, booster fans, etc. The three main parts of the VOD system were: input data system, control system, and controlled devices. The input data were collected through Real-Time Location System (RTLS), environmental monitoring, and system boundaries. The data were then analyzed through the control system, which was NRG1-ECO® used in the mine. According to the control strategies in the control system, devices such as fans, louvers, and doors, were either manually or automatically adjusted to meet the airflow standards. No new additional airflow was introduced to the mine during the VOD controlling process. Instead, airflow was reduced or redistributed according to the intensity of mining activities. According to the outcome from the VOD project implemented in the mine, the benefits were apparent, showing that the VOD system increased the airflow flexibility and generated a $153,000 annual saving in just one mine level.

Basu *et al.* (2013) explained an idea on mine ventilation optimization (MVO)-VOD integration to improve energy efficiency for mine ventilation systems. The authors indicated that fans, VFDs, and duct dimensions should be optimized through MVO. In addition, VOD was used to monitor and control equipment via smart management. The authors believed that the integration would improve the productivity and efficiency of a mine. However, the detailed process and methods were not discussed in the paper.

Janzen *et al.* (2013) conducted another study on the VOD system and demonstrated the importance of successful VOD placement. Air Monitoring Stations (AMS) were utilized to measure airflow properties and determine the airflow requirements in various areas. Data obtained from AMSs

were exported to programmable logic controllers (PLCs) and distributed control system (DCS) for controlling fans and regulators to meet the airflow requirements. Production was escalated due to energy savings and proper air management with the use of VOD. The authors suggested that modular designs should be used extensively in a VOD system for easy maintenance and production flexibility enhancement.

Dasys *et al.* (2014) presented a matrix of the technology and benefits with using VOD and a method to determine the effectiveness of VOD systems. The VOD systems installed in Coleman mine of Vale and Nickel Rim South mine of Glencore were assessed. There were issues with the sensors and their installation in the VOD systems. It was also found that the management structure might need to be changed to operate the VOD systems. It was very important that the locations of vehicles be monitored. With a huge upfront infrastructure cost, energy savings alone from using the VOD system could hardly generate an acceptable rate of investment regarding business development. However, VOD could also maximize production by redirecting the over-supplied air volume to mining areas where productive capacity was available. According to the case study conducted on a sublevel at Coleman mine, $19,000 of energy savings or an additional $250,000 of potential production could be achieved over a month with the VOD system. The effectiveness of VOD systems could be measured by energy utilization intensity and system efficiency. Parameters (e.g., ventilation supply hardware, mine design, scheduling, dispatching, ventilation control, engine type selection, ventilation modeling, and legislation) could be graded based on energy utilization intensity and system efficiency. A VOD system with high system efficiency and a low energy utilization intensity would be the ideal system to implement. Other than the traditional ventilation network solver and process simulator used in a VOD system, a software called VREX was used as a ventilation rules engine to develop control strategies on the ventilation system based

on the data collected from ventilation network solver and production model. Dasys *et al.* (2014) concluded that the VOD system was suggested to be oriented towards maximizing production and minimizing energy usage based on the availability of productive capacity.

Chatterjee *et al.* (2015) pointed out the importance of applying energy efficiency (EE) and load management (LM) to optimizing fan speeds in underground mines. The authors reviewed the VOD technique and indicated that the shortcoming of VOD was that the main fan was not adjusted to optimize the airflow usage in underground mines. The authors then conducted a study to optimize the main fan speed by applying both the EE and LM strategies. According to the results of the case study conducted, 2,540,035 kWh or $277,035 per year were saved.

Li (2019) introduced a dynamic ventilation-modeling package, VREX, to evaluate the energy savings from airflow changes in a VOD system. VREX is a ventilation rule engine (or a decision support tool), which can simulate the mining activities within an operation period and determine the airflow requirement over the period based on production. VREX uses the mine development/production data from the discrete event simulation (DES) in SimMine^{TM} and the airflow data from 3D-CANVENT to determine the ventilation system control strategies over time. SimMine^{TM} uses the control time interval (CTI) to generate production scenarios. In general, more than one solution could lead to the same airflow distribution in a VOD system. VREX could help to select better solutions by taking time into consideration. A case study of using VREX in a VOD system was conducted by Li (2019). Over a 31-day period, the airflow requirements for different production scenarios with different lengths of CTIs (e.g., 10 min, 30 min) were determined. It was found that the longer the CTI is, the higher the air demand is. The reason was that VREX found the mining activity with the highest airflow requirement in each CTI and used the air volume to

determine the air demand in the ventilation system. It was suggested that the CTI should be in the range of 10 to 30 min so that the air demand did not vary much and the VOD system could react to the movements of the vehicles. The results of the case study showed that the total energy consumption was reduced by 28% with using VREX in the VOD system. A higher energy saving, 34%, could be achieved by using the maximum airflow available in the system.

Genetic algorithm (GA)

Acuña *et al.* (2010) proposed an integrated GA–ventilation network solver approach for free splitting networks to support decision-making on primary mine ventilation system optimization. The free splitting networks refer to ventilation networks controlling only the pressure of fans to fulfill the airflow requirements at the lowest cost. They found that there was no integrated algorithm to minimize the energy consumption of the ventilation system and the proposed integrated approach was able to find feasible solutions for any ventilation system. The results from the integrated approach were compared to the manual results, and an up to 13% reduction in energy cost was achieved.

2.6.2 Mine production schedule optimization and common algorithms

Recently, mine production schedule optimization has been widely discussed recently due to the mining industry downturn. Common algorithms used for mine production schedule optimization are reviewed below.

Genetic algorithm

Denby and Schofield (1995) developed GO-SCHED, which is a software using GA to optimize mine production schedules. Net present value is used as fitness in the software. GO-SCHED uses "Penalty Functions" to handle constraints like fitness value. GO-SCHED is suitable for both short- and long-term scheduling. One disadvantage of the software is that the data type is unique, which is not easy to import data from and export data to other software packages. Yun *et al.* (2003) applied evolutionary algorithms to determine optimal ore grade, production scheduling, and to help select mining methods. Net present value is defined as fitness, which represents the quality of individuals. The algorithm is terminated when the iterations reach the pre-determined maximum number, or the variation of fitness does not change significantly. According to their findings, Yun *et al.* (2003) find that evolution algorithm is an efficient optimization approach to deal with complex problems. Lowndes and Yang (2004) utilized GA to optimize a ventilation network by determining the location, number, and duty of both main fans and booster fans. Two case studies were conducted to show the optimized results from GA. According to the results, the GA technique successfully minimized the ventilation cost by implementing the aforementioned details of the main fans and booster fans.

Maybee *et al.* (2010) presented a case study using the optimization software Schedule Optimization Tool (SOT) to generate high-NPV schedule alternatives and to help validate strategic decisions. SOT was used to generate high-NPV schedules with all the constraints met. Because SOT utilizes GA and there is no certificate of optimality possible for a large problem size, close-to-optimal schedules are produced instead of optimized schedules. In terms of the optimization process, schedules with all the constraints satisfied are carried out first. A "just-in-time" is then

performed to schedule the development activities at the correct time, which means development activities are scheduled as late as possible, but before stopes are ready. Heuristic guidance rules in SOT bias the initial scheduling process. Learning by means of a GA is then conducted to produce more profitable schedules. According to the results from the case study, a 20% NPV increase was achieved compared with that from the manually-made schedules.

Fava *et al.* (2011) presented another case study of applying SOT to a real mine. Three enhancements were made to SOT. Evaluation of schedules over various resource constraints was automated. User-defined ranking was made allowable. Application of primary and secondary stope sequencing rules was automated. The upgraded SOT was able to evaluate different scenarios and help mine planners make strategic decisions.

Another case study using SOT was performed by Fava *et al.* (2012). Results from three investigations on the case study showed that mine planners could reanalyze schedules and figure out dataset issues in a short time with the help of SOT. In addition, mine's NPV was increased by $54.3 million.

Fava *et al.* (2013) conducted a case study using SOT for Newmont's Leeville operation. To maximize NPV, SOT utilizes not only heuristics but also an evolutionary algorithm to generate schedules. Heuristics was used as the starting point of the optimization process. Heuristics examples like the highest mineral mass and the highest mineral grade were presented in the study. The purpose of the evolutionary algorithm was to make sure an optimized schedule met predecessor-successor and resource constraints among activities. "Just-in-time", aiming to schedule stoping activities right after corresponding development activities, was also built into SOT. By using the "just-in-time", SOT was able to make the optimized schedule more reasonable,

while increasing the NPV. According to the results of the case study, a $122 million NPV increase was achieved for the schedule with over 26,000 activities. Most importantly, the entire study lasted only a few days compared with months of planning work carried out by mine planners to achieve similar results.

Samanta *et al.* (2013) applied a multi-objective genetic algorithm (MOGA) in production scheduling to deal with ore grade uncertainty in open pit mines. Compared with other optimization algorithms, MOGA was faster and more efficient. Pareto optimal solutions were generated by MOGA to balance the effects of individual objectives. A case study was presented in the paper with MOGA being applied in an iron ore mine. The results showed that the MOGA became computationally expensive with a relatively big block grade model and the algorithm had difficulties meeting strict grade targets.

Critical Path Method (CPM)

Luxford (2000) shared his fifteen-year scheduling experiences and pointed out critical scheduling issues needed to be considered by mine planners in the paper entitled “Reflections of a mine scheduler.” Luxford listed four scheduling traps: many activities in one place, complicated schedules, many options for development activities, and many priorities. He demonstrated the improvement of scheduling software from 1987 to 2000 in some mines in Australia. Examples of the software were Hornet, Microsoft (MS) Project, program evaluation and review techniques (PERT), critical path method (CPM), and MS Excel. In terms of ventilation, he suggested that the number of dead spots and airway resistances should be minimized.

Linear programming

Kruger *et al.* (2003) published a study on an underground mine planning optimization system, which was called PlanIt-OPTIM. CADSmine™ V4 was utilized for planning, and CADSmine™ Detail Optimization Engine was used for schedule optimizing. PlanIt-OPTIM was a non-linear model that was solved by combining meta-heuristics and linear programming. In the results of a project shown in the study, PlanIT-OPTIM improved NPV by 10% compared with the existing production schedule. As well, profiles of the monthly gold production and monthly revenue from PlanIt-OPTIM were better than those from the baseline schedule.

Mixed integer programming (MIP)

Nehring and Topal (2007) proposed a MIP model for hard rock mines that used the sublevel stoping method to mine minerals. A nine-stope conceptual copper orebody was established for evaluation. Stope sequences and production schedules were carried out using the MIP model and the results were compared with that from a manually generated model. The results indicated that the MIP model increased the NPV by $1,048,218. If the orebody was complex, the advantages of the MIP model would be more evident compared to the manual scheduling process by trying every possible scenario in terms of solution time.

Nehring *et al.* (2010) proposed a new underground production schedule optimization model using MIP. The MIP model was mainly made for mining operations using the sublevel stoping method. An old model, with more variables formulating the MIP model, was simulated and the results compared with that of the new model with a single variable. Both the new and old models were coded in a mathematical programming language (AMPL) and solved in CPLEX 10.3. A case study

was presented to describe the advantages of the new model. According to the results, the new model ran much faster than the old one, while obtaining the same NPV. Results from this study indicated the importance of reducing the number of variables in a mathematical programming model so reduce the computing time.

Nehring *et al.* (2010) conducted a case study on integrating short-term and long-term schedules by using MIP to optimize NPV. The model only took stoping activities into account and did not consider resource assignment, production drilling, and backfilling activities. However, the cash penalty was applied to consider the overproduction and underproduction situations. As a result, the integrated model increased the NPV by 1% compared with single short-term and single long-term models.

Nehring *et al.* (2012) presented an integrated method for underground mine production scheduling. Short-term and medium-term schedules were combined to not only maximize NPV but also meet required mill feed grade. Penalties were applied to account for not meeting the required mill feed grade. A hypothetical underground mine was utilized to test the performance of the integrated method. Compared with a segregated method which represented short-term schedules that were conducted separately from medium-term schedules, the integrated method produced higher NPV schedules and better mill feed grade.

Menabde *et al.* (2007) proposed another optimization tool, named Blasor, for medium-term and long-term schedules of open pit mines. Mixed Integer Linear Programming (MILP) model was used, and CPLEX was applied as the optimization engine. Blasor was used not only to maximize discounted operating cash flow (DOCF) but also to find the ultimate pit boundaries. Compared with traditional pit design plans, plans generated from Blasor increased the DOCF by up to 10%.

Huang *et al.* (2009) developed a MineSight Schedule Optimizer (MSSO) to address short-term and medium-term production scheduling issues by optimizing the NPV. MSSO utilized the MILP technique, and LINDO API was used as the optimization engine. MSSO could be applied to both surface and underground mines with various constraints such as geometrical and equipment constraints considered. However, according to the open pit mine case study, MSSO did not consider activity durations and sequence.

Martinez and Newman (2011) developed a scheduling optimization model for Kiruna mine, Sweden, an underground iron ore mine using the sublevel caving method. A short-term resolution was added to the long-term model, which was presently used, to improve the optimization performance. The model utilized the MIP technique and was solved in CPLEX. The objective function in the model was based on minimizing deviation on monthly production. Two methods used to reduce solution time in the study were variable elimination and problem decomposition. According to the results presented, the model was more robust and was able to achieve better results in a shorter time.

Little *et al.* (2013) proposed an integrated integer programming (IP) model for underground mine scheduling optimization. The IP model was coded in AMPL and solved in CPLEX. The authors pointed out that production scheduling and stope layouts were the significant aspects needed to be considered for mine planning. In the integrated model, stope layouts and production schedules were optimized simultaneously, but separately in isolated models. A case study was conducted in a gold mine using the integrated model and the isolated model. Based on the results of the case study, it is seen that the advantages of using the integrated IP model were prominent in terms of NPV, holistic outlook, devotion to constraints, and simulation time.

Kawahata *et al.* (2013) explained a production scheduling optimization approach used at Twin Creeks, which was one of Newmont's open pit mines. Two optimization software packages used were "the Optimizer" and Minemax Scheduler (Minemax). Both the Optimizer and Minemax used the MILP technique to maximize NPV. The Optimizer was for long-term schedules, and Minemax was for short-term schedules. The coupling of the two software made the optimization successful for Twin Creeks to achieve Nevada regional goals, which were optimizing the use of capital equipment to extract, transport, and process the mineral with the highest grade.

Harmony Search (HS) algorithm

Sui *et al.* (2011) proposed a ventilation optimization approach utilizing the harmony search (HS) algorithm. The HS algorithm was derived from the esthetic process and aimed to find the best state by matching various musical instruments. In addition, more practices led to better quality of harmony in the HS. The HS algorithm was also used to control airflow efficiently in underground mines where there was an emergency. The authors proposed a simple conceptual model using the Newton method, GA, and HS, respectively. According to the results, the solution time for HS was much shorter than that for the other methods while the results were reasonable.

Particle Swarm Optimization (PSO)

Khan and Niemann-delius (2014) illustrated an optimization approach using particle swarm optimization (PSO) for long-term scheduling problems in open pit mines. Initial solutions were created with a heuristic approach. Then the PSO technique was applied to find the optimum or the close-to-optimum solutions. A case study using hypothetical data was conducted to compare the results from PSO with that from integer programming using CPLEX. It showed that the PSO

approach was much quicker in terms of computational time and generated better schedules with higher NPV.

2.6.3 Conclusion

According to the literature review presented above, efforts have been made for ventilation optimization and production schedule optimization individually. However, as far as the author knows, the combination of the two has not been adequately dealt so far. Indeed, for underground mines, the combination of the two is essential because a single optimization of either ventilation or production schedule is not the optimization of the mining system as a whole. Mine ventilation constraints have to be considered into the mine production optimization process. For underground M/MN mines, DPM is the main concern for the ventilation system. Therefore, this research is conducted in a timely fashion to provide improved input for DPM modeling in a ventilation network model with a hybrid methodology.

2.7 Integration of mine ventilation and production schedule optimizations

Brickey (2015) proposed an integer optimization model for underground production schedule optimization and mine ventilation was treated as a consumable resource. Two solvers, which are Open Mine Planner (OMP) and CPLEX, were evaluated, and it was found that the OMP solver was better than the CPLEX solver in terms of solution time and accuracy. The ventilation constraint considers the total airflow of the mine, the airflow consumed by each activity in the schedule, and a fixed amount of airflow for nonscheduled needs (e.g., offices). The fixed amount of airflow was assumed to be 10% of the total airflow of the mine. Airflows for the mine and locations and sizing of booster fans and regulators were not determined by the model. Airflow

required to dilute the DPM in production levels under the regulatory limit was estimated and applied as constraints to the production schedule. According to the results, there was a difference in the cumulative metal production between the schedules with and without ventilation constraints. The proposed integer optimization model was able to assess various scenarios quickly, and the resulted schedules produced more metal than the schedule created manually.

As mentioned above, this schedule optimization model does not determine the airflow of the ventilation system. In the model, the airflow needed to dilute the DPM under the regulatory limit was estimated. Therefore, ventilation optimization was not incorporated with production schedule optimization.

Kocsis *et al.* (2003) mentioned that ventilation was always over-provided in mines and the ventilation design was not integrated into the life-of-mine (LOM) schedule. They proposed an integrated approach using mine process simulators (i.e., Telemining^{TM} (2001)) and ventilation modeling to find the airflow requirements over the LOM. It was suggested to apply this approach in the early stage of a mining operation to avoid making wrong decisions. They also indicated that automated mines would be the future of mining in terms of health, safety, productivity, and cost.

2.8 Mine ventilation concerns and control strategies

Mine ventilation is one of the most important systems of an underground mine. It not only provides the necessary fresh air for personnel working underground but also cleans the contaminated air and harmful gases out of the working area. For underground coal mines, methane concentration is the most prominent concern because explosions can happen when the methane content reaches a critical level in the air. For underground M/NM mines, the most significant concern is the DPM

due to its unhealthy effects on the lungs of human body. For all the underground mines, dust and other contaminants such as nitrogen dioxide and radon are also concerns, which can dictate the ventilation design because of the potential health hazard on human body. Heat can be an issue because it increases as mines expand at depth. The main heat sources in underground mines are auto compression, virgin rock temperature, and mining equipment (McPherson, 2009). Ventilation is often required to remove dust and other contaminants and heat.

Ventilation for DPM reduction is the focus of this thesis.

The source of DPM is the diesel engines of mining equipment used underground. Diesel equipment such as mine trucks and LHDs are prevalent in underground mines due to their higher efficiency and more extended durability compared with the electricity-powered equipment.

DPM is a part of the diesel exhaust, which is a very complex mixture (U.S. EPA, 2002). DPMs are ultra-fine particles that are respirable and can harm the lungs after prolonged exposure. They consist of elemental carbon (EC) and are surrounded by various compounds like sulfate. The components of DPM are shown in Fig. 2-6. The elemental carbon atoms are the solid core in the figure, and they have an extensive surface. Toxic compounds such as hydrocarbons and sulfates shown in the figure are absorbed onto the core and transported with the core.

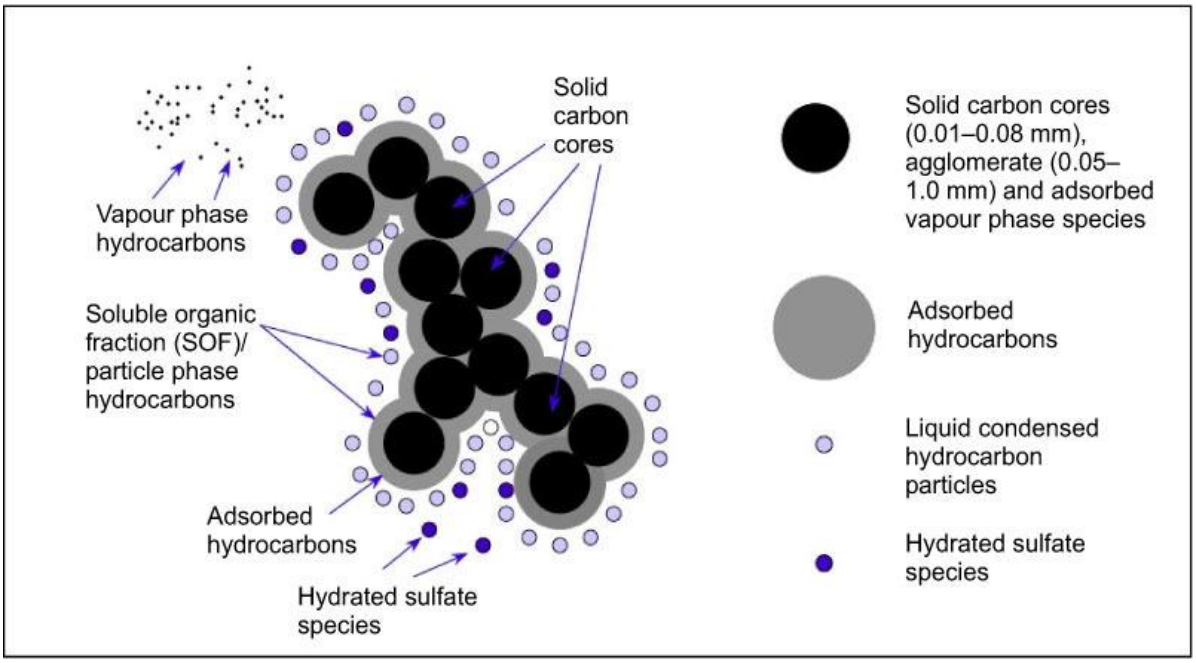

Fig. 2-6. DPM components (Twigg and Phillips, 2009).

According to Mine Safety and Health Administration (MSHA) in the U.S., TC is used as a substitute for DPM (Mine Safety and Health Administration, 2009). TC is the sum of the organic carbon (OC) and EC. In Ontario, the TC can also be calculated as 1.3 times of EC (Government of Ontario, 1990).

Because the DPMs have such small sizes that they are invisible to the naked eyes and can flow with the air underground. Therefore, the downstream of airflow is contaminated by the DPM and will be harmful to people if the DPM concentration is above the TC regulatory limit of 160 $\mu g/m^3$ (Mine Safety and Health Administration, 2001) in the U.S. or 400 $\mu g/m^3$ in Ontario, Canada (Government of Ontario, 1990).

DPM exposure is regulated to varying levels around the world (Gangal, 2012). In Canada, the ventilation requirements for diesel equipment vary in different provinces. In Ontario, the airflow

must be more than 0.06 m^3/s per kW power of the diesel equipment regardless of exhaust air quality (Government of Ontario, 1990). Other Canadian jurisdictions, as summarized by Gangal (2012), use the CANMET/CSA nameplate airflow requirement that recognizes the need to dilute a broad range of contaminants including diesel particulate.

Common DPM control strategies are shown as listed:

a) Turn off the engine if the diesel equipment is not in use.
b) Apply diesel particulate filters to the exhaust pipe of the diesel equipment.
c) Dilution by providing adequate ventilation.
d) Conduct regular maintenance on the diesel equipment.
e) Equip environmental cabs on the diesel equipment to protect the drivers from long-time DPM exposure.
f) People working underground are supposed to wear personal particulate filters which help filter out the DPM in the air.
g) Use high-quality fuels (low sulfur).
h) Plan the truck haul route in the return airway.

2.9 Methods for quantifying DPM

Various DPM monitors have been invented to monitor and quantify the DPM concentration over time. A DPM monitor called D-PDM was introduced by Wu and Gillies (2008). The D-PDM was converted from a Personal Dust Monitor (PDM) with structural changes. It was tested in five Australian mines and compared with the SKC impactor system, which was the only existing DPM monitor prior to the D-PDM in Australia back in 2008 (Wu and Gillies, 2008). The SKC impactor

system does not display real-time DPM data and shows TWA results instead (SKC Inc, 2017); the NIOSH 5040 method (NIOSH, 2003) is used to analyze the results from the SKC impactor system. The NIOSH 5040 method is an analytical method using a thermal-optical technique to determine both the OC and EC (Birch, 2003). Results from the tests (Wu and Gillies, 2008) showed that the D-DPM was robust and accurate for DPM monitoring in underground mines.

The TSI DustTrak™ aerosol monitor was tested (Osei-Boakye *et al.*, 2008), and a calibration model was established to predict the TC concentration according to the NIOSH 5040 method. Based on the test results, the TSI DustTrak™ aerosol monitor was suggested to replace the MSHA compliance instrument due to its real-time monitoring feature and relatively high accuracy. The MSHA compliance instrument refers to an SKC impactor filter cassette media using the NIOSH 5040 method to analyze the collected DPM data. It could take up to two weeks to process the DPM data collected by the MSHA compliance instrument in a laboratory.

Another real-time DPM monitor, the EcoChem Analytics PAC 2000 DPM monitor, was tested at multiple mine sites in Sudbury, Canada (Grenier, 2010). It was concluded that the real-time DPM monitors should be applied to monitor DPM concentrations in underground mines.

Pinssar DPM reader (Pinssar, 2019) provides continuous monitoring and recording of DPM levels up to 800 nanometers range on a 24/7 basis. An impactor is used to filter oversize particles. The Pinssar DPM reader uses the laser-light scattering photometry (LLSP) technology to measure DPM in the air, which eliminates the need for NIOSH 5040 sample analysis (Pinssar, 2019). The DPM mass concentration is proportional to the intensity of the scattered light generated by the particles. The Pinssar DPM reader has been applied in underground mines (Black and Mullins, 2019), tunnels, diesel workshops, and other confined spaces (CCD Group, 2019). Based on the

technical specifications (CCD Group, 2019), the DPM reader's dimensions are 0.66 m in height, 0.25 m in depth, and 0.74 m in width, which makes it not wearable by workers.

Another popular DPM monitor is Airtec Diesel Particulate Monitor (Flir Systems, 2011). It is a portable real-time DPM monitor using the NIOSH 5040 method. Its application to DPM monitoring has been discussed by several researchers (Janisko *et al.*, 2011; Noll *et al.*, 2013, 2014). The unit price for this monitor is about 6000 USD; the consumable parts are also pricey. The unit prices are 40 USD for filter cassette and 85 USD for prefilter cartridge.

According to Grenier's R-436 report (Grenier, 2005) entitled "Measurement of Carbon Monoxide in Diesel Engine Exhaust," carbon monoxide (CO) is a good indicator of the maintenance condition of a diesel engine. Poor maintenance of a diesel engine can lead to an increase in the DPM concentration in the exhaust. Hence, CO concentration measurements could be taken to detect diesel activity and help to validate DPM measurements.

It can be seen that the NIOSH 5040 method is the standard method for analyzing DPM data. The DPM monitors are used to obtain the DPM data so that high-DPM areas can be detected and engineering controls can be taken to dilute the DPM in these areas. Five Airtec diesel particulate monitors and one TSI DustTrak aerosol monitor were available at the mine site where the experiment of this thesis was conducted. The Airtec Diesel Particulate Monitors were selected to collect the DPM data because they are real-time monitors and do not need to be sent to a laboratory to get the results after two weeks.

2.10 DPM modeling using CFD

Zheng *et al.* (2011) conducted a validation study for a CFD model using the species transport model to predict DPM concentrations at various locations. Their study confirmed that the CFD approach could assess options for DPM reduction. Furthermore, Zheng *et al.* (2015) used the species transport model available in ANSYS Fluent to investigate the DPM distribution over a period of 200 s for four alternative auxiliary ventilation systems. It was found that the CFD approach could be used to select the best DPM control strategy. Kurnia *et al.* (2014) evaluated different ventilation strategies for efficient and economic control of hazardous gas released by diesel equipment using the species transport model in ANSYS Fluent.

It should be mentioned that none of the mentioned work provides specific methods for a longer-term (e.g., one hour) DPM modeling using CFD models, which would reflect the actual operation of diesel equipment in a heading of an underground mine. Most of the approaches proposed would be prohibitively computationally expensive and would require the use of high-performance computing (HPC), which is not usually available at a mine site. Thus, a new CFD modeling approach is proposed in this thesis to improve the performance and practical applicability of CFD models.

2.11 Conclusion

In this chapter, ventilation network solver, CFD applications in the mining industry, hybrid models used in mining and other industries, ventilation network basics, equations and theories of underground mine ventilation, DPM and its control strategies, DPM quantification methods, and CFD modeling of DPM are reviewed.

To the best knowledge of the author, it is seen that prior CFD modeling approaches are not able to model DPM over an extended period of time (e.g., one hour) quickly. To the best effort of the author, no network modeling approaches are found for DPM modeling in underground mines.

In the following chapter, a new CFD approach is presented, and it enables quick and accurate DPM modeling over an extended period of time in underground mines. DPM modeling in a network solver is also presented.

Chapter 3

3 Approaches to Model the DPM Concentration over an Hour in Underground Mines

As mentioned in Section 1.2, the VCM and SOT tools provide motivation for this thesis, and the author's contributions are: in developing the new CFD approach of modeling DPM over an extended period of time, in proposing a DPM modeling approach using a ventilation network solver, in developing the framework of a hybrid modeling methodology. The hybrid modeling methodology will be applied to the situation where network modeling is not capable of performing 3D fluid dynamics modeling and getting diesel input (e.g., diesel emission rates) in the model. Ventilation network modeling is performed by using the 1D ventilation network solvers such as Ventsim and VNet. Hence, 3D modeling of different fluid flows cannot be performed by using ventilation network modeling. The fact that the number of DPM real-time monitors is usually limited at the mine sites makes it difficult to install sufficient DPM monitors across the cross-sectional areas at the locations of interest. The DPM data recorded by the monitors will then be input to the ventilation network model with a correction factor so that the DPM data from a monitor at one location can be converted to represent the area-average DPM data. However, the correction factor can vary under different circumstances, which is a concern. The hybrid methodology provides improved input to a ventilation network model without the above concern. The areas of interest will be dead-end headings with auxiliary ventilation, complex airflow (e.g., airflow streams are not in the same direction) zones, and low airflow zones.

Some of the findings from this chapter were published as a peer-reviewed paper titled as "DPM Variation Analysis over Multiple LHD Work Cycles with the Use of CFD" and the paper was presented in the *11th International Mine Ventilation Congress* in Xi'an, China, in 2018. Some other findings from this chapter were presented in the *24th Annual MDEC (Mining Diesel Emissions Council) Conference* in Toronto, Canada, in 2018.

3.1 Introduction

Meeting production targets while ensuring health and safety of the workforce is paramount for mines all over the world. Mine ventilation, which dilutes and removes contaminants and provides fresh air to personnel and equipment, plays a significant role in health and safety in underground mines.

For metal and non-metal mines, a main health and safety concern arises from the DPM concentration due to the fact that it is carcinogenic after long-term exposure (Anon, 1988, 2000, 2001). DPM mainly comes from heavy-duty diesel equipment such as mine trucks and LHDs. DPM consists of very small particles emitted in diesel exhaust (Twigg and Phillips, 2009), mainly OC and EC. The sum of OC and EC is called TC, which is commonly referred to as DPM (Grenier, 2010). Practically, EC is measured according to the NIOSH 5040 method (Birch, 2003).

Mines have employed various methods to protect personnel from exposure to high-DPM exhaust. These methods include the installation of environmental cabs on mine trucks, applying diesel particulate filters to tailpipes, and the use of personal particulate filters (or respirators) (Bugarski, 2007). In addition, a well-designed and controlled ventilation system helps to dilute DPM efficiently.

This chapter proposes a new CFD approach to study the DPM concentration distribution after multiple work cycles of an LHD in the heading of an underground mine. To the best knowledge of the author, this is the first time that DPM was modeled over time in a network solver. Results from the two approaches are compared.

3.2 Details of the field studies

Five field studies have been undertaken in an underground gold mine in the U.S. The purpose of the field studies is to collect the DPM released from LHDs and trucks over time in various working areas and to use the data for validating numerical modeling results. These field studies were conducted along with the normal schedule and were completed in active headings of the mine. Due to safety concerns, personnel were not allowed to stay near the entrance of a heading where equipment frequently moved in and out. Therefore, the cycle time, working path, number and type of diesel equipment were not recorded in all the studies. Another limitation of the experiment is that the diesel emission rates from different diesel equipment were not measured in the studies. Neither the velocity magnitude nor the temperature of the diesel exhaust from the tailpipe of each diesel equipment was recorded. The Airtec Diesel Particulate Monitors were used to collect the DPM data in the field studies. As stated in Section 1.1, the Airtec monitor has a sensitivity of more than 70 $\mu g/m^3$, which is another limitation of the experiments with considering the regulatory limit (160 $\mu g/m^3$). However, the proposed new CFD modeling approach will not be affected by these limitations because the accuracy of the modeling results depends on the accuracy of the input data. The CFD modeling results will get better with better input.

After completing the field studies, equipment timeline reports were acquired from the mine site. The information shown in the equipment timeline report contains: the start and finish time of an

equipment in a heading, the equipment type, which shift the driver of the equipment worked on, the location of the heading, the destination of the equipment, the tonnage of ore or waste transported by the equipment over each work cycle. With this information, the average cycle time could be estimated.

Two of the field studies were conducted in the same heading, and there are four different headings being tested with five DPM monitors available at the mine. Airflow velocity, dimensions of cross-sectional areas, and temperature were recorded at each sampling point in each field study. Details about the experiment design and experiment apparatus are presented below.

3.2.1 Experiment apparatus

The DPM monitor used in the field studies was FLIR Systems Airtec Diesel Particulate Monitor as shown in Fig. 3-1. The FLIR Airtec DPM monitors were the only real-time DPM monitors available on-site at the time. There were five units available at the mine site.

Fig. 3-1. The Airtec DPM monitor with accessories (Figure source: Airtec Diesel Particulate Monitor User Manual (Flir Systems, 2011)). The description of each component is presented in Table 3-1.

Table 3-1. Description of the DPM monitor and its accessories (Table source: Airtec Diesel Particulate Monitor User Manual (Flir Systems, 2011)).

No.	Component	Description
1	Airtec Monitor	Real-time diesel particulate monitor
2	Inlet Prefilter Assembly	Inlet Prefilter and tubing to connect Prefilter to Airtec monitor
3	Filter Cassette	Replaceable cassette captures media for EC analysis
4	Prefilter Cartridge	Replaceable cartridge prefilters larger particles
5	USB cable	Cable to connect the monitor to PC to download data and change settings
6	Power Supply	Charges battery or power the monitor

Main specifications (Flir Systems, 2011) of the DPM monitor are:

1) Dimensions: 13.2 cm × 13.2 cm × 6.4 cm
2) Weight: 0.6 kg
3) Range: 50 to 600 μg/m^3
4) Operating temperature: -20 to 60 ℃
5) Data logging interval: 1, 5, 15, 60 min

The DPM data is stored in the Airtec DPM monitor and can be exported to a comma-separated values (CSV) file through an Airtec software (FLIR Systems, 2015) that comes with the monitor. The software is also able to automatically calculate both the moving average TC and EC concentrations over time from a minimum interval of 5 min to a maximum interval of one shift. Hence, manual calculations are necessary if the DPM concentrations for a one-minute moving average are used.

The monitors had been sent to the manufacturer for calibration before each field study. New prefilter cartridge and the filter cassette were loaded on the monitors for each experiment. The pump flow rate was set to HIGH (1.7 liter per minute). According to the user manual for the Flir Airtec DPM monitor (Flir Systems, 2011), this pump flow rate is recommended for enhanced sensitivity in low EC environments. The pump flow rate was calibrated using a flowmeter for all the DPM units at the beginning of each experiment. The pump flow rate was not measured at the end of each experiment. The battery life is more than 12 hours according to the Flir Airtec website (Flir Systems, 2018). The pump stops working when the battery is dead. All the units were fully charged before each experiment to ensure that the battery would not be dead during an experiment.

The total sampling time of each DPM monitor can be found by connecting the unit with a PC. The detailed information of each sample including the date, time, and EC in weight is accessible from the PC. The EC concentration ($\mu g/m^3$) is calculated based on the flow rate, sampling interval, and the EC weight. The Airtec DPM monitor uses a conversion factor of 1.3 to convert the EC concentration to total carbon (TC) concentration.

No side-by-side NIOSH 5040 method was performed to quantify the accuracy of the DPM data collected from the Airtec DPM monitors.

The quality of the instruments used especially the Flir Airtec real-time DPM monitors is considered not high. As mentioned above, the Flir Airtec DPM monitors were the only real-time DPM monitors available on-site at the time. The "real" accuracy of the Flir Airtec DPM monitors was not indicated based on published papers and the manufacturer's datasheet. According to the Airtec DPM monitor official website (Flir Systems, 2018), the monitor uses a technology developed by the diesel particulate group at the NIOSH Pittsburgh Research Laboratory and has accurately replicated results from their method 5040 test. According to the Airtec website and the user manual, the sensitivity of the DPM monitor is 15 $\mu g/m^3$ (EC), which is less than 4% and 10% compared with the regulated DPM concentrations in Canada and the U.S. (e.g., 400 $\mu g/m^3$ in Ontario, and 160 $\mu g/m^3$ in the U.S.), respectively. It appeared that the Flir Airtec DPM monitor was a good choice for instrument based on its sensitivity and the fact that it was the DPM monitor available on-site. It was then used in the field studies. However, the observed discrete values in the raw DPM data collected from the field studies indicated a lower sensitivity than the specification. Dr. James Noll (personal communication, June 12, 2018) from NIOSH was contacted to provide insight on this matter. He confirmed that the sensitivity of the Flir Airtec DPM monitors would be around the 70 $\mu g/m^3$ range for a 5-minute rolling average, which is calculated from the Airtec DPM monitor with the use of the associated data processing software.

Consequently, due to the low quality airflow and DPM data collected from the field, this study should be viewed as a qualitative study rather than a quantitative study.

The poor quality of the data also explains the differences between the results from the field studies and their corresponding CFD models (shown in the following chapters).

The continuous traverse technique with a rotating vane anemometer was used to measure the air velocity in the cross-sectional areas at various sampling points in each field study.

3.2.2 Experiment setup

After reviewing the prior DPM research, the author finds that little research had real-world DPM data and most of the research was on DPM modeling in software, like ANSYS Fluent. The main reason is that active mines always have busy schedules and researchers seldom find the opportunity to install the DPM monitors in ideal locations, where the DPM concentration is not affected by other unpredicted factors, such as level shut down and different running equipment. In addition, in a real underground mine, areas like intersections and working faces are unsafe for the researchers to stay and collect data over time. The reason is that there is equipment frequently moving in the intersections, and the working faces are usually not supported before the broken rock is mucked out. However, airflow and DPM behavior is complex and needs to be analyzed in these mine areas. The following experiments are conducted to find the real DPM distribution over multiple work cycles. The results are compared with the results from modeling DPM.

The same setup was used in all the five experiments (named 1, 2, 3, 4 and 5 for simplicity), which were conducted in dead-end headings with DPM monitors installed on the back of the drifts. These experiments were conducted to provide a range of various air quantities and the associated DPM concentration distributions over time.

Because important information on the equipment in the experiments 2 and 4 was missing in the equipment timeline report provided by the mine, the DPM data collected from these two experiments could not be compared with those from CFD models. Moreover, the DPM data

collected in experiment 1 were heavily affected by the DPM from upstream, which had an irregular distribution over time. This made it difficult to validate the CFD model for experiment 1. As a result, only the experiments 3 (EXP3) and 5 (EXP5) were used in this thesis. 99 and 109 minutes of continuous data collected at each monitoring location in the EXP3 and EXP5 were eligible to be used to establish the CFD models. In other words, the DPM simulation time of the EXP3 and EXP5 CFD models are 99 min and 109 min, respectively. Results from the experiments were compared with those from the associated CFD models and were used to demonstrate the new CFD modeling approach.

In terms of result accuracy, the field data were not suitable to validate the CFD models. Realizing the limitations of the collected field data (see the following sections), this research has been positioned as a qualitative study rather than a quantitative study, with a primary goal of developing a framework of a hybrid methodology for modeling of diesel particulate matter concentration in underground mine ventilation systems.

EXP3

EXP3 was carried out in a dead-end heading and the plan view of the experiment area is shown in Fig. 3-2. Arrows in Fig. 3-2 indicate the airflow direction. A diesel-powered LHD trammed into the test area from location C, mucked ore/waste from the working face, and exited the area through location C. Four Flir Airtec DPM monitoring (Flir Systems, 2011) units were installed at four different locations A, C, D, and E, on the back of a heading. There are no monitors at location B but airflow measurements were taken, and results were used as references for the results at location A. The fifth DPM monitor, which is not shown in Fig. 3-2, was mounted near the air filter outside of the cab of an LHD to measure the DPM concentration near the LHD. A ventilation survey was

performed at locations A, B, C, D, and E using the traverse methodology (McPherson, 2009) to obtain the dimensions of the experiment area and velocities to calculate the air volumes. An example of the location of a DPM monitor in the cross-sectional area is shown in Fig. 3-3. Data from the airflow measurements are shown in Table 3-2.

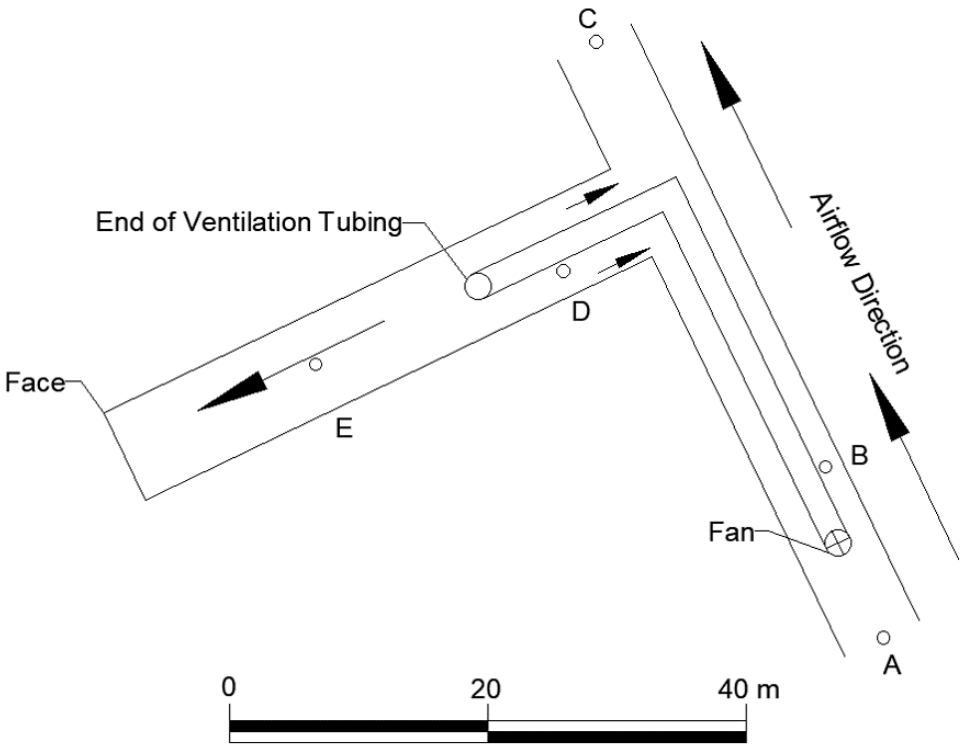

Fig. 3-2. Plan view of the design and the DPM monitor locations in the EXP3.

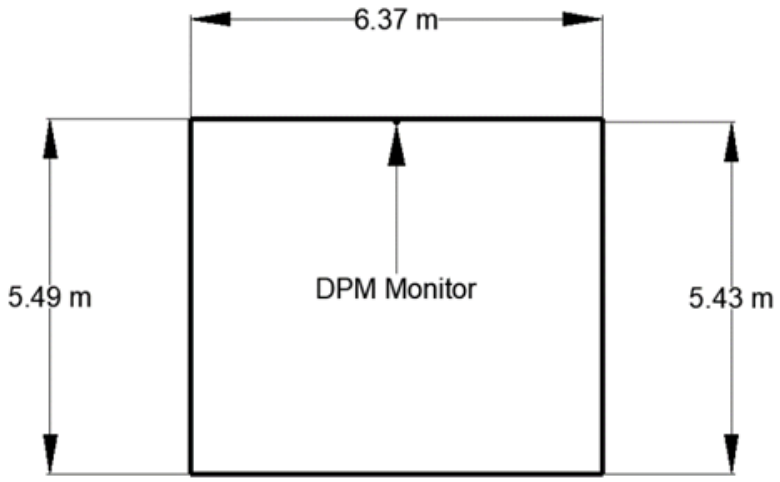

Fig. 3-3. Cross-section of the heading, showing the location of a DPM monitor at location C in the EXP3.

Table 3-2. Raw data collected from EXP3

DPM monitor	Dimension (m)				Velocity (m/s)		Temperature (°C)		Humidity (%)
	Width (W)		Height (H)				Dry-bulb (DB)	Wet-bulb (WB)	
	W1	W2	H1	H2	V1	V2			
A	4.57	4.62	5.60	5.59	2.80	2.81	24.44	16.50	46.50
B	5.00	4.88	4.87	5.15	1.61	1.62	25.83	17.00	43.70
C	5.03	4.90	4.71	5.06	2.93	2.93	26.17	18.11	47.50
D	5.68	6.05	5.35	4.80	0.42	0.43	25.94	19.78	58.20
E	6.57	6.39	5.12	5.11	1.09	1.12	26.33	20.72	61.20
F	Outside of the cab of an LHD								

The monitors were left underground to collect real-time DPM data for over 24 hours continuously. Each DPM monitor was set to collect data at a one-minute interval. The air pump of the DPM monitors was calibrated with a flowmeter, and the airflow rate of the pump was set at 1.7 liter per min. The raw DPM data was expressed as EC in weight, and one-minute DPM concentration data were then manually calculated according to (Flir Systems, 2013).

Ventilation surveys were conducted at location A, B, C, D, and E. The volumetric flow rate (in m^3/s) of air inside the fan was indirectly calculated by subtracting the flow rate at location B from

that at location A. Air leakage from the ventilation tubing was not measured because the measurements would potentially cause a production delay for the mine.

The experimentation process at the mine site had some limitations imposed by operating conditions (such as leakage in ventilation tubing) and by the quality of the installed air monitors purchased by the mine. As a result, the quality of the gathered airflow data is poor. However, the gathered temperature and humidity data are within the expected range. Table 3-3 is used as a reference for the explanation.

Table 3-3. Comparisons between the measured and expected volumetric airflow data collected from EXP3

Sampling location	Measured air quantity (m^3/s)	Expected air quantity (m^3/s)	Difference (m^3/s)
A	71.8	70.7	1.1
B	39.8	39.8	0
C	70.7	70.7	0
D	12.6	30.9	-18.3
E	36.5	30.9	5.6

As mentioned above, the continuous traverse technique with a rotating vane anemometer was used for the airflow measurements. Firstly, there were visible holes along the ventilation tubing both in the drift and in the heading. The leakage near the 90-degree turn explains why there is a difference of 18.3 m^3/s (as shown in Table 3-3) between the expected air quantity (70.7 – 39.8 = 30.9 m^3/s) and the measured air quantity (12.6 m^3/s) at locations D.

Secondly, in theory, the air quantities at locations A and C should be equal (refer to Table 3-3). The difference (71.8 – 70.7= 1.1 m^3/s) is 2%, which is within the 5% acceptable range for air surveys using the traverse technique as shown in McPherson's book Chapter 6 (McPherson, 2009).

Thirdly, in theory, the air quantities at locations D and E should be equal if there is no leakage along the tubing. The change of the airflow direction or the airflow turbulence contributed to the poor airflow data measured at location E. The air coming out of the tubing near the back of the heading would pass location E near the back and travel to the face. Then the air would return from the face and pass location E a second time with an opposite airflow direction. Hence, the traverse measurement at location E would be affected.

Regarding the temperature and humidity data, the same Humidity & Temperature Meter from Kestrel Instruments was used to record the dry-bulb temperature, wet-bulb temperature, and relative humidity at each sampling location. EXP3 was conducted at the 4,450 muck bay, where 4,450 referred to 1,356 m above sea level in altitude. At sampling location C, with a dry-bulb temperature of 26.2°C, the barometric pressure at the altitude of 1,356 m is expected to be 86.6 kPa. With the measured dry-bulb and wet-bulb temperature and the altitude of 1,356 m at location C, barometric pressure of 86.1 kPa was indicated according to ASHRAE Handbook Fundamentals 2001 Chapter 6 (ASHRAE, 2001). Therefore, the barometric pressure is within the expected range.

EXP5

EXP5 was conducted in a different dead-end heading other than the EXP3 and the plan view of the experiment area is shown in Fig. 3-4. Four Flir Airtec DPM monitors were installed on the back of the drift at locations A, B, C, and D. The fifth DPM monitor was attached on an LHD as in EXP3. Ventilation surveys were conducted at the locations as well. Data from the airflow measurements are shown in Table 3-4. The ventilation tubing was not located in the center of the heading in EXP5.

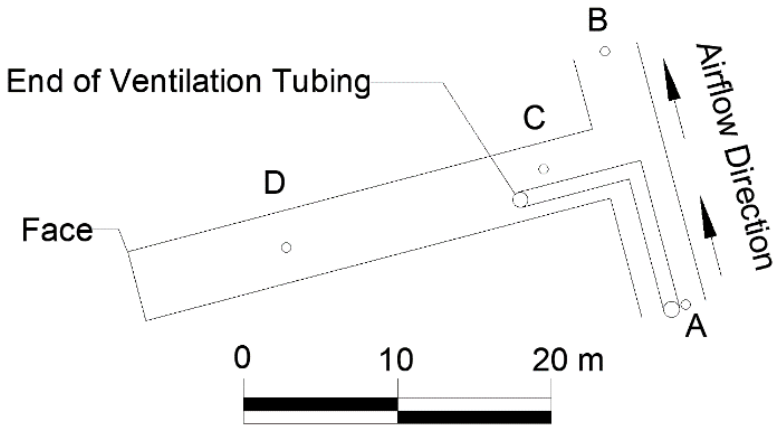

Fig. 3-4. Plan view of the design and the DPM monitor locations in the EXP5.

Table 3-4. Raw data collected from EXP5

DPM monitor	Dimension (m)				Velocity (m/s)		Temperature (°C)		Humidity (%)
	Width (W)		Height (H)				Dry-bulb (DB)	Wet-bulb (WB)	
	W1	W2	H1	H2	V1	V2			
A	4.30	4.26	5.42	5.42	0.09	0.08	25.83	20.78	65.20
B	4.27	4.53	5.64	5.66	1.62	1.62	28.17	21.28	56.40
C	4.74	4.53	4.50	4.47	3.02	3.00	27.94	21.00	55.50
D	5.42	5.27	4.47	4.66	1.67	1.67	28.22	22.22	61.00
E	Outside of the cab of an LHD								

For both the experiments, the fifth DPM monitor was attached on an LHD to get a general idea of the DPM concentration level. This DPM monitor was not placed directly in front of the diesel exhaust tailpipe because the high-temperature diesel exhaust may potentially damage the monitor. It was placed near the fresh air intake of the environmental cab instead. The DPM data collected from this monitor did not have a regular pattern because the diesel engine was either working or idle when it was turned on.

Table 3-5. Comparisons between the measured and expected volumetric airflow data collected from EXP5

Sampling location	Measured air quantity (m^3/s)	Expected air quantity (m^3/s)	Difference (m^3/s)
A	1.9	1.9	0
B	40.1	40.1	0
C	62.3	38.2	24.1
D	40.6	38.2	2.4

Regarding the airflow data, firstly, for Table 3-5, in theory, the expected air quantity at location B (40.1 m^3/s) should be equal to the sum (1.9+38.2 = 40.1 m^3/s) of the expected air quantities at locations A and C if the ventilation tubing does not have any leakage. The leakage on the ventilation tubing and the strong vibrations of the ventilation tubing near location C disrupted the continuous traverse airflow measurement. As a result, the average air velocity measured at location C was increased because of the holes on the tubing near location C. This explains why there was greater air volume measured at location C (62.3 m^3/s) than that measured at location B (40.1 m^3/s). A hot-wire anemometer should have been used to measure the air velocity at location A because the rotating vane anemometer is not sensitive to low airflow (with air velocity less than 0.25 m/s).

Secondly, in theory, the air quantities at locations C and D should be equal if there is no leakage along the tubing. The change of the airflow direction or the airflow turbulence contributes to the poor airflow data measured at this location. The air coming out of the tubing near the back of the heading would pass location D near the back and travel to the face. Then the air would return from the face and pass location D a second time with an opposite airflow direction. Hence, the traverse measurement at location D would be affected.

Regarding the temperature and humidity data, the same Humidity & Temperature Meter from Kestrel Instruments was used to record the dry-bulb temperature, wet-bulb temperature, and

relative humidity at each sampling location. EXP5 was conducted at the 4,100 sump, where 4,100 referred to 1,250 m above sea level in altitude. At sampling location B, with a dry-bulb temperature of 28.2°C, the barometric pressure at the altitude of 1,250 m is expected to be 87.8 kPa. With the measured dry-bulb and wet-bulb temperature and the altitude of 1,250 m at location B, barometric pressure of 87.2 kPa was indicated according to ASHRAE Handbook Fundamentals 2001 Chapter 6 (ASHRAE, 2001). Therefore, the barometric pressure is within the expected range.

3.2.3 Observations

The continuous traverse technique with a rotating vane anemometer was used for the airflow measurements. The lack of agreement on the anemometer data collected in EXP3 was resulted from leakage on the ventilation tubing. For EXP5, only the anemometer data collected at location B could be trusted. The measurement at location C was not reliable because of the swinging ventilation tubing and the leakage on the tubing. A hot-wire anemometer should have been used to measure the air velocity at location A because the rotating vane anemometer was not sensitive to low airflow (with air velocity less than 0.25 m/s).

Consequently, due to the low quality airflow and DPM data collected from the field, this study should be viewed as a qualitative study rather than a quantitative study.

The intention to take measurements at location E in EXP3 and location D in EXP5 was that these locations were the closest ones to the diesel equipment, and the DPM concentration spikes were assumed to show up earlier than those at the other locations.

DPM monitors with a higher accuracy should have been used in this study. An electronic tagging system would give accurate timing and location information for diesel equipment moving into or

out of the study area. More experiments (such as the sampling locations across the cross-sectional area and the record of the diesel equipment cycle time and maintenance schedule) with better DPM sampling instrumentation should be conducted in the future for quantitative studies.

A side-by-side NIOSH 5040 method could have been used as a baseline. Using the NIOSH 5040 method or DPM monitors from different manufacturers at the same sampling locations where the Flir Airtec DPM Monitors were installed could have been conducted for result validation. All the monitors on the site could have been placed at the same location to detect the DPM concentration profile across the cross-sectional area over time in an experiment where the diesel equipment does not move and continuously releases DPM in a heading upstream of the sampling location.

3.3 Proposed DPM modeling approach using CFD

In this study, a new CFD approach was introduced to model the DPM concentration over 1.5 hours efficiently. A single diesel source was created in the CFD model to release DPM in order to mimic the exhaust emissions of diesel equipment (in this case, an LHD) over multiple work cycles. The boundary conditions for DPM concentration and velocity magnitude of diesel plume from the diesel source in the CFD model was controlled by two User Defined Functions (UDFs). With the UDFs, the boundary conditions varied over time and results from the CFD model could match those collected from an underground mine.

One work cycle of an LHD consists of three sections: tramming into the heading, mucking at the working face, and tramming out of the heading. The LHD enters the test area from the outlet and trams into the working face. Then the LHD stays near the working face where the DPM source is

located and mucks the broken ore or waste. Afterward, the LHD moves out of the test area through the outlet.

The DPM emissions from the tailpipe of the LHD vary in each part of the work cycle. The concentration is highest when the LHD is mucking and lowest when the LHD is tramming into the heading. Due to the long duration of the period modeled, an average DPM concentration over each work cycle was used to represent the DPM concentration over each work cycle of the LHD. The averaged DPM concentration was obtained through trial-and-error in the CFD model with reference data from Zheng (2011).

In this approach, the single DPM source can be considered as a point source with a timed on/off profile. The DPM source is not a mobile source. Therefore, the turbulence generated by the movement of the diesel equipment cannot be captured by the CFD model. As a result, the DPM concentration affected by turbulence cannot be modeled. Because this approach is proposed for efficient DPM modeling over an extended period of time (e.g., an hour), the TWA DPM concentrations from using this approach are assumed not to be significantly affected. Future studies may be necessary to investigate the effects on the TWA DPM concentrations from a moving source.

3.3.1 Assumptions

Several assumptions are made on the inputs of the CFD model to formulate reasonable boundary conditions.

The DPM concentration and velocity magnitude of the diesel exhaust is constant when the LHD works.

The shape of LHD does not significantly affect the DPM concentration distribution at the outlet of a dead-end heading over an hour.

When there is DPM coming from the upstream outside of the experiment area, the raw DPM data collected by an Airtec monitor on the back of the upstream drift is adjusted by multiplying a correction factor of 0.5, which is obtained through trial-and-error with knowing the fact that the area-average DPM is smaller than DPM near the back of a draft. The adjusted DPM data represents area-average DPM across the cross-sectional area and is applied in the CFD model.

3.3.2 3D CFD model for EXP3

A 3D view of the CFD model is shown in Fig. 3-5. The 3D CFD model with dimensions is shown in Fig. 3-6. The ventilation tubing has a diameter of 1.067 m. The DPM source represents the diesel exhaust tailpipe. The dimensions of the DPM source are 0.3 m by 0.3 m by 0.3 m. The source was located 7.5 m away from the working face. The DPM source did not move over time like a real LHD. The boundary conditions of the DPM source inlet were set to vary over time to represent the movement of the diesel equipment. A 3D view of the CFD model with the coarse mesh is shown in Fig. 3-7.

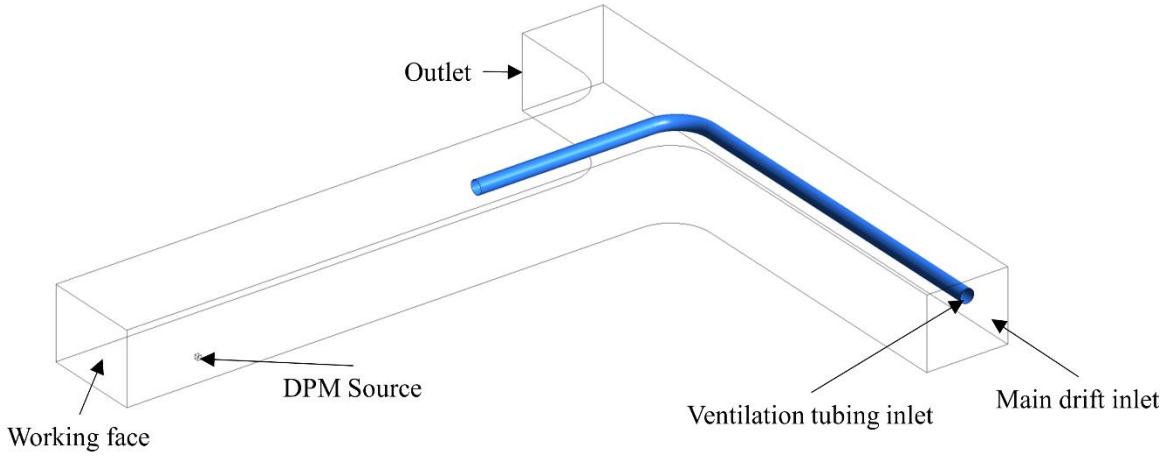

Fig. 3-5. 3D view of the CFD model for EXP3

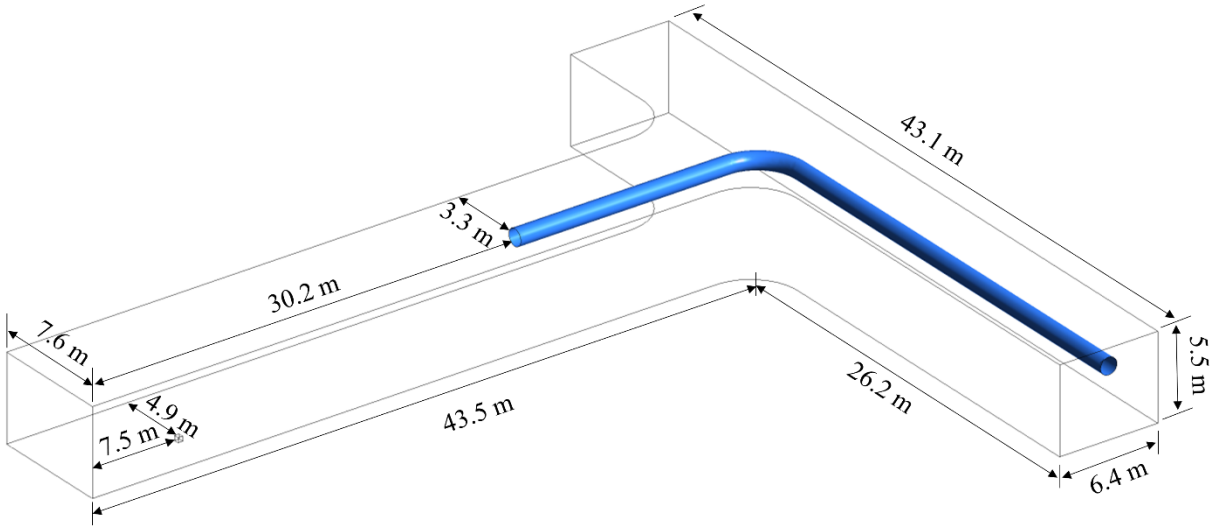

Fig. 3-6. 3D CFD model of EXP3 with detailed dimensional information

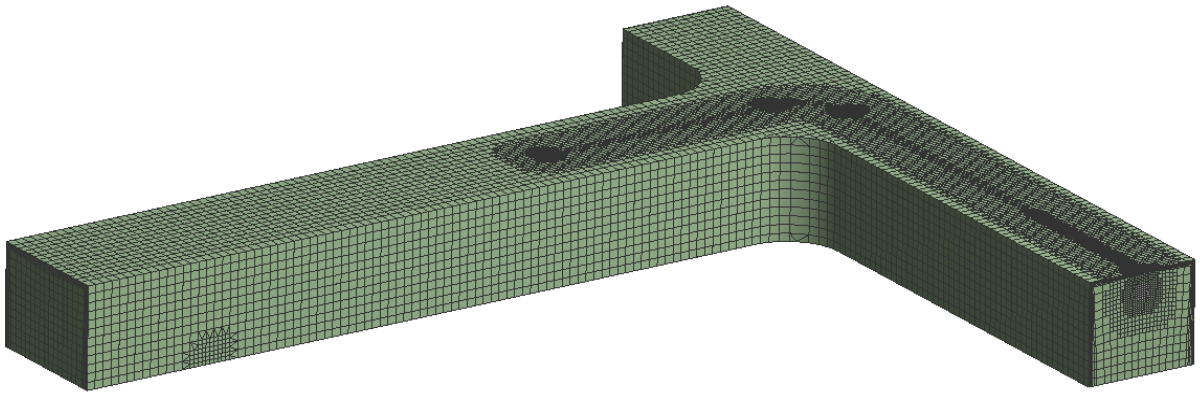

Fig. 3-7. 3D CFD model of EXP3 with the coarse mesh

The CFD model was created with ANSYS Workbench (ANSYS Inc., 2013b) 17.2. The geometry of the CFD model was established in DesignModeler, and the mesh was built in Meshing. The CutCell assembly meshing method (ANSYS Inc., 2013a) was applied. A mesh independence study was conducted to make sure the CFD results were independent of mesh sizes while saving computing time with a smaller mesh size. Inflation layers, which allow near-wall laminar flow to transit to away-from-wall turbulent flow, were applied at the boundaries of the CFD model to take care of the low-airflow zone near the wall (Feroze and Genc, 2016). Governing equations including mass, momentum, energy, and species transport equations are solved in the CFD model. ANSYS Fluent was used as the CFD solver. The governing equations were solved by using the SIMPLE algorithm in ANSYS Fluent. The standard k-epsilon turbulence model (ANSYS Inc., 2009a) was used to model the turbulent flow in the flow domain. The boundary condition for the wall was the no-slip stationary wall. A steady-state airflow simulation was conducted first with the DPM source turned off. After the airflow reached a steady-state, a transient simulation with the DPM source turned on was conducted to model the airflow and DPM concentration over time.

In the CFD model, three monitoring points and three monitoring planes were created at locations C, D, and E, respectively. An example of the location of the monitoring point is shown in Fig. 3-2. The DPM data recorded at the monitoring points over time in the CFD model were compared with the experimental data in order to fit the CFD model. This is a fitting process other than a calibration because this CFD model cannot be used to predict DPM concentration distribution beyond the experiment duration.

DPM was modeled as octane (C_8H_{18}) (Zheng, 2011). The species transport model was employed to model DPM concentration in the fluid domain. Hence, the following species transport equation was solved in addition to the Eqs. (2-1), (2-3), and (2-4).

Species transport equation:

$$\frac{\partial}{\partial t}(\rho Y_i)+\nabla\cdot(\rho\vec{v}Y_i)= -\nabla\cdot\vec{J_i}+R_i+S_i \tag{3-1}$$

where R_i is the production rate of species i chemical reaction, S_i is the additional production rate resulted from user-defined sources and the dispersed phase, $\vec{J_i}$ is the diffusion flux of species i.

Boundary conditions used in the CFD model are presented in Table 3-6. The temperature of the diesel exhaust from the DPM source was not measured in EXP3 and was set to 594 K according to a study conducted by Zheng (2011). The rest of the data shown in Table 3-6 were obtained from the ventilation survey.

Table 3-6. Boundary conditions

	Area (m^2)	Velocity (m/s)	DPM mass fraction	Temperature (K)
Ventilation tubing inlet	0.89	35.97	0	300
Main drift inlet	34.08	1.61	0	300
Outlet	Outflow boundary condition			
DPM source inlet	0.09	DPM and velocity profiles are shown in Fig. 3-8 and Fig. 3-9 respectively		594

The DPM concentration and velocity of the diesel plume from the tailpipe were not measured in EXP3 and were obtained through trial-and-error based on the experimental data from Zheng (2011). The DPM data measured by Zheng (2011) provided a starting point for the trial-and-error process. The velocity magnitude of 24.1 m/s measured by Zheng (2011) was used in this study. The DPM concentration profile and the velocity profile over time for the DPM source are shown in Fig. 3-8 and Fig. 3-9, respectively. The DPM concentrations were applied to the CFD model as mass fractions. The DPM concentrations shown in Fig. 3-8 have been converted from mass fraction to $\mu g/m^3$ by using Eq. (3-2) (Zheng, 2011).

$$\text{DPM mass fraction (unitless)} = \frac{\text{DPM concentration } (\frac{\mu g}{m^3})}{\text{Air density } (\frac{kg}{m^3})} \times \frac{1kg}{10^9 \mu g} \qquad (3\text{-}2)$$

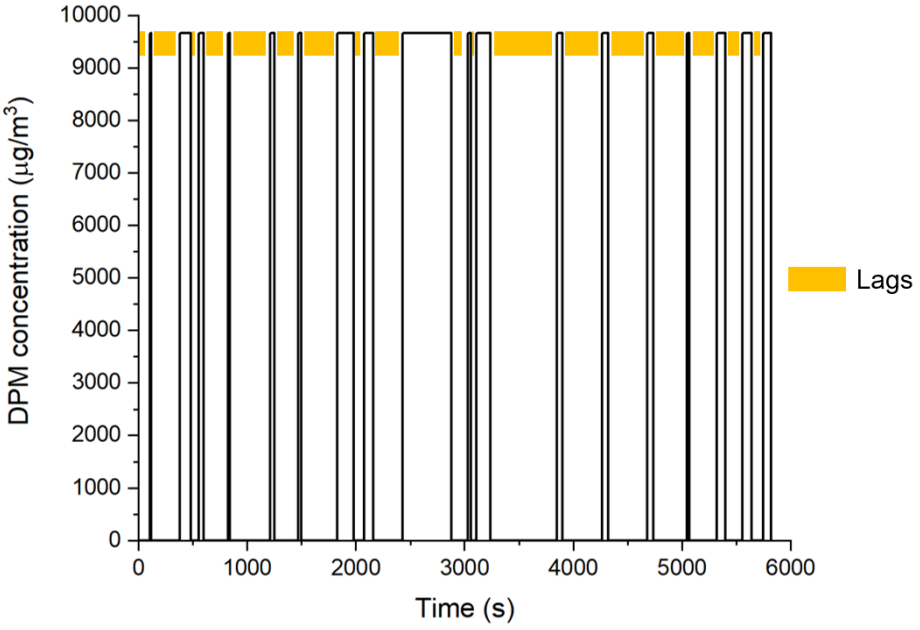

Fig. 3-8. DPM concentration (μg/m^3) profile over time at the DPM source in the CFD model. The DPM concentration in the diesel exhaust plume toggles between a constant value and zero. The lags, highlighted in orange, are periods when no DPM is released.

The equipment timeline report provided by the mine indicated that both the LHD and the truck were in the experiment area to carry out the mucking and dumping tasks. Based on the data collected by the DPM monitors, neither the LHD nor the truck was always working in the experiment area, and there were lags when neither of them was operating, or they were out of the experiment area. Here, a lag refers to a period of time when there is no DPM released into the heading. In the CFD model, the lags were modeled as the DPM source stopped releasing DPM for a period of time. The lags, determined through trial-and-error in the CFD model, are shown in both Fig. 3-8 and Fig. 3-9.

The total simulation time was 99 min. The magnitude of the averaged DPM concentrations is indicated in Fig. 3-8. This DPM profile from the source was applied in ANSYS Fluent by using a UDF (ANSYS Inc., 2009b), which was used to define the boundary conditions.

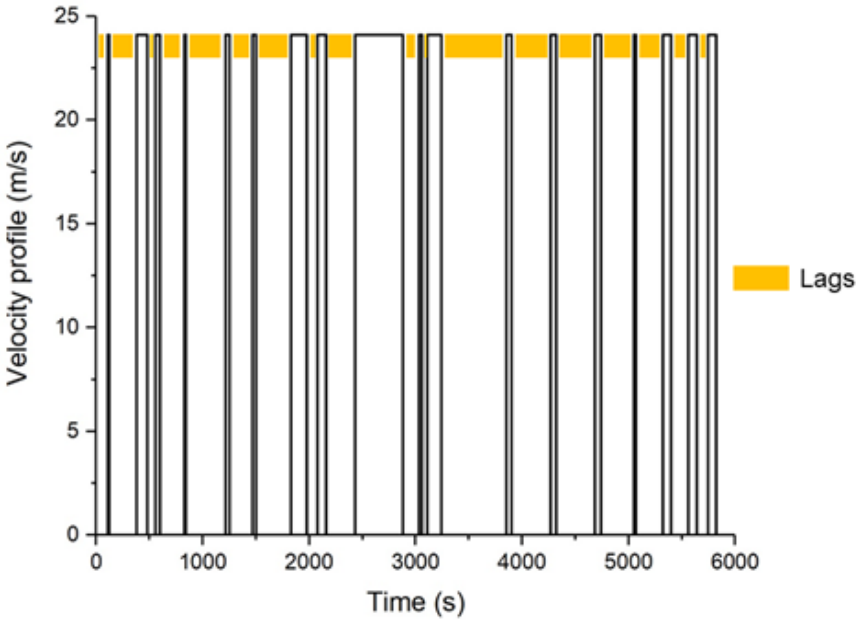

Fig. 3-9. Velocity (m/s) profile over time at the DPM source. The modeled velocity of the diesel exhaust plume toggles between a constant value and zero. The lags, highlighted in orange, are periods when no DPM is released.

The velocity profile over time is shown in Fig. 3-9. The velocity magnitude is 24.1 m/s (Zheng, 2011). The velocity profile was also programmed to a UDF. The UDF of velocity magnitude over time was loaded to ANSYS Fluent to define the boundary conditions.

3.3.3 Mesh independence study for EXP3

A mesh independence study was performed to ensure the CFD modeling results were independent of various mesh sizes and to save the computing time with a smaller mesh size while keeping the same accuracy of the results.

Three meshes were generated. The total elements in the coarse mesh, medium mesh, and the fine meshes are 221,855, 353,397, and 495,812, respectively. From Fig. 3-10, two horizontal

monitoring lines, located in the center of the cross-sectional areas at two locations, were created in the 3D CFD models with the three meshes, respectively.

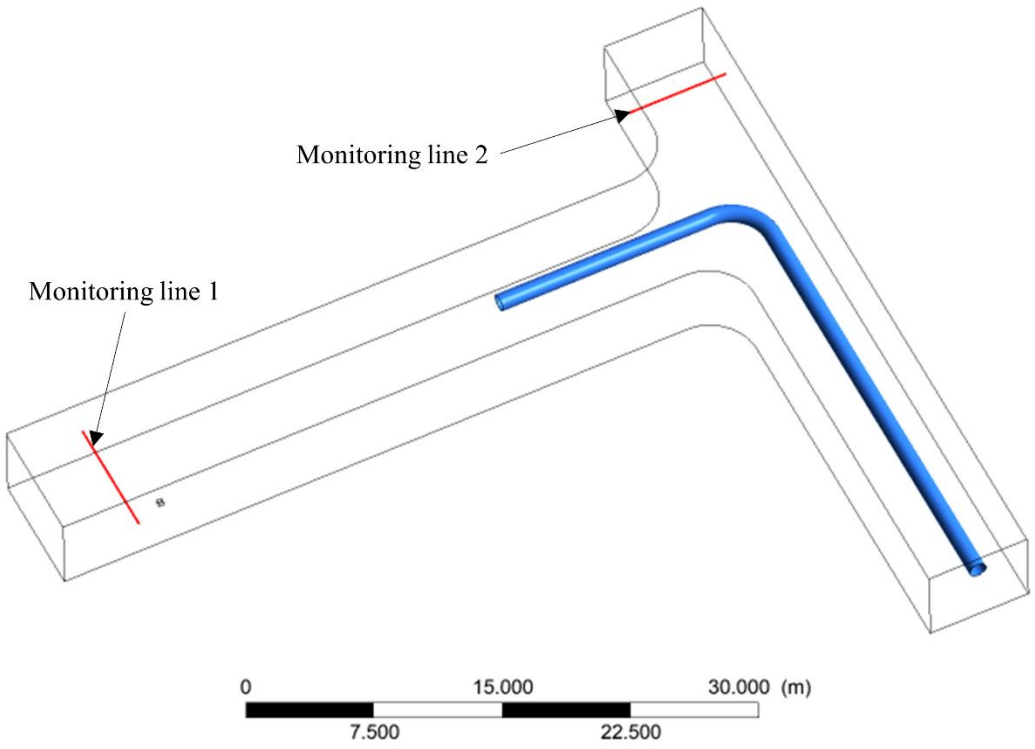

Fig. 3-10. Locations of the two monitoring lines in the CFD model of EXP3

The velocity magnitude of airflows along the two monitoring lines for each 3D CFD model was recorded. The results along the monitoring lines 1 and 2 from the three CFD models with the three meshes are shown in Fig. 3-11 and Fig. 3-12, respectively.

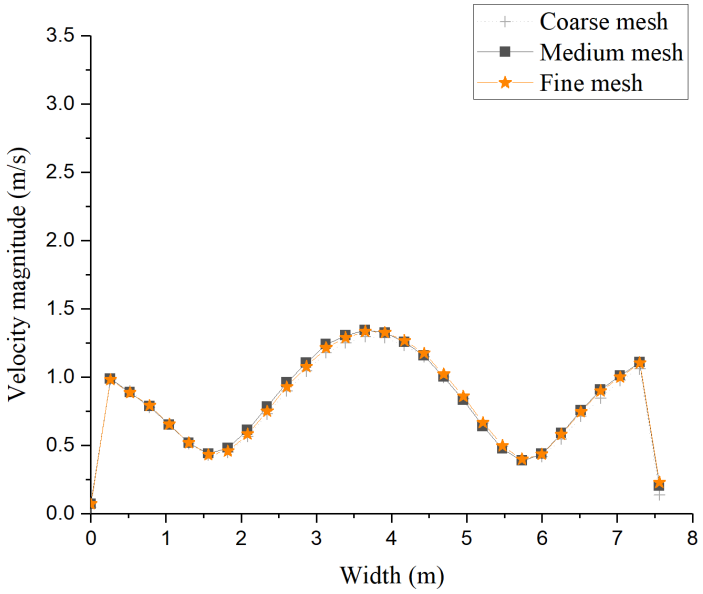

Fig. 3-11. Velocity magnitude profile comparisons along the monitoring line 1 in the CFD models with the three meshes.

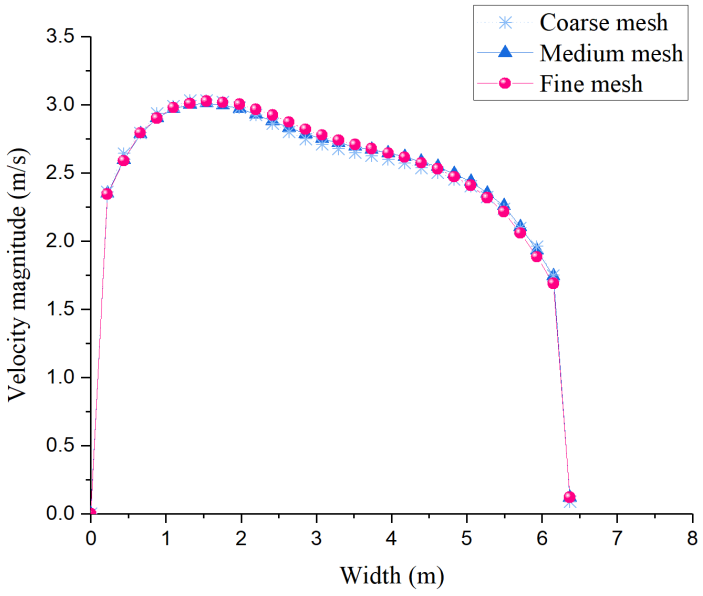

Fig. 3-12. Velocity magnitude profile comparisons along the monitoring line 2 in the CFD models with the three meshes.

From Fig. 3-11 and Fig. 3-12, the results from the CFD model with the coarse mesh have a good agreement with those from the other two CFD models with the medium and fine meshes. Hence, the coarse mesh is selected for the CFD model of EXP3.

3.3.4 3D CFD model for EXP5

Similar to EXP3, a 3D CFD model (as shown in Fig. 3-13) was built for EXP5. The 3D CFD model with dimensions is shown in Fig. 3-14. The ventilation tubing has a diameter of 1.067 m. The DPM source represents the diesel exhaust tailpipe. The dimensions of the DPM source are 0.3 m by 0.3 m by 0.3 m. The source was located 7.5 m away from the working face. The DPM source did not move over time like a real LHD. The boundary conditions of the DPM source inlet were set to vary over time to represent the presence in the heading or absence of the diesel equipment. A 3D view of the CFD model with the coarse mesh is shown in Fig. 3-15.

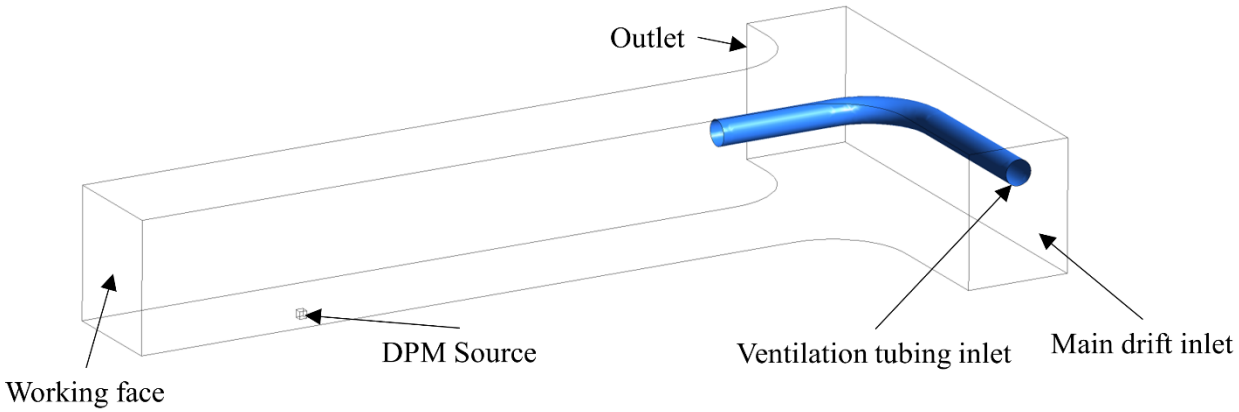

Fig. 3-13. 3D view of the experiment area in the CFD model for EXP5

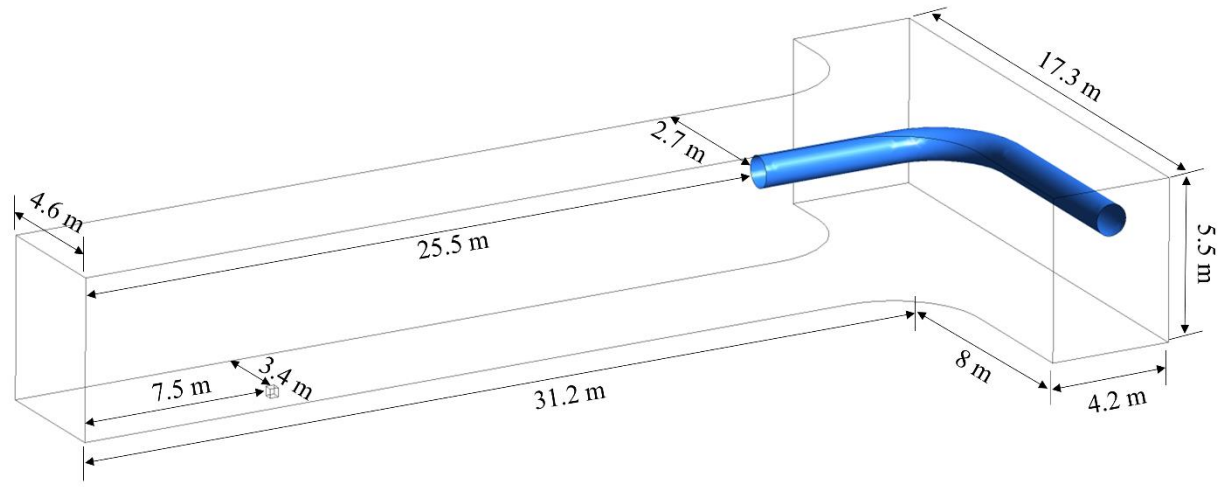

Fig. 3-14. 3D CFD model of EXP5 with detailed dimensional information

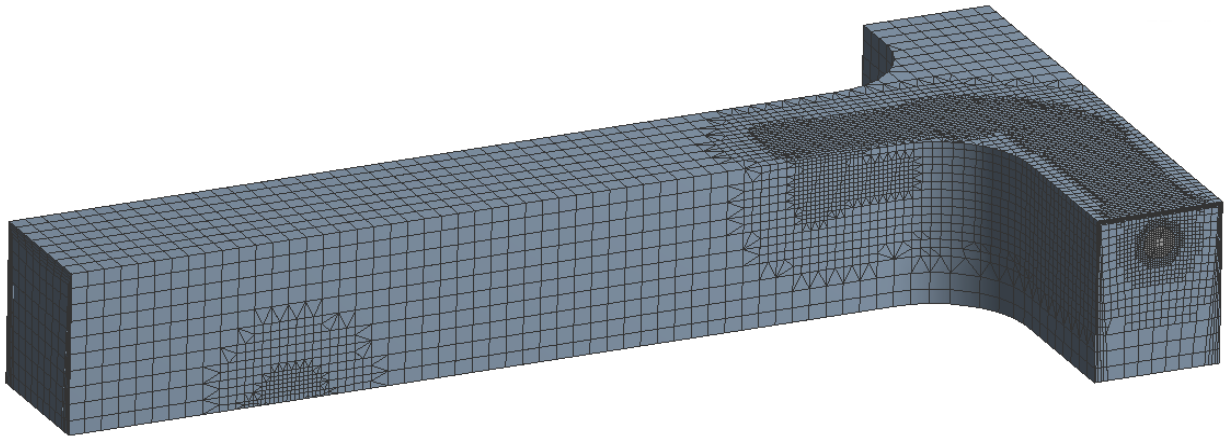

Fig. 3-15. 3D CFD model of EXP5 with the coarse mesh

The CFD model was created with ANSYS Workbench (ANSYS Inc., 2013b) 17.2. The geometry of the CFD model was established in DesignModeler, and the mesh was built in Meshing. The CutCell assembly meshing method (ANSYS Inc., 2013a) was applied. A mesh independence study was conducted to make sure the CFD results were independent of mesh sizes while saving computing time with a smaller mesh size. Inflation layers were created to take care of the low-

airflow zone near the wall (Feroze and Genc, 2016). Governing equations including mass, momentum, energy, species transport equations are solved in the CFD model. ANSYS Fluent was used as the CFD solver. The governing equations were solved by using the SIMPLE algorithm in ANSYS Fluent. The standard k-epsilon turbulence model (ANSYS Inc., 2009a) was used to model the turbulent flow in the flow domain. The boundary condition for the wall was no-slip stationary wall. A steady-state airflow simulation was conducted first with the DPM source turned off. After the airflow reached a steady-state, a transient simulation with the DPM source turned on was conducted to model the airflow and DPM concentration over time.

As shown in Fig. 3-14, the ventilation tubing was not located in the center of the heading. There was DPM coming from the upstream of the main drift. The DPM profile was adjusted from the raw data collected by the monitor at the main drift inlet and it has been applied to both the main drift inlet and the ventilation tubing inlet in the CFD model. Details of the boundary conditions are shown in Table 3-7. The temperature of the diesel exhaust from the DPM source was not measured in EXP5 and it was set to 594 K according to a study conducted by Zheng (2011). The remaining data shown in Table 3-7 was obtained from the ventilation survey.

Table 3-7. Boundary conditions

	Area (m^2)	Velocity (m/s)	DPM mass fraction	Temperature (K)
Ventilation tubing inlet	0.89	35.97	Varies over time as shown in Fig. 3-16	300
Main drift inlet	23.33	0.084	Varies over time as shown in Fig. 3-16	300
Outlet	Outflow boundary condition			
DPM source inlet	0.09	DPM and velocity profiles are shown in Fig. 3-17 and Fig. 3-18 respectively		594

The DPM concentration profile at the main drift inlet and at the ventilation tubing inlet are the same. The DPM data over time collected by the Airtec monitor at location A (shown in Fig. 3-4) is shown in Fig. 3-16.

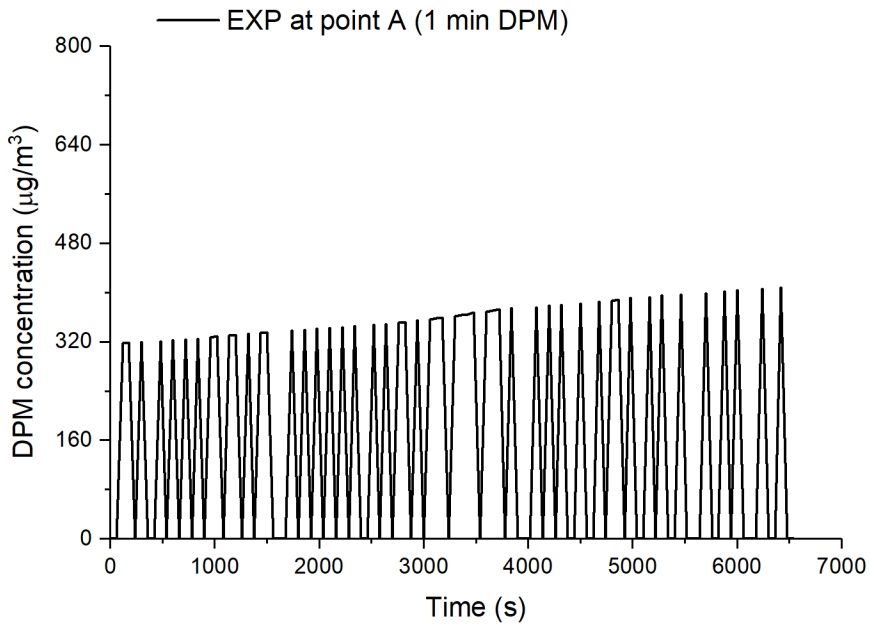

Fig. 3-16. DPM concentration distribution over time at location A from the experiment.

From Fig. 3-16, the average DPM concentration from upstream of the main drift inlet in EXP5 is calculated at 157 μg/m^3, which is high compared to the regulatory limit (160 μg/m^3) and consideration for the boundary conditions of the main drift inlet in the CFD model is required.

The DPM concentration and velocity of the diesel plume from the tailpipe were not measured in EXP5 and were obtained through trial-and-error. The DPM data measured by Zheng (2011) provided a starting point for the trial-and-error process. The velocity magnitude of 24.1 m/s measured by Zheng (2011) was used in this study. The DPM concentration profile and the velocity

profile over time for the DPM source are shown in Fig. 3-17 and Fig. 3-18, respectively. The DPM concentrations were applied to the CFD model as mass fractions.

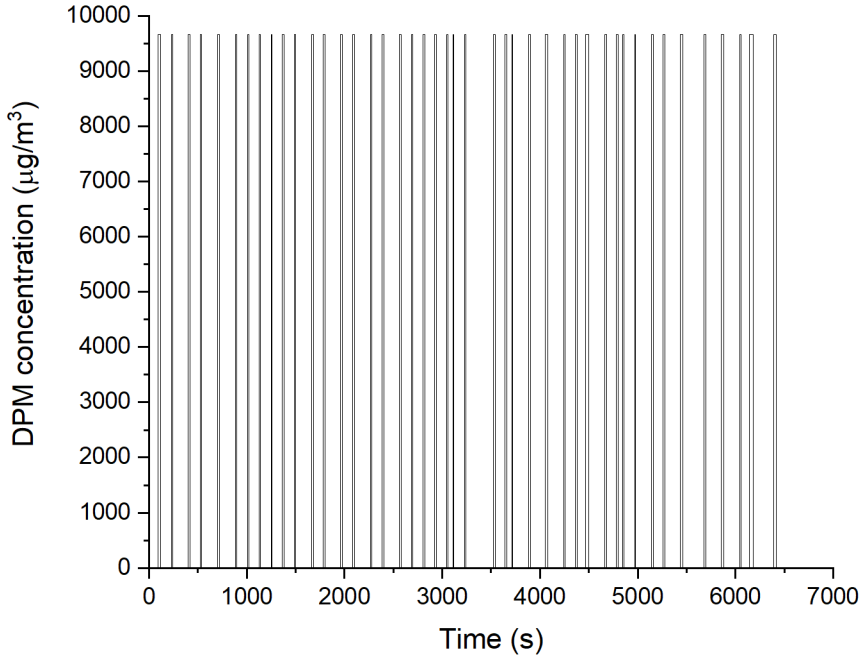

Fig. 3-17. DPM concentration (μg/m^3) profile over time at the DPM source in the CFD model

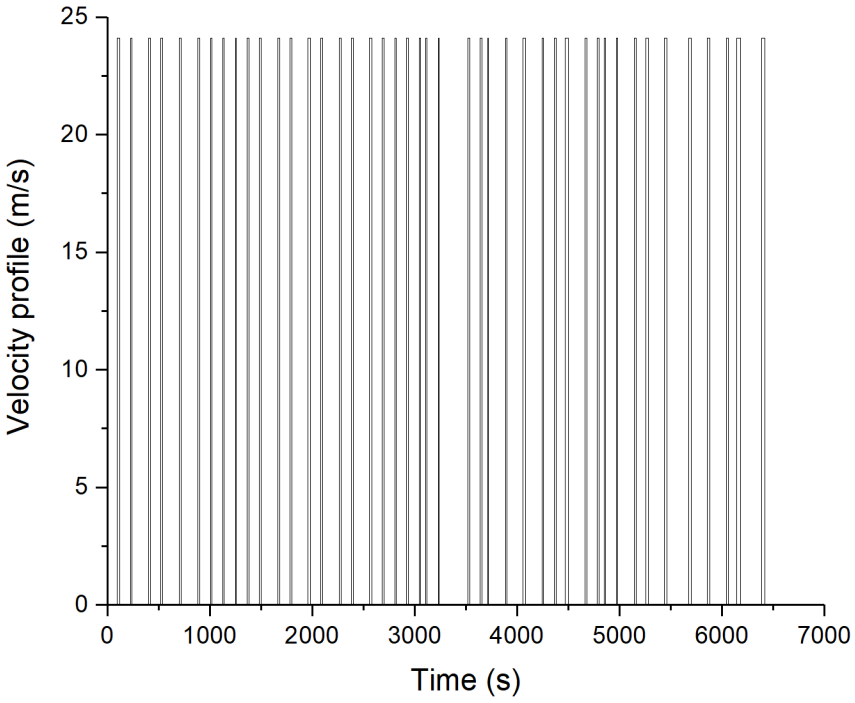

Fig. 3-18. Velocity (m/s) profile over time at the DPM source.

3.3.5 Mesh independence study for EXP5

Similar to EXP3, a mesh independence study was conducted for EXP5. Three meshes were generated. The total elements in the coarse mesh, medium mesh, and the fine meshes are 101,107, 153,858, and 272,953, respectively. From Fig. 3-19, two horizontal monitoring lines, located in the center of the cross-sectional areas at two locations, were created in the 3D CFD models with the three meshes, respectively.

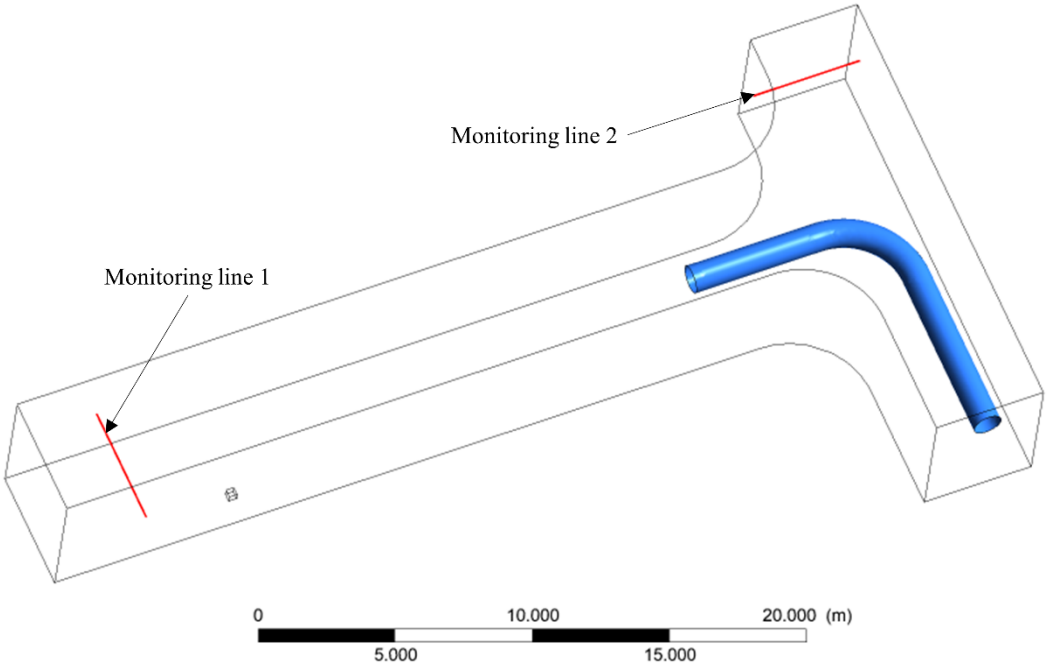

Fig. 3-19. Locations of the two monitoring lines in the CFD model of EXP5

The velocity magnitude of airflows along the two monitoring lines for each 3D CFD model was recorded. The results along the monitoring lines 1 and 2 from the three CFD models with the three meshes are shown in Fig. 3-20 and Fig. 3-21, respectively.

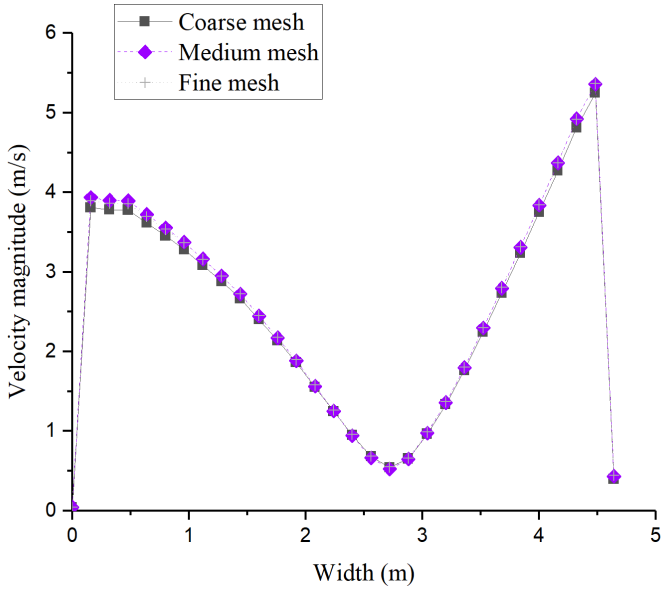

Fig. 3-20. Velocity magnitude profile comparisons along the monitoring line 1 in the CFD models with the three meshes.

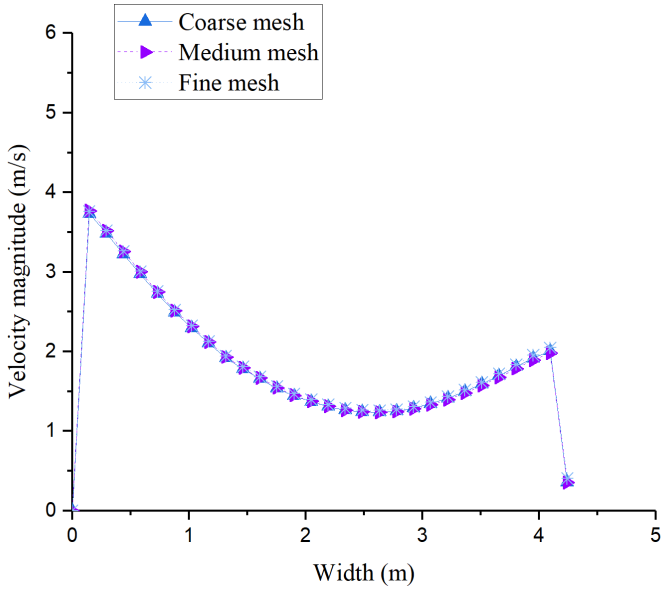

Fig. 3-21. Velocity magnitude profile comparisons along the monitoring line 2 in the CFD models with the three meshes.

From Fig. 3-20 and Fig. 3-21, the results from the CFD model with the coarse mesh indicate a good agreement with those results from the other two CFD models with the medium and fine meshes. Hence, the coarse mesh is selected for the CFD model of EXP5.

3.3.6 Results

EXP3 results

The results from the 3D CFD model are shown in the following figures. This model could have been conducted on a desktop computer, but HPC from SHARCNET (the Shared Hierarchical Academic Research Computing Network) (Bauer, 2007) was used to save time (e.g., more than 6 hours), and it took 2.9 hours to obtain the results.

Fig. 3-22, Fig. 3-23, and Fig. 3-24 present the DPM concentration comparisons over time between the experiment and the 3D CFD model at locations D (before the end of the ventilation tubing), C (the outlet), and E (close to the working face), respectively.

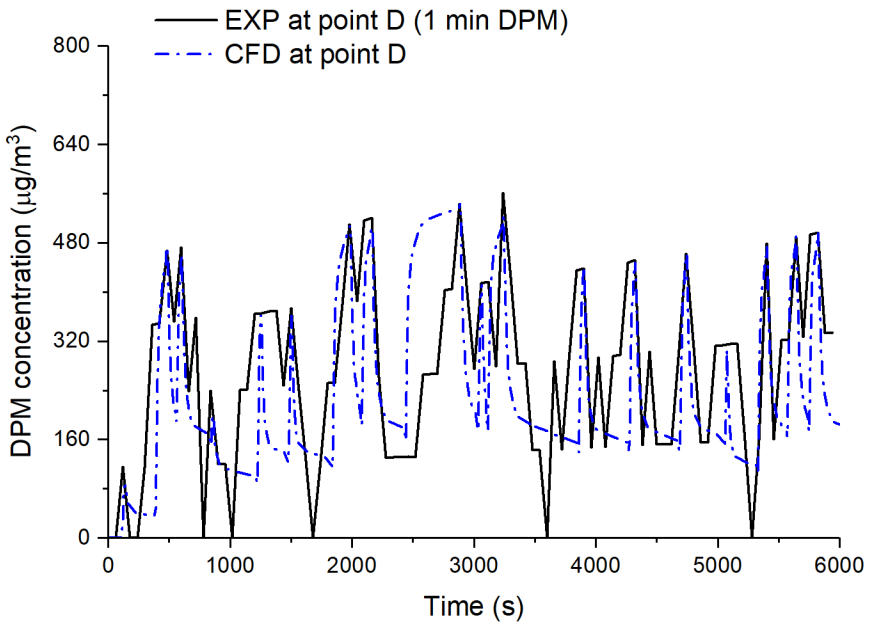

Fig. 3-22. Comparison of DPM concentrations over time at location D, between the 3D CFD model and the experiment. The DPM concentration profile from the CFD model matches well with the experiment.

Fig. 3-22 indicates that the results at location D from the CFD model match the experimental data well. To statistically compare the two data sets, the differences of the two data sets were calculated at first and the t-test (Ross and Willson, 2017) was then conducted on the differences. The p-value (Ross and Willson, 2017) was calculated as 0.021. The mean of the samples' differences is not significantly different from the test mean (0) under the significance level of 0.01, which means the two data sets are statistically comparable and have a good agreement.

The DPM data from the experiment consists of discrete values 0, 140, 280, 420, and 560 μg/m^3. Unlike the experimental data, in the CFD model, the DPM concentration is not restricted to discrete values and never falls to zero. It is also obvious that the DPM concentration would not change sharply in the heading because it takes time to dilute DPM. Instead, the DPM should be gradually

diluted. The data indicate that the DPM concentrations in the experiment could have errors in the range of 70 µg/m^3, which is within the author's expectation as mentioned in Section 3.2.1.

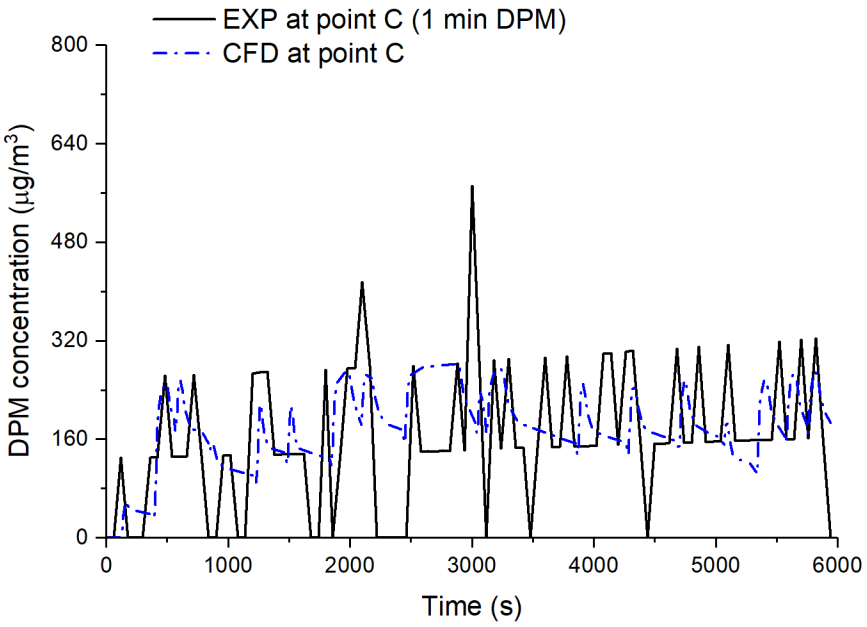

Fig. 3-23. Comparison of DPM concentration distributions over time at location C between the CFD model and the experiment. The main trend of the DPM concentration over time is captured by the CFD model.

Similarly, the DPM concentration trend at location C in the CFD model is a good match to the trend from the experiment as shown in Fig. 3-23. Considering the long duration of the period modeled, the results from the CFD model have a good agreement with that from the experiment. To statistically compare the two data sets, the differences of the two data sets were first calculated and a t-test was then conducted on the differences. The p-value was calculated as 0.094. The mean of the samples' differences is not significantly different from the test mean (0) under the significance level of 0.01, which means the two data sets are statistically comparable and have a

good agreement. There are two DPM concentration spikes over 400 µg/m^3 in the experiment, while the DPM concentration is always below 320 µg/m^3 in the CFD model.

For both the experiment and the CFD model, the DPM concentration at location C is lower than the DPM concentration at location D. This is expected because location C is near the outlet and there is additional fresh air coming from the inlet (location A in Fig. 3-2) to dilute the DPM.

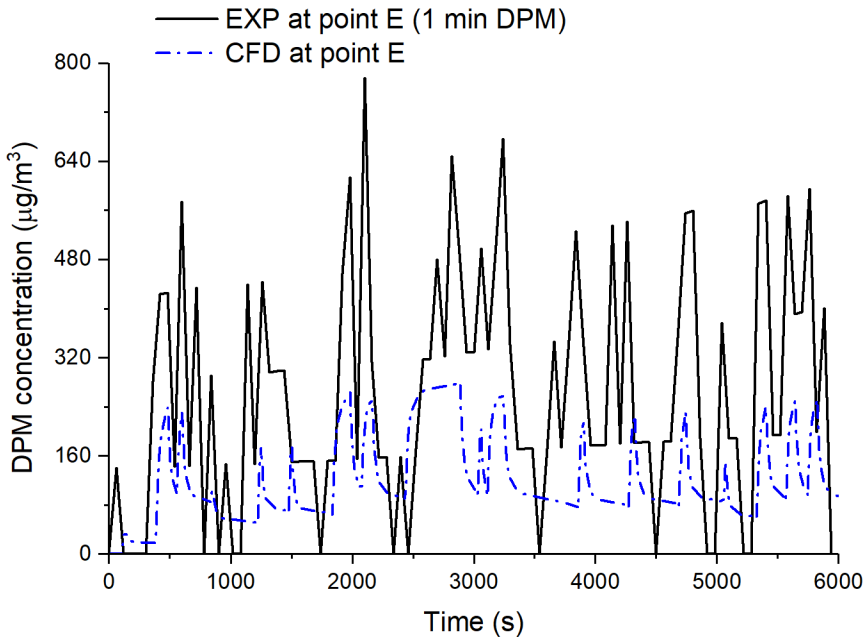

Fig. 3-24. Comparison of DPM concentration distributions over time at location E between the CFD model and the experiment. Magnitudes of the DPM concentration over time do not match well, but the trend matches.

As seen in Fig. 3-24, the trend of the DPM concentration at location E in the CFD model has a good agreement with that from the experiment. To statistically compare the two data sets, the differences of the two data sets were calculated first and the t-test was then conducted on the differences. The p-value was calculated as 7.583E-13. The mean of the samples' differences is

significantly different from the test mean (0) under the significance level of 0.01, which means the two data sets are not statistically comparable and do not have a good agreement. The DPM concentration peaks in the CFD model are far below those in the experiment. This may occur due to the turbulence at location E. Also, in the experiment, the DPM concentrations at location E are higher than the DPM concentrations at locations C and D, however, in the CFD model the DPM concentrations at location E are lower than those at locations C and D.

A summary of the results from the statistical analysis is shown in Table 3-8.

Table 3-8. Summary of the t-test results at the locations C, D, and E in EXP3

	Location C	Location D	Location E
P-value at the confidence level of 0.01	0.094	0.021	7.583E-13
Level of agreement between the CFD results and the experimental results	Good	Good	Bad

EXP5 results

Results from the EXP5 CFD model are compared with those from the experiment and are shown in the following figures. The t-test was not used for the result comparisons of EXP5. The reason is that the DPM concentration downstream was significantly affected by the DPM coming from the upstream as shown in Fig. 3-16. The t-test is too rigorous, and a different (referring to EXP3) approach was used to compare the results from the CFD model with the results from the experiment at locations B, C, and D. At first, linear fitted lines were established for both the CFD and experimental results. Then the differences (in percentage) of the two sets of fitted results were calculated. At last, the average difference was calculated, which represents how different the two data sets are.

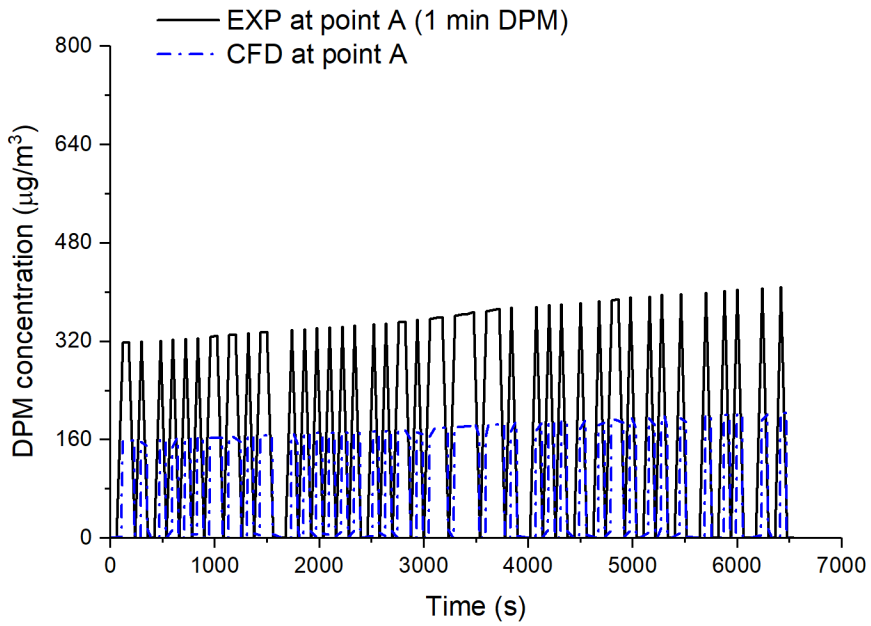

Fig. 3-25. Comparison of DPM concentration distributions over time at location A between the CFD model and the experiment.

It can be seen that the DPM data being applied in the CFD model is half of the raw DPM data. The reason is that the DPM raw data is monitoring point data and not monitoring plane average data. The Airtec monitor was installed on the back of the drift, and the DPM data recorded by the monitor cannot represent the DPM concentration at the cross-sectional area. In addition, the DPM concentration is the highest near the back of the drift because of buoyancy (Zheng *et al.*, 2017). Hence, the area-average DPM is smaller than the raw DPM data. The correction factor is assumed to be 0.5 (discussed in Section 3.3.1) in this study.

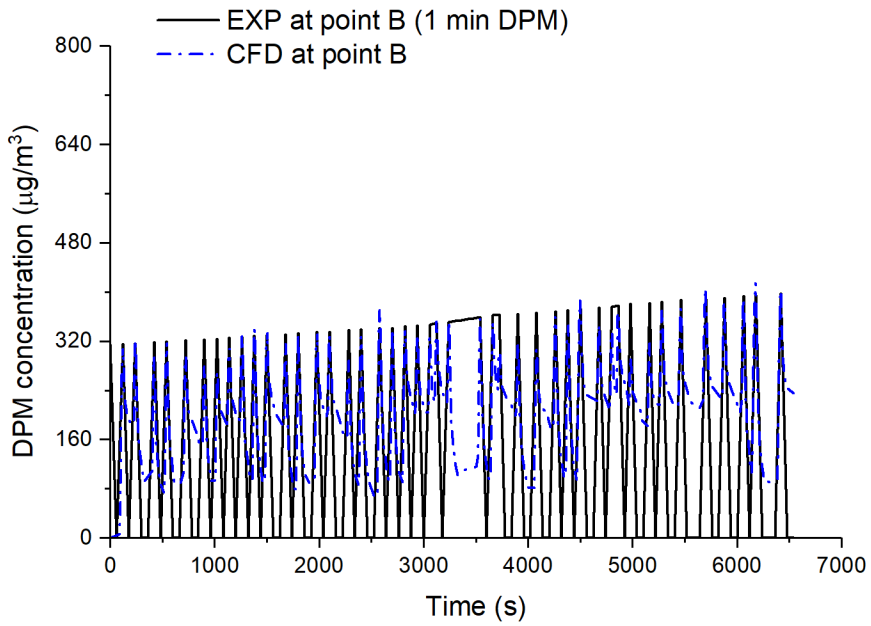

Fig. 3-26. Comparison of DPM concentration distributions over time at location B between the CFD model and the experiment.

It is seen from Fig. 3-26 that the results at location B from the CFD model match the experimental data well. By using the previously mentioned statistical approach, the average difference is calculated at 26.03%, which shows a 74% agreement between the CFD data and the experimental data over time. Considering the long duration of the period modeled and the significant amount of DPM from upstream, the results from the CFD model with a 74% accuracy are considered to be acceptable.

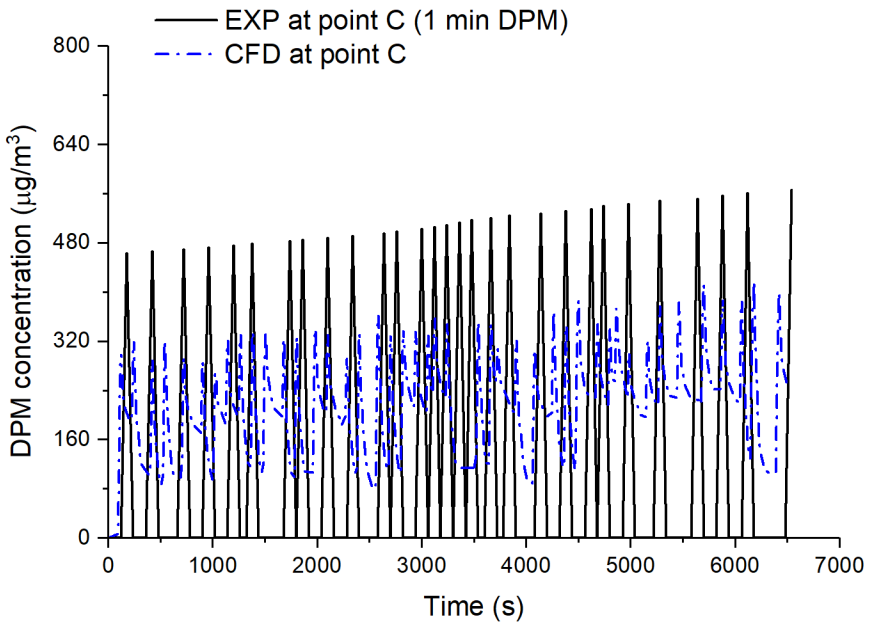

Fig. 3-27. Comparison of DPM concentration distributions over time at location C between the CFD model and the experiment.

The DPM concentration trend at location C in the CFD model matches the DPM concentration trend from the experiment as shown in Fig. 3-27. The DPM peaks from the CFD model are shorter than those from the experiment. By using the above mentioned statistical approach, the average difference is calculated at 54.47%, which shows a 46% agreement between the CFD and the experimental data over time. There are a couple of reasons for the discrepancy. The end of the ventilation tubing vibrated a lot when the EXP5 was conducted. In addition, there were open holes on the body of the tubing, which created leakage of airflow from the tubing to the ambient environment. The flow near the end of the tubing was complex and the Airtec monitor was installed at location C, which is near the complex flow area. Furthermore, the sensitivity of the Airtec monitor is more than 70 µg/m^3.

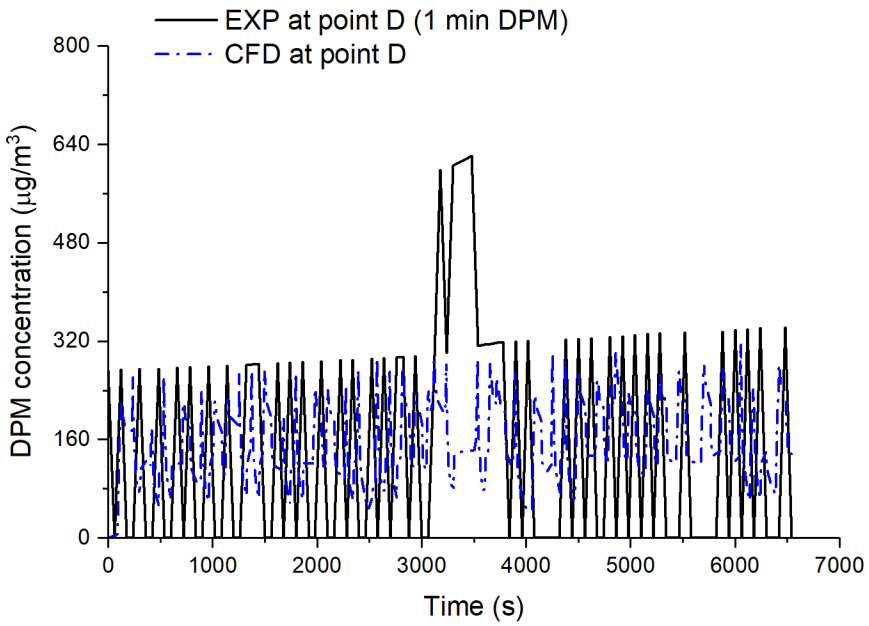

Fig. 3-28. Comparison of DPM concentration distributions over time at location D between the CFD model and the experiment.

As seen in Fig. 3-28, the trend of the DPM concentration at location D in the CFD model has a good agreement with the trend of the DPM concentration from the experiment. By using the previously mentioned statistical approach, the average difference is calculated at 7.06%, which shows a 93% agreement between the CFD and the experimental data over time.

A summary of the results from the statistical analysis is shown in Table 3-9.

Table 3-9. Summary of the average difference (%) between the CFD and experimental results at the locations B, C, and D in EXP5

	Location B	Location C	Location D
Average difference (%) between CFD results and experimental results	26.03	54.47	7.06
Level of agreement between the CFD results and the experimental results	Good	Bad	Good

3.3.7 Discussion (limitations)

For EXP3, there was no DPM coming from the upstream. Based on the statistical analysis, the CFD results have a good agreement with the experimental data at locations C and D. The CFD results did not match the experimental data very well at location E and it may be due to the air turbulence.

For EXP5, DPM coming from the upstream significantly affects the results at locations B, C, and D. A correction factor of 0.5 was used to convert the raw DPM data to area-average DPM data being applied to both the main drift inlet and the ventilation tubing inlet in the CFD model. A different statistical analysis was used to analyze the CFD results. As a result, the CFD results have a good agreement with the experimental data at locations B and D. The CFD results did not match the experimental data very well at location C.

For both CFD models of the EXP3 and EXP5, DPM concentration and velocity magnitude profiles at the DPM source were obtained through trial-and-error with reference data from Zheng (2011). Both the DPM concentration and the velocity magnitude were assumed to be constant when the diesel equipment was working.

This CFD approach has some limitations. The single DPM source does not move like real diesel equipment. The shape of the real diesel equipment is not modeled. Due to the limited number of Airtec monitors, only one monitoring point in the CFD model is created to be compared with the experimental data at each location. Because of the busy schedule at the mine site and for safety purposes, the author was not allowed to stay near the experiment areas to record the time and location of the diesel equipment. Hence, the cycle time of the equipment was estimated through

trial-and-error based on the equipment timeline reports. Together with the cycle time, the DPM concentration and velocity magnitude of the diesel exhaust were estimated with the reference data from Zheng (2011) in the trial-and-error process.

Regarding the accuracy and precision in the CFD modeling, accuracy refers to how close a measurement is to a true value, whereas precision refers to how consistent results are when measurements are repeated. Results from the CFD models are precise but may not be accurate. The reason is that the accuracy of the modeling results depends on the accuracy of the input data, which are based on the field data gathered. If the field data is not accurate, results from the CFD model will not be accurate. The results from the CFD models are precise compared with the field data because the CFD models can be calibrated by applying corresponding boundary conditions based on the field data.

3.3.8 Conclusion

Two DPM simulations of 99 min and 109 min were presented and discussed. According to the literature review, this is the first time that DPM simulations with this time length have been attempted. This was made possible mainly because of the reduced mesh size (with a single DPM source ignoring the shape effect of the LHD) with only one dead-end heading (other than the entire mine) in the CFD model. Also, the complexity of the flow domain was reduced by using the single DPM source and ignoring the shape of the LHD. As well, the DPM concentration and velocity magnitude of the diesel exhaust were kept constant in the proposed CFD approach. This further reduces the computing time compared with a CFD approach with changing DPM concentration and velocity magnitude of the diesel exhaust over time. Based on the results, the proposed CFD approach successfully models the DPM concentration over the defined periods of time. The DPM

profile over time, which is an essential input to the CFD model, was estimated based on the experimental data. For the same heading with the same equipment fleet and the same auxiliary fan speed, the fitted CFD model can be used to predict the DPM concentration distribution over time to assist the mine in preventing the formation of a high-DPM zone in the heading.

Compared with the approaches reported in Section 2.10, this approach is advantageous, especially with a larger experiment area and a longer time period. It is impossible and impractical to always have a 3D CFD model for modeling the shape and movement of the diesel equipment and transient simulations of the DPM over an hour for a whole mine ventilation system due to the enormous mesh size and the significant amount of time (e.g., days) required to build and solve the CFD model. This does not even account for the time required to update the CFD model with the mining advancement at different points of the LOM. The proposed CFD approach reduces the time required to build and solve the CFD model with the reduced mesh size and the simplified flow domain. This is an advantage over the previous CFD modeling approaches. The advantage will be more apparent when there are multiple mining areas with various diesel equipment employed. This CFD approach for DPM modeling is a part of a hybrid methodology, which aims to quickly and accurately model DPM over time. The idea of the hybrid methodology is to apply ventilation network modeling to an entire mine while applying the CFD modeling approach to the dead-end headings. The CFD results are used to update the DPM results from the ventilation network model at the shared locations. More details of the hybrid methodology are shown in Chapter 4. Hence, the time required to build and solve the CFD model is a significant factor to consider as part of the hybrid methodology. This study provides an important step to achieve the proposed hybrid methodology by reducing the computing time while keeping the accuracy of the results and to obtain more accurate input for the ventilation network model.

More experiments with more monitoring points from many locations are required to test the repeatability of this approach. Of course, the lags in DPM and velocity profiles will need to be recalculated for each experiment. In addition, the application of statistical analysis will still be required to quantify the confidence level of the CFD results compared with the experimental data.

3.4 Proposed DPM modeling approach using a ventilation network solver

A DPM modeling approach using a ventilation network solver is proposed. In this study, Ventsim is selected as the ventilation network solver because Ventsim is able to perform both static and dynamic DPM modeling and the author has a valid license. In this study, dynamic modeling of DPM is the focus.

Ventsim is a ventilation network solver with 3D graphics. The computing time of Ventsim is significantly shorter than that of CFD. One limitation of Ventsim is that it is not capable of creating monitoring points or DPM sources at locations across a cross-sectional area in the model. However, the DPM concentration data collected in the field is usually the data recorded by a real-time DPM monitor installed at a location of a cross-sectional area in an underground mine. Ventilation engineers use the data to determine if the DPM concentration is over the regulatory limit, in which case measures will be taken to reduce the DPM concentration. Another use of the data is for predicting the DPM concentration at other locations within the mine by conducting a DPM simulation in Ventsim.

The number of real-time DPM monitors is usually limited at mine sites, and usually only one monitor is installed at one location in a drift. Furthermore, the data from the real-time DPM monitor is used as input in a Ventsim model. However, the DPM data from the real-time monitors

at each location cannot represent the area-average DPM data across the cross-sectional area because the DPM data is from one monitor rather than from the average data from multiple monitors at the same location. This means the DPM data from the DPM monitors will have to be applied to the Ventsim model with a correction factor, which changes under different situations.

According to the gas concentration equation shown in Section 4.5.1 in McPherson (2009) and the equation for total engine out emissions (Saseen, 2007), the DPM concentration calculation in Ventsim is derived and expressed in the following Eq. (3-3). The DPM concentration is calculated based on the engine power (kW) of diesel equipment, the diesel emission rate (g/kW·h), and the air volume (m^3/s).

$$\text{DPM concentration } (\mu g/m^3) = \frac{\text{engine power (kW)} \times \text{diesel emission rate } (\frac{g}{kW \cdot h}) \times \frac{1h}{3600s}}{\text{air volume } (\frac{m^3}{s})} \times \frac{10^6 \mu g}{1g} \qquad (3\text{-}3)$$

In Ventsim, engine power and diesel emission rate are two user inputs for the DPM source(s) in dynamic DPM modeling. If the DPM concentration data is recorded by a real-time DPM monitor and the engine power of diesel equipment is known, the diesel emission rate can be calculated using Eq. (3-3). For the DPM data over time (dynamic DPM modeling), the diesel emission rates at each period of time can be calculated and entered into the Ventsim model.

Another alternative for DPM modeling in Ventsim is to measure the diesel emission rates from the diesel exhaust pipe. The diesel emission rate is not constant over time because the diesel equipment is not always operating under the same conditions (e.g., idling, working, traveling uphill or downhill).

According to Eq. (3-3), with known diesel power and measured diesel emission rates over time, the DPM concentration can be calculated and input to the DPM source in the Ventsim model. However, complex procedure and analysis are required to accurately measure the diesel emission rates for each type of diesel engine. Hence, it is not practical to conduct such measurements in an operating mine.

As a result, collecting DPM data from real-time DPM monitors, converting the data to diesel emission rates over time, and applying the calculated diesel emission rates together with a known diesel engine power to a DPM source are the steps proposed to be followed for conducting a DPM simulation in Ventsim.

3.4.1 Model setup

The layout and some of the ventilation survey data of EXP3 were used to demonstrate the proposed DPM modeling approach in Ventsim. Two modeling approaches were created to show the application:

> Modeling approach 1: An LHD mucks near the working face for 90 min and the diesel emission rate from the exhaust pipe varies over the 90 min period.
>
> Modeling approach 2: Using the data collected from the DPM monitor at the outlet in the Ventsim model from scenario 1 and updating the downstream DPM profile over time.

Ventsim models for the two modeling approaches are shown in Fig. 3-29 and Fig. 3-30, respectively.

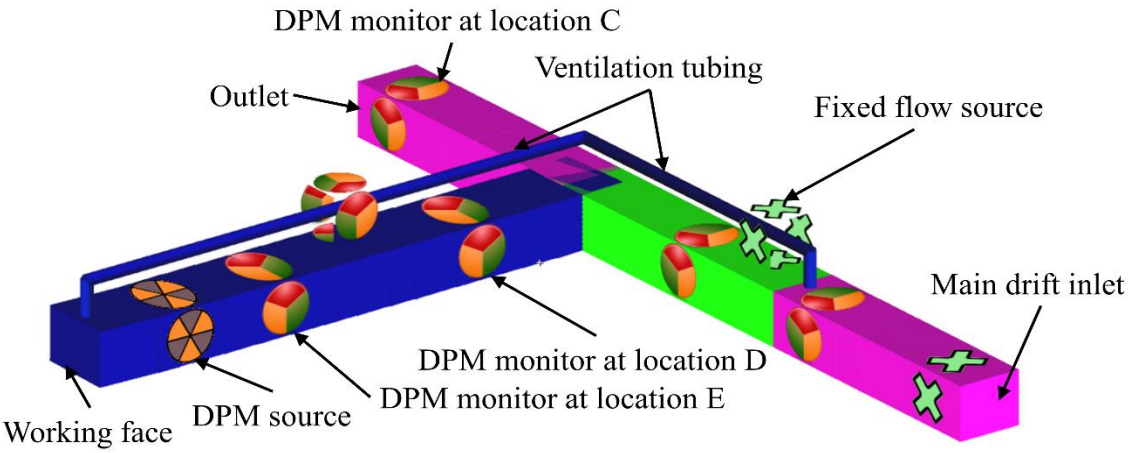

Fig. 3-29. Ventsim model for scenario 1

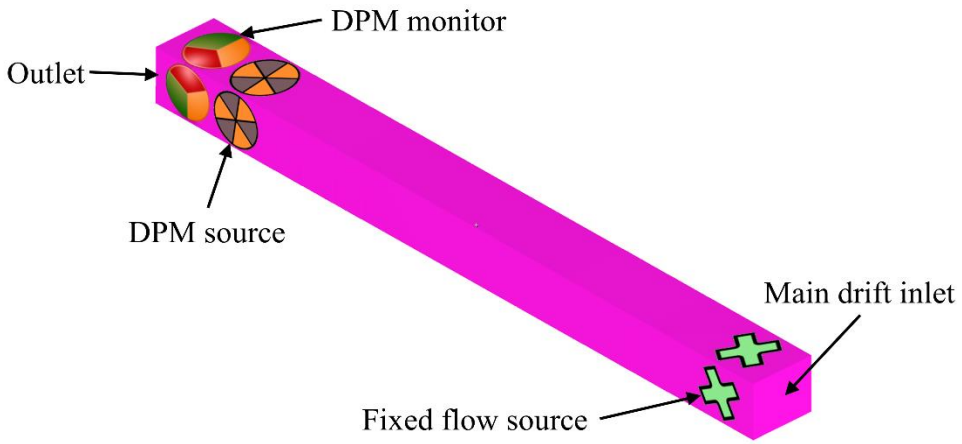

Fig. 3-30. Ventsim model for scenario 2

The purpose of modeling approach 1 was to provide a DPM modeling approach in Ventsim when parameters of a DPM source (including the diesel power and diesel emission rate profiles over time) were known. From Fig. 3-29, the DPM source represents an LHD working near the working face. A ventilation tubing was installed to provide the fresh air to the dead-end heading. Three DPM monitors were placed at three locations in the Ventsim model to record the DPM concentration over time.

The purpose of modeling approach 2 was to provide a similar DPM modeling approach in Ventsim when the number of DPM monitors at a mine site is limited (e.g., only one near the outlet) and an LHD is working near the working face. Compared to Fig. 3-29, there is no ventilation tubing and dead-end heading in Fig. 3-30. Besides, the DPM source is near the outlet rather than at the end of the heading.

3.4.2 Assumptions

For modeling approach 1, assumptions made on the diesel power and diesel emission rate profiles over the 90 min are shown in Table 3-10.

Table 3-10. Diesel power and diesel emission rate profiles of the DPM source in the Ventsim model for modeling approach 1

From (min)	To (min)	Diesel power (kW)	Diesel emission rate (g/kW·h)
0	30	200	0.1
30	60		0.3
60	90		0.2

There are three time periods and the diesel emission rate from the DPM source varies in the three periods. The air volume from the main drift is 87 m^3/s and the air volume drawn into the ventilation tubing is 32.2 m^3/s.

For modeling approach 2, the total air volume in the main drift is 87 m^3/s. The DPM data ($\mu g/m^3$) recorded at location C in scenario 1 is used at the diesel input to the DPM source in modeling approach 2. With a constant diesel power of 200 kW over time, DPM results ($\mu g/m^3$) from the outlet in modeling approach 1 are converted to equivalent diesel emission rates over time by using Eq. (3-3). The diesel emission rates together with the constant diesel power make up the input of the DPM source in modeling approach 2. The DPM monitor behind the DPM source in Fig. 3-30

is used to verify if the DPM generated by the DPM source in modeling approach 2 match the DPM at location C in modeling approach 1. An example of how the DPM results at location C in modeling approach 1 are converted to the input of the DPM source in modeling approach 2 is shown in Table 3-11.

Table 3-11. An example of DPM data conversion for modeling approach 2

Results from modeling approach 1		Input to modeling approach 2					
Flow time (s)	DPM (μg/m^3) data at location C in scenario 1	Air volume (m^3/s)	Diesel power (kW)	Calculated equivalent diesel emission rate (g/kW·h)	From (s)	To (s)	Average diesel emission rate (g/kW·h)
0	0	87	200	0	-	-	-
10	0			0.00	0	10	0.00
20	0.00			0.00	10	20	0.00
30	0.00			0.00	20	30	0.00
40	0.00			0.00	30	40	0.00
50	0.00			0.00	40	50	0.00
60	48.72			0.08	50	60	0.04
70	64.95			0.10	60	70	0.09
80	64.95			0.10	70	80	0.10
90	64.95			0.10	80	90	0.10
100	64.95			0.10	90	100	0.10

As mentioned in modeling approach 1, the total modeling time is 90 min (5,400 s) and only the DPM results from the first 100 s are converted to diesel input of the DPM source in modeling approach 2 as shown in Table 3-11. The DPM results from modeling approach 1 are recorded every second, which means there are 5,400 DPM data points at each monitor in modeling approach 1. However, not all of these data points can be entered into the DPM source in modeling approach 2 because of the data entry limit (maximum 250 different types of data points) in Ventsim. Hence, the DPM data at every 10 s is filtered out from modeling approach 1, which reduces the total DPM data size from 5,400 to 540.

With known air volume and diesel power, the DPM results from modeling approach 1 in Table 3-11 can be converted to equivalent diesel emission rates based on Eq. (3-3). In Ventsim, the diesel emission rate and diesel power data have to be entered based on periods of time (the length of the periods can vary) for dynamic DPM modeling. In this case, one time-period is 10 s and there are 540 periods. For example, the sixth period in modeling approach 2 is from 50 s to 60 s and the diesel emission rate is 0.04 g/kW·h, which is the average of the equivalent diesel emission rates (0 at 50 s and 0.08 g/kW·h at 60 s).

3.4.3 Results

DPM results from modeling approaches 1 and 2 are shown in Fig. 3-31 and Fig. 3-32, respectively. Computing time for both the scenarios is within 5 s.

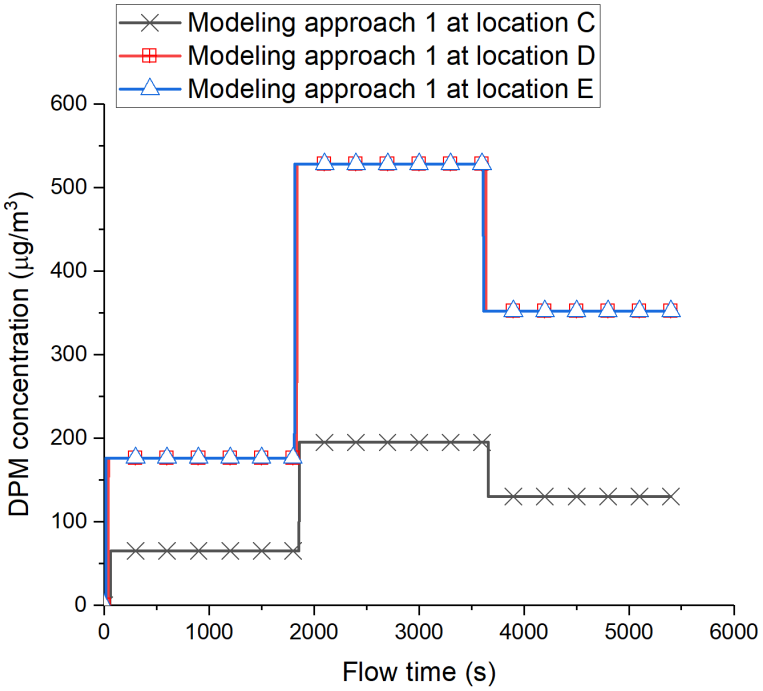

Fig. 3-31. DPM concentration profiles over time recorded by the three DPM monitors in the Ventsim model of modeling approach 1

From Fig. 3-31, the DPM concentration over time at locations D and E are almost the same. Because location E is much closer to the DPM source than location D, the DPM monitor at location E detects DPM quicker than the monitor at location D. Besides, it can be seen that the DPM concentration at locations D and E is greater than the DPM concentration at location C. This is because the air volume at location C is greater than the air volume at the other two locations, which results in more DPM dilution at location C. Furthermore, the DPM data at locations C, D and E in Fig. 3-31 is proportional to the diesel emission rates in Table 3-10.

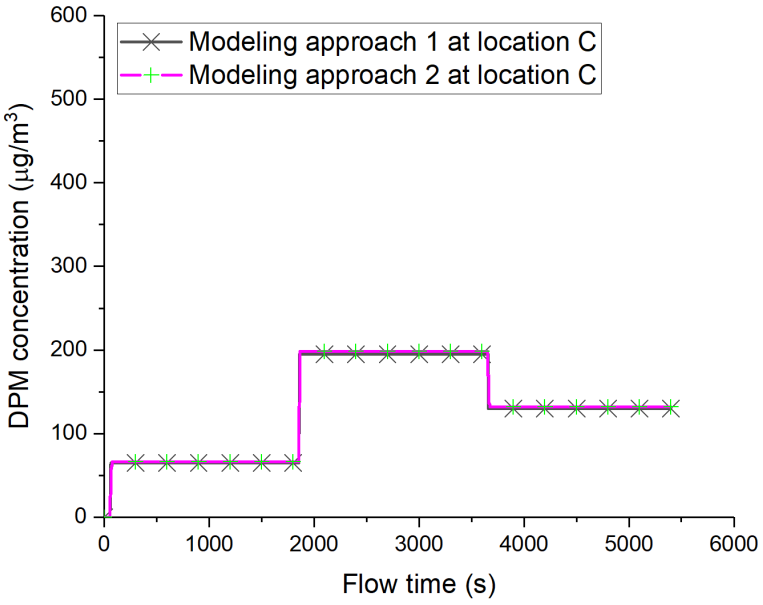

Fig. 3-32. DPM concentration profiles over time recorded by the three DPM monitors in the Ventsim model of modeling approach 2

Table 3-12. Result comparisons at location C in the two modeling approaches

Time (s)	DPM concentration (µg/m^3) from modeling approach 1	DPM concentration (µg/m^3) from modeling approach 2	Error (%)
614	64.95	66.07	1.71
2143	194.86	198.20	1.71
4522	129.91	132.13	1.71

Eq. (3-4) shows how the error was calculated in Table 3-12.

$$\text{Error} = \frac{|\text{DPM data from modeling approach 2-DPM data from modeling approach 1}|}{\text{DPM data from modeling approach 1}} \times 100\% \qquad (3\text{-}4)$$

As mentioned, the DPM data from modeling approach 1 is converted to the equivalent diesel emission rates, which are then applied to modeling approach 2 as input. From Fig. 3-32, the DPM data over time at the outlet from modeling approach 2 match the DPM data at the same location from modeling approach 1.

Three sampling points are taken from the two scenarios shown in Fig. 3-32 and they are compared in Table 3-12. It can be seen that the results from the two modeling approaches are within a 2% error. One reason for the error is that not all the DPM data from modeling approach 1 is converted due to the limit of data entry in Ventsim. The other reason is that the equivalent diesel emission data (shown in Table 3-11) is averaged over the time periods. Nevertheless, the DPM data from modeling approach 2 with a 2% error is considered acceptable.

3.4.4 Discussion (limitations)

Because Ventsim is a network model, monitoring points cannot be created at any location across a cross-sectional area. If the air volumes and DPM sources are the same at two locations, DPM concentration at the two locations will be the same, for instance, the DPM data at locations D and E in modeling approach 1. However, the results can be different with two real-time DPM monitors installed at a point at two locations at the mine site.

The limit of the number of data entries for the DPM source in Ventsim makes it hard to completely convert all the DPM data from either a model or an experiment to equivalent diesel emission rates and to apply the rates as input for a DPM source in a Ventsim model. As a result, the DPM data needs to be either filtered or averaged to reduce the number of data entries. Hence, there will be discrepancies between the DPM results (for instance, the 2% error on the DPM results from modeling approach 2).

The DPM data collected by the real-time monitors from EXP3 is not used in both the modeling approaches. The reason is that the real-time monitors were installed on the back of the drift at different locations in EXP3 and each location only had one monitor. Hence, correction factors

need to be applied to the DPM data to convert the monitoring point data to monitoring plane data. The factors vary under different flow conditions. With more assumptions on boundary conditions applied to the Ventsim model and on the collected DPM data from EXP3, a Ventsim model can be built and result comparisons can be carried out.

3.4.5 Conclusion

A DPM modeling approach using a ventilation network solver, which in this research work is Ventsim, is proposed. The accuracy of the DPM results from the Ventsim model mainly depends on the diesel power and diesel emission rate input. Two modeling approaches are presented. Modeling approach 1 presents an LHD mucking at the working face with known diesel power and diesel emission rate profiles over time. Modeling approach 2 presents how DPM data ($\mu g/m^3$) over time from a heading can be converted to equivalent diesel emission rates ($g/kW \cdot h$) over time, which are then entered into a Ventsim model to update the downstream DPM data. Computing time for both the two modeling approaches (with 90 min dynamic DPM modeling) is within 5 s.

The DPM results at three locations in modeling approach 1 use Eq. (3-3) to handle DPM concentration calculation in Ventsim. The results from modeling approach 2 show that DPM data generated by diesel equipment in a heading can be inserted to a location downstream with correct settings in Ventsim. Thus, the Ventsim model can be simplified but still produce high-accuracy results with reliable diesel input to the model.

As mentioned, the reliable diesel input, which refers to the area-average DPM concentration over time from a number of DPM monitors or the diesel emission rates over time from a DPM source in Ventsim, can be obtained either with sufficient real-time DPM monitors across cross-sectional

areas at different locations in an underground mine or by following a complex procedure to measure the diesel emission rates over time in a laboratory. Both processes are hard to follow at a mine site because the number of real-time DPM monitors is usually limited and the busy mine schedules make it hard to leave diesel equipment being tested and measured in a laboratory. Hence, another way of gathering reliable or improved diesel input to a ventilation network solver is required. A hybrid methodology is proposed in Chapter 4 to provide improved diesel input for DPM modeling in a ventilation network solver.

3.5 A Comparison of two numerical modeling approaches (CFD and a ventilation network solver) for DPM distribution over an hour in underground mines

As far as the author knows, no publications have been found on dynamic DPM modeling by using a mine ventilation network solver. There are few publications indicating DPM simulation in a ventilation network solver, but access to these publications is limited (e.g., membership restrictions). In addition, the abstracts of these publications indicate that no dynamic DPM modeling has been carried out. Hence, a DPM modeling technique using a ventilation network solver is proposed. The purpose is to compare the DPM results from the ventilation network model to the DPM results from the 3D CFD model.

The modeling time was 99 min and 109 min for EXP3 and EXP5, respectively. Several structured cycle times of diesel equipment were proposed based on the equipment timeline report. From Fig. 3-22 to Fig. 3-28, the cycle time of the LHD in both the experiments varied over time. Here, the cycle time is considered constant, which means the duration of diesel equipment in and out of the

heading is fixed in each cycle. The cycle repeats one after another throughout the 99 min and 109 min periods.

The DPM concentration and velocity profiles from the fitted CFD models of EXP3 and EXP5 in Section 3.3 were applied to the CFD model in this section. Results from DPM monitoring points in the CFD model with the proposed structured cycle times were compared with the experimental data through statistical analysis. The cycle time with the best agreement with the experimental data was chosen as the standard cycle time for the CFD model in this study. The CFD model with the standard cycle time was treated as the calibrated CFD model. The standard cycle time of the DPM source in both the EXP3 and EXP5 was 11 min with 3 min in the heading and 8 min out of the heading. Seven structured cycle times were proposed and details of how the standard cycle time was determined are shown in Chapter 4.

With the same cycle time, a transient DPM simulation can be carried out in the ventilation network solver. Ventsim was selected as the ventilation network solver because it is able to perform both steady-state and dynamic DPM modeling (Chasm Consulting, 2016) and it has been widely used in the mining industry as discussed in Section 2.1. The software was also accessible to the author.

Monitoring planes were built in the CFD models at locations C, D, and E in EXP3 and the locations B, C, and D in EXP5 to record the area-average DPM data over time. The DPM data were compared with the results from the ventilation network models. The reason was that monitoring points could not be created in Ventsim and only area-average DPM data is available in Ventsim. The structured cycle time was used in both the CFD model and the ventilation network model for better comparisons in order to minimize the inconsistent cycle times over time. The accuracy and efficiency (time to solve the ventilation network) of the two approaches were analyzed. It was

found that the ventilation network model requires accurate diesel emission rate input, which is not easy to estimate and assumptions are made in order to obtain accurate DPM results. The CFD approach could provide better input for the ventilation network approach, but it takes a longer time to calculate the results.

3.5.1 Assumptions

When the diesel equipment is in the heading, the DPM concentration and velocity magnitude of the diesel exhaust obtained from the following Section 3.5.2 represent the average diesel emission rate considering the diesel equipment trams into the heading, mucks (loads its bucket), and trams out of the heading.

In the ventilation network model, the diesel exhaust is well-mixed with the air at the outlet in the experiment area. The DPM data recorded by the DPM monitor on the back of the drift at the outlet is used as the area-average DPM data at the cross-sectional area. The non-zero DPM data recorded in both the EXP3 and EXP5 during the 99 min and 109 min periods are averaged, and the two average DPM datasets were used to calculate the equivalent diesel emission rates of the DPM sources in both the ventilation network models.

3.5.2 DPM modeling in a ventilation network solver

In this study, Ventsim was chosen as the ventilation network solver, and the DPM modeling was conducted in Ventsim. Results from the Ventsim model were compared with the results from the CFD model. As mentioned, the structured cycle time was applied to both the Ventsim model and the CFD model. With a structured cycle time, it is easier to find the differences between the results from the CFD and the Ventsim models.

EXP3

A 3D view of the Ventsim model is shown in Fig. 3-33. The Ventsim model shown in Fig. 3-33 presents a conventional way to build the ventilation tubing, which was built all the way to the end of the heading.

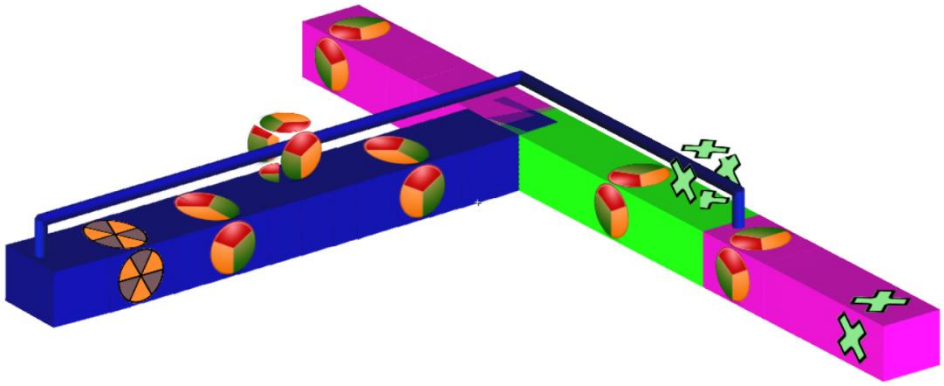

Fig. 3-33. 3D view of the EXP3 Ventsim model.

Several DPM monitors were created at the fresh air intake, return, on the tubing, and along the heading, to record the DPM over time. The fixed flow was used in the model to provide the air volume in the network. The DPM source was placed near the end of the heading as to where it was in the 3D CFD model.

According to the DPM data at location C from the experiment, the average of the non-zero DPM data over the 99 min was calculated at 202.32 μg/m^3. According to the assumption, this average DPM concentration was used as the area-average DPM at location C in the Ventsim model. With an air volume of 87 m^3/s in the drift and with the diesel engine power of 200 kW (Caterpillar.Inc, 2011), the diesel emission rate was calculated at 0.32 g/kW·h. This diesel emission rate was used as the base emission rate in the following Ventsim models and it has been adjusted to match the CFD results.

Fig. 3-34 shows the diesel power profile over time. When the LHD is in the heading, the diesel power is 200 kW. When it is out of the heading, the diesel power is zero (0) kW because there were no DPM sources in the heading anymore.

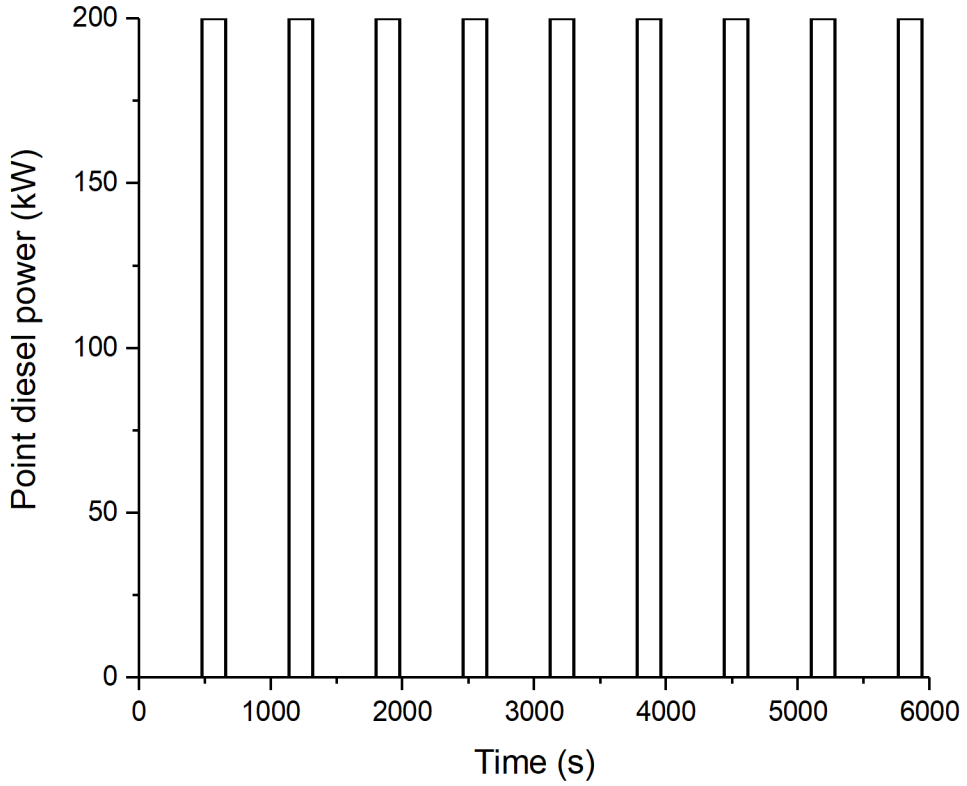

Fig. 3-34. Point diesel power (kW) profile over time at the DPM source in the EXP3 Ventsim model.

The DPM simulation was carried out by using Multi Sim (Chasm Consulting, 2016) with airflow and diesel simulations in the Ventsim model. Heat sources with zero (0) kW and 200 kW diesel power, and diesel emission rate (i.e., 0.32 g/kW·h) were created in the model. VentFIRE (Chasm Consulting, 2016) was used to apply the diesel power profile over time into the DPM simulation. It took less than 10 seconds of computation for the results from this transient DPM simulation in the Ventsim model.

EXP5

A 3D view of the Ventsim model is shown in Fig. 3-35. The Ventsim model shown in Fig. 3-35 presents a conventional way to build the ventilation tubing, which was built all the way to the end of the heading.

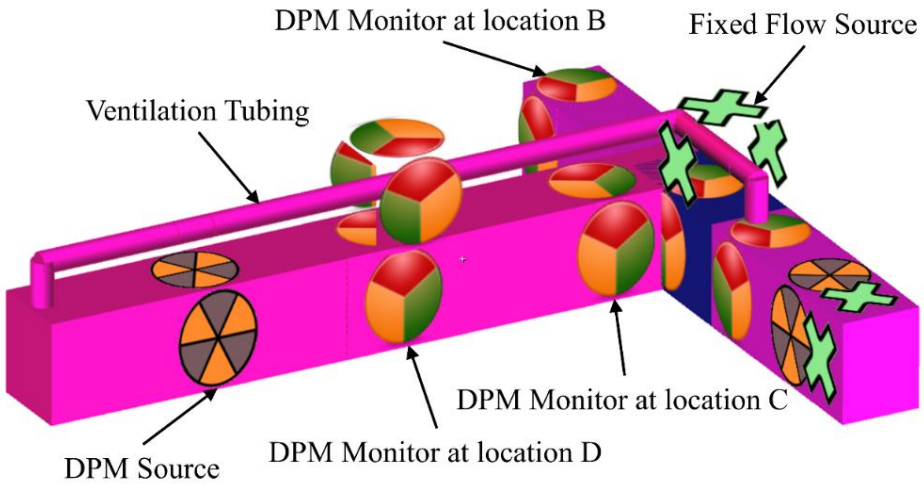

Fig. 3-35. 3D view of the EXP5 Ventsim model.

It can be seen that there are two DPM sources in the Ventsim model. One is near the inlet side, and the other one is near the end of the working face. This is because DPM from the upstream does have a significant influence on the downstream DPM concentration in the experiment area.

According to the DPM data at location B from the experiment, the average of the non-zero DPM data over the 109 min was calculated at 352.37 μg/m^3. With an air volume of 33.17 m^3/s in the drift and diesel engine power of 200 kW (Caterpillar.Inc, 2011), the diesel emission rate was calculated at 0.21 g/kW·h. This diesel emission rate was used as the base emission rate in the following Ventsim models and it has been adjusted to match the CFD results.

Fig. 3-36 shows the diesel power profile over time, for the DPM source near the working face. When the LHD is in the heading, the diesel power is 200 kW. When it is out of the heading, the diesel power is zero (0) kW because there were no DPM sources in the heading anymore.

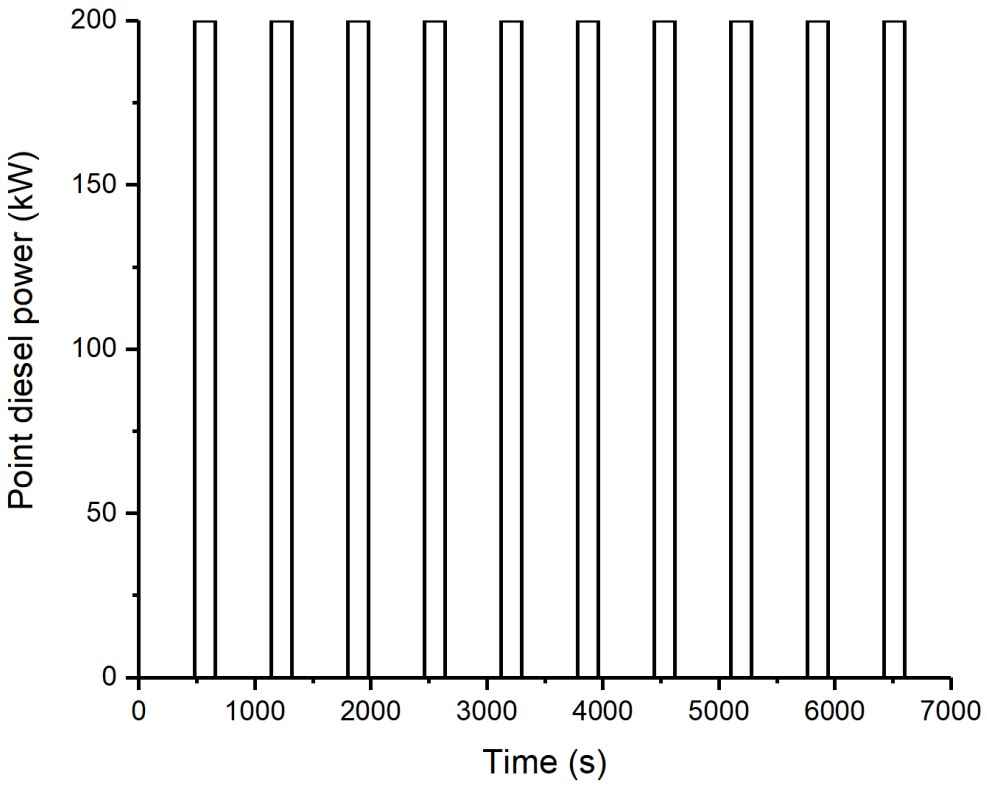

Fig. 3-36. Point diesel power (kW) profile over time at the DPM source in the EXP5 Ventsim model.

The upstream DPM concentration profile shown in Fig. 3-16 has been converted to equivalent diesel emission rate with a 200 kW diesel engine power by using Eq. (3-3). The equivalent diesel emission rate profile is shown in Fig. 3-37.

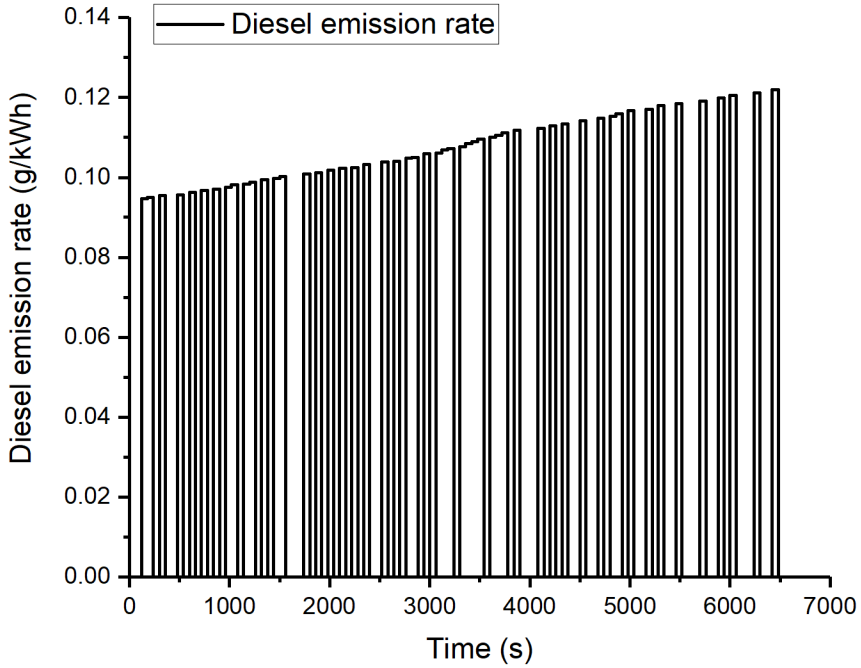

Fig. 3-37. Equivalent diesel emission rate profile from the upstream in the Ventsim model.

3.5.3 DPM modeling in CFD

EXP3

In the CFD model, the DPM concentration (shown in Fig. 3-38) and the velocity (shown in Fig. 3-39) profiles applied to the DPM source were similar to those shown in Fig. 3-8 and Fig. 3-9. Because the CFD model in Section 3.3.2 has been fitted with the experimental data, this CFD model uses the same boundary conditions except for the fixed cycle time. This CFD model is also considered as a (close to) calibrated model.

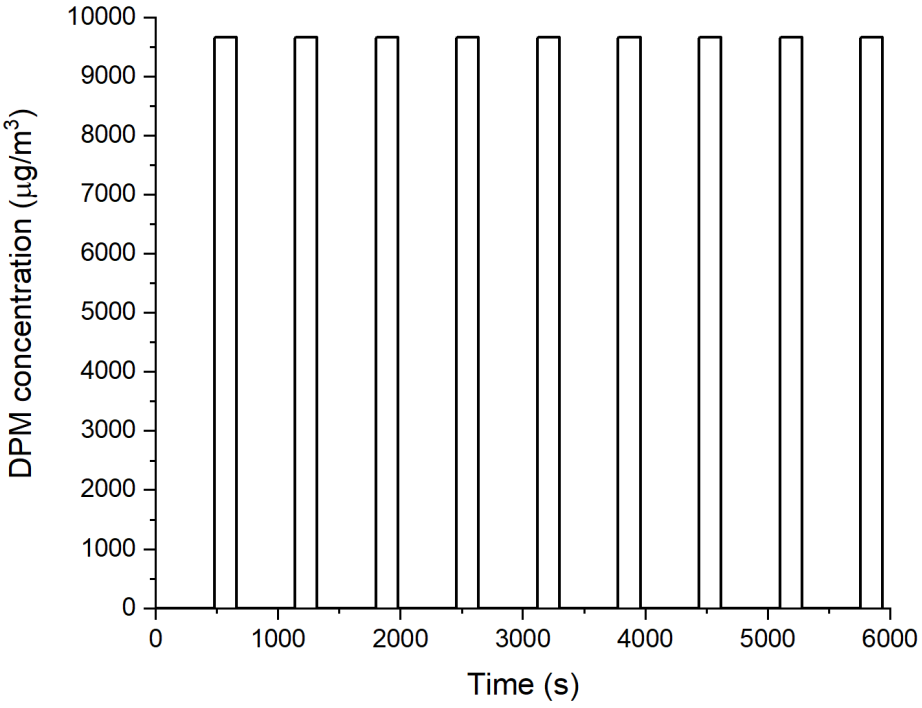

Fig. 3-38. DPM concentration (μg/m^3) profile over time at the DPM source in the CFD model.

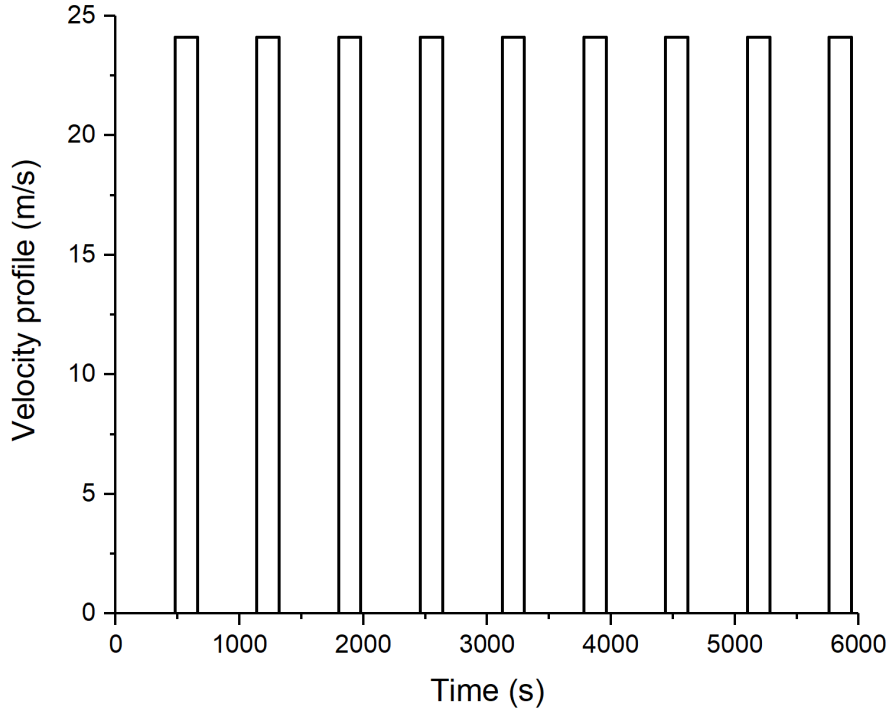

Fig. 3-39. Velocity (m/s) profile over time at the DPM source in the CFD model.

The CFD model is the same as the CFD model shown in Fig. 3-5. The boundary conditions in this CFD model are almost the same as those shown in Table 3-6 except for the applied DPM concentration and velocity magnitude profiles (as shown in Fig. 3-38 and Fig. 3-39 respectively) at the DPM source inlet. Steady-state simulation of airflow was first conducted in the CFD model. Then a transient simulation with turned on DPM source was carried out. It took less than 2 hours for the results from this transient DPM simulation in the CFD model with the use of a High-Performance Computer (HPC). If this model was executed in a laptop, it would have taken 8 to 10 hours for the calculation of the results.

EXP5

The DPM concentration and velocity profiles applied to the DPM source are shown in Fig. 3-40 and Fig. 3-41, respectively. The upstream DPM profile (shown in Fig. 3-16) was used in the CFD model as well. Because the CFD model in Section 3.3.2 has been fitted with the experimental data, this CFD model uses the same boundary conditions except for the fixed cycle time. This CFD model is also considered as a (close to) calibrated model.

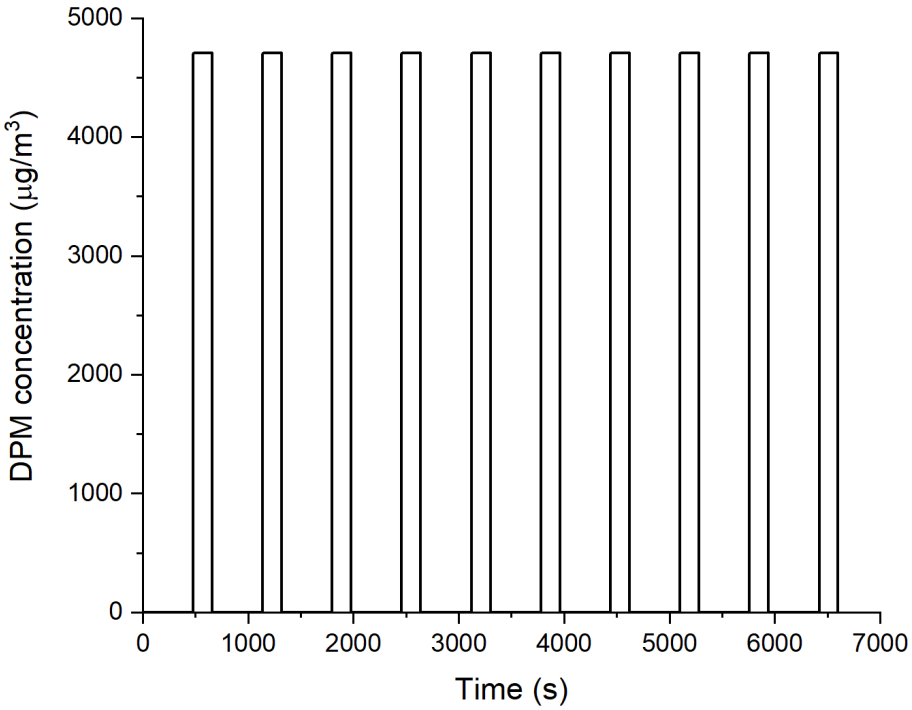

Fig. 3-40. DPM concentration (μg/m^3) profile over time at the DPM source in the CFD model

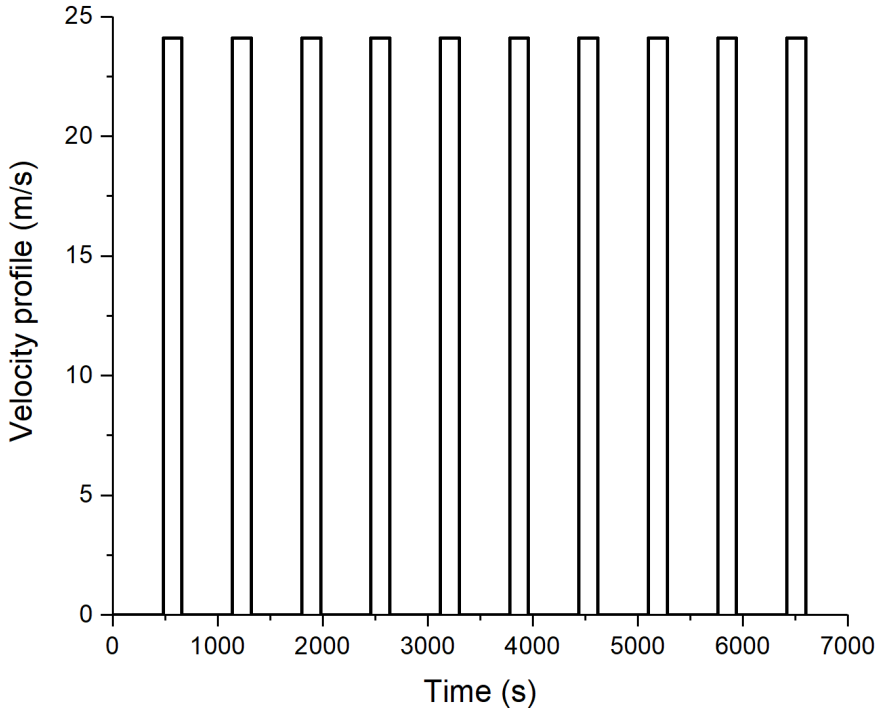

Fig. 3-41. Velocity (m/s) profile over time at the DPM source in the CFD model

Steady-state simulation of airflow was first conducted in the CFD model. Then a transient simulation with DPM source turned on was carried out. It took less than 5 hours for the calculation of the results from this transient DPM simulation in the CFD model with the use of HPC. If this model was executed in a laptop, it would have taken more than 24 hours for the results to be calculated, which is not practical.

3.5.4 Result comparisons

EXP3

Results from the CFD model with the structured cycle time were compared with the results from the Ventsim model. For the EXP3 Ventsim model, the starting diesel emission rate was 0.32 g/kW·h, and the diesel engine power was 200 kW. According to the United States Environmental Protection Agency (U.S. EPA, 2016), a Tier 3 engine is expected to have an emission rate of 0.2 g/kW·h at 200 kW power and a Tier 1 engine is expected to have an emission rate of 0.54 g/kW·h at 200 kW power. Because the results with the 0.32 g/kW·h diesel emission rate were not close to the CFD results, the diesel emission rate was adjusted for the Ventsim model. The new diesel emission rate is 0.57 g/kW·h, which is close to the diesel emission rate of a Tier 1 engine. Hence, there are two sets of results being compared because of the new diesel emission rate being applied in the Ventsim model. Results at locations C, D, and E were compared between the two models and were presented in Fig. 3-42, Fig. 3-43, and Fig. 3-44, respectively. TWA DPM data was calculated and shown in Table 3-13 and Fig. 3-45. Because the DPM data at location C will affect the downstream DPM concentration out of the experiment area, the focus of the comparison is at location C.

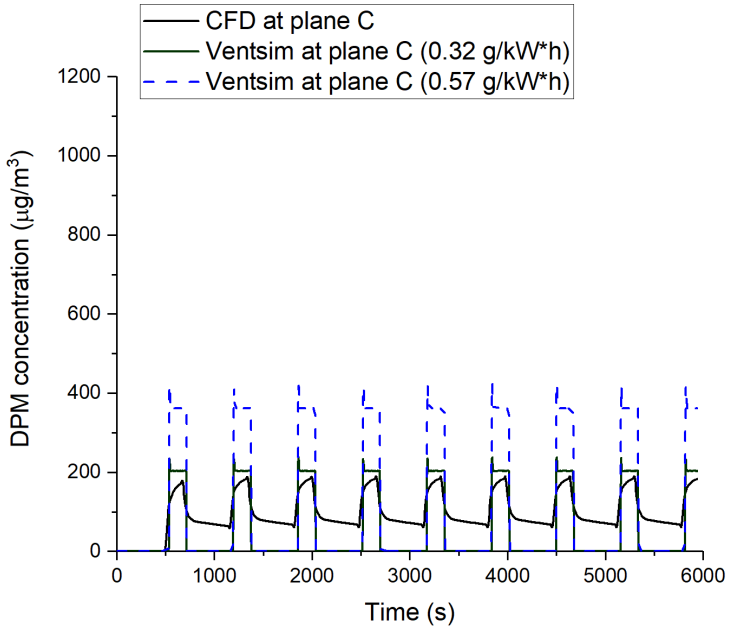

Fig. 3-42. DPM concentration comparisons between the CFD model and the Ventsim model at location C (as shown in Fig. 3-2).

As seen in Fig. 3-42, the DPM results over time from the Ventsim models follow the diesel power profile shown in Fig. 3-34. The DPM does not accumulate over time in the Ventsim model while the peak DPM concentration increases after the first cycle and stays the same for the remaining cycles in the CFD model. The DPM concentration disappears immediately as long as the DPM source stops releasing, which means Ventsim is not able to handle DPM residuals in the heading after the DPM source stops releasing. The DPM profile in the CFD model makes more sense than the DPM profiles in the Ventsim model with different diesel emission rates. The DPM concentration should not reach peak instantly, and it should gradually increase over time until it reaches a peak. Similarly, the DPM concentration should not drop to zero (0) instantly in the Ventsim model. The underlying cause for these relatively unreasonable DPM profiles in the

Ventsim model is that the governing equations being solved are simple. This results in incorrect calculations of accumulation and dilution of the DPM over time.

In the Ventsim model, the DPM peaks of the results from the two diesel emission rates are both greater than the DPM peaks of the results from the CFD model. After several parametric tests in the Ventsim model, the diesel emission rate of 0.57 g/kW·h can lead to a good agreement with the TWA DPM results between CFD and Ventsim as shown in Table 3-13. From Fig. 3-42, the DPM peaks of the results from the Ventsim model with the diesel emission rate of 0.57 g/kW·h are greater than the DPM peaks of the results from the CFD model and from the Ventsim model with the diesel emission rate of 0.32 g/kW·h.

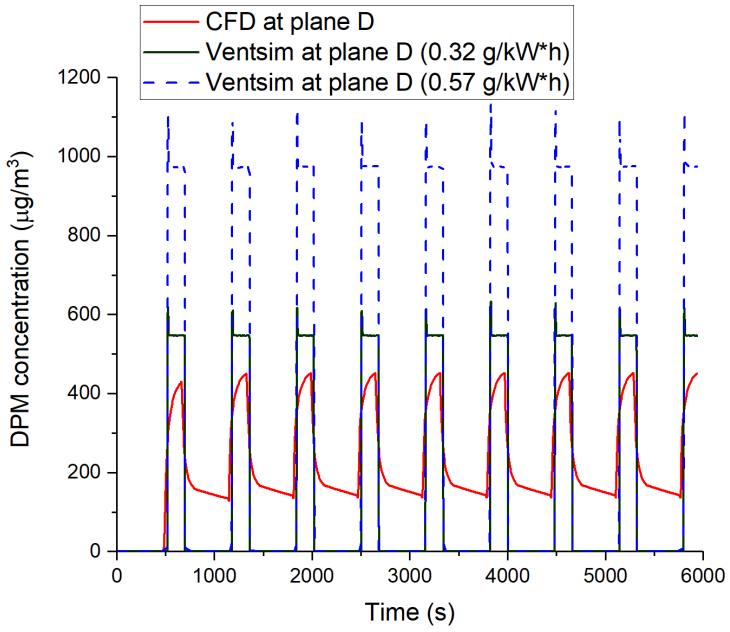

Fig. 3-43. DPM concentration comparisons between the CFD model and the Ventsim model at location D (as shown in Fig. 3-2).

As seen in Fig. 3-43, the DPM data patterns from the three models at location D are similar to those (shown in Fig. 3-42) at location C. The magnitudes of the DPM peaks at location D are all greater than the magnitudes of the DPM peaks at location C. The reason is that air volume in the main drift is higher than air volume in the heading. Hence, the DPM at location C is diluted more than the DPM at location D. Again, Ventsim is not able to handle DPM residuals in the heading after the DPM source stops releasing.

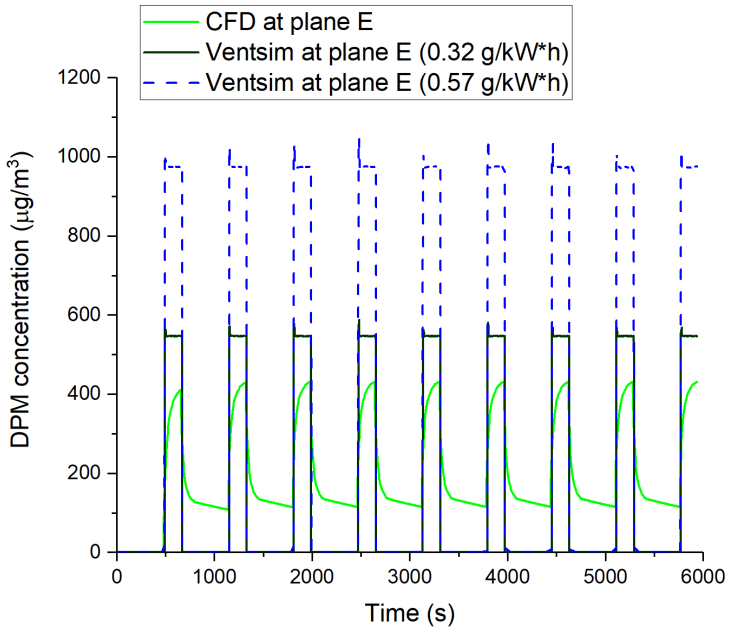

Fig. 3-44. DPM concentration comparisons between the CFD model and the Ventsim model at location E (as shown in Fig. 3-2).

As seen in Fig. 3-44, the DPM data patterns and peaks at location E in the Ventsim model are both same to those at location D. The DPM over time in the CFD model at location E is similar to the DPM data at location D.

To quantify the results, the TWA DPM was calculated according to the following Eq. (3-5), and all the TWA DPM data is shown in Table 3-13.

$$\text{TWA} = \frac{t_1 * c_1 + t_2 * c_2 + \ldots + t_n * c_n}{t_1 + t_2 + \ldots + t_n} \tag{3-5}$$

where *t* represents a time interval, *c* represents the DPM concentration, *n* represents the number of samples.

Table 3-13. Comparison of TWA DPM concentration ($\mu g/m^3$) in the CFD and Ventsim models

Location	CFD (plane)	Ventsim (with emission rate of 0.32 g/kW·h)	Error (%)	Ventsim (with emission rate of 0.57 g/kW·h)	Error (%)
C	95.06	53.80	43.40	96.02	1.01
D	218.18	146.05	33.06	260.59	19.44
E	194.03	147.86	23.80	263.67	35.89

Eq. (3-6) shows how the error was calculated in Table 3-13.

$$\text{Error} = \frac{|\text{DPM data from Ventsim-DPM data from CFD}|}{\text{DPM data from CFD}} \times 100\% \tag{3-6}$$

As mentioned earlier, the comparison of the results at location C is the focus. According to results at location C in Table 3-13, the TWA DPM data from the Ventsim model with the emission rate of 0.57 g/kW·h matches the TWA DPM data from the CFD model quite well. The errors with the Ventsim model with the emission rate of 0.57 g/kW·h at locations C and D are smaller than the errors with the Ventsim model with the emission rate of 0.32 g/kW·h. These comparisons are also shown in the following figure.

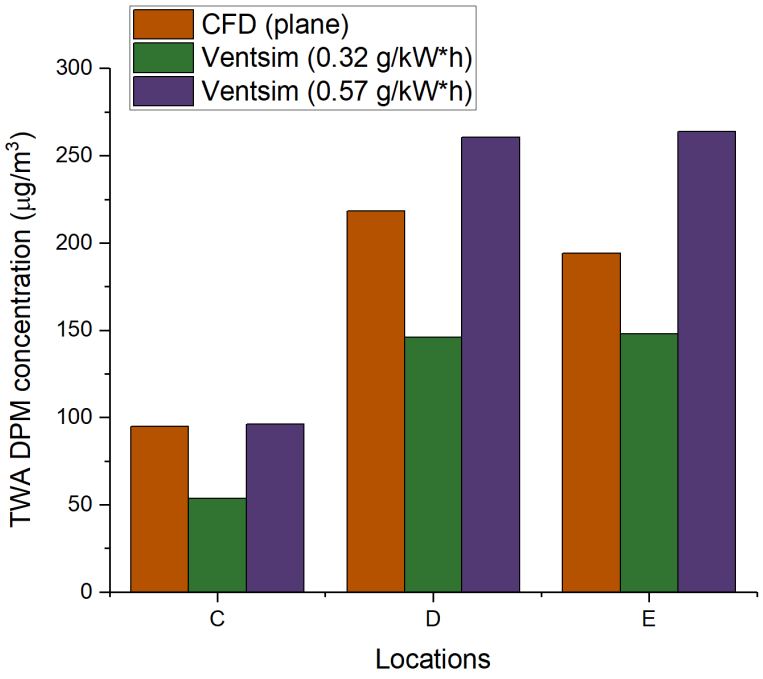

Fig. 3-45. TWA DPM data comparisons between the CFD and Ventsim models.

According to Fig. 3-45, it is apparent that TWA DPM data from the Ventsim model with the emission rate of 0.57 g/kW·h has a better agreement with the DPM data from the CFD model compared to the TWA DPM data from the Ventsim model with the emission rate of 0.32 g/kW·h.

EXP5

For the EXP5 Ventsim model, the starting diesel emission rate was 0.21 g/kW·h, and the diesel engine power was 200 kW. The results with the 0.21 g/kW·h diesel emission rate were close to the CFD results. The diesel emission rate was adjusted for the Ventsim model to improve the results. The new diesel emission rate is 0.19 g/kW·h. Hence, there are two sets of results being compared because of the new diesel emission rate being applied in the Ventsim model. Results at locations B, C, and D were compared from the two models as well and were presented in Fig. 3-46,

Fig. 3-47, and Fig. 3-48, respectively. TWA DPM data was calculated and shown in Table 3-14 and Fig. 3-49. Because the DPM data at location B will affect the downstream DPM concentration out of the experiment area, the focus of the comparison is at location B.

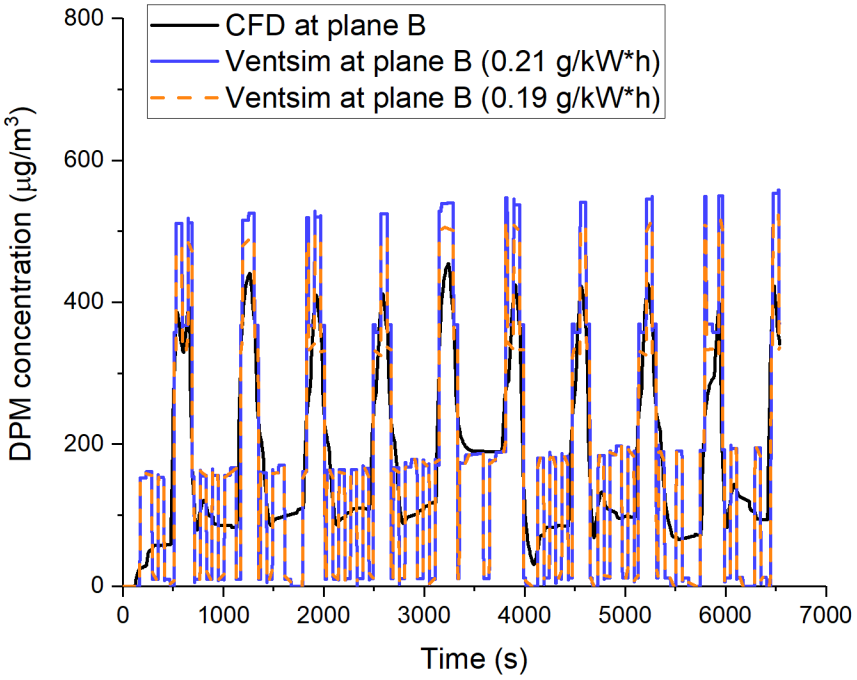

Fig. 3-46. DPM concentration comparisons between the CFD model and the Ventsim model at location B (as shown in Fig. 3-4).

As seen in Fig. 3-46, the DPM results over time from the Ventsim model follow the diesel power profile shown in Fig. 3-36. The DPM slightly accumulates over time in the Ventsim model while the peak DPM concentration fluctuates around 400 µg/m^3 in the CFD model. The DPM profiles in both the CFD model and the Ventsim model are affected by the DPM coming from the upstream. There are DPM residuals in the CFD model after each work cycle but no DPM residuals in the Ventsim model.

The DPM peaks of the results from the Ventsim model with the two diesel emission rates are both greater than the DPM peaks of the results from the CFD model. The differences of results from the Ventsim model with the two diesel emission rates are small. The diesel emission rate of 0.19 g/kW·h can lead to a better agreement of the TWA DPM results between CFD and Ventsim as shown in Table 3-14.

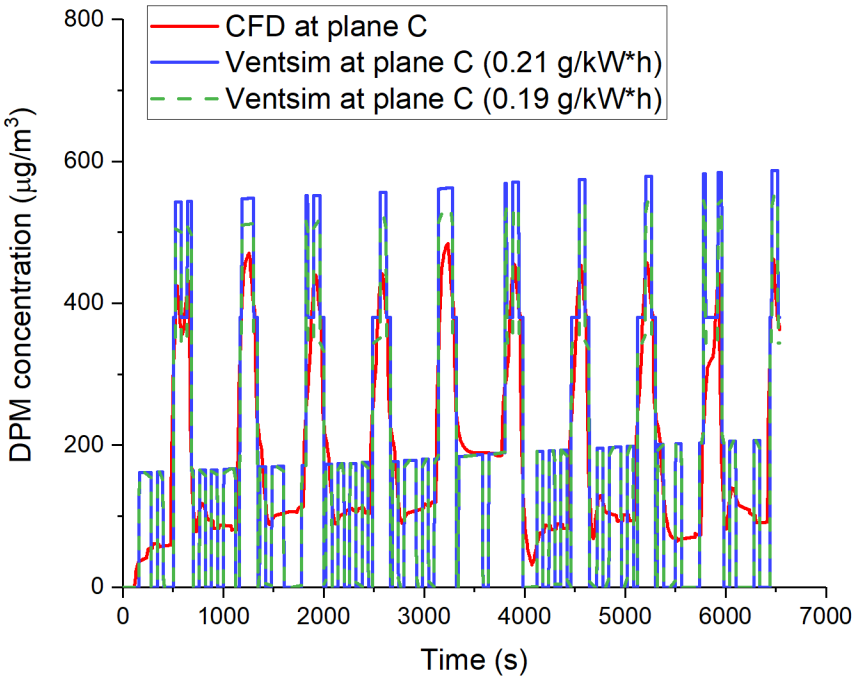

Fig. 3-47. DPM concentration comparisons between the CFD model and the Ventsim model at location C (as shown in Fig. 3-4).

As seen in Fig. 3-47, the DPM data patterns from the CFD and Ventsim models at location C are similar to those (shown in Fig. 3-46) at location B. The magnitudes of the DPM peaks at location C are all greater than those at location B. The reason is that air volume in the main drift is higher than air volume in the heading. Hence, the DPM at location B is more diluted than the DPM at location C.

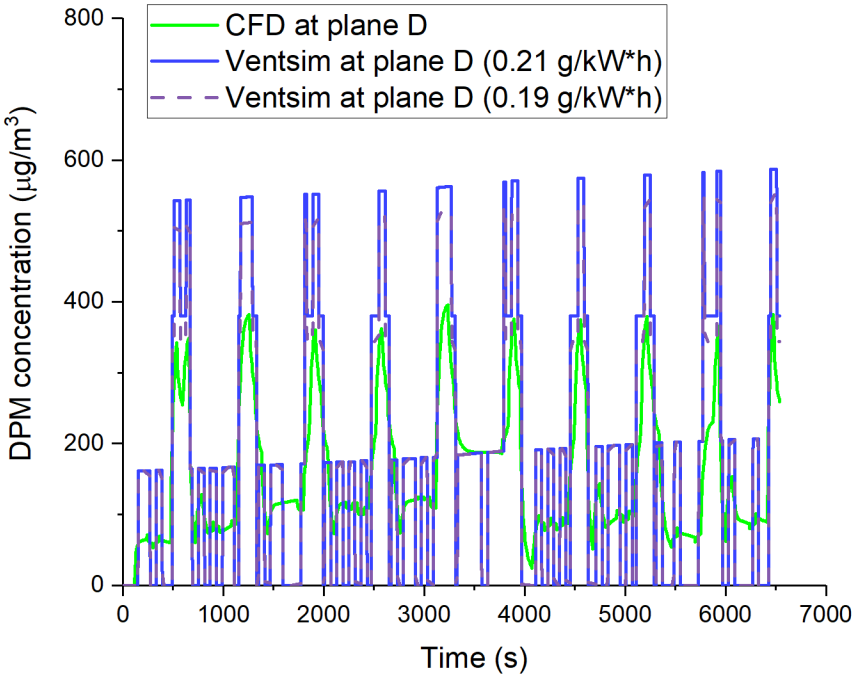

Fig. 3-48. DPM concentration comparisons between the CFD model and the Ventsim model at location D (as shown in Fig. 3-4).

As seen in Fig. 3-48, the DPM data patterns and peaks at location D in the Ventsim model are both same to those at location C. The DPM trend over time in the CFD model at location D is similar to the trend at location C. The DPM peaks at location D are all smaller than the DPM peaks at location C.

TWA DPM was calculated to quantify the results, and all the TWA DPM data is shown in Table 3-14.

Table 3-14. Comparison of TWA DPM concentration (μg/m^3) in the CFD and Ventsim models

Location	CFD (plane)	Ventsim (with emission rate of 0.21 g/kW·h)	Error (%)	Ventsim (with emission rate of 0.19 g/kW·h)	Error (%)
B	172.74	179.82	4.10	170.92	1.05
C	176.69	186.12	5.34	176.59	0.06
D	155.62	187.05	20.20	177.53	14.08

As mentioned earlier, the comparison of the results at location B is the focus. According to results at location B in Table 3-13, the TWA DPM data from the Ventsim model with the emission rate of 0.19 g/kW·h matches that from the CFD model quite well. The errors of the Ventsim model with the emission rate of 0.19 g/kW·h at locations B and C are smaller than the errors of the Ventsim model with the emission rate of 0.21 g/kW·h. These comparisons are also shown in the following figure.

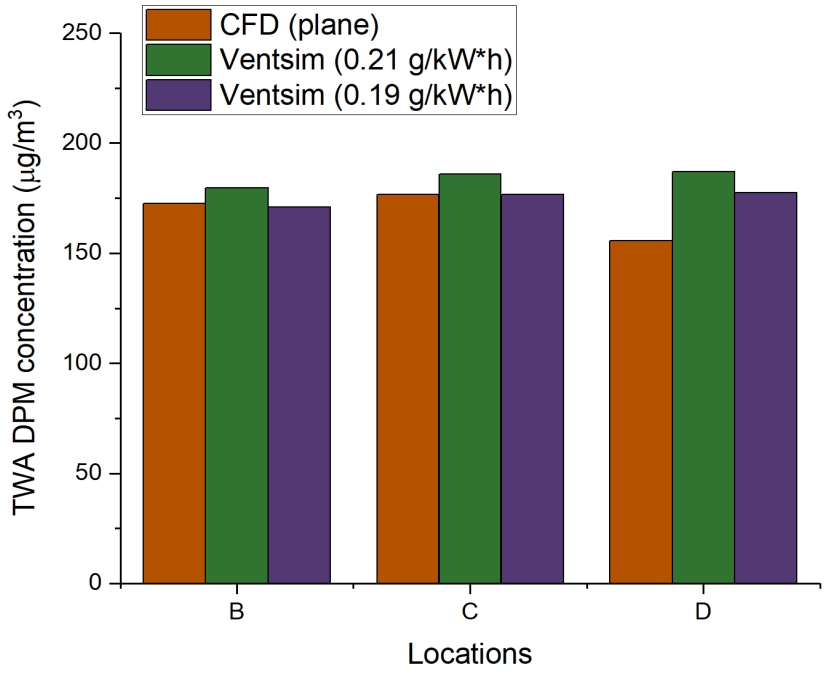

Fig. 3-49. TWA DPM data comparisons between the CFD and Ventsim model.

According to Fig. 3-49, it is apparent that TWA DPM data from the Ventsim model with the emission rate of 0.19 g/kW·h has a better agreement with the data from the CFD model than the data from the Ventsim with the emission rate of 0.21 g/kW·h.

3.5.5 Conclusion

Two approaches, CFD modeling and ventilation network modeling were explored for modeling DPM over one hour in this section. To the author's best knowledge, this is the first time that the DPM was modeled over one hour in a ventilation network solver.

A structured/fixed/constant cycle time, which is 3 min in the heading and 8 min out of the heading, was used for both the CFD and Ventsim models. The area-average DPM data recorded by the monitoring planes in the calibrated CFD model was considered accurate. TWA DPM data was calculated from the modeled DPM data over time.

For EXP3, the diesel engine power of 200 kW and the diesel emission rate of 0.32 g/kW·h were used as the standard inputs in the Ventsim model. The diesel emission rate has been adjusted to 0.57 g/kW·h for a better agreement of the DPM results with the results from the CFD model at locations C and D. In reality, the diesel emission rate of 0.57 g/kW·h can be possible with inferior maintenance on an aging diesel engine.

For EXP5, the diesel engine power of 200 kW and diesel emission rate of 0.21 g/kW·h were used as the standard inputs in the Ventsim model. The diesel emission rate has been adjusted to 0.19 g/kW·h for a better agreement of the DPM results with the results from the CFD model at locations B and C. The two diesel emission rates are close enough in EXP5. The reason is that the DPM

concentration from upstream has a significant effect on the downstream DPM concentration, which leaves a reduced probability for diesel emission rate adjustments.

It is apparent that the diesel emission rate is a significant input for modeling DPM in the Ventsim model. Both diesel engine power and diesel emission rate should be correctly entered into the ventilation network model for the results to better match the results from the CFD model. For future DPM modeling practices in Ventsim, the diesel emission rate is suggested to be carefully and accurately measured for various diesel engines to ensure the accuracy of the DPM modeling output.

The Ventsim model can be used to model DPM over time. However, the fact that the ventilation tubing needs to be extended all the way to the end of a heading for airflow distribution from the main drift may not generate the correct DPM results over time. This issue in the Ventsim model can be taken care of in the CFD models as shown in Fig. 3-5 and Fig. 3-13. Because the Ventsim model requires significantly less time to calculate the results than the CFD model for the modeling DPM over one hour, it will be beneficial to combine the two models by using a hybrid methodology, to be discussed in the next chapter.

Chapter 4

4 A Hybrid Methodology for Investigating DPM Concentration Distribution in an Underground Mine

A section of the results from this chapter was published in the *17th North American Mine Ventilation Symposium*, which was held in April 2019 in Montréal, Canada.

4.1 Introduction

The mine ventilation system is one of the most significant elements of an underground mine since it has to provide sufficient fresh air to the personnel working underground. It also helps clear the contaminants generated from the diesel-powered equipment. In terms of DPM modeling approaches for underground mines, both network modeling and CFD are able to perform steady-state and transient or dynamic simulations. A hybrid methodology is proposed to provide improved diesel input to a ventilation network model by using CFD.

The hybrid methodology combines the two solvers through commonly shared boundary conditions, making it possible to conduct mine-scale ventilation simulations. Results in the ventilation network model are updated with those in the CFD model. In this manner, the ventilation model is computationally efficient and it can produce improved results than those from using the network model alone. The ultimate goal of this hybrid methodology is to make it possible to use the ventilation network solver to model the entire mine ventilation system while the CFD models the flow domains where the ventilation network solver may not be able to perform accurate and detailed simulations (like the active working faces). Mining operations can benefit from the

updated network model using the hybrid methodology and quickly assess different ventilation plans without additional capital investments.

4.2 Proposed hybrid methodology

4.2.1 Methodology

The overall workflow of the hybrid methodology is shown in Fig. 4-1. There are three steps. The first step is to fit a CFD model with the experimental data through trial-and-error. Section 3.3 shows the details on how to fit a CFD model to the experimental data. A flow chart, as shown in Fig. 4-2, is made to present the workflow of the fitting process. The DPM concentration and velocity magnitude of the diesel exhaust applied in the fitted CFD model from the first step is used in the second step to calibrate another CFD model to the experimental data.

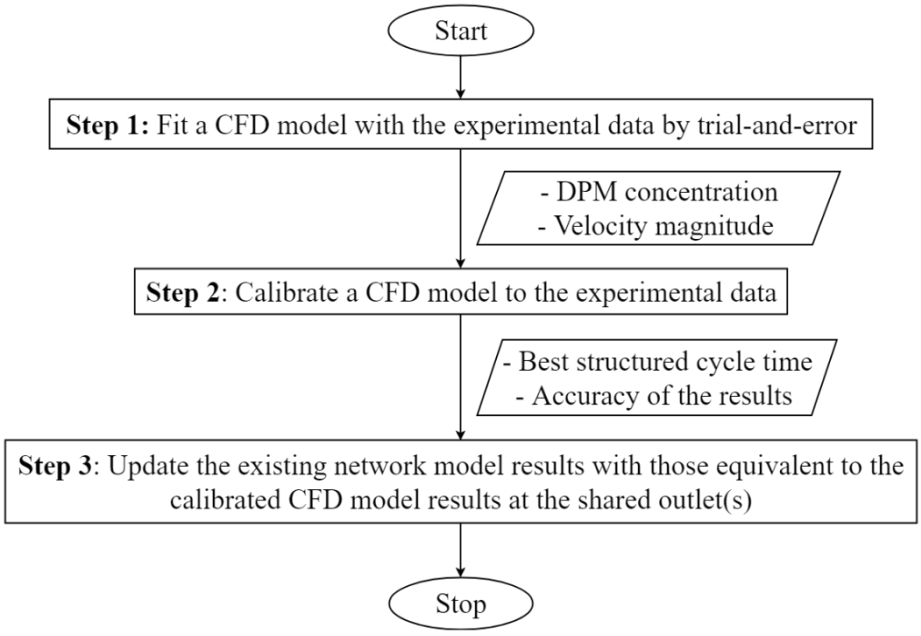

Fig. 4-1. Overall workflow of the hybrid methodology.

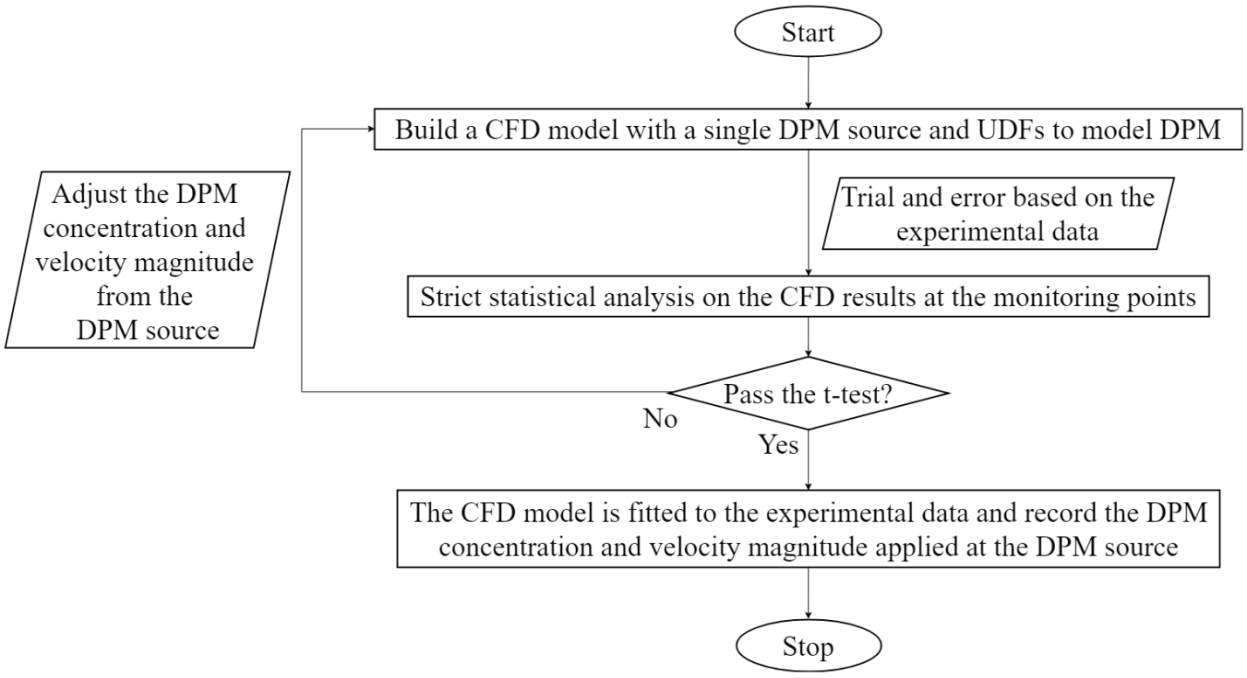

Fig. 4-2. Workflow for fitting a CFD model with experimental data

The workflow shown in Fig. 4-2 can be applied to fit a CFD model for an experiment where DPM coming from upstream does not significantly affect the downstream DPM concentration distribution over time. If there is a large amount of DPM coming from upstream and the concentration varies over time, the t-test shown in Fig. 4-2 will need to be replaced by another statistical analysis, which is not as strict. For instance, the statistical analysis used for EXP5 in Section 3.3.6. The reason is that the irregular upstream DPM profile adds difficulty to fit the CFD model with changing DPM concentration and velocity magnitude of the diesel exhaust from the single DPM source. The statistical analysis may reduce the accuracy of the fitted CFD model. As long as the accuracy is within an acceptable range (i.e., greater than 70%), the DPM concentration and velocity magnitude of the diesel exhaust from the DPM source determined from the CFD model fitted with experimental data can be used to calibrate another CFD model.

As discussed in Section 3.5, the idea of structured/fixed/constant cycle time was proposed to calibrate a CFD model. The structured cycle time was defined as the time when diesel equipment is in a heading and out of the heading, where both times are constant. For instance, an LHD mucks the ore from a heading and dumps it to an ore pass. It takes 2 hours for the LHD to finish mucking in the heading. The average cycle time is 10 min. The average time when the LHD is in and out of the heading is 3 min and 7 min, respectively. Here, the 3 min and 7 min are "fixed," and the LHD repeats this work cycle pattern for 2 hours until it finishes mucking. Besides, it is assumed that the DPM concentration and velocity magnitude of the diesel exhaust from the DPM source is constant when the LHD is in the heading. They are both zero (0) when the LHD is out of the heading where no DPM data was collected. The detailed steps to calibrate a CFD model is shown in Fig. 4-3. If a CFD model is calibrated to experimental data with a set of structured cycle time, the CFD model can be used to predict the DPM concentration.

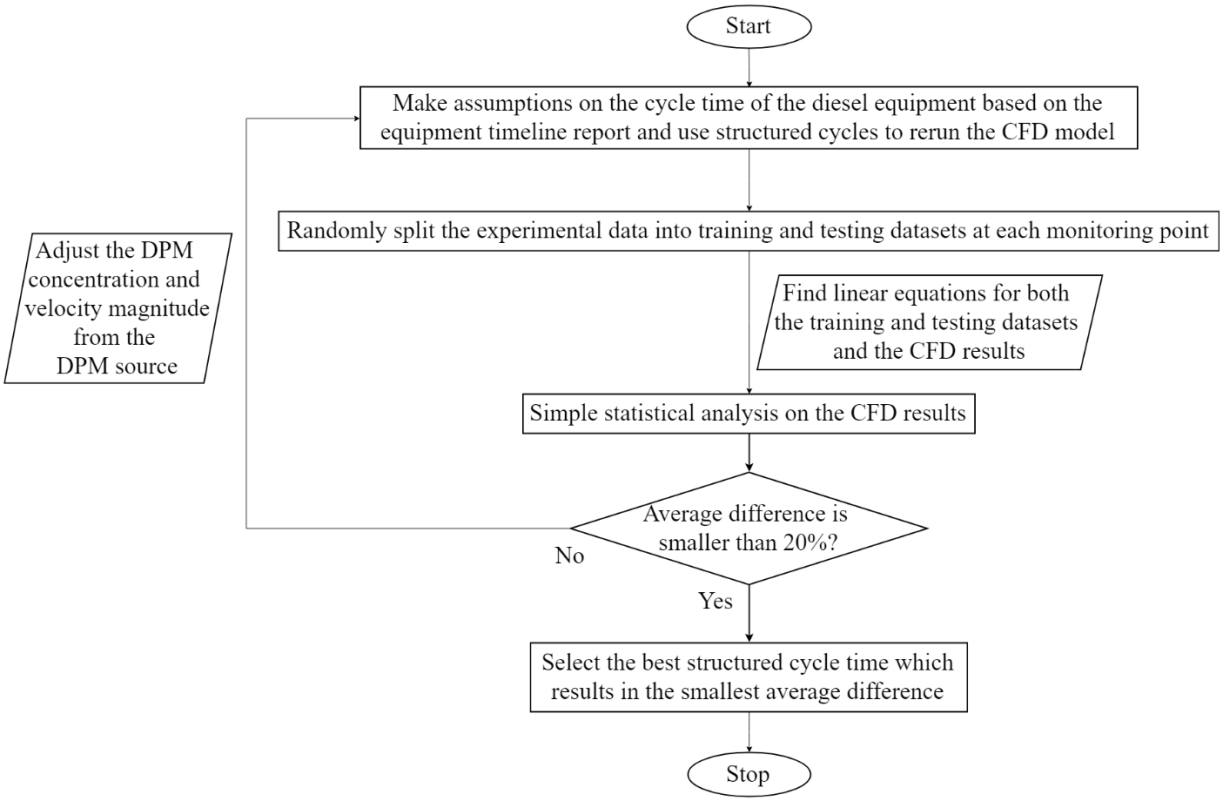

Fig. 4-3. Workflow for calibrating a CFD model to experimental data

According to the equipment timeline report or other similar equipment reports from a mine site, assumptions can be made on the average cycle time of the diesel equipment. For a 10 min cycle, the time when the LHD is in and out of the heading can be assumed. For EXP3 and EXP5, seven structured/fixed times were proposed as shown in Table 4-1 and Table 4-2, respectively. A scenario refers to a combination of several key parameters (such as the cycle time, the DPM concentration and velocity magnitude of the diesel exhaust from the DPM source) entered into the CFD model.

Table 4-1. EXP3 modeling scenarios with various structured times

Scenario	Cycle time (min)		DPM concentration (PPM) of the diesel exhaust from the DPM source	Velocity magnitude (m/s) of the diesel exhaust from the DPM source	Velocity of airflow from ventilation tubing (m/s)
	DPM source on	DPM source off			
1	2	6	19.02	24.10	35.97
2	3	5			
3	4	5			
4	3	6			
5	3	7			
6	4	6			
7	3	8			

Table 4-2. EXP5 modeling scenarios with various structured times

Scenario	Cycle time (min)		DPM concentration (PPM) of the diesel exhaust from the DPM source	Velocity magnitude (m/s) of the diesel exhaust from the DPM source	Velocity of airflow from ventilation tubing (m/s)
	DPM source on	DPM source off			
1	2	6	9.14	24.10	35.00
2	3	5			
3	4	5			
4	3	6			
5	3	7			
6	4	6			
7	3	8			

It can be seen in both the tables that the cycle time consists of DPM source on time and DPM source off time. The DPM source on time represents the period when diesel equipment is inside the heading while the DPM source off time represents the period when the diesel equipment is out of the heading. The DPM source on time ranges from 2 min to 4 min while the off time ranges from 5 min to 8 min. Hence, the cycle time ranges from 8 min to 11 min, which also matches that inferred on the equipment timeline reports. The equipment timeline report shows when and where

equipment is during a shift. The DPM concentration and velocity magnitude of the diesel exhaust from the DPM source in the CFD model are obtained from the fitting process in Fig. 4-1. They are kept constant for the seven scenarios. The velocity of airflow coming from the ventilation tubing in EXP3 and EXP5 are 35.97 m/s and 35 m/s, respectively, which were indirectly calculated according to the ventilation survey data.

A statistical learning approach (Hastie *et al.*, 2008) is chosen to calibrate a CFD model with experimental data. The experimental data collected at each monitoring point is randomly split into training and testing datasets. Results from the CFD model with the seven structured cycle times are compared with the training data at each monitoring location first. Afterward, they are compared with the testing dataset. Linear equations are fitted to the CFD results, training data, and testing dataset. The average difference can be calculated. The criterion to determine if the CFD results are accurate enough is user-defined. In this study, 20% is set as the criterion, that is, the CFD model is calibrated with an 80% accuracy. If more than one structured cycle time can result in a calibrated CFD model, the structured cycle time that results in the lowest average difference between the model and the experimental data is chosen. EXP3 and EXP5 calibration results are shown in the following figures.

EXP3

An example of the DPM concentration over time and its fitted linear line in a CFD modeling scenario is shown in Fig. 4-4.

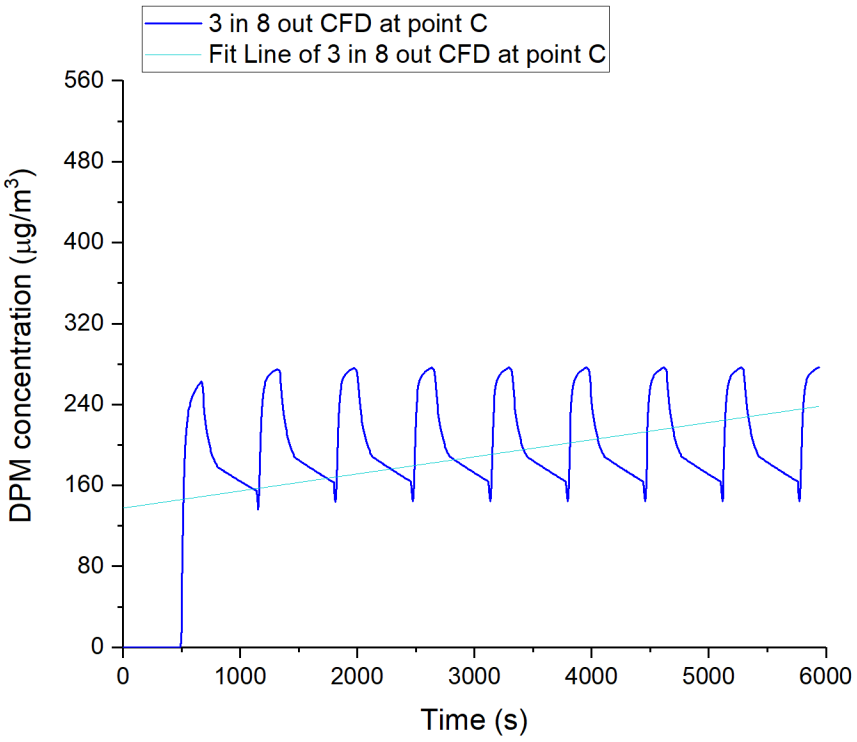

Fig. 4-4. An example of DPM concentration over time at monitoring point C in the CFD model and the fitted line for the DPM data.

Similar to the above example, the linear fitted lines for the other scenarios in the CFD model can be generated. From Fig. 4-5 to Fig. 4-7, linear fitted CFD results from the seven scenarios are compared with the linear fitted training and testing datasets from the experimental data at locations C, D, and E, respectively.

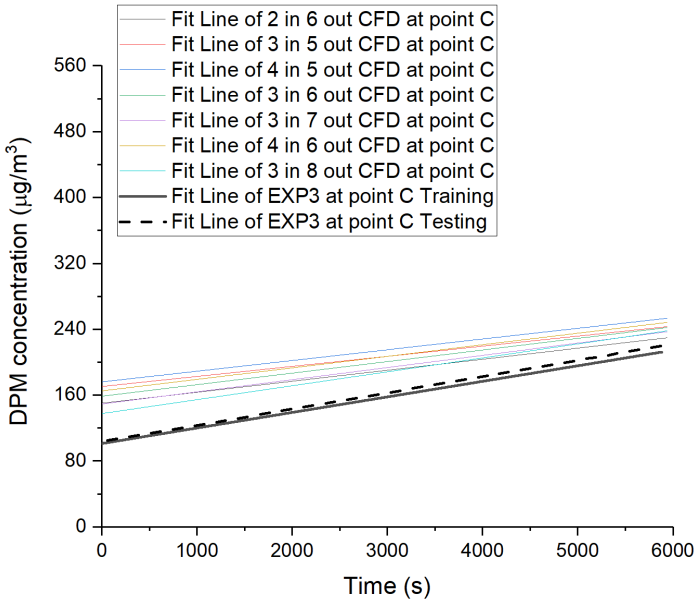

Fig. 4-5. Comparisons of results from the seven scenarios in the CFD model with training and testing datasets at location C.

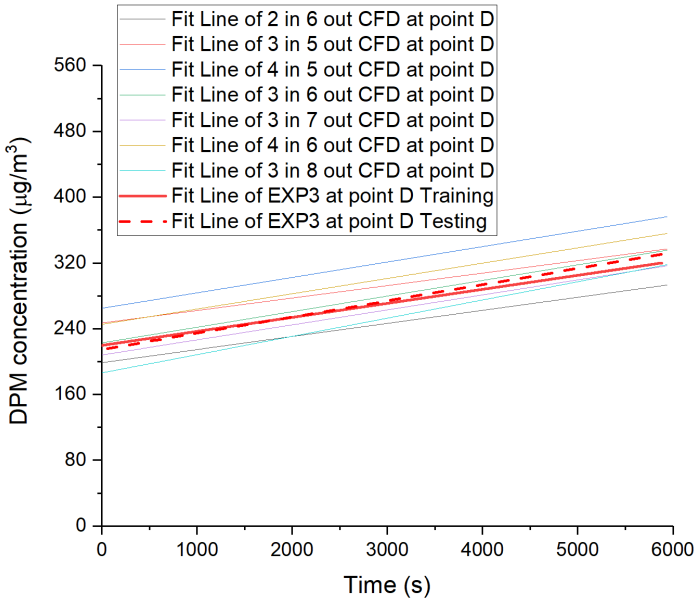

Fig. 4-6. Comparisons of results from the seven scenarios in the CFD model with training and testing datasets at location D.

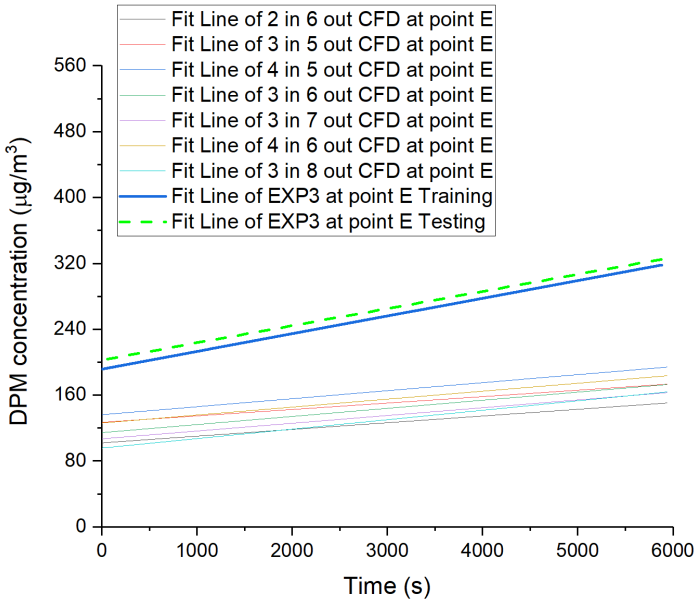

Fig. 4-7. Comparisons of results from the seven scenarios in the CFD model with training and testing datasets at location E.

According to the above figures, the scenario with a structured cycle time of 3 min in the heading and 8 min out of the heading produces the smallest difference compared with both the training and testing datasets of the experimental data. Hence, the CFD model with this structured cycle time is considered as the calibrated model. DPM results from the monitoring planes at locations C, D, and E in the calibrated model are considered as correct area-average DPM data.

EXP5

An example of the DPM concentration over time and its fitted linear line in a CFD modeling scenario is shown in Fig. 4-8.

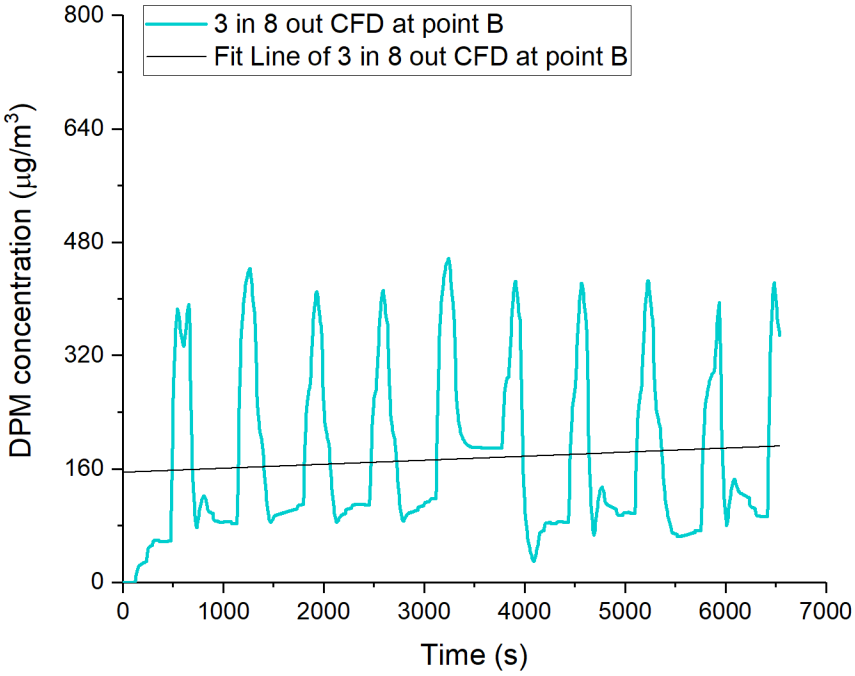

Fig. 4-8. An example of DPM concentration over time at monitoring point B in the CFD model and the fitted line for the DPM data.

Similar to the above example, the linear fitted lines for the remaining scenarios in the CFD model can be generated. From Fig. 4-9 to Fig. 4-11, linear fitted CFD results from the seven scenarios are compared with the linear fitted training and testing datasets from the experimental data at locations B, C, and D, respectively.

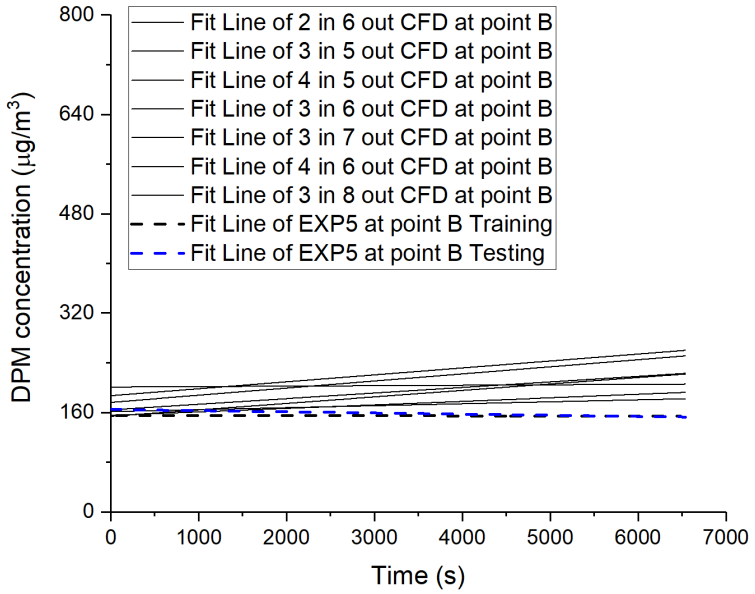

Fig. 4-9. Comparisons of results from the seven scenarios in the CFD model with training and testing datasets at location B.

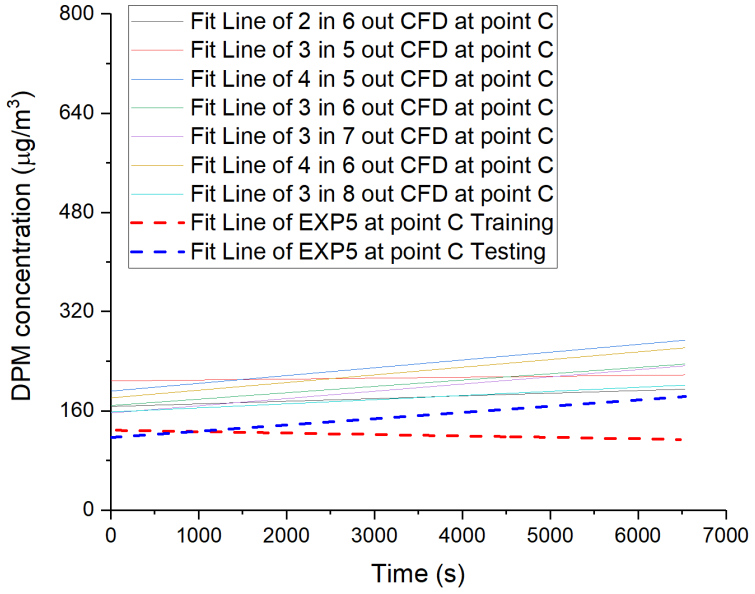

Fig. 4-10. Comparisons of results from the seven scenarios in the CFD model with training and testing datasets at location C.

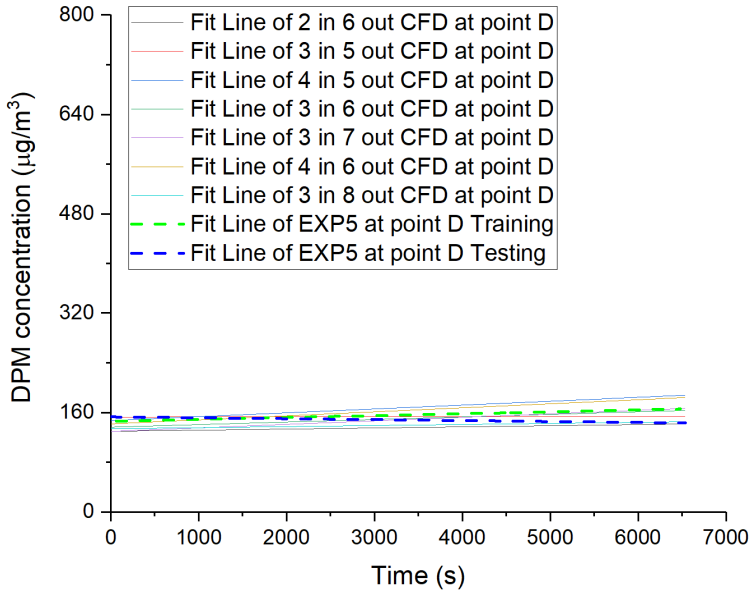

Fig. 4-11. Comparisons of results from the seven scenarios in the CFD model with training and testing datasets at location D.

According to the above figures, the scenario with a structured cycle time of 3 min in the heading and 8 min out of the heading produces the smallest difference compared with both the training and testing datasets of the experimental data. Hence, the CFD model with this structured cycle time is considered as the calibrated model. DPM results from the monitoring planes at locations B, C, and D in the calibrated model are considered as correct area-average DPM data.

As discussed, the best-structured cycle time and the accuracy of the results from the calibrated CFD model can be found from step 2 in Fig. 4-1. The next step of the hybrid methodology is to use the DPM data from the calibrated CFD model to update the ventilation network model, which is Ventsim in this study. Details of step 3 are shown in Fig. 4-12.

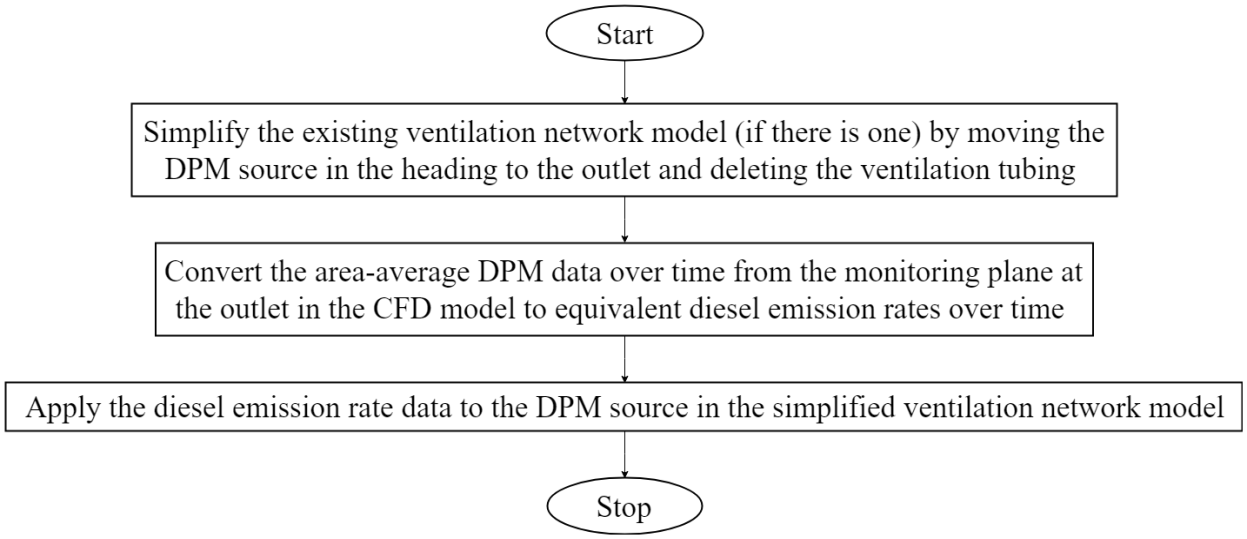

Fig. 4-12. Update the existing network model results with those equivalent to the calibrated CFD model results at the shared outlet(s).

If there is an existing ventilation network model (as shown in Fig. 3-33 and Fig. 3-35), the DPM source is placed near the end of the heading as it is in the CFD model (as shown in Fig. 3-5 and Fig. 3-13). In the Ventsim model, ventilation tubing is required to distribute fresh air to the heading. With the hybrid methodology, the Ventsim models shown in Fig. 3-33 and Fig. 3-35 can be simplified by moving the DPM source to the outlet from the heading and by removing the ventilation tubing because the CFD results will be updated in the Ventsim model. The monitoring plane data from the CFD model will be converted to equivalent diesel emission rates in Ventsim at the outlet(s) for both the CFD and the Ventsim models. Eq. (3-3) is used to carry out the data conversion from CFD to Ventsim.

In this study, the experimental data was recorded over time by the DPM monitors installed on the back of the drift. Thus, these datasets are considered as monitoring point data and cannot represent the area average DPM data over time unless enough DPM monitors are installed in the cross-sectional area at each monitoring location. However, the number of available DPM monitors are

usually limited, and it is difficult to conduct an experiment with many DPM monitors installed in the cross-sectional areas at several locations in an active underground mine because this will interrupt the production activities in the mine. Hence, with the calibrated CFD model, monitoring planes can be created where the monitoring points are located and area average DPM data over time can be recorded. The monitoring plane data can also be used to update the DPM data in the existing ventilation network model.

4.2.2 Solution interface

To demonstrate where the hybrid methodology can be applied and how to update the DPM data in the Ventsim model with the calibrated CFD model, a dead-end heading in a hypothetical underground mine ventilation system is presented in Fig. 4-13 and an enlarged view of the heading is presented in Fig. 4-14.

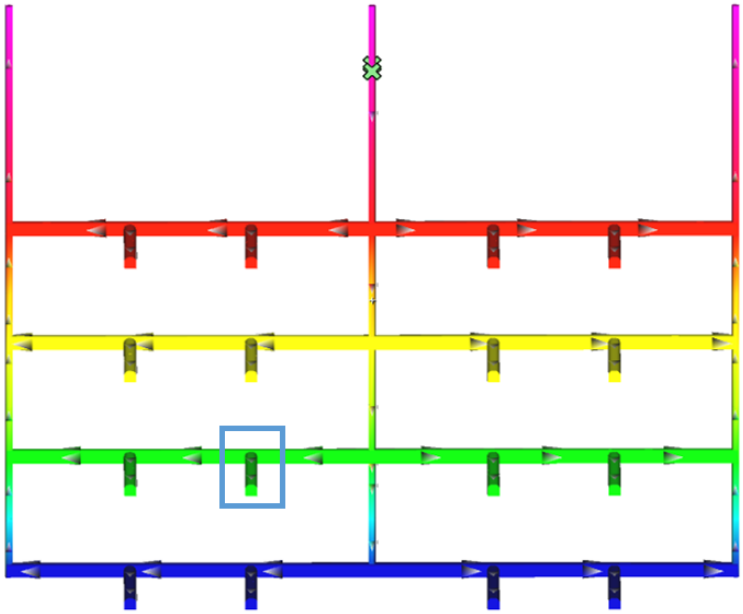

Fig. 4-13. Front view of a hypothetical mine in Ventsim.

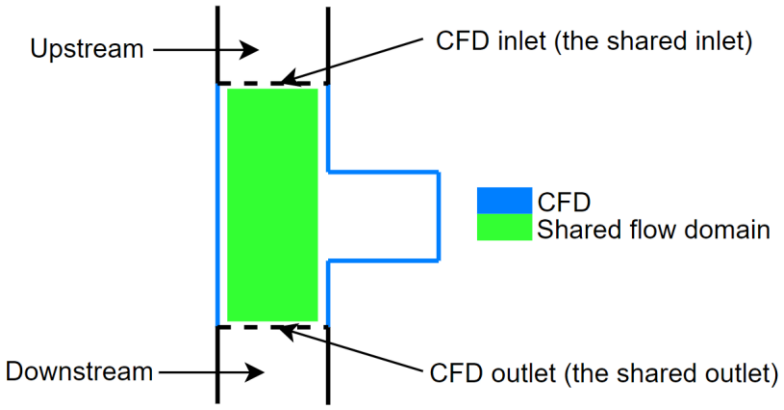

Fig. 4-14. A schematic of data transfer between the Ventsim and CFD models using the hybrid methodology.

From Fig. 4-13, CFD will be used to model the specific areas where detailed information is required, while the Ventsim model will model the remaining ventilation network where general airflow information is enough to support decision-making by on-site ventilation engineers. As seen in Fig. 4-14, the drift between the CFD inlet and outlet and its heading are modeled in CFD. The drift between the CFD inlet and outlet is modeled in Ventsim but not the heading. According to step 3 (as shown in Fig. 4-12) of the hybrid methodology, the area-average DPM data at the CFD outlet is used to update the existing DPM data in the Ventsim model. If there is DPM coming from the upstream, either experimental data (usually monitoring point data) or the Ventsim data (area-average data) can be applied. The upstream baseline data will be normalized with a correction factor and added to the existing equivalent diesel emissions at the shared outlet. The updated Ventsim model then carries the new DPM data downstream in the network as shown in Fig. 4-13. As a result, the entire mine ventilation system can be updated.

4.3 Demonstration

As mentioned earlier, the DPM data over time from the calibrated CFD model is used to update the DPM data from the Ventsim model at the shared outlet. These DPM datasets are compared with the data from the CFD model to validate the DPM data from the updated Ventsim model. If there is a good agreement between the two sets of DPM data, the hybrid methodology is valid and can be applied in modeling and predicting DPM over an extended period of time. EXP3 and EXP5 are used to demonstrate the hybrid methodology.

4.3.1 The original ventilation network model

3D views of the EXP3 and EXP5 in the original Ventsim model are shown in Fig. 4-15 (a) and (b), respectively.

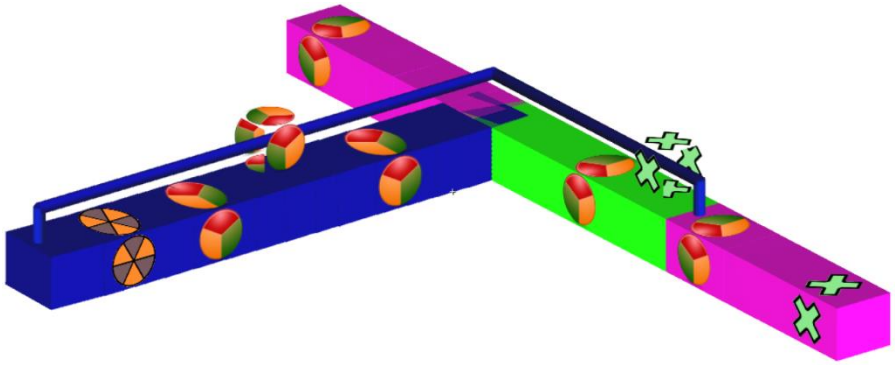

(a)

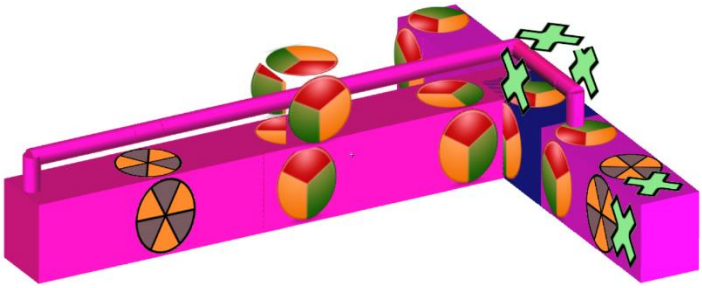

(b)

Fig. 4-15. 3D views of the EXP3 and EXP5 in the Ventsim model.

As seen in Fig. 4-15, a DPM source was placed near the working face in the Ventsim model. The ventilation tubing was built all the way to the end of the heading. For EXP5, another DPM source was placed near the inlet to represent the upstream DPM.

4.3.2 The updated ventilation network model

EXP3

After applying the hybrid methodology, the updated Ventsim model is shown in Fig. 4-16. There are two versions of the updated model with either the dead-end heading included or excluded from the Ventsim model. This does not affect the DPM results at the outlet.

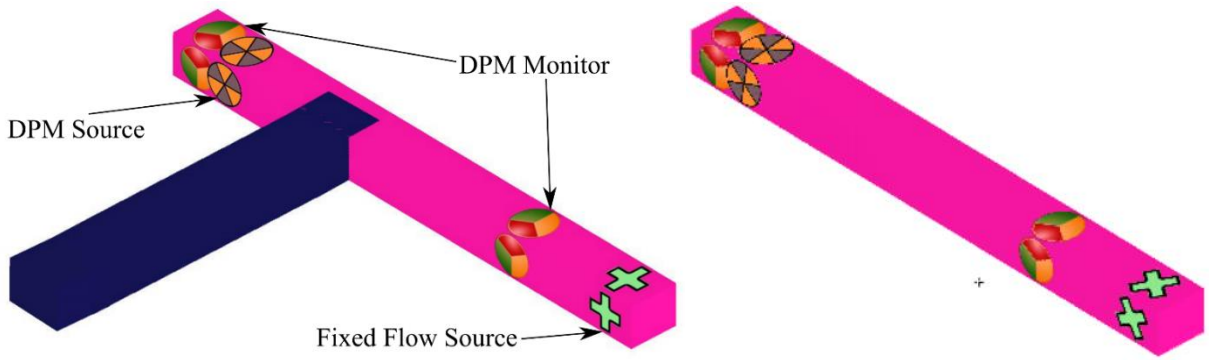

(a) (b)

Fig. 4-16. Two versions of the updated network model for EXP3.

As seen in Fig. 4-16 and Fig. 4-15 (a), the ventilation tubing was removed, and the DPM source was moved from the end of the heading to the outlet. The DPM monitors in the Ventsim model were set to record the DPM data over time in the updated model.

EXP5

After applying the hybrid methodology, the updated Ventsim model is shown in Fig. 4-17. Similar to EXP3, there are two versions of the updated model.

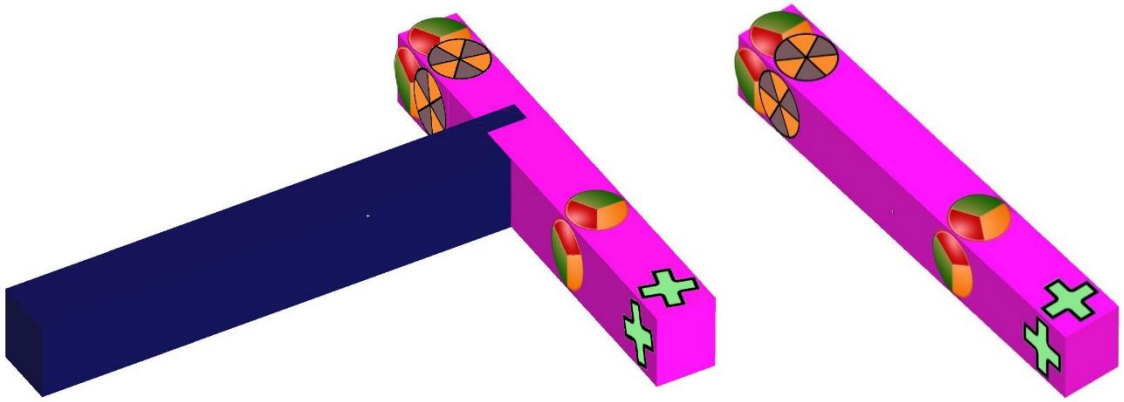

(a) (b)

Fig. 4-17. Two versions of the updated network model for EXP5.

As seen in Fig. 4-17 and Fig. 4-15 (b), the ventilation tubing was removed, and the DPM source was moved from the end of the heading to the outlet. The upstream DPM source was also removed. The new DPM source at the outlet represented the overall DPM concentration profile from the experiment area. The DPM monitors in the Ventsim model were set to record the DPM data over time in the updated model.

4.3.3 Results

EXP3

Results from the CFD model, updated Ventsim, experimental raw data (with a 70 $\mu g/m^3$ error band) at location C are presented in Fig. 4-18.

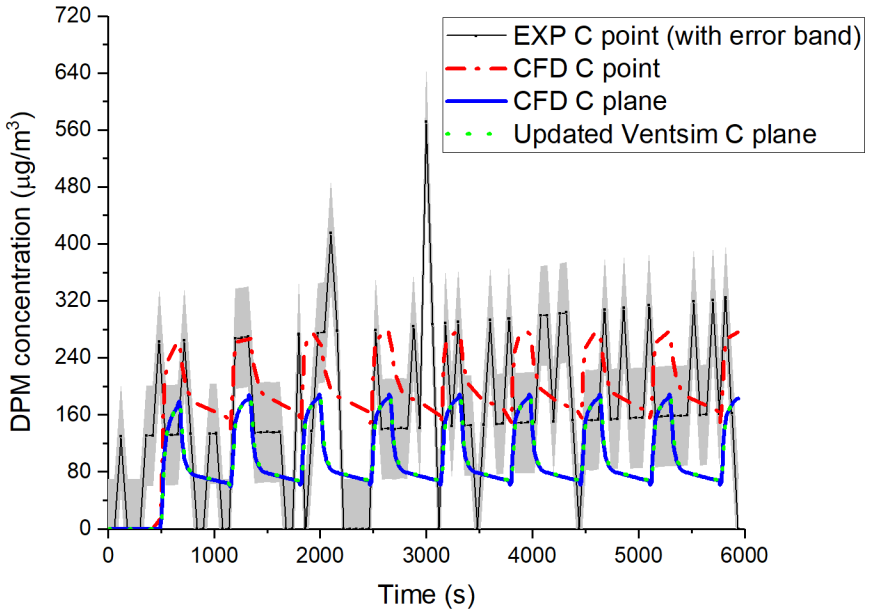

Fig. 4-18. EXP3 result comparisons at location C.

According to Fig. 4-18, the results from the updated Ventsim model perfectly match the monitoring plane results from the calibrated CFD model. The monitoring point data in the calibrated CFD model appears to have a good agreement with the experimental data.

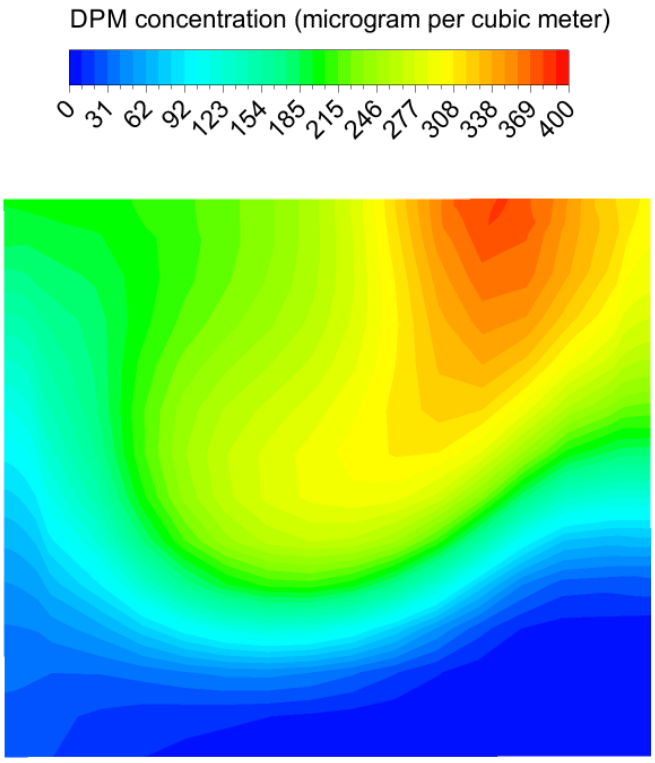

Fig. 4-19. The DPM contour in the cross-sectional area at 660 s at location C (outlet) in the calibrated CFD model.

As seen in Fig. 4-19, the DPM concentration varies over the cross-sectional area at the outlet. The DPM concentrates near the top right corner, and this explains why the monitoring point data is greater than the monitoring plane data.

EXP5

Results from the CFD model, updated Ventsim, experimental raw data (with a 70 $\mu g/m^3$ error band) at location B are presented in Fig. 4-20.

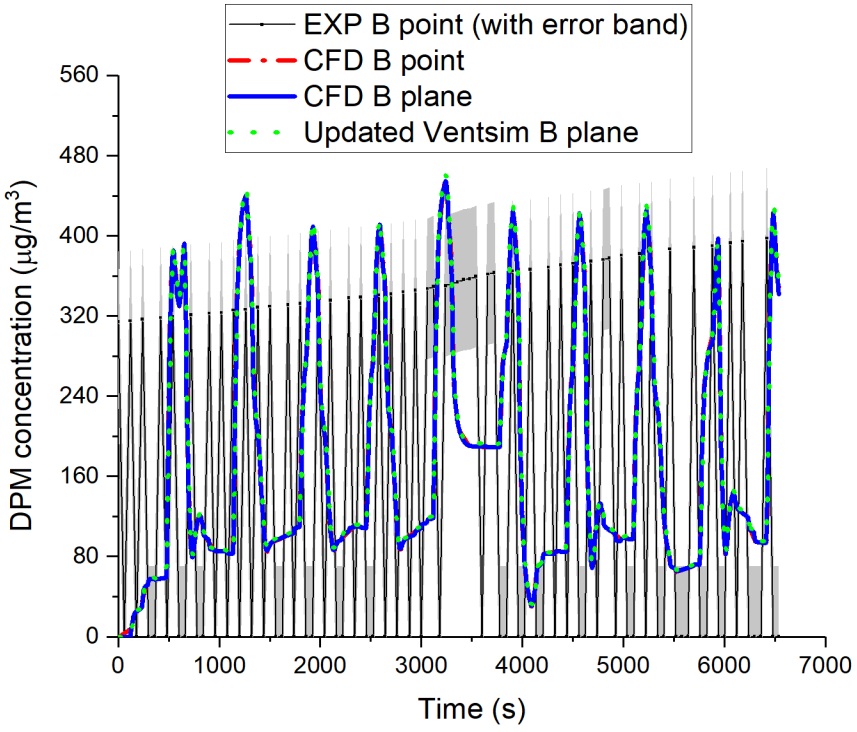

Fig. 4-20. EXP5 result comparisons at location B.

According to Fig. 4-20, the results from the updated Ventsim model perfectly match the monitoring plane results from the calibrated CFD model. The monitoring point data in the calibrated CFD model has a good agreement with the experimental data, and the monitoring point data is almost the same as the monitoring plane data. This is different compared with EXP3.

Fig. 4-21. The DPM contour in the cross-sectional area at 660 s at location B (outlet) in the calibrated CFD model.

As seen in Fig. 4-21, the DPM concentration does not change much over the cross-sectional area at the outlet, and this explains why the monitoring point data is almost the same as the monitoring plane data.

4.4 Demonstration of the applicability of the hybrid methodology

4.4.1 Introduction

The updated Ventsim model using the hybrid methodology can be used to model a mine-scale ventilation system. Nowadays, mining operations use ventilation network solvers to model their ventilation systems due to the user-friendly-interface, short computing time, and acceptable accuracy of the results. As the focus of the thesis, DPM can be modeled by using either Ventsim alone or using Ventsim with the hybrid methodology. Two case studies were presented in this section. Comparisons between the DPM results from the (mine-scale) Ventsim model using the hybrid methodology and the results from using (mine-scale) Ventsim alone were made to present the differences and the potential application of the hybrid methodology in the mining industry. Additional benefits of using the hybrid methodology, like generating 3D visualization of the DPM concentration distribution at any location and any point of the modeling period, are also presented in this section.

In this section, side-by-side comparisons between using Ventsim alone and using Ventsim with the hybrid methodology for 8-hour dynamic DPM modeling are presented. Two case studies are created to demonstrate the benefits of using the hybrid methodology. The geometry and calibrated CFD model of EXP3 are used as initial inputs of the case studies.

4.4.2 Using Ventsim alone for DPM modeling

As mentioned in Section 3.4, Ventsim uses two inputs, which are the diesel emission rate and the diesel engine power for DPM modeling. Generally, the diesel engine power of diesel equipment can be found on the user's guide of the diesel equipment whereas the diesel emission rate is often

not available. Then the Ventsim user needs to estimate the diesel emission rate for the DPM source (i.e., diesel equipment) because the emission rate varies with factors like fuel and engine type, maintenance schedule, workload, exhaust gas treatment. To the best knowledge of the author, there are two options to estimate the diesel emission rate when using Ventsim alone.

One is using the diesel emission rate from the report from the U.S. EPA on Nonroad Compression-Ignition Engines: Exhaust Emission Standards (U.S. EPA, 2016). For instance, the diesel emission rate for a Tier 3 diesel engine with a diesel engine power of 200 kW is 0.2 g/kW·h. The other is applying an estimated correction factor on the emission rate obtained from the U.S. EPA report to account for the factors mentioned above (e.g., maintenance schedule). For example, 0.44 g/kW·h with a correction factor of 2.2 compared with option 1. The correction factor of 2.2 is chosen according to McGinn (2000) that an emission reduction of up to 55% for DPM was achieved through maintenance procedures. However, the estimated correction factor may or may not be reliable because it all depends on the user's experience and knowledge on how well the diesel equipment is maintained. Both the options are used in the case studies using Ventsim alone.

4.4.3 Using Ventsim with the hybrid methodology for DPM modeling

The diesel emission rates obtained from the calibrated CFD model, as a part of the hybrid methodology, are different from the two options from using Ventsim alone. Two options of the diesel emission rates are proposed when using Ventsim with the hybrid methodology.

One option is the equivalent diesel emission rate calculated based on the DPM mass flowrate from the diesel exhaust tailpipe in the calibrated CFD model (or field studies or lab tests) of an experiment (EXP3 in this study). According to Table 4-1, DPM concentration (in parts per million

(PPM)) of the diesel exhaust from the DPM source in the calibrated CFD model of EXP3 is 19.02 PPM. EXP3 was conducted at the 4,450 muck bay in the underground mine, where 4,450 referred to 1,356 m above sea level in altitude. According to an online air pressure calculator (Mide Technology Corp, 2019), the barometric pressure at the altitude of 1,356 m is expected to be 86,574 Pa at an average dry-bulb temperature of 25.72 °C (based on the dry-bulb temperature readings at the locations A, B, C, D, and E in Table 3-2). With the barometric pressure of 86,574 Pa, the air density from the exhaust tailpipe can be calculated to 0.508 kg/m^3 at the temperature of 320.85 °C (equivalent to 594 K shown in Table 3-6) based on an online air density calculator (Czernia and Haponiuk, 2019). The DPM concentration in the exhaust is calculated to 9,658 µg/m^3 (19.02 × 1E-6 × 0.508 × 1E9 µg/m^3). The volume of air coming from the exhaust pipe is 2.17 m^3/s (24.1 m/s × 0.09 m^2). As a result, the mass flowrate of DPM from the exhaust tailpipe is calculated to 2.1E-5 kg/s (9658 × 1E-9 kg/m^3 × 2.17 m^3/s). Assuming the engine power of the diesel equipment is 200 kW, the equivalent diesel emission rate of the diesel equipment is calculated to 0.378 g/kW·h (2.1E-5 × 1E3 g/s × 3600 s/h / 200 kW) based on conservation of mass.

The other option is the equivalent diesel emission rate calculated based on the 8-hour TWA DPM data at the outlet (refer to location C in EXP3 as shown in Fig. 3-2) in the calibrated CFD model. A 99-min DPM modeling in a dead-end heading using the hybrid methodology in EXP3 was presented in Section 4.3. Because the regulatory DPM concentration limit is measured on a shift-average basis in any heading with mining activities, the shift-average DPM is worthwhile being investigated. Generally, the time of a shift for personnel working underground is either eight hours or ten hours, or sometimes twelve hours. Besides, DPM concentration, 400 µg/m^3, is a TWA value based on the Ontario Mining Regulation (Government of Ontario, 1990). Hence, the 8-h period is chosen as the time in a shift and the 8-h TWA DPM is calculated. From Section 4.2.1, the best

structured cycle time is that 3 min in the heading and 8 min out of the heading. The total simulation time in the calibrated CFD model for EXP3 is 5940 s (99 min) as shown in Fig. 4-22.

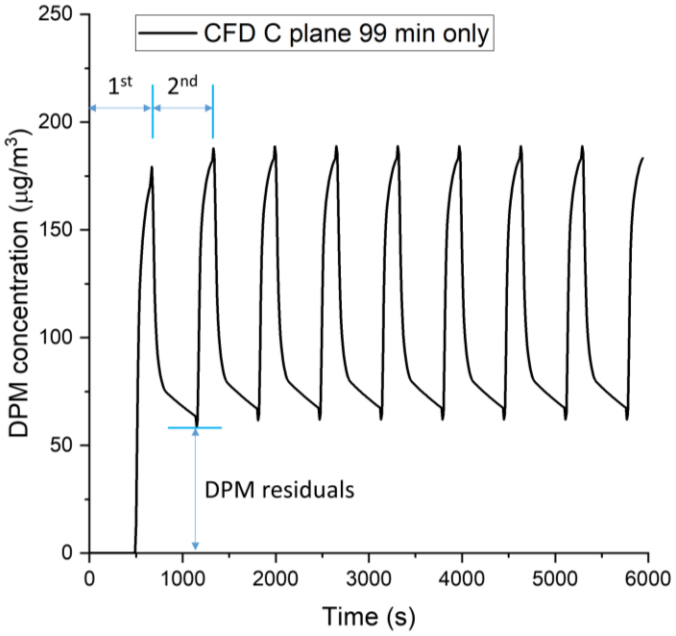

Fig. 4-22. DPM concentration over 99 min at monitoring plane C in the calibrated CFD model of EXP3.

From Fig. 4-22, there are DPM residuals at monitoring plane C after the DPM source in the CFD model stops releasing. The DPM concentration at the monitoring plane at the outlet (location C) does not change after the second cycle in the calibrated CFD model. Therefore, the DPM concentration profiles over the 8-h modeling period at monitoring plane C from the third cycle until 8 h (28,800 s) are the same.

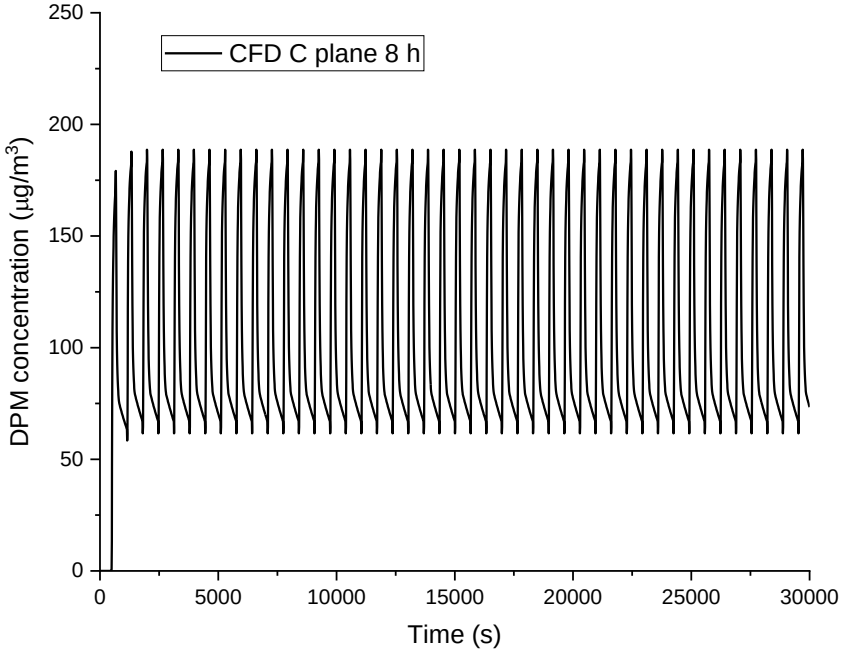

Fig. 4-23. DPM concentration over 8 h at monitoring plane C in the CFD model.

From Fig. 4-23, the 8-h TWA DPM data at monitoring plane C is calculated to 101 μg/m^3, which can be achieved with an equivalent diesel emission rate of 0.57 g/kW·h and a diesel engine power of 200 kW in Ventsim. The emission rate of 0.57 g/kW·h is determined based on the fact that the emission rate from the exhaust tailpipe and the 8-hour TWA DPM at a location downstream of the tailpipe are positively correlated in Ventsim. It should be noticed that the emission rate of 0.57 g/kW·h from this option is different from the emission rate of 0.378 g/kW·h from the previous option. The reason for the difference is that Ventsim is not capable of capturing the DPM residual after the DPM source stops releasing whereas CFD is capable. More details regarding the DPM residuals are shown in the following case studies.

4.4.4 Case studies

Two case studies are created to compare the DPM modeling using Ventsim alone directly and the DPM modeling using Ventsim with the hybrid methodology.

Case study 1: Four diesel equipment work on the same level in the hypothetical mine. The total number of diesel equipment in the mine is four.

Case study 2: Two diesel equipment work on every one of four different levels in the hypothetical mine. The total number of diesel equipment in the mine is eight.

For each case study, the DPM modeling using Ventsim alone with the two diesel emission rates (0.2 g/kW·h and 0.44 g/kW·h) and the DPM modeling using Ventsim with the hybrid methodology with the other two diesel emission rates (0.378 g/kW·h and 0.57 g/kW·h) are conducted and results are compared. The total simulation time for each model is 8 h. The diesel emission rate of 0.2 g/kW·h is the emission rate for a Tier 3 diesel engine with a diesel engine power of 200 kW based on the U.S. EPA report (U.S. EPA, 2016). The diesel emission rate of 0.44 g/kW·h represents the emission rate of 0.2 g/kW·h with a correction factor of 2.2, which is chosen according to McGinn (2000). The diesel emission rate of 0.378 g/kW·h is the equivalent diesel emission rate, which is calculated based on conservation of mass, of the diesel equipment with a 200 kW engine power from the calibrated CFD model. The diesel emission rate of 0.57 g/kW·h represents an equivalent diesel emission rate, which leads to the same 8-h TWA DPM data at monitoring C, for the diesel equipment with a 200 kW engine power from the calibrated CFD model.

Both the Ventsim models in each case study have the same model setup. The only difference is the diesel emission rate of the DPM source in each of the models. The Ventsim models for case studies 1 and 2 are shown in Fig. 4-24 and Fig. 4-25, respectively.

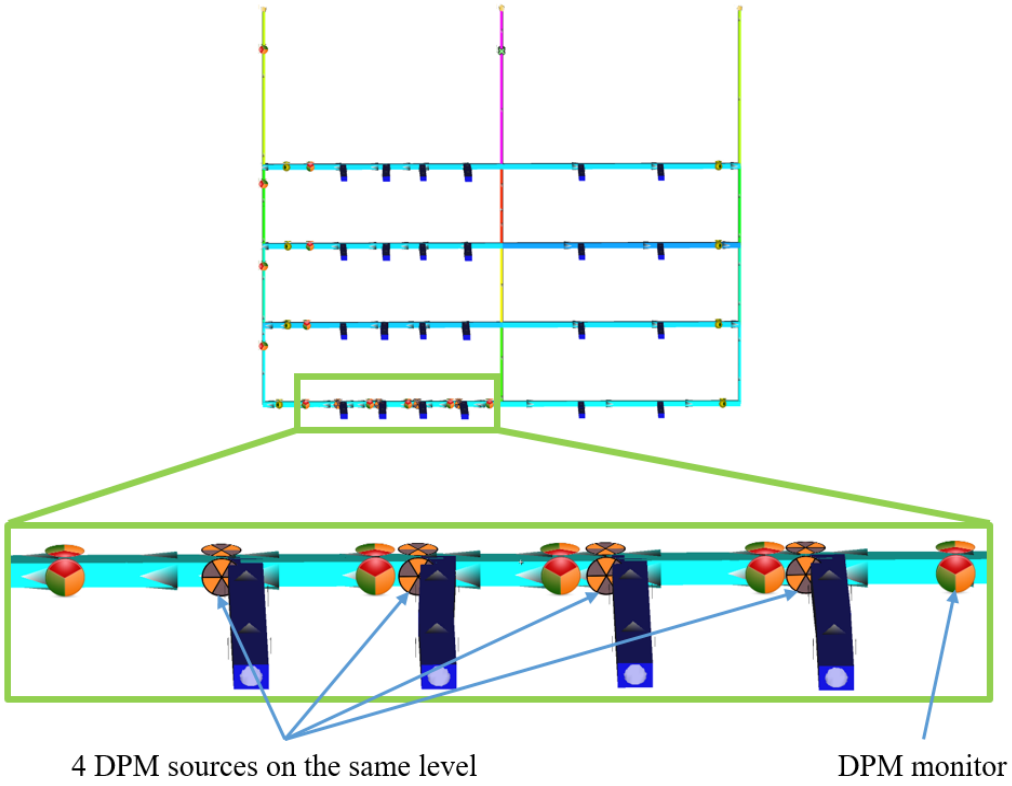

Fig. 4-24. Overview of the Ventsim model for case study 1.

It is seen from Fig. 4-24 that there are four levels in the hypothetical mine. The intake shaft in the middle delivers a fixed amount of 400 m^3/s of airflow into the mine. The return air raises on both the left (204 m^3/s) and the right (196 m^3/s) sides of the mine exhaust the contaminated air out of the mine. Four pieces of the same diesel equipment, which are represented by four DPM sources of the same type, work at four headings on the bottom level of the mine. The DPM sources are moved from the heading to a downstream location near each heading because the DPM concentration over time at the locations downstream of the headings is the focus.

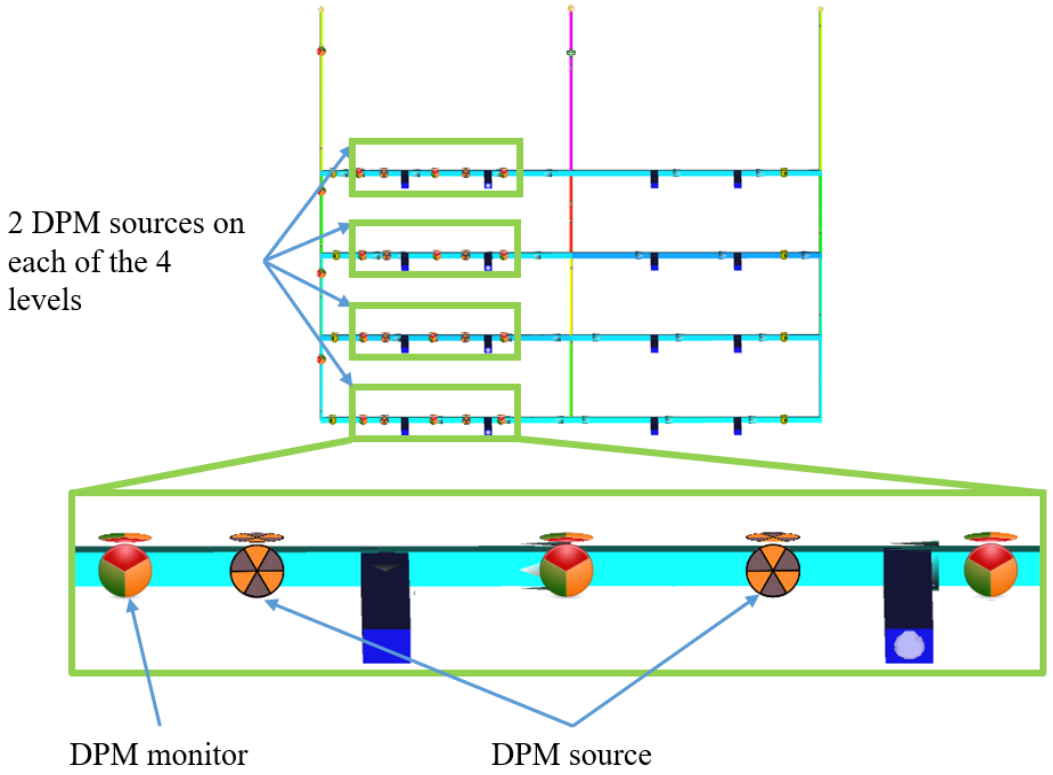

Fig. 4-25. Overview of the Ventsim model for case study 2.

It is seen from Fig. 4-25 that there are four levels in the hypothetical mine. Same as that in case study 1, the intake shaft in the middle delivers a fixed amount of 400 m^3/s of airflow into the mine. The return air raises on both the left (204 m^3/s) and the right (196 m^3/s) sides of the mine exhaust the contaminated air out of the mine. Two pieces of diesel equipment of the same type, which are represented by two same DPM sources, work at two headings on every level of the mine. Similar to that in case study 1, the DPM sources are moved from the heading to a downstream location near each heading.

4.4.5 Assumptions

Assumptions made in the case studies include:

- All the diesel equipment has Tier 3 engines with the same diesel engine power (200 kW).
- In the case studies, the diesel emission rates of 0.2 g/kW·h and 0.44 g/kW·h are used for DPM modeling using Ventsim alone. The emission rate of 0.2 g/kW·h for a Tier 3 engine comes from the report from the U.S. EPA on Nonroad Compression-Ignition Engines: Exhaust Emission Standards (U.S. EPA, 2016). The emission rate of 0.44 g/kW·h is calculated based on the emission rate of 0.2 g/kW·h with an estimated correction factor of 2.2, which is chosen according to McGinn (2000) that an emission reduction of up to 55% for DPM was achieved through maintenance procedures. Hence, a Tier 3 diesel engine with the emission rate of 0.44 g/kW·h represents poor maintenance on the engine.
- The emission rates of 0.378 g/kW·h and 0.57 g/kW·h are used for DPM modeling using Ventsim with the hybrid methodology. The emission rates are based on EXP3 and the calibrated CFD model of the experiment. The emission rate of 0.378 g/kW·h for a Tier 3 engine is calculated based on the conservation of DPM mass flowrate from the DPM source in the calibrated CFD model. The emission rate of 0.57 g/kW·h is calculated based on the 8-h TWA DPM concentration at location C in the calibrated CFD model.
- The emission rate is constant when the diesel equipment is in the heading. The emission rate is zero when the diesel equipment is out of the heading.
- The cycle time of each diesel equipment is 11 min in total, with 3 min in the heading and 8 min out of the heading.
- The diesel equipment works for 8 hours continuously and repeats the cycle (3 min in and 8 min out of the heading).

4.4.6 Results

An 8-h dynamic DPM modeling was conducted in Ventsim for both case studies. Results from the two case studies are presented below.

Case study 1

Fig. 4-26 shows the sampling locations in the Ventsim models for case study 1. The DPM concentrations over the 8-h period were recorded by the DPM monitors at the four sampling locations. The 8-h TWA DPM data from using Ventsim alone and from using Ventsim with the hybrid methodology at each sampling location are calculated and the results are shown in Table 4-3 and Table 4-4, respectively.

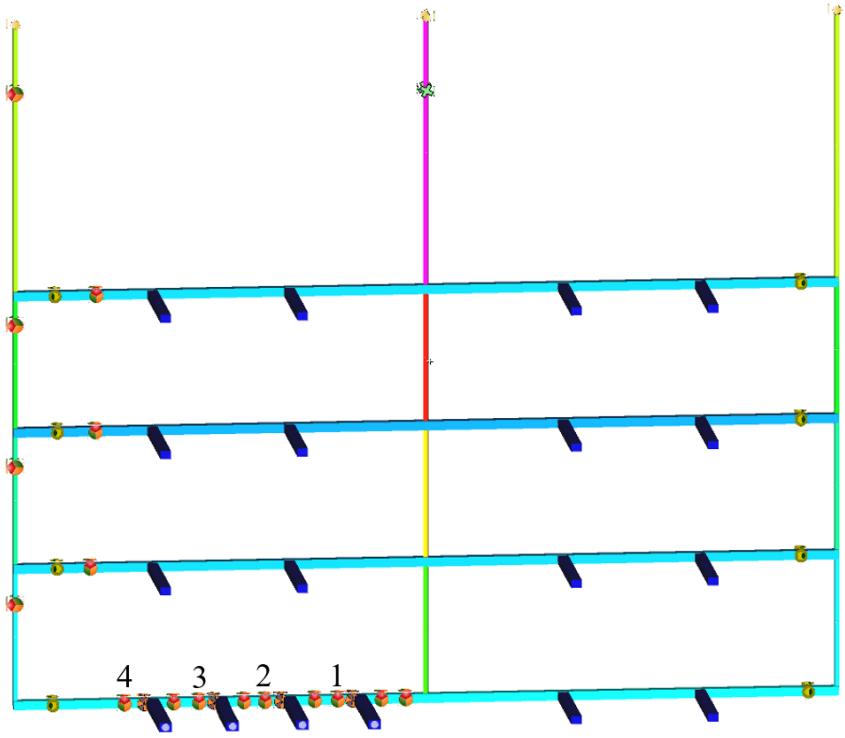

Fig. 4-26. Sampling locations in the Ventsim model for case study 1.

Table 4-3. TWA DPM results from using Ventsim alone

Location	Airflow (m^3/s)	0.2 g/kW·h	0.44 g/kW·h
		8-hr TWA DPM ($\mu g/m^3$)	
1	87	35	78
2	87	70	155
3	87	106	233
4	87	141	310

Table 4-4. TWA DPM results from using Ventsim with the hybrid methodology

Location	Airflow (m^3/s)	0.378 g/kW·h	0.57 g/kW·h
		8-hr TWA DPM ($\mu g/m^3$)	
1	87	67	100
2	87	133	201
3	87	200	301
4	87	266	**402**

From Table 4-3 and Table 4-4, it can be seen that the 8-h TWA DPM data have a linear relationship with the diesel emission rate. The 8-h TWA DPM data from Ventsim using the diesel emission rate of 0.2 g/kW·h, 0.378 g/kW·h and 0.44 g/kW·h are all smaller than the TWA DPM from the emission rate of 0.57 g/kW·h. With the diesel emission rate of 0.57 g/kW·h, the TWA DPM concentration goes over 400 $\mu g/m^3$, which is the Ontario regulatory limit, at sampling location 4. The 8-h TWA DPM concentration adds up along downstream of the DPM source from each heading. For example, with the diesel emission rate of 0.2 g/kW·h, each heading generates 35 $\mu g/m^3$ of DPM, which has been carried over along the downstream areas, and the DPM monitor after the second heading indicates 70 $\mu g/m^3$ of DPM.

Case study 2

Fig. 4-27 shows twelve sampling locations in the Ventsim models for case study 2. The DPM concentrations over the 8-h period were recorded by the DPM monitors at the sampling locations. The 8-h TWA DPM data from using Ventsim alone and from using Ventsim with the hybrid

methodology at each sampling location are calculated and the results are shown in Table 4-5 and Table 4-6, respectively.

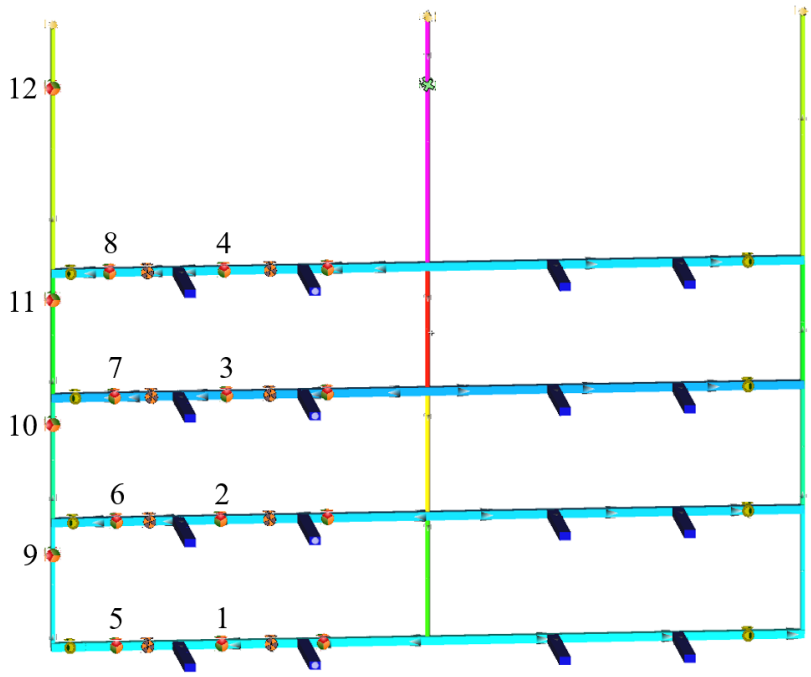

Fig. 4-27. Sampling locations in the Ventsim model for case study 2.

Table 4-5. TWA DPM results from using Ventsim alone

Location	Airflow (m^3/s)	0.2 g/kW·h	0.44 g/kW·h
		8-hr TWA DPM ($\mu g/m^3$)	
1	87	35	77
2	35.8	85	188
3	41.7	73	161
4	39.4	78	171
5	87	70	155
6	35.8	171	375
7	41.7	147	322
8	39.4	155	342
9	87	70	155
10	122.8	100	219
11	164.5	111	245
12	203.9	120	264

Table 4-6. TWA DPM results from using Ventsim with the hybrid methodology

Location	Airflow (m^3/s)	0.378 g/kW·h	0.57 g/kW·h
		8-hr TWA DPM ($\mu g/m^3$)	
1	87	66	100
2	35.8	161	243
3	41.7	138	209
4	39.4	147	221
5	87	133	200
6	35.8	322	**486**
7	41.7	277	**418**
8	39.4	293	**443**
9	87	133	200
10	122.8	188	284
11	164.5	211	318
12	203.9	227	342

From Table 4-5 and Table 4-6, it can be seen that the 8-h TWA DPM data have a linear relationship with the diesel emission rate. With the same diesel emission rate, the 8-h TWA DPM data and airflow quantity are negatively correlated. With the diesel emission rate of 0.57 g/kWh, the DPM concentration goes over 400 $\mu g/m^3$, which is the Ontario regulatory limit, at sampling locations 6, 7, and 8. Similar to case study 1, the 8-h TWA DPM concentration adds up along downstream of the DPM source from each heading.

4.4.7 Conclusion

The TWA DPM data need to be carefully analyzed when there are multiple DPM sources working on the same level at the same time to improve the estimation of the TWA DPM concentration. In case study 1, with the diesel emission rate of 0.57 g/kW·h (from the calibrated CFD model), the DPM monitor at heading 4 detects 402 $\mu g/m^3$ of DPM, which is over the regulatory limit of 400 $\mu g/m^3$ in Ontario. With the diesel emission rate of 0.2 g/kW·h from U.S. EPA, the DPM monitor at sampling location 4 detects 141 $\mu g/m^3$ of DPM, which is still below the regulatory limit of 400

$\mu g/m^3$. To be safe, a relatively large correction factor needs to be applied to the diesel emission rate when performing DPM modeling in Ventsim.

The hybrid methodology with the use of CFD can serve as another option when estimating the diesel emission rate for DPM modeling in Ventsim. Although it is more time-consuming and more complex, it provides better calibrated emission rates. The hybrid methodology can be practical with the completion of a database containing tables of correction factors on diesel emission rates under various situations.

4.4.8 The benefits of using the hybrid methodology

As mentioned in the previous section, the hybrid methodology offers a calibrated estimation of the diesel emission rate for DPM modeling in Ventsim. It provides an improved estimation of the diesel emission rate for DPM modeling in Ventsim especially when there are multiple diesel equipment working on the same level.

The hybrid methodology considers the DPM residuals after the DPM source stops releasing when calculating the TWA DPM concentration.

In addition, the hybrid methodology provides a database (future work) of the correction factors for diesel emission rates under various situations so that engineers can quickly look for a correction factor when conducting DPM modeling in Ventsim. An example of the database of the correction factor for diesel emission rates is presented as follows.

Monitoring points and planes were created in the calibrated CFD model of EXP3. The locations of the monitoring points and planes are shown in Fig. 4-28.

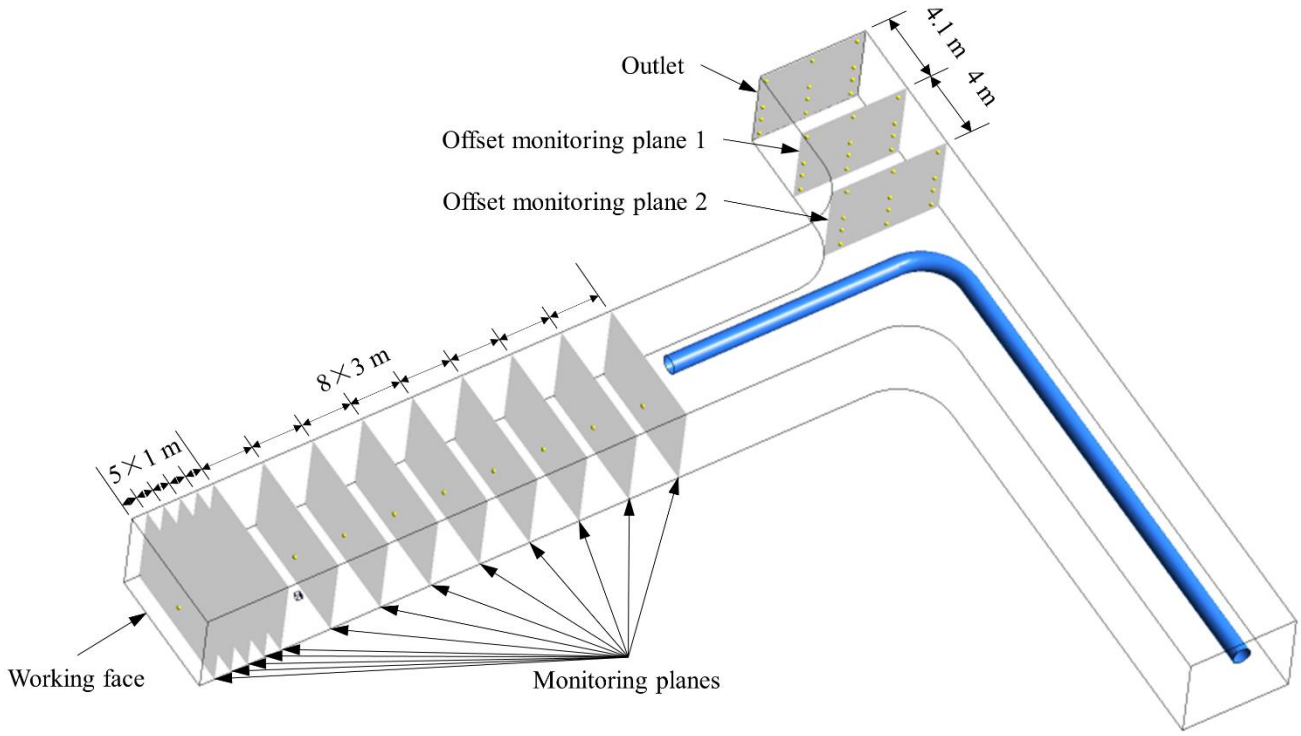

Fig. 4-28. Monitoring points and planes in the CFD model.

As shown in Fig. 4-28, two groups of monitoring planes are created in the CFD model to record DPM concentration over time. One group consists of three monitoring planes near the outlet. A monitoring plane is created at the outlet. Offset monitoring plane 1 is 4.1 m away from the outlet and offset monitoring plane 2 is 4 m away from offset monitoring plane 1. Twelve monitoring points (from SP1 to SP12) are created on each of the three monitoring planes near the outlet and the locations of the monitoring points can be seen in Fig. 4-29.

The other group has thirteen monitoring planes in the heading. Five of the thirteen monitoring planes are located close to the working face and in front of the DPM source with a 1 m spacing between each other. The remaining eight monitoring planes are located behind the DPM source

with a 3 m spacing between each other. Only one monitoring point is created on each monitoring plane. The location of the monitoring point on each monitoring plane can be seen in Fig. 4-30.

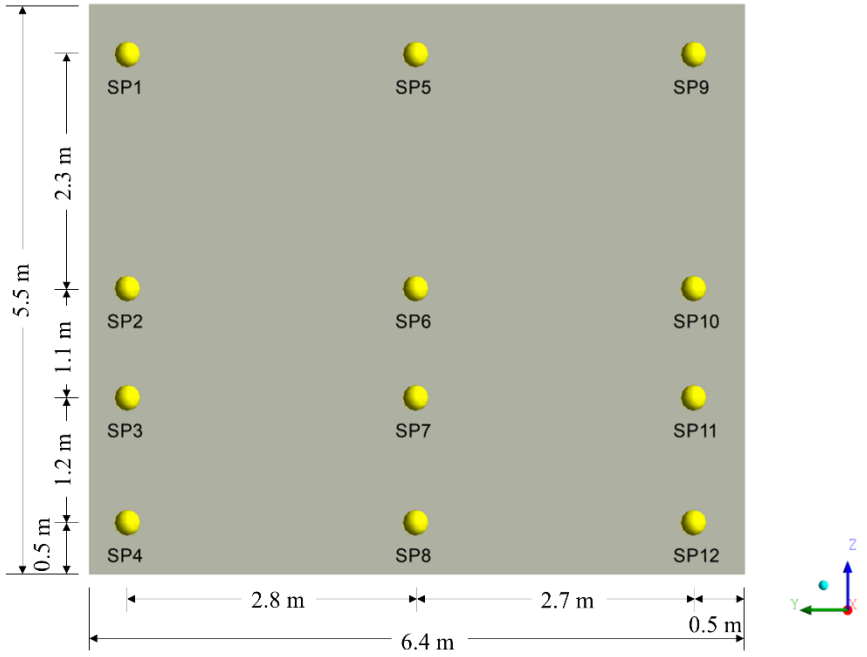

Fig. 4-29. Locations of the monitoring points on the monitoring planes at the outlet.

As shown in Fig. 4-29, twelve monitoring points are created on each of the three monitoring planes near the outlet. Three monitoring points (SP1, SP5, and SP9) are located near the back, three (SP2, SP6, and SP10) are located in the middle, and three (SP4, SP8, and SP12) are located near the floor. Three monitoring points (SP3, SP7, and SP11) are created at the height of 1.7 m, which represents an average height of a person working underground.

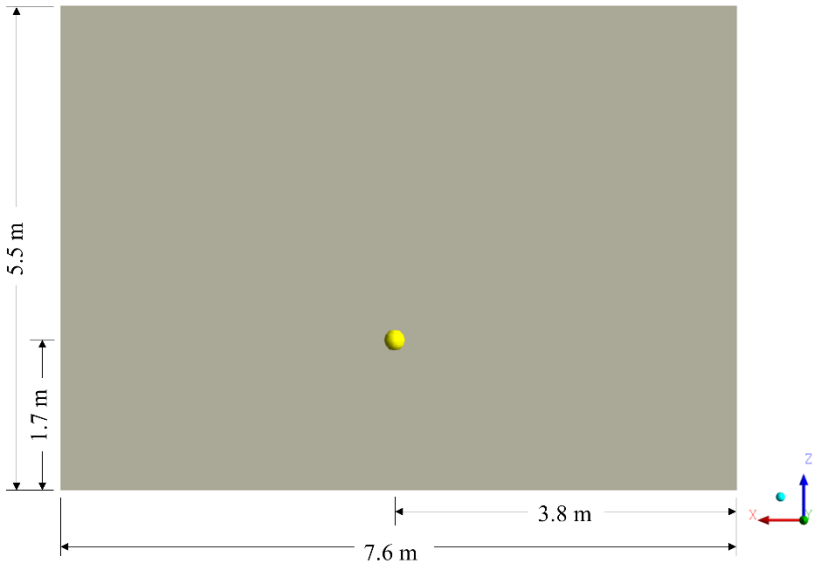

Fig. 4-30. Location of the monitoring point on monitoring planes near the working face.

As shown in Fig. 4-30, only one monitoring point is created on each of the monitoring planes near the working face. The monitoring point is located 1.7 m above the floor and 3.8 m away from the wall on the right side.

The DPM data over 99 min on the monitoring points and planes are included in the results from the transient DPM simulation of 99 min in the calibrated CFD model of EXP3 (refer to Section 4.2.1). Similar to the DPM concentration profile shown in Fig. 4-22, the DPM concentration profile on the monitoring points and planes do not change after the second work cycle of the diesel equipment. Therefore, the DPM concentration profiles over the 8-h modeling period at the monitoring points and planes from the third cycle until 8 h (28,800 s) are the same. The 8-h TWA DPM data at the monitoring points and planes are calculated and shown from Table 4-7 to Table 4-10. A correction factor is calculated by dividing the 8-h TWA DPM data from the monitoring plane by that from the monitoring point. As mentioned above, the number of real-time DPM monitors is usually limited at mine sites. Therefore, the correction factor can be used to estimate

the TWA DPM concentration across a cross-sectional area when the TWA DPM concentration at a monitoring point in the cross-sectional area is known from using a real-time DPM monitor. The correction factors are also shown from Table 4-7 to Table 4-10.

Table 4-7. Comparisons of the 8-h TWA DPM concentrations on the monitoring points and planes in the heading

Location	8-h TWA DPM (μg/m^3)	Location	8-h TWA DPM (μg/m^3)	Correction factor
Monitoring plane - 1 m away from the working face (plane-1m)	176.2	Monitoring point - 1 m away from the working face (point-1m)	176.4	1.0
Monitoring plane - 2 m away from the working face (plane-2m)	176.6	Monitoring point - 2 m away from the working face (point-2m)	176.8	1.0
Monitoring plane - 3 m away from the working face (plane-3m)	176.6	Monitoring point - 3 m away from the working face (point-3m)	176.9	1.0
Monitoring plane - 4 m away from the working face (plane-4m)	176.6	Monitoring point - 4 m away from the working face (point-4m)	177.1	1.0
Monitoring plane - 5 m away from the working face (plane-5m)	176.5	Monitoring point - 5 m away from the working face (point-5m)	177.6	1.0
Monitoring plane - 8 m away from the working face (plane-8m)	186.9	Monitoring point - 8 m away from the working face (point-8m)	184.1	1.0
Monitoring plane - 11 m away from the working face (plane-11m)	208.5	Monitoring point - 11 m away from the working face (point-11m)	212.0	1.0
Monitoring plane - 14 m away from the working face (plane-14m)	207.9	Monitoring point - 14 m away from the working face (point-14m)	229.5	0.9
Monitoring plane - 17 m away from the working face (plane-17m)	201.7	Monitoring point - 17 m away from the working face (point-17m)	225.2	0.9
Monitoring plane - 20 m away from the working face (plane-20m)	199.3	Monitoring point - 20 m away from the working face (point-20m)	220.9	0.9
Monitoring plane - 23 m away from the working face (plane-23m)	202.9	Monitoring point - 23 m away from the working face (point-23m)	221.2	0.9
Monitoring plane - 26 m away from the working face (plane-26m)	211.0	Monitoring point - 26 m away from the working face (point-26m)	226.2	0.9
Monitoring plane - 29 m away from the working face (plane-29m)	219.5	Monitoring point - 29 m away from the working face (point-29m)	230.6	1.0

It is seen from Table 4-7 that the 8-h TWA DPM concentrations at each monitoring point and plane at the same location in the heading are similar, which leads to correction factors ranging from 0.9 to 1.0. The comparisons are also shown in Fig. 4-31.

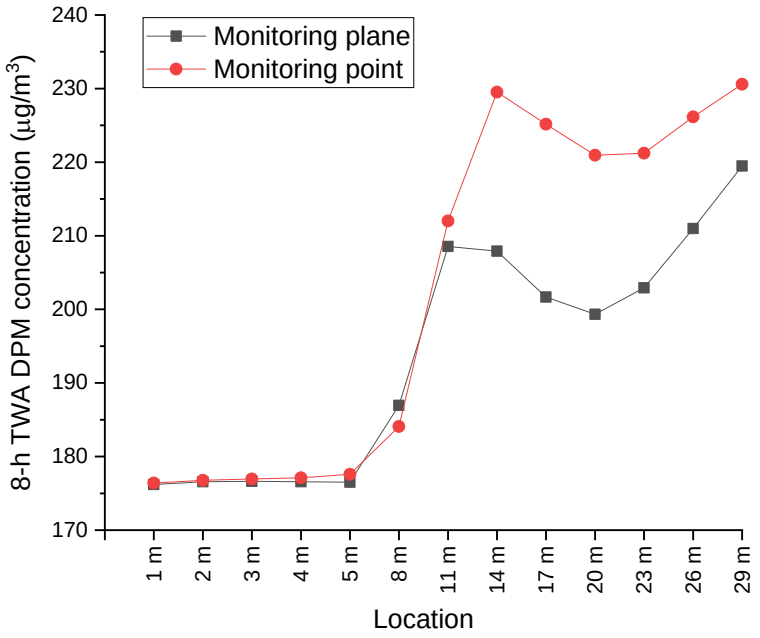

Fig. 4-31. 8-h TWA DPM concentration (µg/m^3) at the monitoring points and planes in the heading.

To better understand the 8-h TWA DPM concentrations shown in Table 4-7, the DPM concentration over 3,000 s (50 min) at the monitoring planes in the heading are shown in Fig. 4-32 and Fig. 4-33. The DPM concentrations over 3,000 s (50 min) at the monitoring points in the heading are shown in Fig. 4-34 and Fig. 4-35. For visualization purposes, not all the DPM concentrations over 28,800 s (8 h) are shown because the DPM concentration pattern in the figures can be vague.

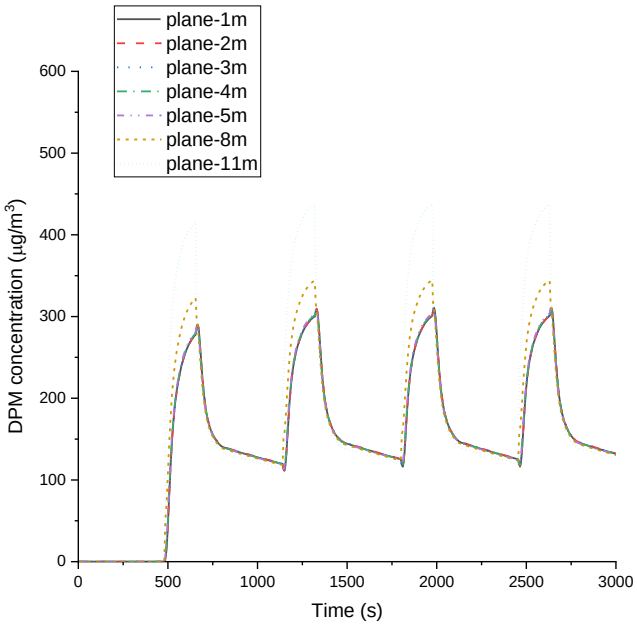

Fig. 4-32. DPM concentration (μg/m^3) over time at the monitoring planes (from 1 m to 11 m away from the working face) in the heading.

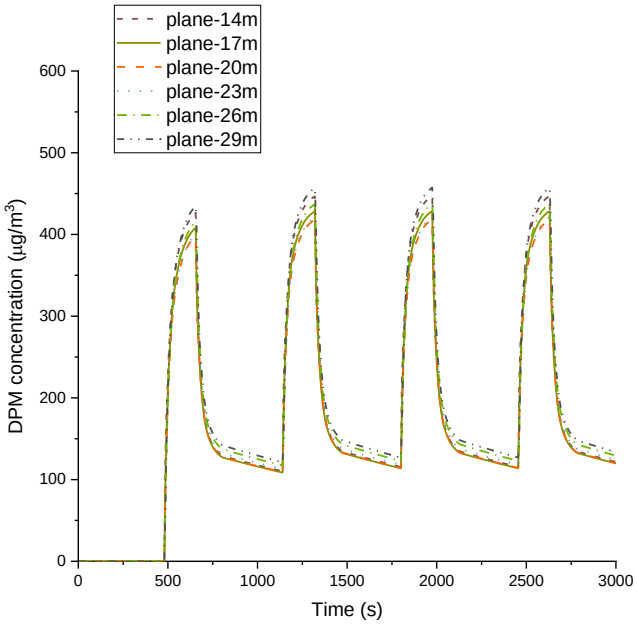

Fig. 4-33. DPM concentration (μg/m^3) over time at the monitoring planes (from 14 m to 29 m away from the working face) in the heading.

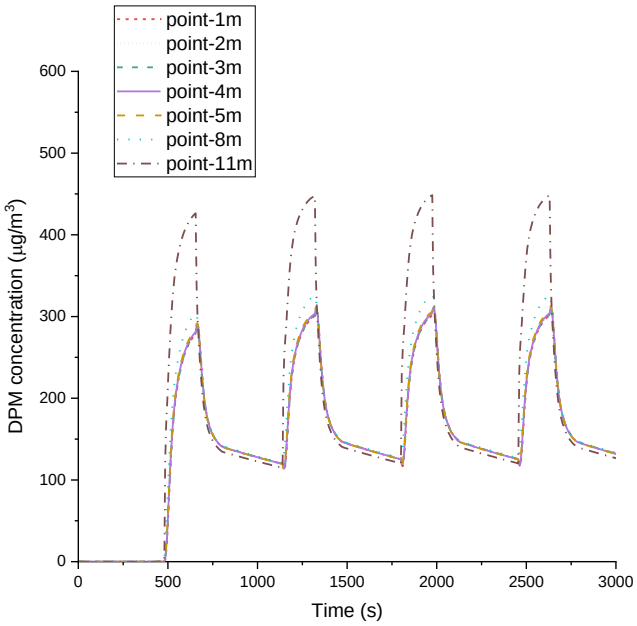

Fig. 4-34. DPM concentration (μg/m^3) over time at the monitoring points (from 1 m to 11 m away from the working face) in the heading.

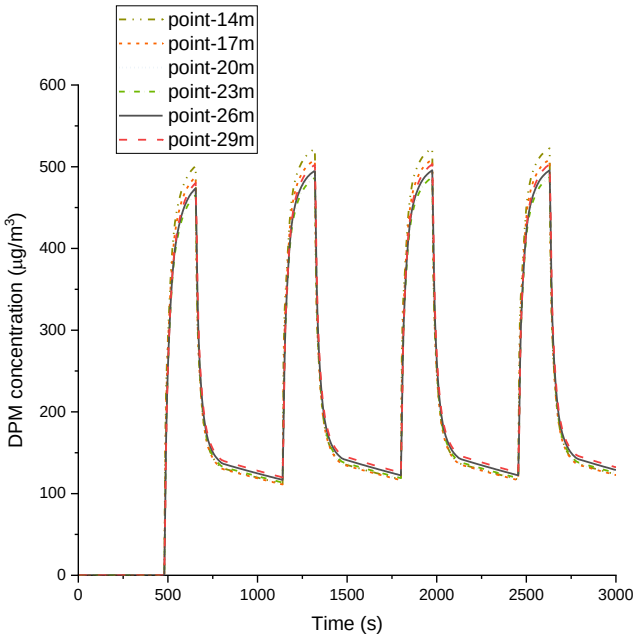

Fig. 4-35. DPM concentration (μg/m^3) over time at the monitoring points (from 14 m to 29 m away from the working face) in the heading.

From Fig. 4-32 and Fig. 4-34, it is clear that the DPM concentrations over time at the monitoring points and at the planes (from 1 m to 11 m away from the working face) in the heading are similar, which are also reflected by the correction factors in Table 4-7. More details on the DPM concentration over time at the monitoring points and planes (from 1 m to 11 m away from the working face) can be found in Fig. 4-36, Fig. 4-37, and Fig. 4-38.

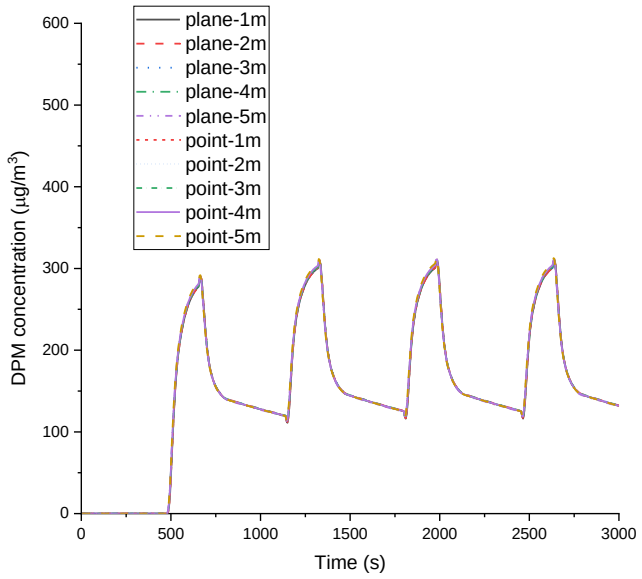

Fig. 4-36. DPM concentration (μg/m^3) over time at the monitoring points and planes (from 1 m to 5 m away from the working face) in the heading.

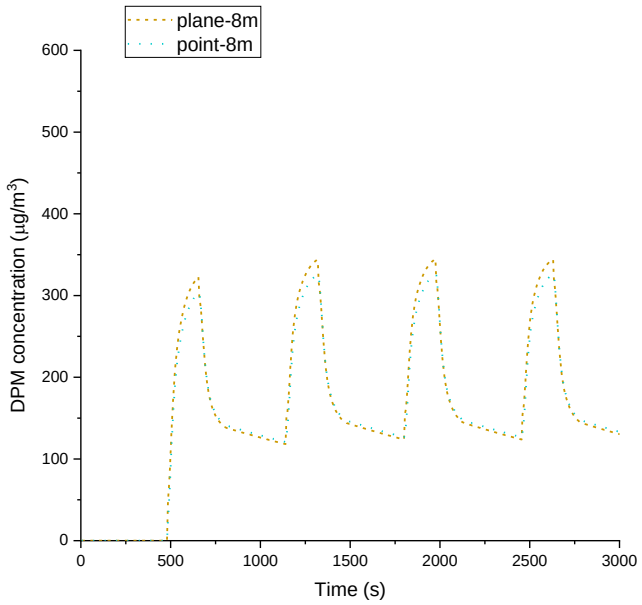

Fig. 4-37. DPM concentration (μg/m^3) over time at the monitoring point and plane (8 m away from the working face) in the heading.

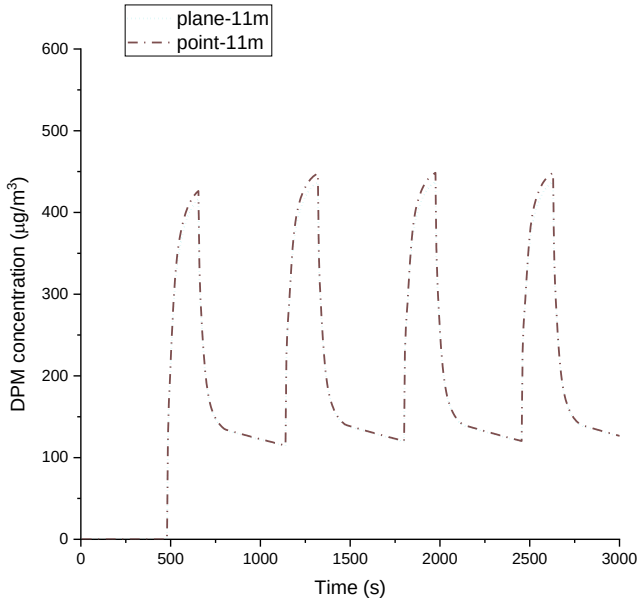

Fig. 4-38. DPM concentration (μg/m^3) over time at the monitoring point and plane (11 m away from the working face) in the heading.

It is seen from Fig. 4-33 and Fig. 4-35 that the DPM concentrations over time at the monitoring points (from 14 m to 29 m away from the working face) are greater than that at the monitoring planes. This relationship is also reflected by the correction factors in Table 4-7. More details on the DPM concentration over time at the monitoring points and planes (from 14 m to 29 m away from the working face) can be found from Fig. 4-39 to Fig. 4-44.

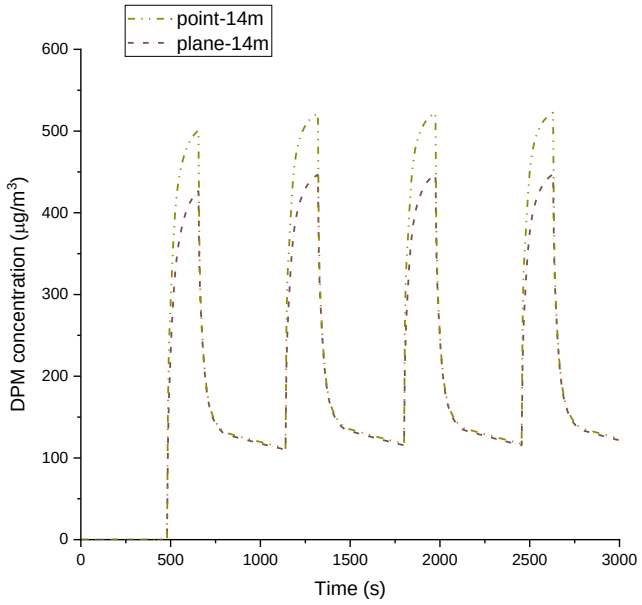

Fig. 4-39. DPM concentration (µg/m^3) over time at the monitoring point and plane (14 m away from the working face) in the heading.

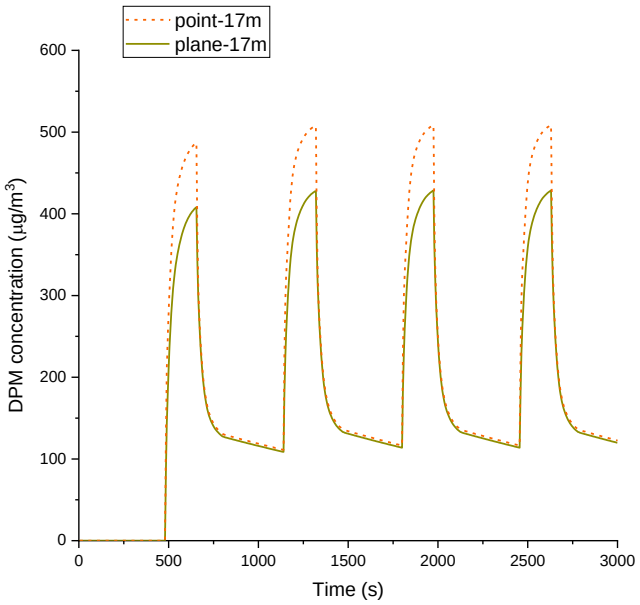

Fig. 4-40. DPM concentration (μg/m^3) over time at the monitoring point and plane (17 m away from the working face) in the heading.

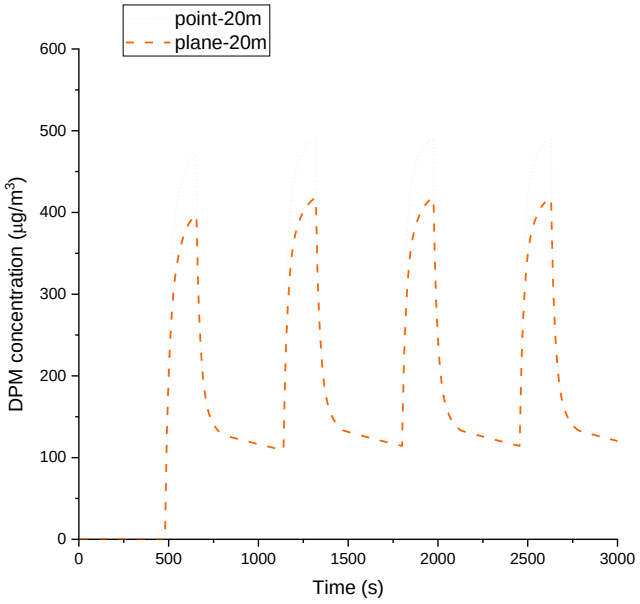

Fig. 4-41. DPM concentration (μg/m^3) over time at the monitoring point and plane (20 m away from the working face) in the heading.

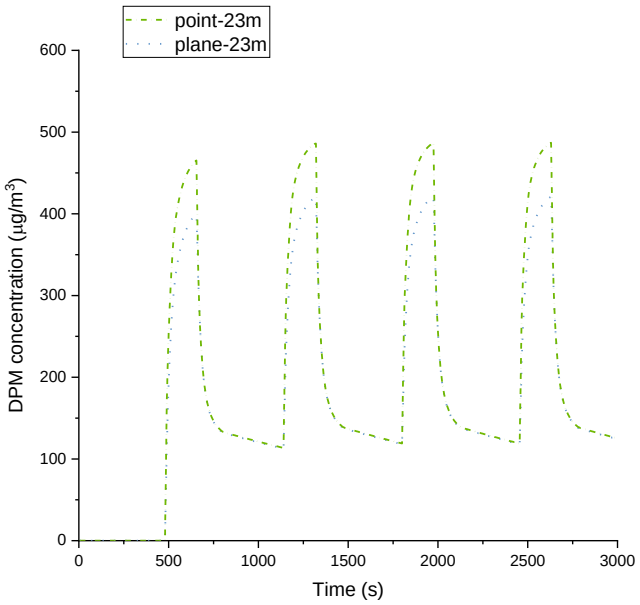

Fig. 4-42. DPM concentration (μg/m^3) over time at the monitoring point and plane (23 m away from the working face) in the heading.

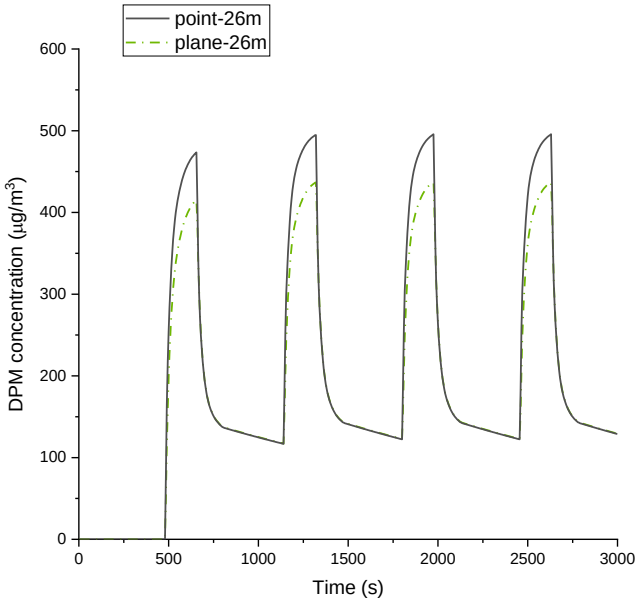

Fig. 4-43. DPM concentration (μg/m^3) over time at the monitoring point and plane (26 m away from the working face) in the heading.

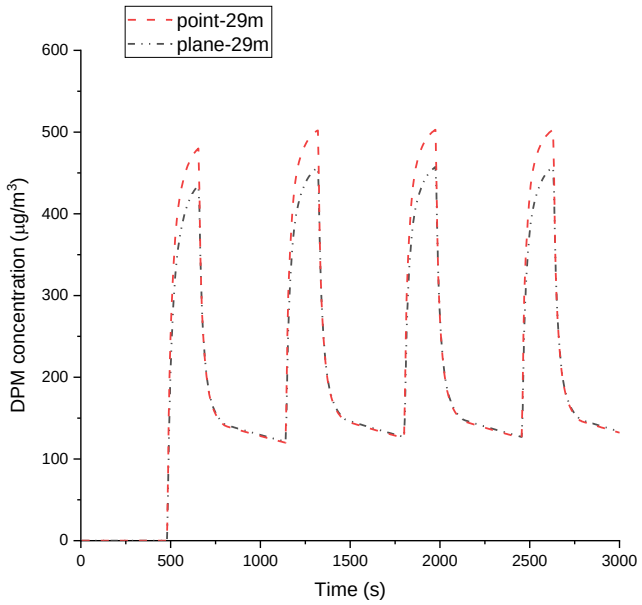

Fig. 4-44. DPM concentration (μg/m^3) over time at the monitoring point and plane (29 m away from the working face) in the heading.

Table 4-8 shows the 8-h TWA DPM concentrations on the twelve monitoring points and on the monitoring plane at the outlet. The correction factors at each monitoring point are also shown in the table.

Table 4-8. Comparisons of the 8-h TWA DPM concentrations on the monitoring points and plane at the outlet

Location	8-h TWA DPM (μg/m^3)	Correction factor
Outlet-plane	100.5	NA
Outlet-SP1	144.1	0.7
Outlet-SP2	73.6	1.4
Outlet-SP3	44.6	2.3
Outlet-SP4	22.7	4.4
Outlet-SP5	196.0	0.5
Outlet-SP6	174.8	0.6
Outlet-SP7	106.7	0.9
Outlet-SP8	6.6	15.2
Outlet-SP9	146.0	0.7
Outlet-SP10	39.3	2.6
Outlet-SP11	4.8	20.9
Outlet-SP12	0.04	2,408.6

It is seen from Table 4-8 that depending on the location of the monitoring point on the plane, the 8-h TWA DPM concentrations on the monitoring points and plane have a significant difference. As a result, the correction factors vary significantly. When the number of real-time DPM monitors is limited and the space to install the DPM monitors is constrained (e.g., no monitor can be installed at the height of 1.7 m on the wall), the 8-h TWA DPM concentrations across the cross-sectional area, especially at the average height of a person, can be difficult to be predicted without the use of CFD. More details on the DPM concentration over time at the monitoring points (from SP1 to SP12) and the plane can be found in Fig. 4-45 and Fig. 4-46.

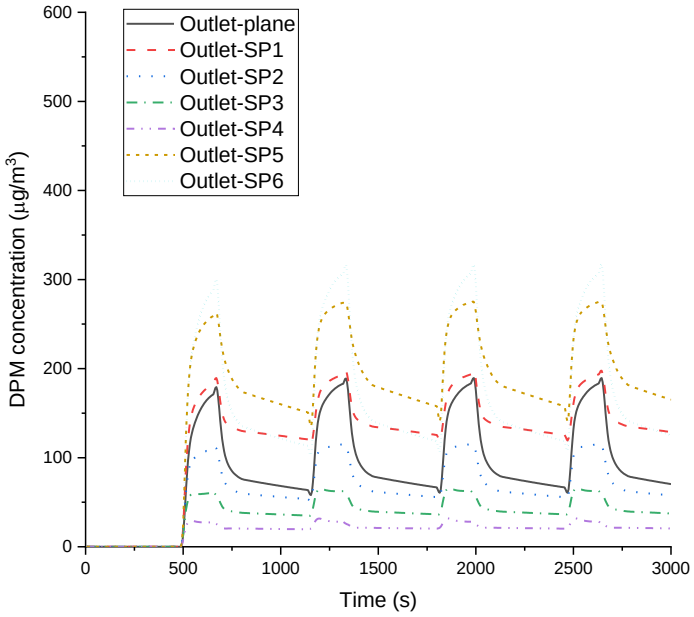

Fig. 4-45. DPM concentration (μg/m^3) over time at the monitoring points (from SP1 to SP6) and the monitoring plane (outlet).

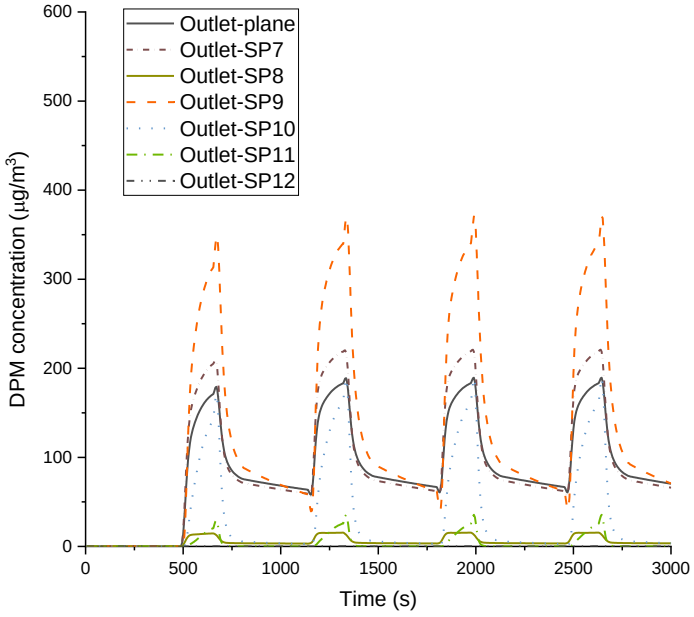

Fig. 4-46. DPM concentration (μg/m^3) over time at the monitoring points (from SP7 to SP12) and the monitoring plane (outlet).

Table 4-9 shows the 8-h TWA DPM concentrations on the twelve monitoring points and on the monitoring plane at offset monitoring plane 1. The correction factors at each monitoring point are also shown in the table.

Table 4-9. Comparisons of the 8-h TWA DPM concentrations on the monitoring points and plane at offset monitoring plane 1

Location	8-h TWA DPM (μg/m^3)	Correction factor
Offset monitoring plane 1-plane (Offset1-plane)	101.8	NA
Offset monitoring plane 1-SP1 (Offset1-SP1)	184.8	0.6
Offset monitoring plane 1-SP2 (Offset1-SP2)	94.3	1.1
Offset monitoring plane 1-SP3 (Offset1-SP3)	62.1	1.6
Offset monitoring plane 1-SP4 (Offset1-SP4)	32.1	3.2
Offset monitoring plane 1-SP5 (Offset1-SP5)	227.2	0.4
Offset monitoring plane 1-SP6 (Offset1-SP6)	180.3	0.6
Offset monitoring plane 1-SP7 (Offset1-SP7)	95.7	1.1
Offset monitoring plane 1-SP8 (Offset1-SP8)	3.5	29.1
Offset monitoring plane 1-SP9 (Offset1-SP9)	114.0	0.9
Offset monitoring plane 1-SP10 (Offset1-SP10)	9.6	10.6
Offset monitoring plane 1-SP11 (Offset1-SP11)	0.2	543.8
Offset monitoring plane 1-SP12 (Offset1-SP12)	0.001	165,012.8

It is observed from Table 4-9 that the 8-h TWA DPM concentrations on the monitoring points and plane at offset monitoring plane 1 are similar to the 8-h TWA DPM concentrations on the monitoring points and plane at the outlet. The 8-h TWA DPM concentrations vary significantly, which is from 0.001 μg/m^3 to 227 μg/m^3. More details on the DPM concentration over time at the monitoring points (from SP1 to SP12) and the plane can be found in Fig. 4-47 and Fig. 4-48.

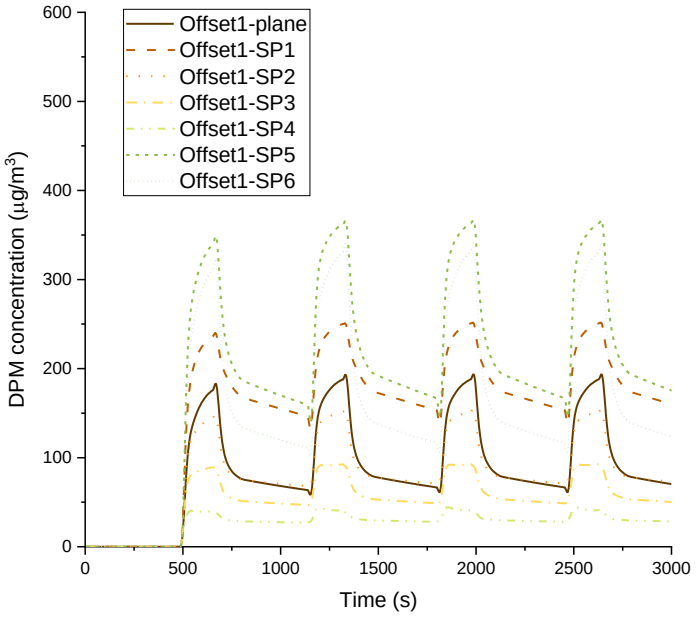

Fig. 4-47. DPM concentration (µg/m^3) over time at the monitoring points (from SP1 to SP6) and the monitoring plane (offset monitoring plane 1).

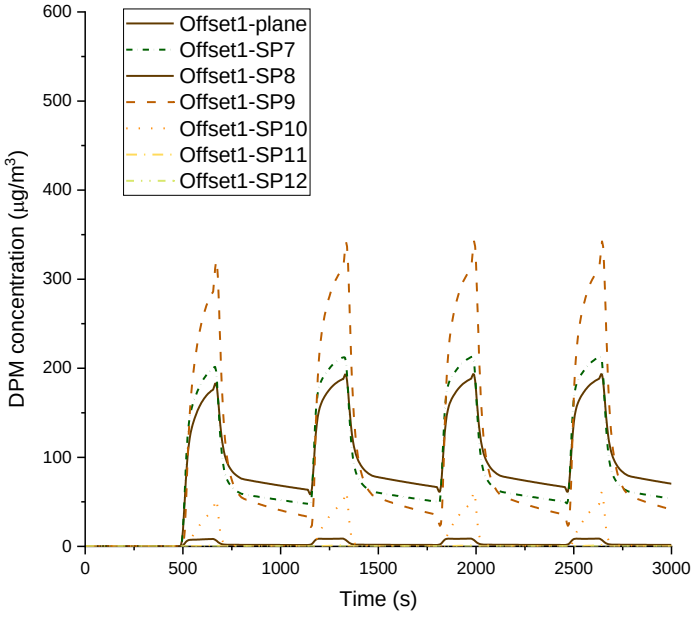

Fig. 4-48. DPM concentration (µg/m^3) over time at the monitoring points (from SP7 to SP12) and the monitoring plane (offset monitoring plane 1).

Table 4-10 shows the 8-h TWA DPM concentrations on the twelve monitoring points and on the monitoring plane at offset monitoring plane 2. The correction factors at each monitoring point are also shown in the table.

Table 4-10. Comparisons of the 8-h TWA DPM concentrations on the monitoring points and plane at offset monitoring plane 2

Location	8-h TWA DPM ($\mu g/m^3$)	Correction factor
Offset monitoring plane 2-plane (Offset2-plane)	103.8	NA
Offset monitoring plane 2-SP1 (Offset2-SP1)	218.8	0.5
Offset monitoring plane 2-SP2 (Offset2-SP2)	149.7	0.7
Offset monitoring plane 2-SP3 (Offset2-SP3)	115.1	0.9
Offset monitoring plane 2-SP4 (Offset2-SP4)	41.2	2.5
Offset monitoring plane 2-SP5 (Offset2-SP5)	251.5	0.4
Offset monitoring plane 2-SP6 (Offset2-SP6)	162.7	0.6
Offset monitoring plane 2-SP7 (Offset2-SP7)	51.5	2.0
Offset monitoring plane 2-SP8 (Offset2-SP8)	0.7	148.7
Offset monitoring plane 2-SP9 (Offset2-SP9)	66.5	1.6
Offset monitoring plane 2-SP10 (Offset2-SP10)	0.5	216.5
Offset monitoring plane 2-SP11 (Offset2-SP11)	0.001	89,457.5
Offset monitoring plane 2-SP12 (Offset2-SP12)	0.000001	182,366,995.2

It is seen from Table 4-10 that the 8-h TWA DPM concentrations on the monitoring plane and each of the monitoring points at offset monitoring plane 2 vary significantly. More details on the DPM concentration over time at the monitoring points (from SP1 to SP12) and the plane can be found in Fig. 4-49 and Fig. 4-50.

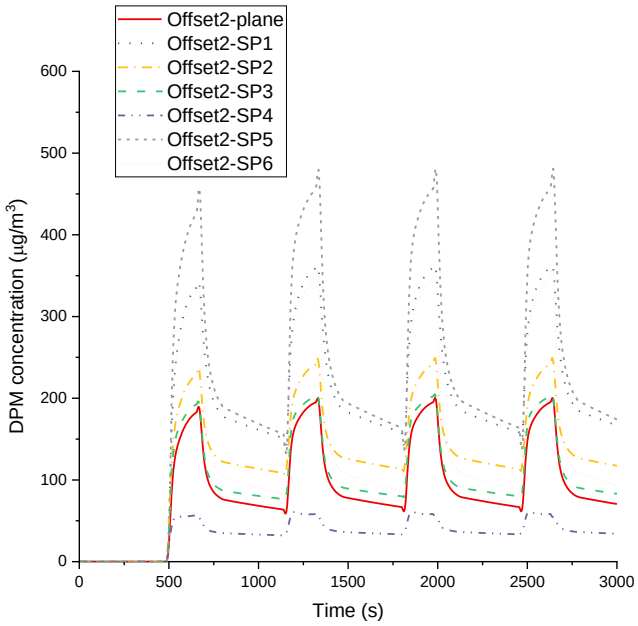

Fig. 4-49. DPM concentration (μg/m^3) over time at the monitoring points (from SP1 to SP6) and the monitoring plane (offset monitoring plane 2).

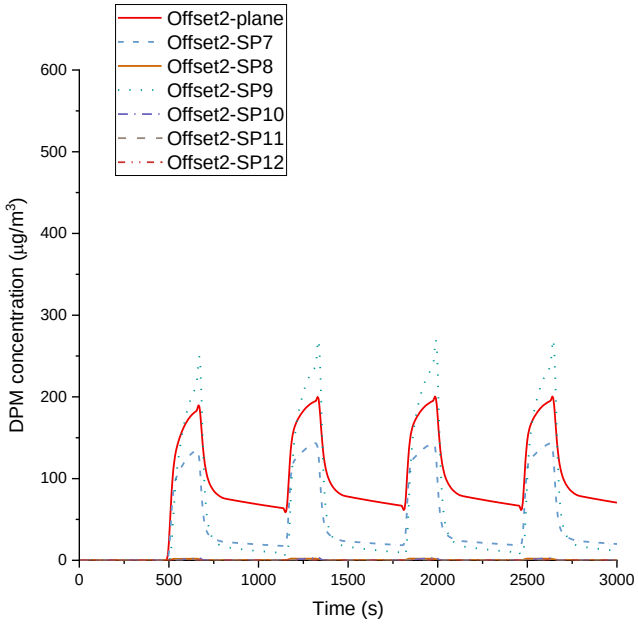

Fig. 4-50. DPM concentration (μg/m^3) over time at the monitoring points (from SP7 to SP12) and the monitoring plane (offset monitoring plane 2).

The DPM concentrations over 3,000 s at the three monitoring planes near the outlet are presented in Fig. 4-51, showing that the area-average DPM concentrations over time at the three monitoring planes are similar. More details can be found in Table 4-8, Table 4-9, and Table 4-10.

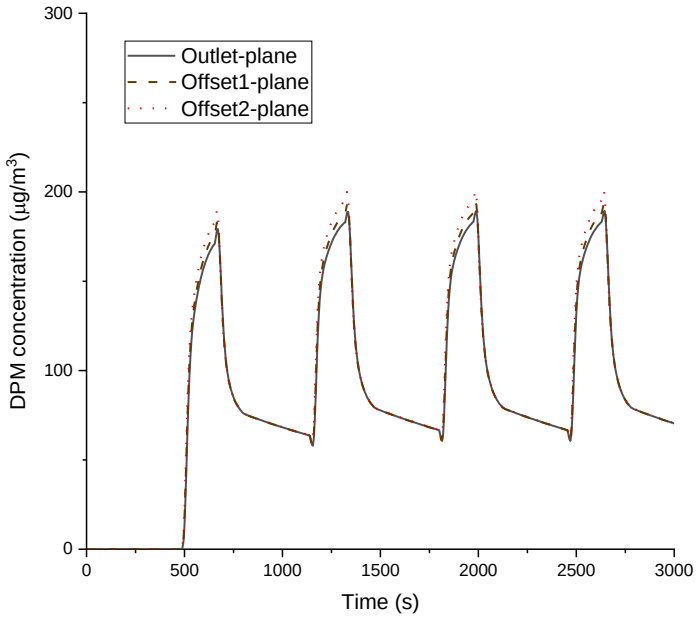

Fig. 4-51. Area-average DPM concentration (μg/m^3) over time at the outlet, offset monitoring plane 1, and offset monitoring plane 2.

As mentioned in the assumptions (refer to Section 4.4.5), the cycle time of the diesel equipment in the calibrated CFD model is 11 min in total with 3 min in the heading and 8 min out of the heading. It was found that the first DPM peak showed up at 670 s (11 min and 10 s) and the first DPM residual showed up at 1,150 s (19 min and 10 s) at the monitoring plane at the outlet. The contours of the velocity magnitude and the DPM concentration at 670 s and 1,150 s at the three monitoring planes near the outlet are shown from Fig. 4-52 to Fig. 4-55.

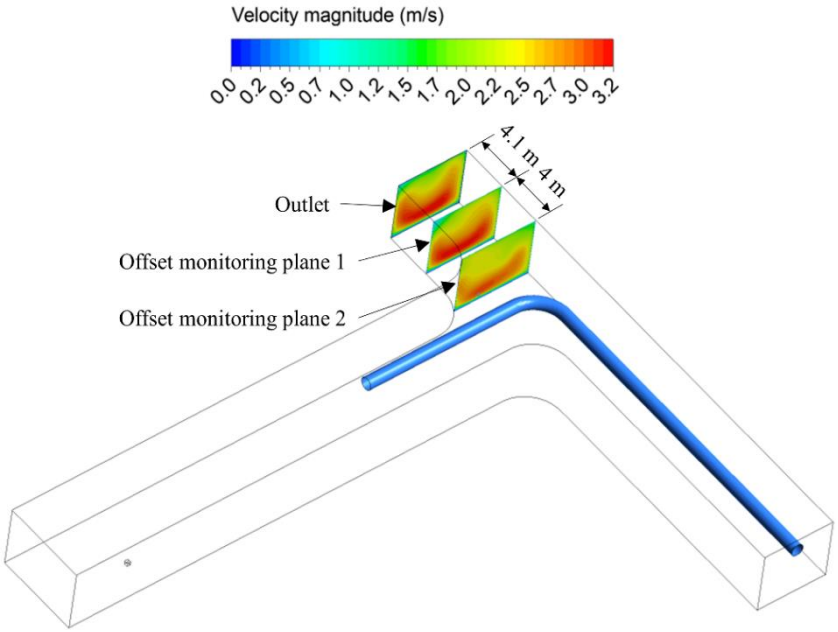

Fig. 4-52. The contour of velocity magnitude at the monitoring planes near the outlet at 670 s.

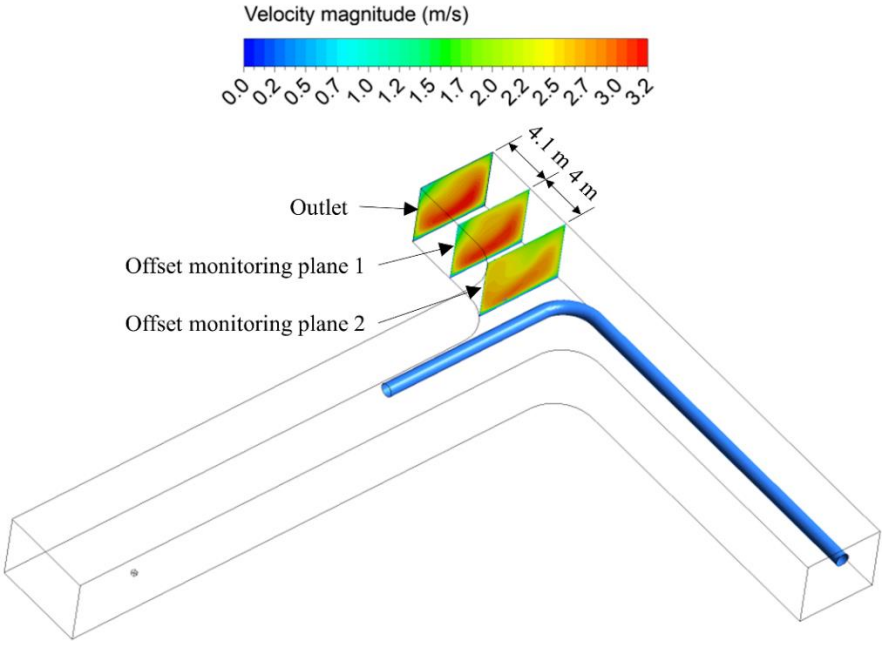

Fig. 4-53. The contour of velocity magnitude at the monitoring planes near the outlet at 1,150 s.

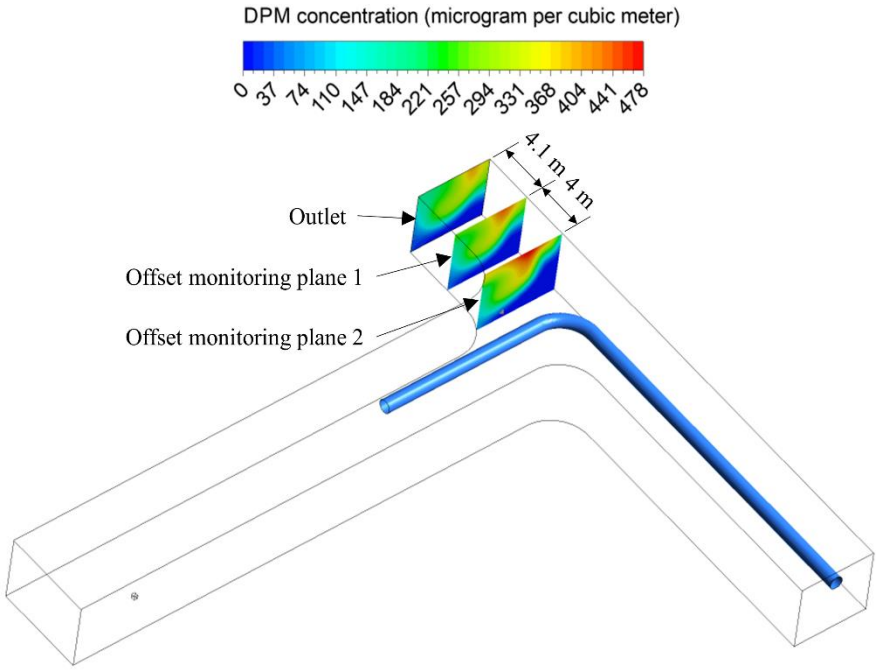

Fig. 4-54. The contour of DPM concentration at the monitoring planes near the outlet at 670 s.

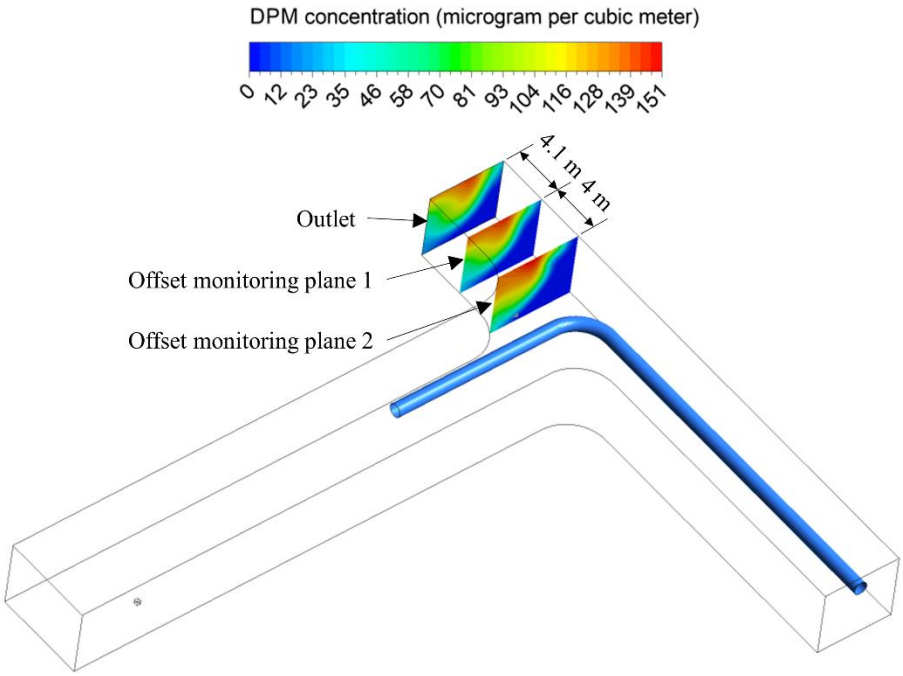

Fig. 4-55. The contour of DPM concentration at the monitoring planes near the outlet at 1,150 s.

It can be seen from Fig. 4-52 to Fig. 4-55 that the DPM concentration and velocity magnitude are negatively correlated. The higher the velocity magnitude, the lower is the DPM concentration. The DPM concentration decreases at all the planes after the DPM source stops releasing in the heading. Enlarged views of the DPM concentration contours at the outlet, offset monitoring plane 1, and offset monitoring plane 2 are shown in Fig. 4-56, Fig. 4-57, and Fig. 4-58, respectively.

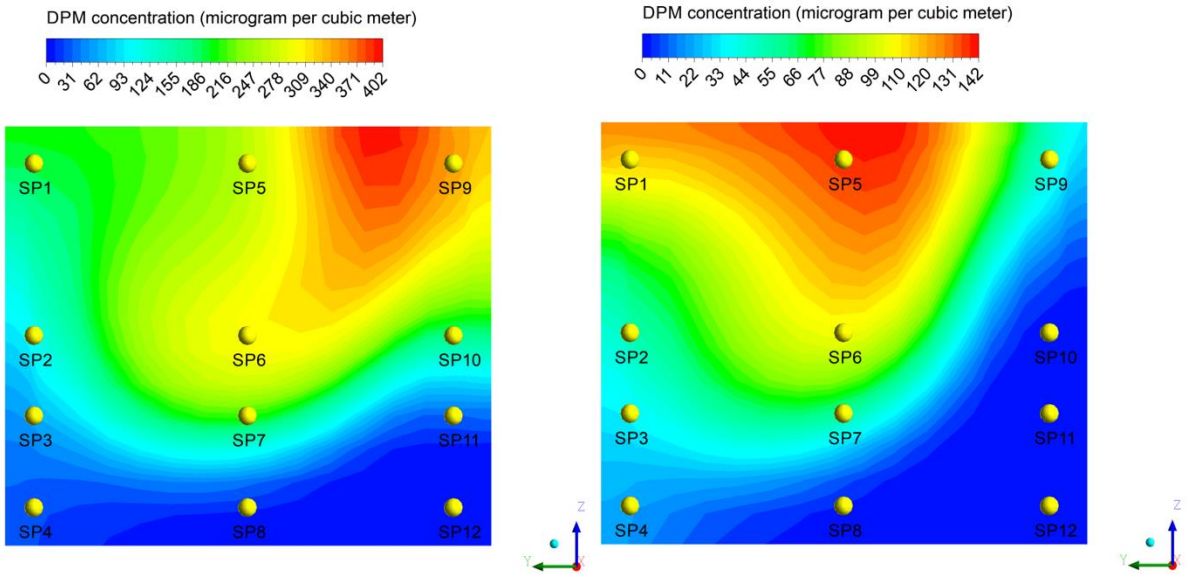

(a) (b)

Fig. 4-56. Figure (a) shows the contour of DPM concentration at the outlet at 670 s. Figure (b) shows the contour of DPM concentration at the outlet at 1,150 s.

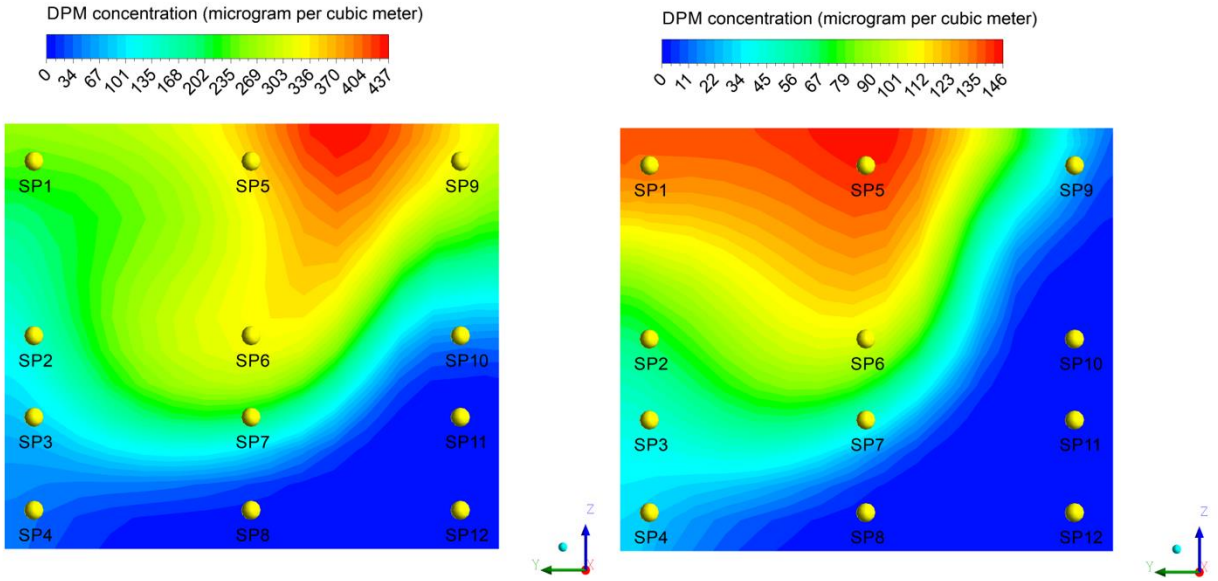

(a) (b)

Fig. 4-57. Figure (a) shows the contour of DPM concentration at offset monitoring plane 1 at 670 s. Figure (b) shows the contour of DPM concentration at offset monitoring plane 1 at 1,150 s.

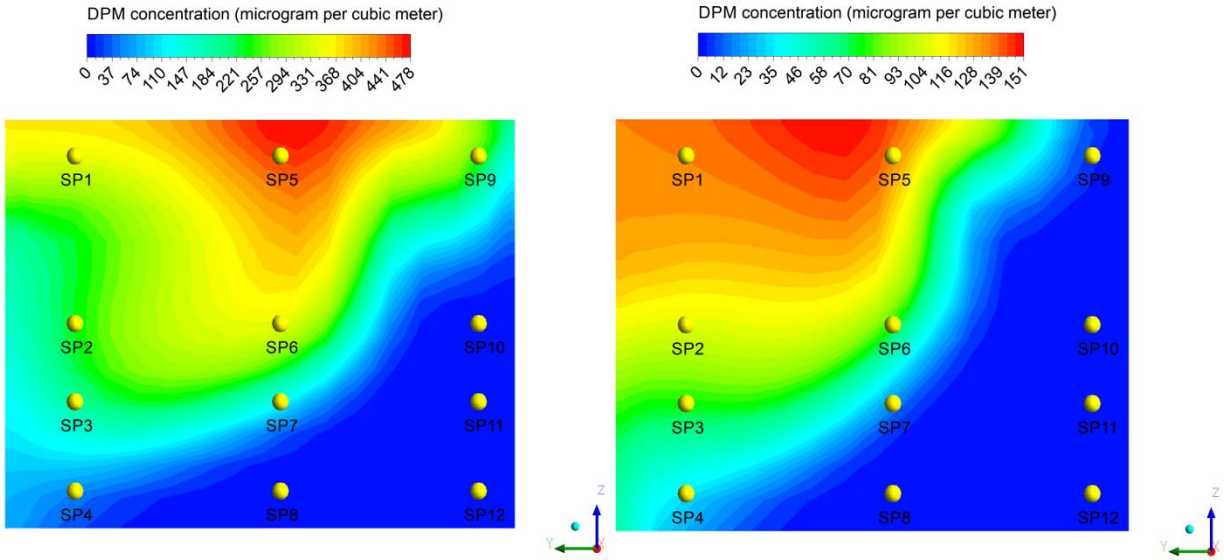

(a) (b)

Fig. 4-58. Figure (a) shows the contour of DPM concentration at offset monitoring plane 2 at 670 s. Figure (b) shows the contour of DPM concentration at offset monitoring plane 2 at 1,150 s.

It is seen from Fig. 4-56, Fig. 4-57, and Fig. 4-58 that the high-DPM-concentration zone shifts to the left at all the planes after the DPM source stops releasing. The DPM concentration significantly varies across the cross-sectional area of the three planes. This also explains the significant variation of the 8-h TWA DPM concentration data shown in Table 4-8, Table 4-9, and Table 4-10.

To summarize, the hybrid methodology takes the DPM residuals (after the DPM source stops releasing) into account when calculating the TWA DPM concentration. The calibrated CFD model, as part of the hybrid methodology, can be used to indicate where the DPM measurements should be taken. For instance, the sampling locations with large correction factors should be avoided when taking the DPM measurements. The hybrid methodology can provide 3D visualizations of the DPM concentration distribution at any location, point, and time of the modeling period. It can also provide the correction factors for DPM measurements to estimate the area-average DPM concentration at a specific location. With the area-average DPM concentration, the equivalent diesel emission rate for a known diesel engine power of the DPM source in Ventsim can be determined. Thereafter, DPM modeling in Ventsim can be conducted with a better calibrated diesel emission rate.

The hybrid modeling is complex and time-consuming. The hybrid methodology will be practical if a database (future work) of the correction factors for diesel emission rates under various scenarios is created. Then, on-site mine engineers can quickly look for a correction factor when conducting DPM modeling in Ventsim.

4.5 Findings and discussion

This chapter presented a hybrid methodology for investigating DPM concentrations over time in an underground mine. The methodology is used to provide improved input to ventilation network models. A calibrated CFD model and an updated Ventsim model using the hybrid methodology were presented. Results from the updated Ventsim model match the monitoring plane data from the calibrated CFD well. Using results from the CFD model to update the ventilation network model at the outlet significantly saves computing time. Results from the updated ventilation network model are considered accurate enough because they are the results from the CFD model, which has been calibrated using experimental data. Unfortunately, due to the low quality airflow and DPM data collected from the field, this study should be viewed as a qualitative study rather than a quantitative study. It should be noted here that the experimental data used are also limited in size, and more field studies are required to enhance the knowledge and value of the proposed hybrid methodology.

It is not practical to use a CFD model alone to simulate mine-scale ventilation due to a large amount of time required to build and solve a model. In terms of a mine-scale ventilation system, the hybrid methodology is a practical option because it is relatively computationally quick. Because this study was conducted only at one heading, the computational time of the updated Ventsim model is equal to that of the CFD model. The computational time depends on the number of LHD work cycles and the complexity of the mine geometry. The efficiency of the updated Ventsim model will be evident when multiple headings are modeled.

The hybrid methodology will be practical if a database (future work) of the correction factors for diesel emission rates under various scenarios is created. On-site mine engineers can quickly look

for a correction factor when conducting DPM modeling in Ventsim. With the hybrid methodology, the main data sampling parameters impacting the DPM concentration at a sampling location near a heading can be grouped into four categories: main drift and heading conditions, ventilation tubing conditions, diesel equipment conditions, and sampling point location.

The main drift and heading conditions include:

1) Dimensions of the main drift and the heading
2) Air density, barometric pressure, and temperature in the sampling area
3) Velocity magnitude, and temperature of the air coming from the main drift inlet
4) Upstream DPM concentration

The ventilation tubing conditions include:

1) The distance from the end of the ventilation tubing to the working face in a heading
2) The diameter of the ventilation tubing
3) The position of the ventilation tubing across the cross-sectional area in the drift (e.g., in the center or biased to one side)
4) Velocity magnitude of the air coming from the ventilation tubing
5) Air leakage along the ventilation tubing

The diesel equipment conditions include:

1) Moving path of diesel equipment (e.g., entering the heading from upstream or downstream direction)

2) Location and time records of diesel equipment in the experiment area (for fitting the CFD model)

3) Standard cycle time of diesel equipment (for calibrating the CFD model)

4) Diesel engine power and diesel emission rate of diesel equipment

5) Position of the diesel exhaust pipe (e.g., against or along with the airflow direction)

6) Dimensions of the diesel exhaust tailpipe

7) The velocity, temperature of diesel exhaust from the tailpipe

8) DPM concentration in the diesel exhaust from the tailpipe

9) The maintenance schedule of diesel equipment

The sampling point location refers to the spatial location(s) (across the cross-sectional area and along the drift) of the sampling point(s).

With the help of the hybrid methodology, the database will contain input data (e.g., the main data sampling parameters) and output data. The output data will contain:

1) The estimated diesel emission rate of the diesel equipment from the calibrated CFD model
2) A correction factor for the current diesel emission rate used in a Ventsim model
3) TWA (e.g., 8 h TWA or 12 h TWA) DPM concentrations at monitoring points and planes at the same location and the correction factors (for converting the DPM concentrations at monitoring points to that at the monitoring plane) in the experiment area

- When the number of DPM monitors is limited on-site, the correction factor can be used to estimate the area-average DPM concentration at the location. The area-average DPM concentration can be used as input for DPM modeling in Ventsim at that location.

4) Figures or time series of data (e.g., the DPM concentration over time at the monitoring points and planes as shown from Fig. 3-32 to Fig. 4-51)
5) The contour of DPM concentration distribution on a monitoring plane at key points in time (e.g., when the DPM peak and residual show as presented from Fig. 4-56 and Fig. 4-58)

An example of the database is shown in Table 4-11. The numbers shown in the table are all hypothetical. The purpose is to show the structure of the database and how the database can be applied.

Table 4-11. An example of the database

Input															Output						
Main drift and heading condition						Ventilation tubing condition				Diesel equipment condition					Sampling plane location				Sampling point location		
Dimensions of the main drift (H×W) (m×m)	Dimensions of the heading (H×W) (m×m)	Air density in the sampling area (kg/m^3)	Air velocity at the main drift inlet (m/s)	Air temperature at the main drift inlet (K)	Upstream DPM concentration (μg/m^3)	The distance from the end of the ventilation tubing to the working face (m)	The diameter of the ventilation tubing(m)	Velocity magnitude of the air coming from the ventilation tubing (m/s)	Air leakage along the ventilation tubing(m^3/s)	Standard cycle time (time in and out of the heading) (min×min)	The velocity of diesel exhaust (m/s)	DPM concentration in the diesel exhaust (μg/m^3)	Engine power (kW)	Diesel emission rate (g/kW·h)	-	8-hr TWA DPM (μg/m^3)	Estimated diesel emission rate (g/kW·h) from the DPM source	Correction factor on the diesel emission rate	-	8-hr TWA DPM (μg/m^3)	Correction factor
5x6	5x7	1.2	1.5	300	0	30	1.07	30	5	3x8	24	8000	200	0.2	Monitoring plane 1	100	0.4	2	SP1	196	0.51
																			SP2	107	0.93
																			…	…	…
…	…	…	…	…	…	…	…	…	…	…	…	…	…	…	…	…	…	…	…	…	…

Both the input (i.e., the main data sampling parameters) and the output data are presented in Table 4-11. Due to the limited space, not all the data sampling parameters are included in the input. For the same reason, no figure (or time series of data) and contour of DPM concentration distribution on a monitoring plane at key points in time are included in the output. Results from more experiments can be filled into the table, which will make the database useful for on-site mine engines to make short-term and long-term ventilation plans.

A user can use the database to understand how the DPM distributes over time at different locations (e.g., across a cross-sectional area or along the drift). When conducting an experiment using real-time DPM monitors, the user can determine where the DPM monitor should be installed with the help of the DPM concentration contours on monitoring planes at key points in time. The DPM monitors should be installed at locations where the airflow and DPM are as well-mixed as possible and the DPM concentration is relatively high compared with other points across a cross-sectional area.

Regarding DPM modeling in Ventsim, either the estimated diesel emission rate from the DPM source or the correction factor on the existing diesel emission rate in the database can be used to provide the correct diesel emission rate from the DPM source. Then a DPM model in Ventsim can be quickly set up with the diesel emission rate and the known diesel engine power.

To summarize, the database makes it possible to consider air quality during ventilation planning. On-site engineers can quickly look for a correction factor for diesel emission rate when conducting DPM modeling in Ventsim. The database will be useful when there is a major change in the diesel fleet at a mine site. This change can be the increasing number of diesel equipment for production

demand. With additional diesel equipment working underground, a considerable amount of DPM can be emitted into the air. Detailed analysis of the DPM concentration profile across the entire mine site will be valuable with the use of the database induced from the hybrid methodology. The observations from the analysis can provide guidance for short-term and long-term ventilation plans and production schedules. An example of the guidance is the maximum number of diesel equipment working on a specific level based on the mine-scale DPM modeling (using the estimated diesel emission rate from the database) in Ventsim. For a given production schedule, different ventilation plans can be quickly assessed.

Chapter 5

5 Conclusion and Future Work

5.1 Conclusion and remarks

The framework to develop a hybrid methodology for modeling of diesel particulate matter concentration in underground mine ventilation systems is proposed and assessed in this research. The methodology uses DPM results from a calibrated CFD model to update the results from a simplified ventilation network model at the shared outlet(s) in both the models. ANSYS Fluent is chosen as the CFD solver because it is commonly used in mining-related research in North America and it is able to perform all the tasks required by this research. In addition, the author is familiar with how ANSYS Fluent works, and other researchers use it for DPM modeling as well. Ventsim is chosen as the ventilation network model because it is able to perform both steady-state and dynamic DPM modeling. In addition, it is commercially available and has been used for several years in mine sites in North America. The CFD DPM results are converted to equivalent diesel emission rates for input in Ventsim. It is found that the results from the updated ventilation network model match the results from the calibrated CFD model very closely.

DPM modeling in CFD is not a new topic. However, to the best knowledge of the author, no approach has been found in the literature that can perform a transient simulation of DPM over an hour in a timely manner. The prior approaches had the geometry of the diesel equipment included in the CFD model, which not only increased the mesh size (e.g., more than one million elements) but increased the complexity of the flow domain as well. As a result, the computing time was

extremely long (e.g., days or weeks). Moreover, the prior approaches modeled the diesel equipment either moving in one straight direction (without going back and forth in a drift or any turns) or staying at one location but kept releasing DPM for less than 300 s. However, it still took days or weeks to derive a solution from CFD. In contrast, the proposed DPM modeling approach in CFD makes it possible to conduct a DPM modeling over an extended period (e.g., an hour, eight hours) in a timely manner. Consequently, the DPM concentration over a full working cycle of diesel equipment, which is much closer to the real situation for diesel equipment in underground mines, can be modeled.

Because DPM concentration is measured by an 8-hour average or shift-average in underground mines, existing DPM modeling approaches in CFD cannot be used in this research. Hence, a new DPM modeling approach in CFD was proposed. In the CFD approach, a single DPM source is created on the floor of a heading to represent the diesel exhaust pipe of diesel equipment. The DPM source does not move, but DPM concentration and velocity magnitude of the diesel exhaust vary over time, which imitates the movement of the diesel equipment in and out of the experimental area. The DPM concentration and velocity magnitude of the diesel exhaust are adjusted to calibrate the model based on statistical analysis. According to the results for both EXP3 and EXP5 presented in Chapter 3, good agreements between the CFD results and experimental data are found at two out of three locations in both experiments. In addition, the simulation time (i.e., hours) of this approach is much less than that of existing CFD approaches (i.e., days or weeks) due to smaller mesh size and less complex flow domain.

The CFD model is a fitted model because the results from it only represent the current DPM distribution and cannot be used to predict future DPM distribution. Therefore, the concept of

structured/fixed/constant cycle time is introduced. The structured cycle time is estimated based on the equipment timeline reports from the mine site and represents an average cycle time for diesel equipment in a heading. The impact of cycle time on DPM concentration over time is also explored by using the CFD model. After testing (e.g., seven scenarios used in this study), the cycle time leading to the best CFD results is considered as the standard cycle time. The CFD model with this standard cycle time is calibrated to the experimental data with an 80% accuracy. With more cycles added to the calibrated CFD model, DPM distribution can be predicted. Results from the calibrated CFD model are also compared with the results from a Ventsim model with the standard cycle time.

DPM modeling in Ventsim is not new. However, to the best knowledge of the author, no publications (or publications with limited access) have been found on dynamic DPM modeling in Ventsim. Hence, a Ventsim model is built to perform DPM modeling over an hour, and the results are compared with that from the calibrated CFD model. It was found that the diesel emission rate directly affects DPM modeling in Ventsim. For example, a 10% increase in the diesel emission rate will lead to a 10% increase in the DPM concentration when the diesel power and airflow are kept constant. The results from the calibrated CFD model can be used to provide more accurate diesel emission rates in the Ventsim model. Without the calibrated CFD model, the diesel emission rate has to be either measured or inferred from the real-time DPM monitors installed in the experimental area. However, both the measurements and the use of real-time DPM monitors are not cost-effective and they are time-consuming. Besides, mines always have busy schedules and the number of real-time monitors is limited, which makes it harder to conduct such experiments. Hence, using the calibrated CFD model to improve the diesel emission rate input in Ventsim is beneficial. The workflow for integrating a CFD model with a ventilation network solver is developed.

With the hybrid methodology, the updated Ventsim DPM results are the same as those from the calibrated CFD. In terms of a mine-scale ventilation network, DPM in all the dead-end headings can be modeled in CFD, and the existing Ventsim model can be updated. Then, the mine-scale DPM modeling can be processed in a timely manner.

To summarize, the framework of the hybrid methodology consists of four main components: data sampling (i.e., raw field data collected with high accuracy instrument), model development and modeling methodology (e.g., CFD modeling, Ventsim model using the hybrid methodology), a database with the DPM concentration and the correction factors for diesel emission rates under various conditions (e.g., Table 4-11), and application of the database (e.g., short-term and long-term ventilation planning, production schedule optimization).

This work can also be used to better indicate where DPM measurements should have been taken. The DPM measurements should have been taken in headings without a large amount of DPM coming from upstream of the experiment area, e.g., DPM measurements in the fresh air upstream with the diesel equipment as the only DPM source. Besides, the measurements could have been taken further downstream of the heading to allow the DPM well-mixed with the air. In addition, multiple DPM monitors could have been installed across the same cross-sectional area downstream heading to capture the DPM concentration distribution over time at the sampling location.

5.2 Future work

Future work related to this research can focus on the following topics:

- In this study, two experiments were conducted and studied. The CFD results remain to be validated using better field data (both raw airflow and DPM data). More experiments and more real-time DPM monitors are necessary to test the repeatability of the hybrid methodology. Additional field studies would also provide better validation and this should be considered in future work.
- The maintenance data on the diesel engine was unknown at the time when the experiments were conducted. This data, captured in future studies, will provide a more accurate diesel emission rate in Ventsim.
- Sensitivity studies on the location of the DPM source in the CFD model can be carried out to ensure that the results are consistent.
- A sensitivity analysis on the velocity magnitude of airflow coming out of the ventilation tubing can be carried out to estimate an improved airflow quantity to dilute the DPM concentration (if above the regulatory limit). Savings on ventilation cost can be assessed with the improved airflow quantity.
- The Dekati DePS (Dekati Ltd., 2018), which is a real-time DPM monitor made in Finland, can be a substitute for the Airtec monitor because it has better accuracy. In addition, parts of the monitors do not need to be regularly changed.
- The process of updating a Ventsim model using the hybrid methodology can be automated because both the model setup and data conversions can be automated with some programming effort. User-friendliness can be improved.

- With enough experiments and calibrated CFD models, a database of TWA DPM or DPM profile over time under various conditions (including cycle times, DPM concentration and velocity magnitude of diesel exhaust from diesel equipment, velocity of the airflow coming from the ventilation tubing and main drift inlet, different length of simulation time, etc.) can be established for predicting DPM distribution. The database should be updated with more studies. The database can be made available to the mining industry.
- The DPM concentration inside the environmental cab of diesel equipment should be studied. It is important because the operator of the LHD may be exposed to higher DPM concentrations than the regulatory limit over a shift (e.g., 8 hours of operation).
- The updated Ventsim model with the hybrid methodology can be used in mine production schedule optimization. The updated Ventsim model has the potential to provide accurate DPM results, which can be used by VCM and SOT for schedule optimization purposes.

Lessons were learned from this study. The following list summarizes the essential aspects that need to be considered for future field studies.

- Have a detailed plan, design, and methodology of the field study beforehand (e.g., the available time and number of the personnel, equipment, and production headings provided by the mine site).
- Budget appropriately for the experiments and make sure funds are available after completing the design of experiments and before conducting the experiments.
- Select proper sampling locations where airflow is as fully developed as possible.

- Use several instruments made by different manufacturers at each sampling location for result validation.
- Limit the uncertainties (e.g., high DPM concentration from upstream, more than one diesel equipment work in the experiment area) when measuring DPM concentration.
- An electronic tagging system would provide accurate timing and location information for diesel equipment moving into or out of the study area.
- Check accuracy of the instrument (e.g., DPM monitor, vane anemometer).
- Check the diesel engine condition and its maintenance schedule.
- Check the airflow balance from the airflow measurements.
- Check leakage on the ventilation tubing.

The introduction of this hybrid methodology opens new opportunities and challenges for research. However, the benefits of the practical application of this methodology in real-life mine scenarios can be cost-effective and time-saving with the completion of a DPM database based on various scenarios.

References

Acuña, E., Maynard, R., Hall, S., Hardcastle, S. G., Li, G., Lowndes, I. S. and Tonnos, A. (2010) 'Practical mine ventilation optimization based on genetic algorithms for free splitting networks', in *13th United States/North American Mine Ventilation Symposium*. Sudbury, Ontario, Canada.

Acuña, E. I. and Lowndes, I. S. (2014) 'A review of primary mine ventilation system optimization', *Interfaces*, 44(2), pp. 163–175. doi: 10.1287/inte.2014.0736.

Allen, C. L. and Tran, T. T. (2011) 'Ventilation-On-Demand control system's impact on energy savings and air quality', in *CIM*. Montreal, Canada.

Álvarez, R., Acuña, E. and Hurtado, J. P. (2011) 'A comparison of main mine ventilation optimisation methodologies—manual and genetic algorithms', in *2nd International Conference on Mine Planning*. Antofagasta, Chile.

Anon (1988) 'Carcinogenic Effects of Exposure to Diesel Exhaust', in. National Institute for Occupational Safety and Health (NIOSH), Department of Health and Human Services, pp. 88–116.

Anon (2000) 'Health Assessment Document for Diesel Exhaust', in. U.S. Environmental Protection Agency (EPA), p. Report EPA/600/8-90/057E.

Anon (2001) 'Threshold Limit Values for Chemical Substances and Physical Agents and Biological Exposure Indices', in. American Conference of Governmental Industrial Hygienists (ACGIH).

ANSYS Inc. (2009a) *ANSYS Fluent 12.0 Theory Guide*. Canonsburg, PA.

ANSYS Inc. (2009b) *ANSYS Fluent 12.0 UDF Manual*. Canonsburg, PA.

ANSYS Inc. (2009c) *ANSYS Fluent 12.0 User's Guide*. Canonsburg, PA.

ANSYS Inc. (2013a) *ANSYS Fluent Meshing User's Guide*. Canonsburg, PA.

ANSYS Inc. (2013b) *Workbench User's Guide*. Canonsburg, PA.

ASHRAE (2001) 'The 2001 ASHRAE Handbook Fundamentals', in. Atlanta, GA, USA.

Atkinson, J. J. (1854) 'On the Theory of the Ventilation of Mines', *North of England Institute of Mining Engineers*, 3, p. 118.

Baiden, G. (2001) 'TeleminingTM Systems Applied To Hardrock Metal Mining At INCO Limited', in *Proceedings of the CIM Mine Operators Conference*. Sudbury, Ontario, Canada.

Baiden, G., Bissiri, Y., Hardcastle, S. and Kocsis, C. (2005) 'Justification of "on-demand"

ventilation systems by means of simulation techniques', in *Application of Computers and Operations Research in the Mineral Industry*. Taylor & Francis Group, London. doi: 10.1201/9781439833407.ch61.

Balusu, R., Humpries, P., Harrington, P., Wendt, M. and Xue, S. (2002) 'Optimum inertisation strategies', in *Queensland Mining Industry Health and Safety Conference*. Queensland, Australia, pp. 133–144.

Basu, A. J., Andersen, M. M. and Godsey, A. J. (2013) 'A framework for integrating mine ventilation optimization (MVO) with ventilation on demand (VOD)', in *23rd World Mining Congress*. Montreal, Quebec, Canada. doi: 10.1017/CBO9781107415324.004.

Bauer, M. A. (2007) 'High performance computing: The Software Challenges', in *Proceedings of the 2007 international workshop on Parallel symbolic computation - PASCO '07*. London, Ontario, Canada: ACM Press, pp. 11–12. doi: 10.1145/1278177.1278180.

Belgacem, M. Ben, Chopard, B. and Parmigiani, A. (2012) 'Coupling method for building a network of irrigation canals on a distributed computing environment', in *Cellular Automata*. Santorini Island, Greece, pp. 309–318. doi: 10.1007/978-3-642-33350-7_32.

Birch, M. E. (2003) *NIOSH Manual of Analytical Methods*.

Black, S. and Mullins, B. (2019) *A Study of Nano Diesel Particulate Matter (nDPM) Behaviour and Physico-chemical Changes in Underground Hard Rock Mines of Western Australia MRIWA PROJECT M495*. Perth, Western Australia.

Bluhm, S., Moreby, R., von Glehn, F. and Pascoe, C. (2014) 'Life-of-mine ventilation and refrigeration planning for Resolution Copper Mine', *Journal of the Southern African Institute of Mining and Metallurgy*. The Southern African Institute of Mining and Metallurgy, 114(6), pp. 497–503.

Bluhm, S. J., Marx, W. M., Von Glehn, F. H. and Biffi, M. (2001) 'VUMA Mine Ventilation Software', *Journal of the Mine Ventilation Society of South Africa*, 54(3).

Brickey, A. J. (2015) *Underground production scheduling optimization with ventilation constraints*. Colorado School of Mines. doi: 10.1017/CBO9781107415324.004.

Bugarski, A. (2007) 'Integrated Approach to Reducing Exposure of Underground Miners to Diesel Particulate Matter and Gases', in *DPM Workshop*. Elko, Nevada, p. 36.

Caterpillar.Inc (2011) *Underground Mining Loader*. Available at: http://amalgamatedmining.com/PDFs/R1600G.pdf.

CCD Group (2019) *PINSSAR DPM Monitoring Reader*. Available at: https://ccdgroup.com.au/products/pinssar-dpm-monitoring-reader/ (Accessed: 2 January 2020).

Chang, P., Xu, G., Zhou, F., Mullins, B., Abishek, S. and Chalmers, D. (2019) 'Minimizing DPM

pollution in an underground mine by optimizing auxiliary ventilation systems using CFD', *Tunnelling and Underground Space Technology*. Pergamon, 87, pp. 112–121. doi: 10.1016/J.TUST.2019.02.014.

Chasm Consulting (2016) *Ventsim Visual User Guide*. Capalaba, QLD, Australia.

Chatterjee, A., Zhang, L. and Xia, X. (2015) 'Optimization of mine ventilation fan speeds according to ventilation on demand and time of use tariff', *Applied Energy*. Elsevier Ltd, 146, pp. 65–73. doi: 10.1016/j.apenergy.2015.01.134.

Chen, X., Yang, S., Sun, X. and Wang, L. (2015) 'Research on 1D-2D Co-simulation for Cabin Air Environment Accident', *Procedia Engineering*. Elsevier, 121, pp. 1983–1989. doi: 10.1016/j.proeng.2015.09.196.

Cross, H. (1936) *Analysis of flow in networks of conduits or conductors*.

Czernia, D. and Haponiuk, B. (2019) *Air Density Calculator*. Available at: https://www.omnicalculator.com/physics/air-density.

Dasys, A., Hardcastle, S. G., Hughes, G. and Parsons, H. (2014) 'Increasing production capacity with ventilation on demand a new paradigm for VOD - enabling production', in *CIM Convention*. Vancouver, BC, Canada.

Dekati Ltd. (2018) *Dekati DePS Brochure*. Kangasala, Finland.

Denby, B. and Schofield, D. (1995) 'The Use of Genetic Algorithms in Underground Mine Scheduling', in *APCOM XXV 1995: Application of Computers and Operations Research in the Minerals Industries*. Brisbane, Australia: Australasian Institute of Mining and Metallurgy.

Duckworth, I. J., Wallace Jr, K. G. and Wise, R. (1995) 'Ventilation Planning and Design of the Skyline Mines', in *Proceedings of the 7th US/North American Mine Ventilation Symposium*. Littleton, CO, USA, pp. 9–14.

Edwards, J. C. and Hwang, C. C. (1999) 'CFD analysis of mine fire smoke spread and reverse flow conditions', in *Proc. of 8th US Mine Ventilation Symposium*. Rolla, MO, USA, pp. 91–99.

Edwards, J. C. and Hwang, C. C. (2006) 'CFD Modeling of Fire Spread along Combustibles in a Mine Entry', in *Proceedings of the SME Annual Meeting*, pp. 1–5.

Fava, L., Saavedra-Rosas, J., Tough, V. and Haarala, P. (2013) 'Heuristic optimization of scheduling scenarios for achieving strategic mine planning targets', in *23rd World Mining Congress*. Montreal, Canada.

Fava, L., Maybee, B. and Millar, D. (2012) 'Decision Support for an Underground Gold Mining Operation – A Case Study', in *Project Evaluation Conference*. Melbourne, VIC.

Fava, L., Millar, D. and Maybee, B. (2011) 'Scenario evaluation through mine schedule

optimisation', in *MinePlanning 2011*. Antofagasta, Chile.

Feroze, T. and Genc, B. (2016) 'Estimating the effects of line brattice ventilation system variables in an empty heading in room and pillar mining using CFD', *Journal of the Southern African Institute of Mining and Metallurgy*. The Southern African Institute of Mining and Metallurgy, 116(7), pp. 1143–1152. doi: 10.17159/2411-9717/2016/v116n12a8.

Flir Systems (2011) *Airtec Diesel Particulate Monitor Operators Manual*. Albuquerque, NM, USA.

Flir Systems (2013) *Airtec Measurement Calculations*. Albuquerque, NM, USA.

Flir Systems (2018) *FLIR AIRTEC™ DPM MONITOR*. Available at: www.flir.com/airtec.

FLIR Systems (2015) *Airtec Diesel Particulate Monitor SOFTWARE HELP GUIDE*. Nashua, New Hampshire.

Gangal, M. (2012) 'Summary of worldwide underground mine diesel regulations', in *Proceedings of the 18th MDEC Conference*. Toronto, Canada.

Gillies, A. D. S., Wu, H. W., Tuffs, N. and Sartor, T. (2004) 'Development of a Real Time Airflow Monitoring and Control System', in *Proceedings of the 10th US/North American Mine Ventilation Symposium*. Anchorage, Alaska, USA.

Gillies, A. D. S. (2012) 'Some approaches and methods for real-time DPM ambient monitoring in underground mines ventilation considerations in handling DPM', pp. 1–6.

Gillies, A. D. S., Wu, H. W. and Harvey, T. (2008) 'Mine Real-Time Personal Respirable Dust and Diesel Particulate Matter Monitoring', (April), pp. 14–16.

Gillies, S., Slaughter, C., Calizaya, F. and Wu, H. W. (2010) 'Booster Fans-Some Considerations for their Usage in Underground Coal Mines-Mining Innovation', in Hardcastle, S. and McKinnon, D. L. (eds) *13th United States/North American Mine Ventilation Symposium*. Sudbury, Ontario, Canada. Available at: http://gwmt.com.au/Papers/2010/B117 2010 - June - 13USMVC Booster Fans Paper.pdf.

Gorain, S. and Pandey, J. K. (2015) 'Contaminant Dilution Based Ventilation Study for Narwapahar Mine', *Indian Mining & Engineering Journal*. IME Publication Bhubaneswar, 54(4), pp. 9–13.

Government of Ontario (1990) *R.R.O. 1990, Reg. 854: MINES AND MINING PLANTS*. Canada.

Greberg, J. and Sundqvist, F. (2011) 'Simulation as a tool for mine planning', in *Second International Future Mining Conference*. Sydney, NSW.

Grein, S., Stepniewski, M., Reiter, S., Knodel, M. M. and Queisser, G. (2014) '1D-3D hybrid modeling-from multi-compartment models to full resolution models in space and time.', *Frontiers*

in neuroinformatics. Frontiers Media SA, 8, p. 68. doi: 10.3389/fninf.2014.00068.

Grenier, M., Hardcastle, S. G., Mchaina, D. and Gangal, M. (1991) 'Simultaneous Measurement of Mine Worker Exposure to Respirable Silica and Diesel Exhaust Particulate', *CIM Bulletin*, 85(965), pp. 56–61.

Grenier, M. (2005) *Measurement of Carbon Monoxide in Diesel Engine Exhaust*. Sudbury, Ontario, Canada.

Grenier, M. G. (2010) 'Reducing Miners' Exposure to Diesel Particulate Matter Using Real-time Measurement', in *CIM Conference and Exhibition*.

Hardcastle, S., Gangal, M., Schreer, M. and Gauthier, P. (1999) 'Ventilation-on-Demand: Quantity or Quality — A Pilot Trial at Barrick Gold's Bousquet Mine', in *8th U.S. Mine Ventilation Symposium*. Rolla, MO, USA. Available at: https://scholarsmine.mst.edu/usmvs/8usmvs/8usmvs-theme1/6.

Hardcastle, S., Kocsis, C., Bissiri, Y. and Baiden, G. (2005) 'Optimising Mine Ventilation Through the Use of Life-Cycle Production Models', in *Eighth International Mine Ventilation Congress*. Brisbane, QLD.

Hardcastle, S. G. (1995) '3D-CANVENT: An Interactive Mine Ventilation Simulator', in *7th U.S. mine ventilation symposium*. Lexington, KY, United States: United States: Society for Mining, Metallurgy, and Exploration, Inc.

Hardcastle, S. G., Gangal, M. K. and Leung, E. (1998) 'Green and economic mine ventilation with an integrated air management system', in *Mine Planning and Equipment Selection*. Balkema, Rotterdam, pp. 785–793.

Hardcastle, S. G. and Kocsis, C. K. (2004) 'The ventilation challenge', *CIM (Canadian Mining and Metallurgical) Bulletin*, 97(1080), pp. 51–57.

Hardcastle, S. G., Kocsis, C. and Lacroix, R. (2007) 'Strategic mine ventilation control: a source of potential energy savings', in *Montreal Energy & Mines*. Montreal, Canada, pp. 255–263.

Hardcastle, S. G., Lamond, R. and Willoughby, D. (1999) 'Ventilation Optimization – Balancing The Need For More Power Against Environmental Concerns', in Tien, J. (ed.) *8th U.S. Mine Ventilation Symposium*. Rolla, MO, USA: Missouri-Rolla Press, pp. 305–312.

Hastie, T., Tibshirani, R. and Friedman, J. (2008) *The elements of statistical learning: data mining, inference and prediction*. Stanford, California. Available at: https://web.stanford.edu/~hastie/Papers/ESLII.pdf.

Huang, Z., Cai, W. and Banfield, A. F. (2009) 'A new short- and medium-term production planning tool – MINESIGHT® schedule optimizer (MSSO)', in *SME Annual Meeting*. Denver, CO.

Janisko, S. J., Noll, J. D. and Cauda, E. E. (2011) 'Aerosol sensing technologies in the mining industry', in *Proc. Society of Photo-Optical Instrumentation Engineers (SPIE)*. International Society for Optics and Photonics. doi: 10.1117/12.884315.

Janisko, S. and Noll, J. (2008) 'Near real time monitoring of diesel particulate matter in underground mines', *Safety And Health*, (3), pp. 509–514.

Janisko, S. and Noll, J. D. (2010) 'Field Evaluation of Diesel Particulate Matter Using Portable Elemental Carbon Monitors', in *13th United States/North American Mine Ventilation Symposium* .

Janzen, J., Hortin, K., Lilley, J., Edmond, M., Filiatreault, P., Montgomery, D. and Hindle, K. (2013) 'Ventilation On Demand – the impact of sensors, installation, control strategies, commissioning and advanced controls performance', in *23rd World Mining Congress*. Montreal, Canada.

Kawahata, K., Schumacher, P. and Hufford, R. (2013) 'Mine production scheduling optimization at Newmont's Twin Creeks Mine', *Mining Engineering*, pp. 49–55.

Khan, A. and Niemann-delius, C. (2014) 'Production Scheduling of Open Pit Mines Using Particle Swarm Optimization Algorithm', *Advances in Operations Research*, p. 9.

Khan, M. U. and Gillies, S. (2015) 'REALTIME DIESEL PARTICULATE MATTER MONITORING IN U.S. UNDERGROUND MINES', in *SME Annual Meeting*. Denver, CO.

Kocsis, C. K., Hall, R. and Hardcastle, S. G. (2003) 'The integration of mine simulation and ventilation simulation to develop a 'Life Cycle'mine ventilation system', *South African Institute of Mining and Metallurgy*, pp. 223–230.

Kocsis, C. K., Hardcastle, S. G. and Hall, R. (2004) 'Benefit of using mine process simulators to design a" life-cycle" mine ventilation system', *TRANSACTIONS-SOCIETY FOR MINING METALLURGY AND EXPLORATION INCORPORATED*, 316.

Kok, J. (2014) 'Feasibility studies – what should be considered in terms of ventilation', in *12th AusIMM Underground Operators' Conference 2014*. Melbourne, VIC: The Australasian Institute of Mining and Metallurgy, pp. 197–204.

Kruger, A., Holton, M. and Terblanche, F. (2003) 'PlanIt – OPTIM : An optimal mine planning system for large underground mining corporations', in *APCOM 2003: 31st International Symposium on Application of Computers and Operations Research in the Minerals Industrie*. South African institute of Mining and Metallurgy, pp. 231–238.

Kurnia, J. C., Sasmito, A. P., Wong, W. Y. and Mujumdar, A. S. (2014) 'Prediction and innovative control strategies for oxygen and hazardous gases from diesel emission in underground mines', *Science of The Total Environment*. Elsevier, 481, pp. 317–334. doi: 10.1016/J.SCITOTENV.2014.02.058.

Li, G. (2019) 'Simulation of Airflow Changes in a VOD System and Evaluation of Energy Benefits

through VREX Modeling', in *17th North American Mine Ventilation Symposium*. Montreal, Canada, pp. 361–369.

Li, G., Kocsis, C. and Hardcastle, S. G. (2011) 'Sensitivity analysis on parameter changes in underground mine ventilation systems', *Journal of Coal Science and Engineering (China)*, 17(3), pp. 251–255. doi: 10.1007/s12404-011-0305-z.

Lilic, N. and Kuzmanovl, D. (1994) 'Optimization of air distribution in mine ventilation networks', 4(I), pp. 105–113.

Little, J., Knights, P. and Topal, E. (2013) 'Integrated optimization of underground mine design and scheduling', *Journal of the Southern African Institute of Mining and Metallurgy*, 113(10), pp. 775–785.

Lowndes, I. S. and Yang, Z. Y. (2004) 'The application of GA optimisation methods to the design of practical ventilation systems for multi-level metal mine operations', *Mining Technology*, 113(1), pp. 43–58. doi: 10.1179/037178404225004283.

Luxford, J. (2000) 'Reflections of a Mine Scheduler', in *MassMin*. Brisbane, QLD, pp. 119–126.

Marcer, R., Audiffren, C., Viel, A., Bouvier, B., Walbott, A. and Argueyrolles, B. (2010) 'Coupling 1D System AMESim and 3D CFD EOLE models for Diesel Injection Simulation', in *23rd Annual Conference on Liquid Atomization and Spray Systems*. Brno, Czech Republic.

Martinez, M. A. and Newman, A. M. (2011) 'A solution approach for optimizing long- and short-term production scheduling at LKAB's Kiruna mine', *European Journal of Operational Research*. Elsevier B.V., 211(1), pp. 184–197. doi: 10.1016/j.ejor.2010.12.008.

Maybee, B. M., Fava, L., Dunn, P. G., Wilson, S. and Fitzgerald, J. (2010) 'Towards optimum value in underground mine scheduling', *CIM Journal*, 1(3).

McGinn, S. (2000) *The relationship between diesel engine maintenance and exhaust emissions Final Report*. Available at: www.deep.org (Accessed: 30 November 2019).

McPherson, M. J. (2009) *Subsurface Ventilation and Environmental Engineering*. Fresno, CA, USA: Mine Ventilation Services, Inc.

Menabde, M., Stone, P., Law, B. and Baird, B. (2007) 'Blasor–A generalized strategic mine planning optimization tool', in *SME Annual Meeting*. Denver, CO.

Mide Technology Corp (2019) *Air Pressure at Altitude Calculator*. Available at: https://www.mide.com/air-pressure-at-altitude-calculator.

Mine Safety and Health Administration (2001) *MSHA: Diesel Particulate Single Source Page Metal/Nonmetal Mines*.

Mine Safety and Health Administration (2009) *DPM: What is it? What are the health risks? How*

does MSHA regulate it? Available at: https://arlweb.msha.gov/01-995/2009Docs/DPMOverview.pdf.

Mine Ventilation Services (2016) *VNet User's Manual & Tutorial*. Clovis, CA, USA.

Morla, R., Karekal, S., Godbole, A., Bhattacharjee, R. M., Balasubrahmanyam, N. and Satyanarayana, I. (2019) 'Effect of ventilation air velocities on diesel particulate matter dispersion in underground coal mines', *International Journal of Mining and Geo-Engineering*, 53(2). Available at: https://ijmge.ut.ac.ir/article_70475_a529e9670547e3c8c6f6bfa07f3a1f5b.pdf.

Nehring, M., Topal, E., Kizil, M. and Knights, P. (2010) 'An Investigation to Integrate Optimum Long-Term Planning with Short Planning in Underground Mine Production Scheduling', in *Mine Planning and Equipment Selection*. Fremantle, WA.

Nehring, M., Topal, E., Kizil, M. and Knights, P. (2012) 'Integrated short- and medium-term underground mine production scheduling', *Journal of the Southern African Institute of Mining and Metallurgy*, 112(5), pp. 365–378.

Nehring, M. and Topal, E. (2007) 'Production schedule optimisation in underground hard rock mining using mixed integer programming', in *Project Evaluation Conference*. Melbourne, VIC.

Nehring, M., Topal, E. and Little, J. (2010) 'A new mathematical programming model for production schedule optimization in underground mining operations', *Journal of the South African Institute of Mining and Metallurgy*, 110(8), pp. 437–446.

NIOSH (2003) *NIOSH Method 5040 – Elemental Carbon (Diesel Particulate)*. Atlanta, GA, USA.

Noll, J., Cecala, A., Organiscak, J. and Janisko, S. (2014) 'Real-time DPM Monitoring', *Engineering and Mining Journal*, 215(6), p. 78.

Noll, J., Janisko, S. and Mischler, S. E. (2013) 'Real-time diesel particulate monitor for underground mines', *Analytical Methods*. The Royal Society of Chemistry, 5(12), pp. 2954–2963. doi: 10.1039/c3ay40083b.

Norman, V. B. and Farnsworth, K. D. (1993) 'AutoMod', in Evans, G. W. et al. (eds) *Winter Simulation Conference*. Los Angeles, CA, USA, pp. 249–254.

O'Connor, D. F. (2008) 'Ventilation on demand (VOD) auxiliary fan project–Vale Inco Limited, Creighton Mine', in Wallace, K. G. (ed.) *12th US Mine Ventilation Symposium*. Reno, Nevada, USA, pp. 41–44.

Occupational Health and Safety Act (1990) *R.R.O. 1990, Reg. 833: CONTROL OF EXPOSURE TO BIOLOGICAL OR CHEMICAL AGENTS*.

Osei-Boakye, K., Mousset-Jones, P. and Kins, K. (2008) 'Planning to Meet the Required DPM Concentration Levels in Underground Mines – a Calibration Model', in *12th U.S. North American Mine Ventilation Symposium*, pp. 495–502.

PADT (2013) *Flownex–Fluent Link.*

PADT (2014a) *Flownex ANSYS Integration*.

PADT (2014b) *Flownex General User Manual*.

Pinssar (2019) *How It Works | Pinssar*. Available at: https://pinssar.com.au/technology/how-it-works/.

Prince, J. A. (2015) *Coupled 1D-3D simulation of flow in subway transit networks*. Imperial College London. Available at: https://spiral.imperial.ac.uk/bitstream/10044/1/29431/1/Prince-J-2016-PhD-Thesis.pdf.

Ren, T. and Balusu, R. (2010) 'The use of CFD modelling as a tool for solving mining health and safety problems', in *10th Underground Coal Operators' Conference*. University of Wollongong & the Australasian Institute of Mining and Metallurgy, pp. 339–349.

Ren, T. and Wang, Z. (2013) 'Computational fluid dynamics modelling of respirable dust and gas behaviour on a longwall face', in *Australian Mine Ventilation Conference*. Australia: Australasian Institute of Mining and Metallurgy, pp. 191–200.

Ross, A. and Willson, V. L. (2017) 'ONE-SAMPLE T-TEST', in *Basic and Advanced Statistical Tests*. Rotterdam: SensePublishers, pp. 9–12. doi: 10.1007/978-94-6351-086-8_4.

Ruckman, R. and Prosser, B. (2010) 'Integrating Ventilation Monitoring Sensor Data with Ventilation Computer Simulation Software at the Waste Isolation Pilot Plant Facility', in *13th United States/North American Mine Ventilation Symposium*. Sudbury, Ontario, Canada.

Rueda, N. (2017) 'Co-simulation: 1D to 3D coupling in an underground mine ventilation simulated model', in *16th North American Mine Ventilation Symposium*. Golden, Colorado, USA.

Samanta, B., Raj, K., Battacherjee, A. and Chakravarty, D. (2013) 'Uncertainty-based mine production scheduling for ore grade control using conditional simulation and multiobjective genetic algorithms', *Mining Engineering*.

Sarac, S. and Sensogut, C. (2000) 'A combined method for the analysis of mine ventilation networks', (May), pp. 371–374.

Saseen, G. (2007) *Estimation of Diesel Particulate Matter Emissions (DPM)*. Elko, Nevada.

SKC Inc (2017) *SKC Impactor Sampler Operating Instructions*. Eighty Four, PA, USA.

De Souza, E. (2015) 'Cost saving strategies in mine ventilation', in *Canadian Institute of Mining, Metallurgy and Petroleum (CIM) Convention*. Montreal, Canada, pp. 10–12.

Stewart, C. M., Aminossadati, S. M. and Kizil, M. S. (2015) 'Underground Fire Rollback Simulation in Large Scale Ventilation Models', in *15th North American Mine Ventilation*

Symposium. Blacksburg, VA, USA.

Sui, J., Yang, L., Zhu, Z., Fang, H. and Zhen, H. (2011) 'Mine ventilation optimization analysis and airflow control based on harmony annealing search', *Journal of Computers*, 6(6), pp. 1270–1277. doi: 10.4304/jcp.6.6.1270-1277.

Şuvar, M., Cioclea, D., Gherghe, I. and Păsculescu, V. (2012) 'Advanced Software for Mine Ventilation Networks Solving', *Environmental Engineering and Management Journal*, 11(7), pp. 1235–1239.

Thiruvengadam, M., Zheng, Y., Lan, H. and Tien, J. C. (2016) 'A diesel particulate matter dispersion study inside a single dead end entry using dynamic mesh model', *Int. J. Mining and Mineral Engineering*, 7(3), pp. 210–223. doi: 10.1504/IJMME.2016.078356.

Toraño, J., Torno, S., Menendez, M., Gent, M. and Velasco, J. (2009) 'Models of methane behaviour in auxiliary ventilation of underground coal mining', *International Journal of Coal Geology*, 80(1), pp. 35–43. doi: 10.1016/j.coal.2009.07.008.

Twigg, M. V. and Phillips, P. R. (2009) 'Cleaning the Air We Breathe - Controlling Diesel Particulate Emissions from Passenger Cars', *Platinum Metals Review*, 53(1), pp. 27–34. doi: 10.1595/147106709X390977.

U.S. EPA (2002) *Health Assessment Document for Diesel Engine Exhaust (Final 2002)*. Washington, DC. doi: EPA/600/8-90/057F.

U.S. EPA (2016) *Nonroad Compression-Ignition Engines: Exhaust Emission Standards (EPA-420-B-16-022)*. Available at: https://nepis.epa.gov/Exe/ZyPDF.cgi?Dockey=P100OA05.pdf.

VUMA Software ADCO (Pty) Ltd (2018) *Software for Mine Ventilation, Cooling and Environmental Control*. Available at: http://www.vuma.co.za/Data/Brochures/VUMA3D_Brochure.pdf.

Walker, S. (2013) 'A Good Air Flow', *Engineering and Mining Journal*, 214(12), pp. 60–61, 64–65, 68–69.

Webber-Youngman, R. (2005) 'An Integrated Approach Towards the Optimization of Ventilation, Air Cooling and Pumping Requirements for Hot Mines', in *Eighth International Mine Ventilation Congress*. Brisbane, QLD, Australia.

Wedding, W. C. (2014) *Multiscale modeling of the mine ventilation system and flow through the gob*. University of Kentucky.

Widzyk-Capehart, E. and Watson, B. (2001) 'AGNEW GOLD MINE EXPANSION MINE VENTILATION EVALUATION USING VENTSIM', in *Proceedings of the 7th International Mine Ventilation Congress*. Cracow, Poland.

Wu, H. W., Gillies, A. D. S., Volkwein, J. D. and Noll, J. (2009) 'Real-Time DPM Ambient

Monitoring in Underground Mines', pp. 1–10.

Wu, H. W. and Gillies, A. D. S. (2008) 'Developments in real time personal diesel particulate monitoring in mines', pp. 657–664.

Xu, G., Huang, J., Nie, B., Chalmers, D. and Yang, Z. (2017) 'Calibration of Mine Ventilation Network Models Using the Non-Linear Optimization Algorithm', *Energies*. Multidisciplinary Digital Publishing Institute, 11(1), p. 31. doi: 10.3390/en11010031.

Yuan, L. and Smith, A. C. (2009) 'CFD modeling of spontaneous heating in a large-scale coal chamber', *Journal of Loss Prevention in the Process Industries*, 22(4), pp. 426–433. doi: 10.1016/j.jlp.2009.02.016.

Yun, Q. X., Lian, M. J., Lu, C. W., Chen, Y. F. and Guo, W. W. (2003) 'Applications of Evolutionary Algorithms in Planning and Design of Mines', in *Mine Planning and Equipment Selection*. Kalgoorlie, Western Australia: Carlton, Victoria : AusIMM, 2003.

Zhang, H. (2015) *Approaches to Simulation of an Underground Longwall Mine and Implications for Ventilation System Analysis*. Virginia Polytechnic Institute and State University.

Zhang, H., Hauta, R. and Fava, L. (2016) 'Simultaneous Optimization of a Mine Schedule and a Ventilation Scenario', in *Maintenance, Engineering and Reliability/Mine Operators Conference*. Sudbury, Ontario, Canada.

Zheng, Y. (2011) *Diesel particulate matter dispersion analysis in underground metal/nonmetal mines using computational fluid dynamics*. Missouri University of Science and Technology.

Zheng, Y., Lan, H., Thiruvengadam, M. and Tien, J. C. (2011) 'DPM dissipation experiment at MST's experimental mine and comparison with CFD simulation', *Journal of Coal Science and Engineering (China)*. China Coal Society, 17(3), pp. 285–289. doi: 10.1007/s12404-011-0311-1.

Zheng, Y., Thiruvengadam, M., Lan, H. and Tien, J. C. (2015) 'Effect of auxiliary ventilations on diesel particulate matter dispersion inside a dead-end entry', *International Journal of Mining Science and Technology*, 25(6), pp. 927–932. doi: 10.1016/j.ijmst.2015.09.008.

Zheng, Y., Li, Y., Thiruvengadam, M., Lan, H. and Tien, J. C. (2017) 'DPM dispersion inside a single straight entry using dynamic mesh model', *International Journal of Coal Science & Technology*. China Coal Society, 4(3), pp. 234–244. doi: 10.1007/s40789-017-0179-9.

Zheng, Y. and Tien, J. C. (2008) 'DPM Dispersion Study using CFD for Underground Metal / Nonmetal Mines', in *12th U.S./North American Mine Ventilation Symposium*, pp. 487–494.

Curriculum Vitae

Name	Hongbin Zhang
Post-secondary Education and Degrees	Laurentian University Sudbury, Ontario, Canada 2015-2020 Ph.D.
	Virginia Polytechnic Institute and State University (Virginia Tech) Blacksburg, Virginia, USA 2013-2015 M.Sc.
	University of Kentucky Lexington, Kentucky, USA 2010-2013 B.Sc. (Hons)
	China University of Mining and Technology Xuzhou, Jiangsu, China 2008-2013 B.Sc.
Honors and Awards	Dr. Fergal Nolan Radiation Safety Institute of Canada Graduate Award Canada, 2017
	Per-Anders Persson Scholarship USA, 2014
	International Engineering Transfer Student Scholarship USA, 2010-2013
	Provost International Scholar USA, Fall 2011-Spring 2013
Related Work Experience	Ventilation Engineer and Mine Planning Specialist MIRARCO Mining Innovation, Sudbury, Canada 2015-2019
	Graduate Teaching Assistant Laurentian University, Sudbury, Canada 2019

Mining EIT (Mine Ventilation) Part-Time
Hatch Ltd., Sudbury, Canada
2018-2019

Summer Experience
Newmont Mining Corporation, Leeville, USA
2016

Mine Engineering Summer Intern
Newmont Mining Corporation, Denver, USA
2015

Graduate Research Assistant
Virginia Tech, Blacksburg, USA
2013-2015

Publications

Zhang, H., Fava, L., Cai, M., Vayenas, N., Acuña, E. (2019). "Hybrid CFD-Network Methodology for Improved DPM Modeling." Proceeding of the 17th North American Mine Ventilation Symposium. Montréal, Canada, pp. 784–793.

Zhang, H., Fava, L., Cai, M., Vayenas, N., Acuña, E. (2018). "DPM Variation Analysis over Multiple LHD Work Cycles with the Use of CFD." in: Chang X. (eds), Proceeding of the 11th International Mine Ventilation Congress. Xi'an, China, pp. 493-502.

Zhang, H., Hauta, R., Fava, L. (2017). "Mine schedule optimisation with ventilation constraints: a case study." in: Hudyma, M., Potvin, Y. (Eds.), Underground Mining Technology 2017. Sudbury, Ontario, Canada, pp. 145–152.

Zhang, H., Fava, L., Cai, M., Vayenas, N. (2017). "A hybrid network and CFD model for analyzing DPM concentration as part of underground mine plan optimization." in: Ghodrati, B., Kumar, U., Schunnesson, H. (Eds.), Proceeding of the 26th International Symposium on Mine Planning and Equipment Selection. Luleå, Sweden, pp. 271–277.

Zhang, H. (2015). Approaches to Simulation of an Underground Longwall Mine and Implications for Ventilation System Analysis. Virginia Polytechnic Institute and State University.

Zhang, H., Fayed, H. E., Luxbacher, K. D., and Jong, E. (2014). “The Feasibility of Hybrid Network and CFD Modeling for Mine Ventilation Applications.” SME Annual Meeting, Salt Lake City, Utah, USA.